

RIBONUCLEASES: STRUCTURAL AND BIOCHEMICAL  
INSIGHTS INTO CYTOTOXIC ACTIVITY

by

Randal Jeremy Johnson

A dissertation submitted in partial fulfillment  
of the requirements for the degree of

Doctor of Philosophy  
(Biochemistry)

at the

UNIVERSITY OF WISCONSIN-MADISON

2007

## A dissertation entitled

### Ribonucleases: Structural and biochemical insights into cytotoxic activity

submitted to the Graduate School of the  
University of Wisconsin-Madison  
in partial fulfillment of the requirements for the  
degree of Doctor of Philosophy

by

Randal Jeremy Johnson

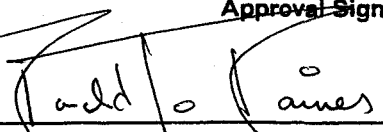
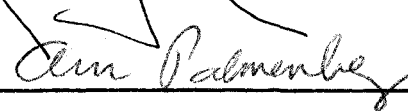
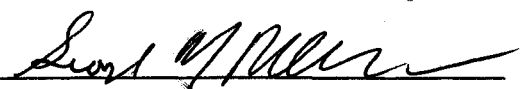
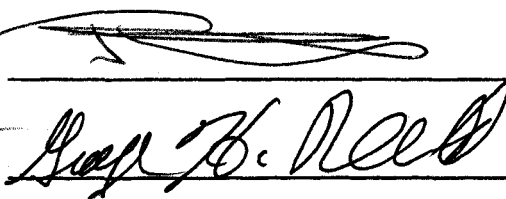
Date of Final Oral Examination: August 6, 2007

Month & Year Degree to be awarded: December

May

August 2007

\*\*\*\*\*  
Approval Signatures of Dissertation Committee

Signature, Dean of Graduate School

/EH

# RIBONUCLEASES: STRUCTURAL AND BIOCHEMICAL INSIGHTS INTO CYTOTOXIC ACTIVITY

Randal Jeremy Johnson

Under the supervision of Professor Ronald T. Raines

At the University of Wisconsin–Madison

The pancreatic ribonuclease superfamily is a vertebrate-specific class of enzymes that degrade RNA and perform a variety of biological activities. Certain superfamily members such as Onconase, a ribonuclease A homologue from the Northern leopard frog, have selective, innate toxicity toward cancerous cells. This selective toxicity can also be engineered into naturally nontoxic family members by designing protein variants that evade the inhibitory action of the ribonuclease inhibitor protein. The overall mechanism of ribonuclease cytotoxicity involves multiple steps, including nonspecific binding to the cell surface, internalization by endocytosis, translocation to the cytosol, interaction with the ribonuclease inhibitor, and ultimately degradation of cellular RNA. This thesis seeks to understand the steps involved in ribonuclease cytotoxicity, especially as they relate to the engineered cytotoxicity of human and bovine members of the enzyme superfamily.

Chapter Two describes the molecular interactions between the human ribonuclease inhibitor (RI) and human pancreatic ribonuclease (RNase 1) through determination of the X-ray crystal structure of the complex and characterization of variants of RNase 1. These variants of RNase 1 evade the binding of RI through engineered electrostatic repulsion and overcome a major hurdle to the development of human ribonuclease chemotherapeutics. In Chapter Three, the competing influences of Coulombic forces on ribonuclease cytotoxicity

are dissected through the use of a latent fluorophore to measure ribonuclease internalization. Chapter Four describes the interspecies regulation of ribonucleases by bovine and human RI, focusing on the co-evolution of the protein–protein interaction between ribonuclease and RI. The application of ribonuclease cytotoxicity to target cells infected with the hepatitis C virus is described in Chapter Five. The strategy is based on the engineering of an inactive precursor, or zymogen, of a ribonuclease that is then activated by the NS3 protease of the hepatitis C virus. Chapter Six is a study on the contribution of a buried, polar residue to the ribonucleolytic activity and conformational stability of ribonucleases. Together Chapters Two–Six provide information about the structure and function of ribonucleases and their inhibitor, RI, and relate this information to the cytotoxic activity of ribonucleases.



## Acknowledgments

My graduate career would not have been as rewarding or successful without the guidance and assistance of many people. First, I am grateful to my advisor, Ron Raines, for helping me develop as an independent researcher through his guidance, resources, and especially enthusiasm for science. He is a talented scientist whose vision and innovative thinking made research exciting in the Raines group.

I am grateful to members of the biochemistry community, including Ann Palmenberg, George Phillips, George Reed, Jon Thorson, and Marv Wickens for their guidance with my research and ongoing career. I am especially thankful for my collaborators in the Phillips lab who performed the crystallography that started much of my research, including Jason McCoy, Craig Bingman, and George Phillips. I appreciate Darrell McCaslin's guidance in the Biophysics Instrumentation Facility, where through his assistance many of the experiments in this dissertation were performed. I am thankful to the BTP especially Tim Donohue and Beth Holden for funding and broadening my education.

I am also grateful to many other members of the Raines group for their help in designing experiments and for making the Raines group an enjoyable place to spend five years. Luke Lavis with his love for fluorescence and creative mind shaped greatly my research directions. Mentoring Shawn Lin was a true joy, as he always desired to learn and pushed me to consider new areas of research. My classmates, Jeet Kalia, Annie Tam, and Tom Rutkoski, were always there to discuss the pressures of science and the intricacies of graduate school. For always acting excited when I had new data, listening to my crazy ideas, and bringing many smiles with their lively conversations, I am grateful to my local lab mates, Rebecca Turcotte, Margie Borra, Kim Dickson, Cindy Chao, and Sunil Chandran. Many other lab members

including Bryan Smith, Brian Miller, Eugene Lee, Steve Fuchs, Betsy Kersteen, Kelly Gorres and Matt Soellner taught me what it meant to be a scientist and helped me through all of the obstacles along the way.

Finally, I thank my wife, Carol, for her love, patience, and never ending support. She always listened intently to my stories about work, my practice talks, or my crazy ideas. I also thank my parents, Randy and Peggy, who cultivated my love for knowledge and nature, for their love and support both for schooling and for life's many other challenges. I also appreciate my many other family members, including Matthew, Jackie, and Graham, who were always there to laugh and remind me what was really important in life.

## Table of Contents

<b>Abstract</b> .....	i
<b>Acknowledgments</b> .....	iii
<b>Table of Contents</b> .....	v
<b>List of Figures</b> .....	viii
<b>List of Tables</b> .....	x
<b>List of Abbreviations</b> .....	xi
<b>Chapter One</b> .....	1
<b>Introduction</b> .....	1
<b>1.1 Overview</b> .....	2
<b>1.2 Pancreatic Ribonuclease Superfamily</b> .....	3
<b>1.3 Ribonuclease Inhibitor Protein</b> .....	5
<b>1.4 Mechanism of Ribonuclease Cytotoxicity</b> .....	7
<b>1.5 Conclusions</b> .....	15
<b>Chapter Two</b> .....	24
<b>Inhibition of Human Pancreatic Ribonuclease by the Human Ribonuclease Inhibitor Protein</b> .....	24
<b>2.1 Abstract</b> .....	25
<b>2.2 Introduction</b> .....	26
<b>2.3 Experimental Procedures</b> .....	28
<b>2.3 Results</b> .....	37
<b>2.4 Discussion</b> .....	44
<b>2.5 Conclusions</b> .....	52

<b>Chapter Three</b> .....	72
<b>Cytotoxic Ribonucleases: The Dichotomy of Coulombic Forces</b> .....	72
<b>3.1 Abstract</b> .....	73
<b>3.2 Introduction</b> .....	73
<b>3.3 Experimental Procedures</b> .....	76
<b>3.4 Results</b> .....	82
<b>3.5 Discussion</b> .....	86
<b>3.6 Conclusions</b> .....	90
<b>Chapter Four</b> .....	102
<b>Intraspecies Regulation of Ribonucleolytic Activity</b> .....	102
<b>4.1 Abstract</b> .....	103
<b>4.2 Introduction</b> .....	104
<b>4.3 Experimental Procedures</b> .....	106
<b>4.4 Results</b> .....	113
<b>4.5 Discussion</b> .....	119
<b>4.6 Conclusions</b> .....	123
<b>Chapter Five</b> .....	143
<b>A Ribonuclease Zymogen Activated by the NS3 Protease of Hepatitis C Virus</b> .....	143
<b>5.1 Abstract</b> .....	144
<b>5.2 Introduction</b> .....	144
<b>5.3 Experimental Procedures</b> .....	147
<b>5.4 Results</b> .....	152
<b>5.5 Discussion</b> .....	158

5.6 Conclusions .....	160
<b>Chapter Six .....</b>	<b>172</b>
<b>Genetic Selection Reveals the Role of a Buried, Conserved Polar Residue.....</b>	<b>172</b>
6.1 Abstract .....	173
6.2 Introduction .....	173
6.3 Experimental Procedures .....	175
6.4 Results.....	179
6.5 Discussion .....	182
6.6 Conclusions .....	186
<b>Chapter Seven .....</b>	<b>195</b>
<b>Conclusions and Future Directions .....</b>	<b>195</b>
7.1 Conclusions .....	196
7.2 Future Directions.....	197
<b>Appendix I .....</b>	<b>199</b>
<b>Expression and ribonucleolytic activity of human ribonucleases 11–13.....</b>	<b>199</b>
A1.1 Abstract .....	200
A1.2 Introduction .....	200
A1.3 Experimental Procedures .....	202
A1.4 Results and Discussion .....	205
<b>References.....</b>	<b>222</b>

## List of Figures

Figure 1.1 Members of the human pancreatic ribonuclease superfamily .....	16
Figure 1.2 Comparison of the molecular contacts within crystalline RI•ribonuclease complexes. ....	18
Figure 1.3 Comparison of the amino acids in RNase A essential to catalysis and the amino acids of RNase A in contact with RI.....	20
Figure 1.4 Correlation between the biochemical properties of a ribonuclease and its cytotoxicity to K-562 cells .....	22
Figure 2.1 Structure of the crystalline complex of hRI and RNase 1 .....	58
Figure 2.2 Contact residues from the crystal structures of hRI•RNase 1 and pRI•RNase A ...	60
Figure 2.3 Comparison of the $\beta 4$ – $\beta 5$ loop of RNase 1 and RNase A when bound to RI (green) .....	62
Figure 2.4 Electron density at $1\sigma$ ( $2F_{\text{obs}} - F_{\text{calc}}$ ) of key contact residues between hRI and RNase 1 .....	64
Figure 2.5 Dissociation rate of the complex between wild-type RNase 1 and hRI .....	66
Figure 2.6 Affinity for hRI and cytotoxic activity of ribonucleases .....	68
Figure 2.7 Electrostatic representation of the interaction between hRI and RNase 1 .....	70
Figure 3.1 Design of ribonuclease variants and latent fluorophore .....	92
Figure 3.2 Cytotoxicity of ribonuclease variants .....	94
Figure 3.3 Kinetics of ribonuclease internalization .....	96
Figure 3.4 Properties of RNase 1, its variants, and RNase A.....	98
Figure 3.5 Coulombic effects on ribonuclease-mediated cytotoxicity.....	100
Figure 4.1 Structure and sequence of RI.....	127

Figure 4.2 Dissociation of RI•ribonuclease complexes.....	129
Figure 4.3 Conformation and conformational stability of RI•ribonuclease complexes .....	131
Figure 4.4 Stability to hydrogen peroxide oxidation of RI and RI•ribonuclease complexes .	133
Figure 4.5 Phylogenetic tree of RIs.....	135
Figure 4.6 Percent identity between RIs and ribonucleases .....	137
Figure 4.7 Multiple sequence alignment of RIs.....	139
Figure 4.8 Multiple sequence alignment of ribonucleases .....	141
Figure 5.1 Structural model of unactivated 2C zymogen with 88/89 termini, 14-residue linker, and seven disulfide bonds .....	164
Figure 5.2 Activation of 1C zymogen by the NS4A/NS3 protease .....	166
Figure 5.3 Ribonucleolytic activity of zymogens in comparison to RNase A.....	168
Figure 5.4 Conformation and conformational stability of unactivated and activated 1C zymogens by circular dichroism .....	170
Figure 6.1 Genetic selection to reveal the influence of substitutions at position 75 to the activity and stability of RNase A .....	191
Figure 6.2 Conformational stability of five variants of RNase A .....	193
Figure A1.1 Comparison of conserved sequence elements within human members of the pancreatic ribonuclease superfamily.....	210
Figure A1.2 Expression of the RNA encoding RNases 11–13 .....	212
Figure A1.3 Quantitation of mRNA expression data .....	214
Figure A1.4 Sequence alignment of RNase 1, RNase 5, and RNase 12 .....	216
Figure A1.5 Protein expression of RNases 11 and 12 in <i>E. coli</i> BL21(DE3) cells. ....	218
Figure A1.6 Genetic selection for the critical residues to RNase 12 ribonucleolytic activity	220

## List of Tables

Table 2.1	Crystallographic, data processing, and refinement statistics; values in parentheses refer to the highest resolution shell .....	54
Table 2.2	Intermolecular hydrogen bonds ( $r_{X...X} < 3.35 \text{ \AA}$ ) in the structures of the crystalline hRI·RNase 1 and pRI·RNase A complexes .....	55
Table 2.3	Biochemical parameters of RNase 1, RNase A, and their variants .....	56
Table 2.4	Rate constants for the binding of hRI to RNase 1 and its variants .....	57
Table 3.1	Properties of wild-type RNase 1 and its variants .....	91
Table 4.1	Biochemical parameters for bRI, hRI, and RI•ribonuclease complexes .....	125
Table 4.2	Conservation of ribonuclease-contact residues in RIs .....	126
Table 5.1	Enzymatic activity of ribonuclease A zymogens .....	162
Table 5.2	Physicochemical properties of a ribonuclease A zymogen .....	163
Table 6.1	Biochemical properties of wild-type RNase A and variants at Ser75 .....	188
Table 6.2	Mass analysis of wild-type RNase A and variants at Ser75 .....	189
Table 6.3	Residues other than serine at position 75 (or the structurally analogous position) in the RNase A superfamily .....	190



**List of Abbreviations**

$\epsilon$	extinction coefficient
6-FAM	6-carboxyfluorescein
6-TAMRA	6-carboxytetramethylrhodamine
ANG	human angiogenin (RNase 5)
ASA	accessible surface area
BCA	bicinchoninic acid
bRI	bovine ribonuclease inhibitor
BSA	bovine serum albumin
BS-RNase	bovine seminal ribonuclease
CD	circular dichroism
CFIS	chain-folding initiation site
CPP	cell-penetrating peptide
DNA	deoxyribonucleic acid
DTNB	5,5'-(dithiobis(2-nitrobenzoic acid))
DTT	dithiothreitol
EDN	eosinophil-derived neurotoxin (RNase 2)
EDTA	ethylenediaminetetraacetic acid
<i>F</i>	fluorescence
FADE	fast atomic density evaluator
FBS	fetal bovine serum
FPLC	fast performance liquid chromatography
h	hour

HCl	hydrochloric acid
HCV	hepatitis C virus
HPLC	high-performance liquid chromatography
hRI	human ribonuclease inhibitor
ITPG	isopropyl-1-thio- $\beta$ -D-galactopyranoside
$k_a$	kinetic association rate constant
$k_{cat}$	first-order enzymatic constant
$K_d$	equilibrium dissociation constant
$k_d$	kinetic dissociation rate constant
kDa	kilodalton
$K_m$	Michaelis constant
LB	Luria-Bertani broth
LRR	leucine-rich repeat
MALDI-TOF	matrix assisted laser desorption/ionization-time-of-flight
MES	2-(N-morpholino)-ethanesulfonic acid
min	minute
MW	molecular weight
NaCl	sodium chloride
NS3	nonstructural protein 3
NS4A	nonstructural protein 4A
NS5A/5B	nonstructural protein 5A/5B
<i>OD</i>	optical density
ONC	Onconase <sup>®</sup> (a registered trademark of Alfacell, Inc.)

OVS	oligo(vinylsulfonic acid)
PBS	phosphate-buffered saline
PCR	polymerase chain reaction
PDB	Protein Data Bank
poly(C)	poly(cytidylic acid)
pRI	porcine ribonuclease inhibitor
RMSD	root mean square deviation
RI	ribonuclease inhibitor
RNA	ribonucleic acid
RNase A	bovine pancreatic ribonuclease
RNase 1	human pancreatic ribonuclease
s	second
SDS-PAGE	sodium dodecyl sulfate-polyacrylamide gel electrophoresis
<i>t</i>	time
TB	terrific broth
TCEP	tris(2-carboxyethyl) phosphine
$T_m$	midpoint of the thermal denaturation curve
Tris	2-amino-2-(hydroxymethyl)-1,3-propanediol

## **Chapter One**

### **Introduction**

## 1.1 Overview

RNA serves many keystone roles in biology, as even previously disregarded segments of noncoding RNA have been discovered to play important structural and regulatory roles in biology (Hannon 2002). For instance, through its structural involvement in large protein-RNA complexes such as the ribosome and spliceosome, RNA facilitates the catalysis of protein synthesis and gene splicing (Reiter et al. 2003; Korostelev et al. 2006; Sashital et al. 2007). Shorter segments of noncoding RNA also regulate biological processes such as development, cell proliferation, and cell survival (Hannon 2002; Dykxhoorn and Lieberman 2005). The identification of these short noncoding RNAs, such as micro RNAs and small interfering RNAs, has shed new light on the complexity of the genome (Lagos-Quintana et al. 2001; Michalak 2006). These short noncoding RNAs function by recognizing short segments of RNA and recruiting large protein complexes to degrade the RNA sequence. Additionally, in the classic paradigm of biochemistry, messenger RNA serves as the transfer medium for the flow of information from DNA to proteins, where the regulation of RNA-turnover and processing controls protein abundance (Goldstrohm et al. 2006; Goldstrohm et al. 2007).

Due to its important roles in biology, multiple disease states have been connected with the misregulation of RNA (Esquela-Kerscher and Slack 2006). For instance, aberrant expression of multiple micro RNAs and small interfering RNAs is correlated with the development and progression of various cancers (Esquela-Kerscher and Slack 2006; Wu et al. 2007). Consequently, alteration of RNA abundance has emerged as a new target for therapeutics (Tafech et al. 2006), and new classes of therapeutics that target RNA

abundance have surfaced; such as small interfering RNAs to downregulate disease-related proteins, ribozymes to degrade specific RNA sequences, and ribonucleases with selectivity for cancer cells to control cell fate (Tafech et al. 2006). As compared to the first two strategies in which the therapeutic is RNA-based and has difficulties crossing the cell membrane (Takeshita and Ochiya 2006), ribonucleases are internalized rapidly and with high specificity for cancer cells (Leland and Raines 2001; Rutkoski et al. 2005). In fact, Onconase<sup>®</sup>, a ribonuclease from the oocytes of the Northern Leopard frog (*Rana pipiens*), is currently in phase III clinical trials for the treatment of malignant mesothelioma and has recently received orphan drug status from the U.S. Food and Drug Administration (Pavlakis and Vogelzang 2006).

## 1.2 Pancreatic Ribonuclease A Superfamily

Onconase is just one member of the the pancreatic ribonuclease A superfamily, where the entire enzyme family encompasses a large class of vertebrate-specific enzymes that catalyze the hydrolysis of RNA (Beintema 1987; Beintema et al. 1988b; Beintema et al. 1997). The characteristics that define the enzyme superfamily are the members ability to degrade RNA, the existence of an N-terminal signal sequence that codes for their secretion from the cell, the presence of multiple conserved disulfide bonds, and their kidney-shaped three-dimensional structure (Beintema 1987; Beintema et al. 1988b; Beintema et al. 1997). The archetypal member of the pancreatic ribonuclease superfamily is bovine pancreatic ribonuclease (RNase A; EC 3.1.27.5). Due to its small size and ease of purification, RNase A has served as a model protein for studies on protein structure,

folding, catalysis, evolution, and semisynthesis (Raines 1998). Despite its extensive applications as a model protein, the biological role of RNase A, the digestion of dietary RNA in the ruminant gut, is fairly narrow in scope (Barnard 1969), but this is not representative of the entire enzyme family.

In humans, thirteen members of the pancreatic ribonuclease superfamily have been identified (Figure 1.1) (Cho et al. 2005). The genes coding for these proteins are all located in close proximity on chromosome 14. These thirteen ribonucleases have sequence identities between 16–75% (Cho et al. 2005), and their sequence diversity foreshadows their diversity of biological activities. For instance, RNase 5, known as angiogenin, induces blood vessel proliferation or angiogenesis (Shapiro et al. 1986) by translocating to the nucleus and binding to ribosomal RNA (Tsuji et al. 2005). Interestingly, mutations in the angiogenin gene indicate higher susceptibility for familial amyotrophic lateral sclerosis (Greenway et al. 2006), making angiogenin an interesting therapeutic target. RNase 2, eosinophil-derived neurotoxin (EDN), and RNase 3, eosinophil-cationic protein (ECP), are major protein components of the eosinophil and are involved in host defense (Rothenberg and Hogan 2006). Similarly, RNase 7 has innate antimicrobial activities that are mediated through its cationic N-terminal residues (Huang et al. 2007). Human pancreatic ribonuclease (RNase 1), the human homologue of RNase A, is expressed more ubiquitously than RNase A and has been adapted for new biological functions in primates (Landre et al. 2002; Zhang 2006). The biological roles of many of the ribonucleases are still to be clarified, but their identification may offer new surprises, especially as preliminary results indicate that RNase 9 and 10 are highly expressed in male reproductive

organs (Zhu et al. 2007). Human ribonucleases 9–13 are also missing at least one of the three canonical active site residues (Cho et al. 2005), raising the possibility that these ribonucleases have biological activities independent of the degradation of RNA (Zhu et al. 2007).

### **1.3 Ribonuclease Inhibitor Protein**

To regulate the biological activities of ribonucleases and protect itself from nonspecific ribonuclease activity, cells produce the ribonuclease inhibitor protein (RI), an extraordinarily tight inhibitor of ribonucleases ( $K_d \sim \text{fM}$ ) (Dickson et al. 2005). RI is a 50-kDa cytosolic protein whose expression is nearly invariant by cell type at approximately 4  $\mu\text{M}$  (Haigis et al. 2003). The proposed biological roles for RI involve regulating the biological activities of ribonucleases, sequestering rogue ribonucleases, and responding to oxidative stress (Dickson et al. 2005). RI fulfills the final role through its 29–32 free cysteine residues that can act as powerful antioxidants (Wang and Li 2006), where oxidation of the cysteine residues to disulfides leads to the rapid inactivation and cellular degradation of RI (Fominaya and Hofsteenge 1992; Blázquez et al. 1996) and to increased DNA-damage in RI-deprived cells (Monti et al. 2007). Additionally, unidentified biological roles for RI are possible, as elevated levels of RI expression have been observed in large scale proteomic studies under various physiological conditions (Coling et al. 2007).

RI forms an extraordinarily tight 1:1 stoichiometric complex with ribonucleases (Lee et al. 1989b). All human ribonucleases tested to date have affinities for RI in the femtomolar range (Dickson et al. 2005), making RI-ribonuclease complexes some of the tightest



tightest protein-protein complexes (Teufel et al. 2003). This tight affinity of RI for ribonucleases is retained even though the sequence identity between ribonucleases is less than 30% (Johnson et al. 2007c). RI achieves this unusually high affinity for its diverse ligands by using its unique three-dimensional structure to bury substantial complex surface area ( $\sim 2800\text{--}3677 \text{ \AA}^2$ ) and by increasing the association rate for complex formation through long-range electrostatics (Iyer et al. 2005; Shaul and Schreiber 2005; Johnson et al. 2007c).

RI has a horseshoe-shaped three-dimensional architecture with alternating  $\alpha$ -helix and  $\beta$ -strands, where the concave interior surface of  $\beta$ -strands forms the ribonuclease binding interface (Figure 1.2). The exact molecular contacts between RI and ribonuclease have been elucidated for four RI-ribonuclease pairs (Kobe and Deisenhofer 1995; Papageorgiou et al. 1997; Iyer et al. 2005; Johnson et al. 2007c). RI inhibits ribonucleolytic activity by forming molecular contacts with at least two of the three canonical active site residues (shown as black boxes in Figure 1.2) and occluding substrate binding. The interactions between RI and three ribonucleases, angiogenin, EDN, and RNase A, highlight the diversity of residues used by RI to bind ribonucleases, where only one hydrogen bond—between Ser460 of RI and Gln12 of angiogenin/Gln11 of RNase A/Trp10 of EDN—is conserved in all three structures (Iyer et al. 2005). Another hydrogen bond to the catalytic lysine residue of the ribonuclease by Asp435 of RI is most likely conserved, but is obscured in the RI-RNase A structure by a bound sulfate atom (Kobe and Deisenhofer 1995; Iyer et al. 2005). The diversity of contact residues between RI and its different ribonuclease ligands has been exploited to inhibit RNase A selectively while

maintaining high affinity for angiogenin. By inserting tryptophan residues at 408/410 in hRI and deleting the intervening residue, a variant of hRI was developed with greater than  $10^9$ -fold selectivity for binding to angiogenin over RNase A (Kumar et al. 2004).

#### **1.4 Mechanism of Ribonuclease Cytotoxicity**

This selective inhibition of ribonucleases by RI also plays an important role in determining the cytotoxicity of a ribonuclease. Naturally cytotoxic ribonucleases, like Onconase and bovine seminal ribonuclease (BS-RNase), have greatly reduced affinity for the ribonuclease inhibitor (Boix et al. 1996). This connection between RI-affinity and cytotoxicity led to the development of new cytotoxic ribonucleases that were engineered to evade the binding of RI (Leland et al. 1998; Leland and Raines 2001). Through investigation of naturally cytotoxic ribonucleases and engineered nontoxic ribonucleases, additional attributes important to the cytotoxicity of a ribonuclease have emerged. These attributes are high ribonucleolytic activity, low affinity for RI, high conformational stability, and high cellular internalization efficiency (Leland and Raines 2001; Matousek 2001; Makarov and Ilinskaya 2003; Benito et al. 2005; Arnold and Ulbrich-Hofmann 2006) and consideration of these variables can assist in designing ribonucleases that are more toxic to tumor cells (Rutkoski et al. 2005).

*Ribonucleolytic Activity.* Ribonucleases are efficient catalysts of RNA degradation with kinetic constants near the diffusion limit (Raines 1998; 2004). They show specificity for cleavage on the 3' side of pyrimidine nucleotides *in vitro*, but the *in vivo* substrate specificity is unclear (Raines 1998). Short interfering RNAs, rRNA, and tRNA have all

been suggested as substrates for various ribonucleases, but the correlation of substrate specificity with cytotoxicity is also unclear (Lin et al. 1994; Ardelt et al. 2003; Suhasini and Sirdeshmukh 2006). For instance, Onconase shows specificity *in vitro* for particular UGG triplets located in the variable loop or D-arm of tRNAs (Suhasini and Sirdeshmukh 2006), but the correlation between cleavage of this substrate and the cytotoxicity of Onconase was not investigated.

To perform the chemistry of RNA degradation, ribonucleases use two histidine residues, as a general acid and base, and a lysine residue to stabilize the transition state (Raines 1998; 2004). Many additional residues perform peripheral roles in nucleobase recognition, phosphoryl group binding, or in structural alignment of the catalytic residues (Raines 2004). Recently, all of the residues in RNase A and angiogenin that are essential to catalysis were identified by genetic selection. Residues essential to catalysis included the active-site residues, buried hydrophobic and polar residues, and disulfide bound cysteines. Overall, 23 residues in RNase A and 29 residues in angiogenin were intolerant to substitution (Smith and Raines 2006). Due its  $>10^5$ -fold higher catalytic activity, most protein engineering to design cytotoxic ribonucleases has begun with RNase A instead of angiogenin (Leland et al. 2002).

The ability to degrade RNA is essential to the cytotoxic activity of a ribonuclease. Ribonuclease variants with significantly reduced ribonucleolytic activity both by chemical or genetic modification lose their cytotoxic activity (Arnold and Ulbrich-Hofmann 2006). For instance, Onconase variants with  $<0.1\%$  residual activity have a greater than 50-fold decrease in cytotoxicity (Lee and Raines 2003). Also, RNase A variants with reduced

catalytic activity but similar RI affinity show decreased cytotoxicity when compared to variants with higher activity (Dickson et al. 2003). Thus, to achieve high cytotoxicity with RNase A, the 23 essential residues for catalysis should be exempt from substitution (Figure 1.3), leaving 80% of the amino acids in RNase A available for substitution to instill the other positive attributes for increased cytotoxicity.

*RI-evasion.* In order to exert their ribonucleolytic activity in the cell, ribonucleases must evade the inhibitory action of RI. By effectively evading RI, variants of RNase A and BS-RNase can be more toxic to erythroleukemia cells than Onconase (Lee and Raines 2005; Rutkoski et al. 2005). Also, changing the intracellular concentration of RI, either positively or negatively, proportionally shifts the cytotoxicity of moderately cytotoxic variants (Haigis et al. 2003; Monti and D'Alessio 2004).

Many strategies have been described to design ribonucleases that evade inactivation by RI, including chemical modification, attachment of targeting moieties, oligomerization, and most commonly site-directed mutagenesis (Suzuki et al. 1999; Futami et al. 2001; Rutkoski et al. 2005; Leich et al. 2006). One strategy to design cytotoxic ribonucleases took advantage of a computational algorithm called FADE (fast atomic density evaluation) that identified regions of high shape complementarity (regions of interlocking “knobs” and “holes”) in the RI-RNase A crystal structure (Mitchell et al. 2001; Rutkoski et al. 2005). Sterically disruptive amino acids, especially arginine, were then substituted at positions of high shape complementarity in RNase A, creating RNase A variants with high cytotoxicity (Rutkoski et al. 2005).

RNase 1, the human homologue of RNase A, has been more a difficult starting point in the design of RI-evasive and cytotoxic variants (Gaur et al. 2001; Leland et al. 2001; Bosch et al. 2004). In RNase A, a single G88R substitution decreases the binding affinity of RI for RNase A by  $>10^4$ -fold (Leland et al. 1998). Conversely in RNase 1, N88R, G89R, or S90R substitutions alone or in concert fail to instill significant RI-evasion (Gaur et al. 2001; Bosch et al. 2004). Previous mutagenesis and modeling studies had suggested that the binding energy for RI·RNase 1 complex formation was more widely distributed than in the RI·RNase A complex, especially in the  $\alpha 2\beta 1$  region (residues 33–43) and the  $\beta 2\beta 3$  region (residues 64–71) (Pous et al. 2000; Gaur et al. 2001), but substitutions distributed over these regions only slightly reduced the affinity of RNase 1 for RI (Gaur et al. 2001; Bosch et al. 2004). Other strategies, such as the fusion of RNase 1 with human basic fibroblast growth factor, site-specific attachment of RNase 1 to targeting antibodies, and incorporation of nuclear localization signals have succeeded in creating variants with limited RI-evasion and cytotoxicity (Bosch et al. 2004; Tada et al. 2004; Erickson et al. 2006; Rodriguez et al. 2006), but basic knowledge about the intraspecies complex between hRI·RNase 1 was still missing. Chapters 2–4 of this thesis address this problem through structural and biochemical investigation of the hRI·RNase 1 complex and provide information about the influence of this complex on the biology of both ribonuclease and RI.

In the crystal structure of RI·RNase A, 23 residues of RNase A were observed to form either hydrogen bonds or van der Waals contacts with RI (Figure 1.3) (Kobe and Deisenhofer 1995; Johnson et al. 2007c). Only three of these 23 residues overlap with the 23 residues essential for ribonucleolytic activity, meaning that a unique set of 20 amino

acids should be amenable to substitution in order to decrease RI-affinity without significant loss in ribonucleolytic activity (Smith and Raines 2006). Thus, 20% of the residues not essential to catalysis (20 out of 101), could serve as possible sites for disruption of RI-ribonuclease complexes.

*Conformational Stability.* Onconase is an extremely stable enzyme with a midpoint for its thermal denaturation ( $T_m$ ) of nearly 90 °C. Decreasing its conformational stability detrimentally affects its cytotoxicity (Leland et al. 2000; Arnold et al. 2006). Onconase's high stability is attained through the energetic contributions of a tightly packed hydrophobic core, a constricted N-terminal residue, and a network of stabilizing disulfide bonds (Arnold et al. 2006). RNase A is stabilized significantly by its four disulfide bonds, as substitution of any of its cystines with alanine residues decreases the  $T_m$  value by >20 °C (Klink et al. 2000; Ruoppolo et al. 2000) and diminishes the cytotoxicity of the resulting variant (Klink et al. 2000). Conversely, introduction of non-natural disulfide bonds to stabilize variants of RNase A increases their conformational stability and cytotoxicity (Klink and Raines 2000; Dickson et al. 2003). The correlation between increased conformational stability and increased cytotoxicity is likely a reflection of the reduced susceptibility to proteolysis and increased cellular half-lives of conformationally stable proteins (Klink and Raines 2000). Most amino acids that directly affect stability are located on the buried interior of the ribonuclease, but certain surface exposed residues also have a significant affect on stability, making the effect of a substitution on conformational stability and cytotoxicity difficult to judge *a priori* (Coll et al. 1999; Bosch et al. 2004;

Smith and Raines 2006). Chapter 6 examines the contribution of a buried polar residue to ribonuclease stability and identifies certain characteristics important for its conservation.

*Cellular Internalization.* In order to reach the cytosol and interact with RI, a ribonuclease must first be internalized into the cell and trafficked to the cytosol (Conner and Schmid 2003). The efficiency of ribonuclease internalization may dramatically impact a ribonuclease's cytotoxicity as microinjected and transiently expressed ribonucleases are toxic at substantially lower concentrations than exogenously delivered ribonucleases (Saxena et al. 1991; Leland et al. 1998; Erickson et al. 2006). The steps known to be involved in ribonuclease internalization are: nonspecific binding of the ribonuclease to the cell surface, internalization via endocytosis, and translocation from the endosomes to the cytosol (Lee and Raines 2005; Notomista et al. 2006).

The first step in ribonucleases internalization, cell-surface binding, proceeds without the necessity for a specific protein receptor, as cell-surface binding is not saturable and incubation of cells with proteases prior to ribonuclease incubation has no effect on ribonuclease internalization (Haigis and Raines 2003). Cell-surface binding for ribonucleases proceeds by a similar mechanism to that observed for other cationic proteins and peptides such as cell-penetrating peptides (CPPs) (Hallbrink et al. 2001; Kaplan et al. 2005; Fuchs and Raines 2006; 2007), where the cationic charge of the biomolecules facilitates interactions with negatively charged cell-surface molecules such as heparan sulfate (Fuchs and Raines 2004). In fact, cationization of ribonucleases leads to increased cytotoxicity, presumably through increased cell-surface binding (Futami et al. 2001; Futami et al. 2002; Fuchs et al. 2007). The cationic charge on the RNA-binding face of the

ribonuclease is particularly important for cell-surface binding and for destabilization of the negatively charged membranes (Notomista et al. 2006). The positive charge of a ribonuclease and its effect on ribonuclease internalization may also be therapeutically relevant, as cancerous cells are known to display higher percentages of anionic phospholipids on their cell surface (Ran et al. 2002; Notomista et al. 2006). Thus, the positive charge on a ribonuclease could be partially responsible for the selectivity of ribonucleases for cancerous cells over normal cells (Notomista et al. 2006).

After binding to the cell surface, RNase A is then internalized and accumulates in endosomes (Lavis et al. 2006). The specific endocytic pathway that RNase A traverses is dynamin- and clathrin-independent, as RNase A does not colocalize with transferrin, the canonical clathrin-dependent pathway marker (Haigis and Raines 2003). RNase A then travels to the late endosomes or lysosomes, but not to the Golgi apparatus, before being translocated to the cytosol (Haigis and Raines 2003). Conversely, two reports show that Onconase internalization diverges from RNase A internalization, but these reports disagree on the degree of divergence as one paper reports that Onconase is internalized by a clathrin-mediated pathway but the other reports that it is clathrin-independent (Haigis and Raines 2003; Rodriguez et al. 2007). Additional endocytic pathways have also been suggested for certain ribonuclease variants, including translocation to the nucleus, and these alternate endocytic pathways may differentially influence their cytotoxicity (Bosch et al. 2004; Rodriguez et al. 2006).

The final step in ribonuclease internalization, involving translocation from the endosomes to the cytosol, is the least well-characterized. Ribonucleases are known to



increased evasion of the cytosolic RI and increased cytotoxicity indicates that ribonucleases reach the cytosol and so must translocate across endocytic membranes (Rutkoski et al. 2005). Additionally, ribonucleases accumulate in endocytic vesicles indicating that translocation is an inefficient process, although visualization or quantitation of translocation has not been achieved (Lavis et al. 2006). Understanding the entire internalization mechanism for ribonucleases could provide additional attributes to consider when designing cytotoxic ribonucleases.

*Cytotoxic Attributes Combined.* Ribonuclease cytotoxicity is a complex phenotype whose measurement encompasses all of the aforementioned biochemical attributes of a ribonuclease. To integrate this data, the biochemical data for pancreatic ribonuclease variants from multiple studies were collated and graphed *versus* the cytotoxicity of these variants (Figure 1.4). To remove any variation due to methodology, ribonuclease variants for comparison were selected based on the similarity of biochemical methods used to determine their cytotoxic attributes. These graphs show the correlation between each variable and cytotoxicity ( $IC_{50}$ ), where  $k_{cat}/K_m$  measures ribonucleolytic activity,  $K_d$  measures affinity for RI,  $T_m$  measures conformational stability, and net charge indirectly measures internalization.

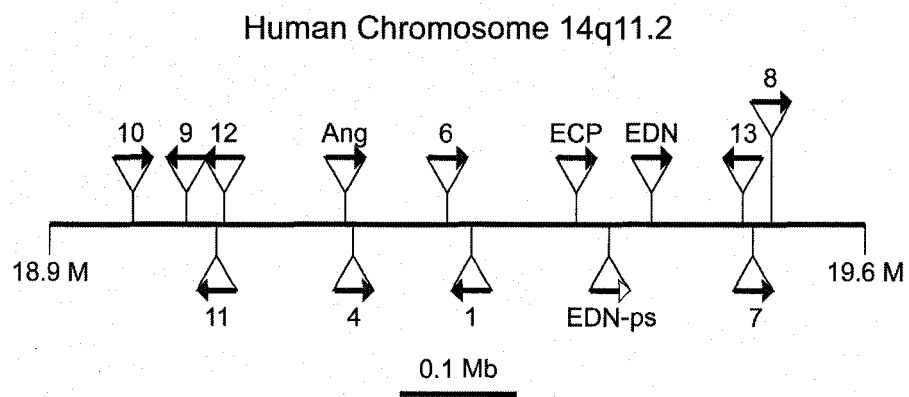
No one factor stands out as the determining factor in ribonuclease cytotoxicity, which is not surprising as these biochemical characteristics are linked with the three-dimensional structure of the enzyme and cannot be decoupled easily. Yet, the log of the  $K_d$  value does seem to have a strong negative trend with  $IC_{50}$ , reinforcing the importance of RI-evasion in ribonuclease cytotoxicity (Rutkoski et al. 2005). Additionally, variants with high

value does seem to have a strong negative trend with  $IC_{50}$ , reinforcing the importance of RI-evasion in ribonuclease cytotoxicity (Rutkoski et al. 2005). Additionally, variants with high ribonucleolytic activity often have high cytotoxicity, but this trend could only reflect the increase in ribonucleolytic activity observed upon removal of the potent low salt inhibitor, oligo(vinylsulfonic acid), from the assay buffer (Smith et al. 2003) and may not reflect the enzymatic variation within a cell. Conformational stability and net charge could also have similar trends, though the spread of data points makes detailed analysis difficult. As new ribonuclease variants are developed and additional data points are added to the graphs, an integrated view of ribonuclease cytotoxicity could emerge that properly weights the influence of each biochemical attribute and emphasizes which attributes to favor when designing more cytotoxic ribonucleases.

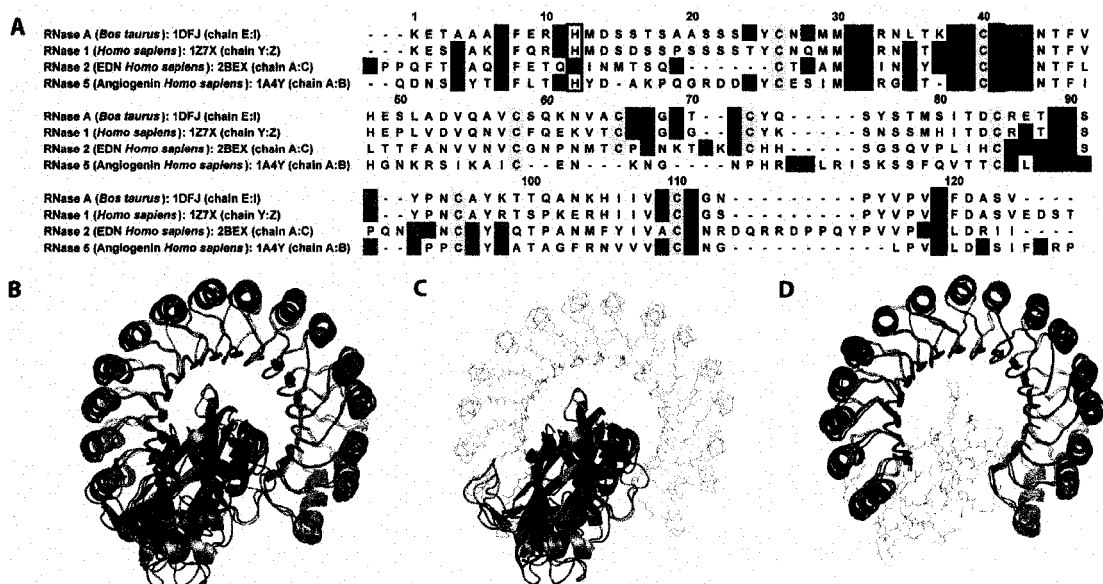
## 1.5 Conclusions

From basic studies on molecular recognition and protein evolution to applied studies related to cancer therapy, ribonucleases and RI provide a medically relevant system to address various questions in biology. Consequently, the information acquired from these studies will further our basic knowledge of protein structure and function, and could assist in the development of promising antitumoral therapeutics.

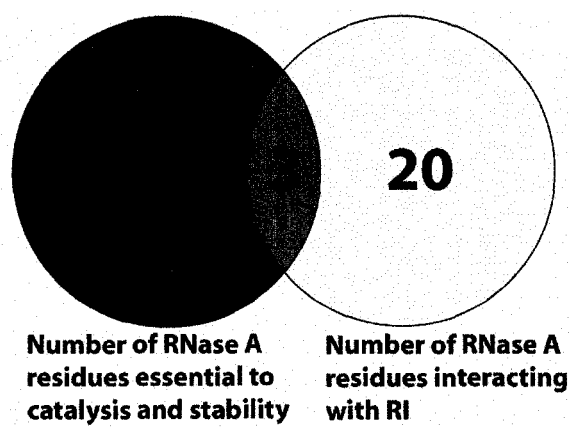
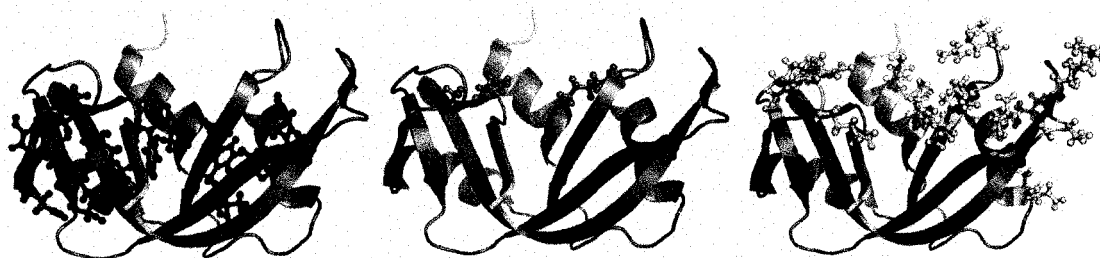
**Figure 1.1** Members of the human pancreatic ribonuclease superfamily depicted with their chromosomal locations. Open arrowheads signify functional genes and closed arrowheads pseudogenes (Cho et al. 2005).



**Figure 1.2** Comparison of the molecular contacts within crystalline RI-ribonuclease complexes. *A*, Amino acid sequence alignment of the four ribonucleases crystallized with RI (Kobe and Deisenhofer 1995; Papageorgiou et al. 1997; Iyer et al. 2005; Johnson et al. 2007c). Residues colored according to residue type and crystal contacts identified by PDBsum (Laskowski et al. 2005). Residues in van der Waals or hydrophobic contact with RI are in red. Residues with a hydrogen bond to RI are in blue. Conserved cysteine residues are in yellow. Catalytic residues are enclosed in black boxes. Residue are numbered according to their alignment with RNase A. *B*, *C*, *D*, Ribbon representation of the structural alignment of hRI-ribonuclease crystal complexes. hRI-RNase 1 is shown in purple, hRI-EDN in red, and hRI-angiogenin in silver. In *C* and *D*, hRI and RNase 1 are depicted as lines, respectively.  $\alpha$ -Carbon atoms of hRI were superimposed with the program Sequoia, and images were created with the program PyMOL.

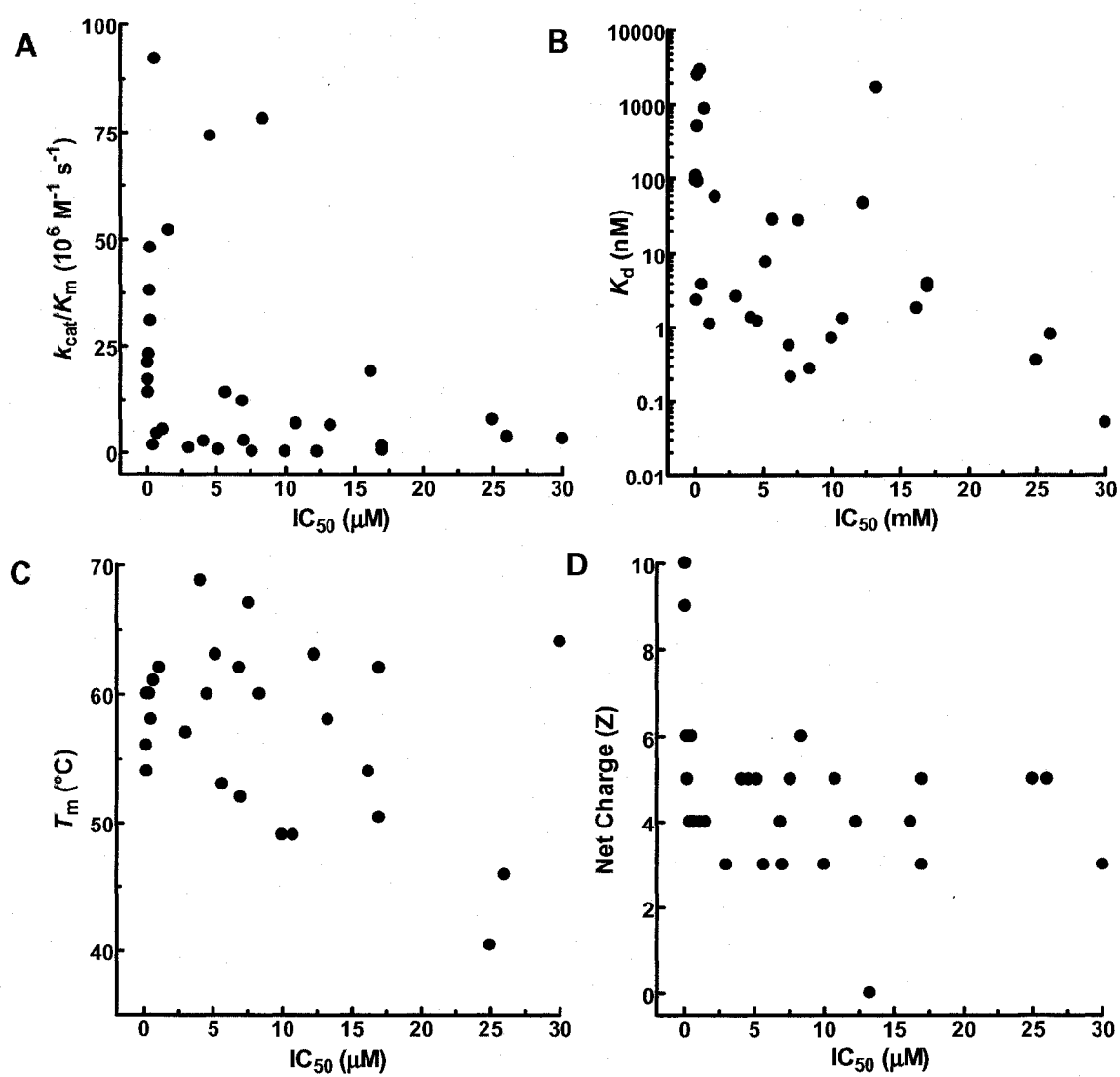


**Figure 1.3** Comparison of the amino acids in RNase A essential to catalysis and the amino acids of RNase A in contact with RI. *A*, Venn diagram of the residues essential for catalysis and stability and those in contact with RI in the crystal structure of the pRI·RNase A complex (PDB accession code 1DFJ) (Kobe and Deisenhofer 1995). The intersection consists of Lys41, Ala109, and His119. Molecular contacts were identified with the program PDBsum (Laskowski et al. 2005). *B*, Ribbon diagram of RNase A depicting the residues essential to catalysis but not in contact with RI in red sticks, residues essential to catalysis and in contact with RI in orange, and residues in contact with RI but not essential to catalysis in yellow.

**A****B**



**Figure 1.4** Relationship between the biochemical properties of a ribonuclease and its cytotoxicity to K-562 cells. *A*,  $k_{\text{cat}}/K_{\text{m}}$  vs  $\text{IC}_{50}$ ; *B*,  $K_{\text{d}}$  vs  $\text{IC}_{50}$ ; *C*,  $T_{\text{m}}$  vs  $\text{IC}_{50}$ ; *D*, Net charge vs  $\text{IC}_{50}$ . Data points were extracted from Leland et al. 1998, Klink and Raines 2000, Leland et al. 2001, Haigis et al. 2002b, Dickson et al. 2003, Lee and Raines 2005, Rutkoski et al. 2005, Johnson et al. 2007a, and Johnson et al. 2007c, wherein data points for ribonucleolytic activity, affinity for RI, and cytotoxicity were determined by using the same experimental procedures.



## **Chapter Two**

### **Inhibition of Human Pancreatic Ribonuclease by the Human Ribonuclease Inhibitor Protein**

Portions of this chapter were published as:

Johnson, R.J., McCoy, J.G., Bingman, C.A., Phillips, G.N., Raines, R.T. (2007) Inhibition of human pancreatic ribonuclease by the human ribonuclease inhibitor protein. *J. Mol. Biol.* **368**, 434–449. I performed all of the research described in this chapter, except the crystallography sections involving model fitting and refinement (JG McCoy, CA Bingman, and GN Phillips).

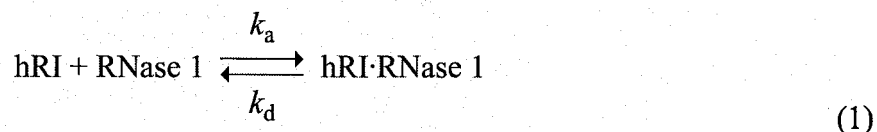
## 2.1 Abstract

The ribonuclease inhibitor protein (RI) binds to members of the bovine pancreatic ribonuclease (RNase A) superfamily with an affinity in the femtomolar range. Here, we report on structural and energetic aspects of the interaction between human RI (hRI) and human pancreatic ribonuclease (RNase 1). The structure of the crystalline hRI·RNase 1 complex was determined at a resolution of 1.95 Å, revealing the formation of 19 intermolecular hydrogen bonds involving 13 residues of RNase 1. In contrast, only 9 such hydrogen bonds are apparent in the structure of the complex between porcine RI and RNase A. hRI, which is anionic, also appears to use its horseshoe-shaped structure to engender long-range Coulombic interactions with RNase 1, which is cationic. In accordance with the structural data, the hRI·RNase 1 complex was found to be extremely stable ( $t_{1/2} = 81$  days;  $K_d = 2.9 \times 10^{-16}$  M). Site-directed mutagenesis experiments enabled the identification of two cationic residues in RNase 1—Arg39 and Arg91—that are especially important for both the formation and stability of the complex, and are thus termed “electrostatic targeting residues”. Disturbing the electrostatic attraction between hRI and RNase 1 yielded a variant of RNase 1 that maintained ribonucleolytic activity and conformational stability but had a  $2.8 \times 10^3$ -fold lower association rate for complex formation and  $5.9 \times 10^9$ -fold lower affinity for hRI. This variant of RNase 1, which exhibits the largest decrease in RI affinity of any engineered ribonuclease, is also toxic to human erythroleukemia cells. Together, these results provide new insight into an unusual and important protein–protein interaction, and could expedite the development of human ribonucleases as chemotherapeutic agents.

## 2.2 Introduction

The stability of a protein-protein complex is governed by intermolecular forces that mediate the rates at which the proteins associate and the complex dissociates. The rate of dissociation is affected largely by forces that act over short distances, including hydrophobic forces, hydrogen bonds, and van der Waals interactions. The rate of association, however, depends primarily on diffusion but can be increased by Coulombic forces (Shoup and Szabo 1982; Sharp et al. 1987; Getzoff et al. 1992; Schreiber and Fersht 1996; Selzer and Schreiber 1999; Selzer et al. 2000; Tang et al. 2006). Although a large energetic penalty is incurred upon desolvation of charged amino acids (Norel et al. 2001; Sheinerman and Honig 2002), the rate of association and, consequently, the stability of a complex can be increased by optimizing Coulombic interactions (Selzer and Schreiber 1999; Selzer et al. 2000; Lee and Tidor 2001).

The ribonuclease inhibitor protein forms a tight ( $K_d = k_d/k_a \approx 10^{-15}$  M) complex with multiple members of the bovine pancreatic ribonuclease (RNase A; EC 3.1.27.5) superfamily, as shown in equation (1) for the human inhibitor (hRI) and enzyme (RNase 1) (Lee et al. 1989b; Boix et al. 1996).



RI achieves its high affinity for ribonucleases through the burial of a large surface area (2908 Å<sup>2</sup> for the hRI-angiogenin complex (Papageorgiou et al. 1997)), along with one of

the largest known electrostatic energies of interaction ( $\Delta U = -12.3$  kcal/mol for the hRI-angiogenin complex (Shaul and Schreiber 2005)). Indeed, among 68 heterodimeric protein-protein complexes, the hRI-angiogenin complex ranked behind only the karyopherin  $\beta 2$ -Ran complex in the relative contribution of electrostatic energy to complex formation (Shaul and Schreiber 2005).

The evasion of RI by ribonucleases has medicinal implications, as variants of RNase A that evade RI are toxic to cancer cells (Leland and Raines 2001; Rutkoski et al. 2005). By using the structure of the complex between porcine RI (pRI) and RNase A (Kobe and Deisenhofer 1996), we designed variants of RNase A that are more toxic to human leukemic cells *in vitro* than is Onconase<sup>®</sup> (ONC), a naturally cytotoxic homologue from *Rana pipiens* that is now in Phase III clinical trials as a cancer chemotherapeutic agent (Rutkoski et al. 2005). Disruption of the pRI-RNase A interface was accomplished by designing RNase A variants with amino-acid substitutions that disturbed regions of high shape-complementarity (Rutkoski et al. 2005). These substitutions targeted short-range pRI-RNase A interactions by instilling steric hindrance or excising hydrogen bonds. We also applied this strategy to bovine seminal ribonuclease (BS-RNase, 87% sequence similarity), another homologue of RNase A that is dimeric in its native state (Kim et al. 1995b; Lee and Raines 2005). A BS-RNase variant with substitutions in the same high shape-complementarity regions was also more cytotoxic than ONC *in vitro* (Lee and Raines 2005).

Designing proteins that have diminished affinity for a cognate protein could be accomplished by targeting either component of the equilibrium dissociation constant:  $k_d$  or

$k_a$ . Previous studies of the RI-ribonuclease interface have focused on short-range intermolecular contacts between the proteins, thereby raising the dissociation rate (Leland et al. 1998; Lee and Raines 2005; Rutkoski et al. 2005). Diminishing the affinity of RNase 1, the human homologue of RNase A, by modulating short-range interactions has, however, proven to be difficult (Gaur et al. 2001; Leland et al. 2001; Bosch et al. 2004). Although RNase 1 and RNase A share 70% sequence identity, mutagenesis studies have indicated substantial variation in how each is recognized by RI (Gaur et al. 2001; Leland et al. 2001; Bosch et al. 2004). We sought to elaborate how RNase 1 is recognized by hRI.

Here, we report the atomic structure of the crystalline hRI-RNase 1 complex. We use this structure to design RNase 1 variants that reveal the contribution of specific residues to the affinity for hRI and to design a variant that has micromolar (rather than femtomolar) affinity for hRI. This variant is toxic to human erythroleukemia cells. Our findings cause us to reevaluate the stability of the wild-type hRI-RNase 1 complex, which we find to have a  $K_d$  value that is nearly  $10^3$ -fold lower than any reported previously. Overall, this work highlights the structural basis for intraspecies regulation of ribonucleolytic activity as well as facilitates the development of chemotherapeutic agents based on human ribonucleases.

## 2.3 Experimental Procedures

*Materials.* *Escherichia coli* strain BL21(DE3) was from Novagen (Madison, WI). 6-FAM-dArU(dA)<sub>2</sub>-6-TAMRA, a fluorogenic ribonuclease substrate, was from Integrated DNA Technologies (Coralville, IA). Enzymes were from Promega (Madison, WI). K-562 cells, which are an erythroleukemia cell line derived from a chronic myeloid leukemia

patient, were from the American Type Culture Collection (Manassas, VA). Cell culture medium and supplements were from Invitrogen (Carlsbad, CA). [*methyl*-<sup>3</sup>H]Thymidine (6.7 Ci/mmol) was from Perkin–Elmer (Boston, MA). Protein purification columns were from Amersham Biosciences (Piscataway, NJ). RNase A Type III-A was from Sigma–Aldrich (St. Louis, MO). Human angiogenin was prepared as described previously (Leland et al. 2002).

MES buffer (Sigma–Aldrich, St. Louis, MO) was purified by anion-exchange chromatography to remove trace amounts of oligomeric vinylsulfonic acid (Smith et al. 2003; Fuchs and Raines 2005). Costar 96-well NBS microtiter plates were from Corning Life Sciences (Acton, MA). Rhodamine 110 (sold as Rhodamine 560) was from Exciton (Dayton, OH). All other chemicals were of commercial grade or better, and were used without further purification.

Terrific Broth (TB) contained (in 1.00 L) tryptone (12 g), yeast extract (24 g), glycerol (4 mL), KH<sub>2</sub>PO<sub>4</sub> (2.31 g), and K<sub>2</sub>HPO<sub>4</sub> (12.54 g). Phosphate-buffered saline (PBS; pH 7.4) contained (in 1.00 L) NaCl (8.0 g), KCl (2.0 g), Na<sub>2</sub>HPO<sub>4</sub>·7H<sub>2</sub>O (1.15 g), KH<sub>2</sub>PO<sub>4</sub> (2.0 g), and NaN<sub>3</sub> (0.10 g).

*Instrumentation.* Matrix-assisted laser desorption/ionization time-of-flight (MALDI–TOF) mass spectrometry was performed with a Voyager-DE-PRO Biospectrometry Workstation (Applied Biosystems, Foster City, CA) at the Biophysics Instrumentation Facility. Fluorescence spectroscopy was performed with a QuantaMaster1 photon-counting fluorimeter equipped with sample stirring (Photon Technology International, South Brunswick, NJ). The fluorescence intensity in microtiter plates was recorded with a



Perkin–Elmer EnVison 2100 plate reader equipped with an FITC filter set (excitation at 485 nm with 14 nm bandwidth; emission at 535 nm with 25 nm bandwidth; dichroic mirror cutoff at 505 nm) in the W.M. Keck Center for Chemical Genomics. Thermal denaturation data were collected using a Cary 3 double-beam spectrophotometer equipped with a Cary temperature-controller (Varian, Palo Alto, CA). [*methyl*-<sup>3</sup>H]Thymidine incorporation into genomic DNA was quantified by liquid scintillation counting using a Microbeta TriLux liquid scintillation and luminescence counter (Perkin–Elmer, Wellesley, MA).

*RNase 1 Purification.* DNA encoding variants of RNase 1 was created by using plasmid pHP-RNase (Leland et al. 2001) and the Quikchange site-directed mutagenesis kit or Quikchange Multi site-directed mutagenesis kit (Stratagene, La Jolla, CA). RNase 1 and its variants were purified from inclusion bodies using the same oxidative folding procedure described previously (Leland et al. 2001). These proteins all lacked the C-terminal threonine residue (Thr128), which was absent from the initial report of the amino acid sequence (Beintema et al. 1984).

Variants of RNase 1 with a free cysteine residue at position 19 were initially protected by reaction with 5,5'-dithio-bis(2-nitrobenzoic acid) (DTNB) (Riddles et al. 1983; Lavis et al. 2006). Immediately before fluorophore attachment, TNB-protected variants were deprotected using a three-fold molar excess of dithiothreitol (DTT) and desalted by chromatography using a PD-10 desalting column (Amersham Biosciences, Piscataway, NJ). Deprotected RNase 1 variants were reacted for 4–6 h at 25 °C with a ten-fold molar excess of 5-iodoacetamido fluorescein (Sigma–Aldrich, St. Louis, MO). Fluorescein-labeled RNase 1 variants were purified by chromatography using a HiTrap SP FF column. The

molecular mass of RNase 1, its variants, and conjugates was confirmed by MALDI-TOF mass spectrometry.

*hRI Purification.* hRI was purified by procedures similar to those described previously (Klink et al. 2001; Lee and Raines 2005; Rutkoski et al. 2005). Briefly, a plasmid (Lee and Raines 2005; Rutkoski et al. 2005) that directs the expression of hRI was transformed into *E. coli* BL21(DE3) cells, and a single colony was used to inoculate LB medium (25 mL) containing ampicillin (150 µg/mL). A starter culture was grown for 16 h at 37 °C and 250 rpm and was used to inoculate cultures of TB medium (1.00 L) containing ampicillin (200 µg/mL). These cultures were grown at 37 °C and 225 rpm until  $OD_{600} \geq 3.0$ . Expression of the hRI cDNA was induced by adding IPTG (0.5 mM) and growing for 16 h at 18 °C and 225 rpm. Bacteria were collected by centrifugation (12,000g for 10 min) and resuspended in 30 mL of 50 mM Tris-HCl buffer, pH 7.5, containing EDTA (10 mM) and DTT (10 mM). Bacteria were lysed by two passes through a French pressure cell, and the cellular debris was removed by ultracentrifugation. RNase A was attached covalently to the resin in two 5-mL HiTrap NHS-ester columns, following the manufacturer's protocol. The supernatant from the ultracentrifuge tubes was loaded onto the RNase A-affinity resin. hRI was eluted in 100 mM sodium acetate-NaOH buffer, pH 6.0, containing NaCl (3.0 M), DTT (5 mM), and EDTA (1 mM), after extensive washing with 50 mM sodium phosphate-NaOH buffer, pH 6.4, containing NaCl (1.0 M), DTT (5 mM), and EDTA (1 mM). The peak eluted from the RNase A-affinity resin was dialyzed for 16 h against 4 L of 20 mM Tris-HCl buffer, pH 7.5, containing DTT (10 mM) and EDTA (1 mM) and purified further by cation-exchange chromatography using a HiTrap Q column (Klink et al.

2001). The purity of the eluted hRI was shown to be >99% by SDS–PAGE (data not shown).

*hRI·RNase 1 Complex Purification.* Purified RNase 1 (50 mg/mL) and hRI (10 mg/mL) were mixed at a 1.2:1.0 molar ratio, and this solution was incubated at 25 °C for 60 min to allow for complex formation. The solution was then loaded onto a 5-mL HiTrap Q column that was pre-equilibrated with 20 mM Hepes–NaOH buffer, pH 7.5, containing DTT (10 mM) and glycerol (2% v/v). The complex was eluted with a linear gradient of NaCl (0–0.4 M) over 30 column volumes. Free RNase 1 eluted with the flowthrough, and the hRI·RNase 1 complex eluted around 0.15 M NaCl. Purified complex was dialyzed for 16 h at 4 °C against 20 mM Hepes–NaOH buffer, pH 7.5, containing DTT (10 mM) and glycerol (2% v/v). Purified complex was concentrated to a final concentration of 10 mg/mL in a Vivaspin 20 mL centrifugal concentrator (Vivascience AG, Hannover, Germany). Aliquots were flash frozen and stored at –80 °C.

*Crystallization.* Crystals of the hRI·RNase 1 complex were obtained by hanging-drop vapor diffusion in 20 mM sodium citrate–HCl buffer, pH 4.2, containing methyl ether PEG 2000 (10% w/v), ammonium sulfate (1 mM), and DTT (25 mM) with the hanging-drop solution containing a mixture of purified hRI·RNase 1 complex (0.9 µL) and crystallization solution (5.1 µL), which was composed of the citrate buffer described above. Diffraction-quality crystals grew within a week at 25 °C. Protein crystals were soaked in reservoir solutions containing increasing amounts of ethylene glycol up to 25% (v/v), and were flash-cooled in a stream of cryogenic N<sub>2</sub>(g).

*Structure Determination.* Diffraction data were collected at SER-CAT Sector 22 at Argonne National Laboratories. The crystal was maintained at 100 K during data collection, and X-rays were tuned to a wavelength of 0.99997 Å. The diffraction images were integrated and scaled using HKL2000 (Otwinowski and Minor 1997). The initial phases were determined through molecular replacement using MOLREP from the CCP4 suite (Bailey 1994; Vagin and Teplyakov 1997) with PDB entry 1DFJ (Kobe and Deisenhofer 1995) as the starting model. Arp-Warp software (Blanc et al. 2004) was used to build the initial model, which was then completed by alternating cycles of model building and refinement using the programs Xfit (McRee 1999) and REFMAC (Murshudov et al. 1997), respectively (Table 2.1). The coordinates have been deposited in the PDB with accession code 1Z7X. To enable a more precise comparison, the structure of the pRI·RNase A complex was refined using ten rounds of refinement in REFMAC with the same parameters ( $R_{\text{cryst}} = 21.4$ ;  $R_{\text{free}} = 28.1$ ). Reflections used for the refinement were from PDB entry 1DFJ (Kobe and Deisenhofer 1995), and 5% of the reflections were chosen randomly to define as  $R_{\text{free}}$ . Both the structure of the hRI·RNase 1 complex and the refined structure of the pRI·RNase A complex were analyzed with the program PDBsum (Laskowski et al. 2005) to identify intermolecular hydrogen bonds and van der Waals contacts. PDBsum uses the algorithm HBPLUS to identify hydrogen bonds ( $r_{\text{X}\cdots\text{X}} < 3.35$  Å) (McDonald and Thornton 1994).

*Ribonucleolytic Activity.* The ribonucleolytic activity of RNase 1 and its variants was determined by quantitating their ability to cleave 6-FAM–dArU(dA)<sub>2</sub>–6-TAMRA, cleavage of this substrate at the uridine ribonucleotide leads to a 180-fold increase in

fluorescence (Kelemen et al. 1999). Assays were carried out at 23 ( $\pm 2$ ) °C in 2 mL of 0.10 M Mes–NaOH buffer, pH 6.0, containing NaCl (0.10 M). Fluorescence data were fitted to equation (2), wherein  $\Delta I / \Delta t$  represents the initial reaction velocity,  $I_0$  is the fluorescence intensity before the addition of a ribonuclease,  $I_f$  corresponds to the final fluorescence intensity after complete substrate hydrolysis, and  $[E]$  is the total ribonuclease concentration.

$$\frac{k_{\text{cat}}}{K_M} = \frac{\Delta I / \Delta t}{(I_f - I_0)[E]} \quad (2)$$

*Conformational Stability.* The conformational stability was determined by following the change in UV absorbance of a solution of ribonuclease at 287 nm with increasing temperature (Klink and Raines 2000). The temperature of PBS containing a ribonuclease (0.1–0.2 mg/mL) was raised from 20 to 80 °C at 0.15 °C/min. The  $A_{287}$  was followed at 1-°C intervals, and the absorbance was fitted to a two-state model of denaturation, in which the temperature at the midpoint of the transition curve corresponds to the value of  $T_m$ .

*RI-evasion.* The affinity of hRI for variants of RNase 1 was determined by using a competition assay reported previously (Abel et al. 2002). Briefly, 2.0 mL of PBS containing DTT (5 mM), fluorescein-labeled G88R RNase A (50 nM), and an unlabeled RNase 1 variant was incubated at 23 ( $\pm 2$ ) °C for 20 min. The initial fluorescence intensity of the unbound fluorescein-labeled G88R RNase A was monitored for 3 min (excitation: 491 nm; emission: 511 nm). hRI was then added to 50 nM and the final fluorescence intensity was measured. Values for  $K_d$  were obtained by nonlinear least-squares analysis of the binding isotherm using the program DELTAGRAPH 5.5 (Red Rock Software, Salt

Lake City, UT). The  $K_d$  value for the complex of hRI and fluorescein-labeled G88R RNase A was assumed to be 1.4 nM (Rutkoski et al. 2005).

*Dissociation Rate.* The dissociation rate constant for the complex between hRI and variants of RNase 1 was determined by a procedure similar to that described previously (Abel et al. 2002). Briefly, equimolar concentrations of hRI and a fluorescein-labeled RNase 1 variant were allowed to reach equilibrium in PBS containing DTT (5 mM). The equimolar concentrations were 20-fold greater than the  $K_d$  value previously determined for each hRI-RNase 1 complex. After equilibrium was reached, wild-type RNase A (100-fold molar excess) was added to the reaction to scavenge free hRI. The increase in fluorescence upon irreversible complex disassociation was followed by fluorescence spectroscopy (excitation: 491 nm; emission: 511 nm). To calculate the value of  $k_d$ , the fluorescence data were fitted to equation (3), wherein  $F_0$  is the fluorescence before the addition of wild-type RNase A and  $F_\infty$  is the fluorescence after complete dissociation of the complex.

$$F = F_0 + (F_\infty - F_0)(1 - e^{-k_d t}) \quad (3)$$

The dissociation rate of the complex between hRI and wild-type RNase 1 was determined using a procedure similar to above except that the experiment was performed using a 96-well microtiter-plate format (L.D. Lavis, T.J. Rutkoski, and R.T. Raines, unpublished results). Briefly, diethylfluorescein-labeled RNase 1 (100 nM) in PBS containing tris(2-carboxyethyl)phosphine (TCEP; 100 $\mu$ M) was added to a 96-well microtiter plate and the initial fluorescence was measured. hRI was then added at

equimolar concentrations and incubated with labeled RNase 1 at 25 °C for 5 min. A 50-fold molar excess of human angiogenin (5  $\mu$ M) was added to scavenge dissociated complex and the change in fluorescence was measured at various time points. To insure that the protein stability was maintained over the duration of the experiment, additional data points were monitored under the same conditions only without the addition of the 50-fold molar excess of angiogenin. Also, to account for drift in the instrument, data are the mean ( $\pm$  SE) from six solutions normalized for the fluorescence of four solutions of rhodamine 110 (10 nM). Fluorescence data were fitted to equation (3) to determine the dissociation rate constant. Initial fluorescence data (<4 h) were not included in the analysis, as these values showed a rapid burst in fluorescence similar to that observed in previous dissociation rate determinations (Lee et al. 1989b).

*Cytotoxicity.* The effect of RNase 1 and its variants on the proliferation of K-562 cells was assayed as described previously (Leland et al. 2001; Haigis et al. 2002b; Rutkoski et al. 2005). Briefly, after a 44-h incubation with ribonuclease, K-562 cells were treated with [*methyl*- $^3$ H]thymidine for 4-h and the incorporation of radioactive thymidine into the cellular DNA was quantified by liquid scintillation counting. Results are shown as the percentage of [*methyl*- $^3$ H]thymidine incorporated into the DNA as compared to the incorporation into control K-562 cells where only PBS was added. Data are the average of three measurements for each concentration, and the entire experiment was repeated in triplicate. Values for IC<sub>50</sub> were calculated by fitting the curves using nonlinear regression to equation (4), wherein  $y$  is the total DNA synthesis following the [*methyl*- $^3$ H]thymidine pulse, and  $h$  is the slope of the curve.

$$y = \frac{100\%}{1 + 10^{(\log(IC_{50}) - \log[\text{ribonuclease}])h}} \quad (4)$$

## 2.3 Results

*Important Interactions Between hRI and RNase 1.* The three-dimensional crystal structure of the hRI·RNase 1 complex was refined to an  $R_{\text{cryst}}$  value of 0.175 ( $R_{\text{free}} = 0.236$ ) at a resolution of 1.95 Å (Table 2.1). The asymmetric unit of the crystal of the hRI·RNase 1 complex resembles that of the hRI·angiogenin complex in its containing two molecular complexes (Figure 2.1) (Papageorgiou et al. 1997). The two complexes are held together by 24 residue-to-residue hydrogen bonds formed between the N-terminal β-strand of the two hRI molecules. This dimerization of the hRI molecules buries an additional 1700 Å<sup>2</sup> of surface area.

In chain X of RNase 1 (Figure 2.2a), a bound citrate molecule forms hydrogen bonds to all three of the key catalytic residues in the enzymic active site (His12, Lys41, and His119). The bound citrate perturbs the substrate binding cleft of RNase 1, causing Arg10 and Lys66 to undergo conformational changes. To exclude the effect of citrate, the complex between chain Z of RNase 1 (without citrate bound) and chain Y of hRI will serve herein for comparisons to the structure of the pRI·RNase A complex (Kobe and Deisenhofer 1995).

The root-mean-square deviation (rmsd) between the alpha carbons of hRI·RNase 1 and pRI·RNase A is 2.8 Å (Kobe and Deisenhofer 1995). Much of the deviation between the



complexes originates from the structural variation between hRI and pRI (rmsd = 1.6 Å) because pRI, unlike hRI, was observed to undergo a conformational change upon ribonuclease binding. The alpha carbons of RNase 1 and RNase A have less deviation (rmsd = 0.6 Å). In contrast, angiogenin and eosinophil-derived neurotoxin (EDN), the other human ribonucleases that have been co-crystallized with hRI, have rmsd values of 7.4 and 6.3 Å from RNase 1, respectively (Papageorgiou et al. 1997; Iyer et al. 2005), underscoring the similarity between RNase 1 and RNase A.

The conservation of contact residues between the hRI-RNase 1 and pRI-RNase A complexes is shown in Figure 2.2a. The location of hRI-contact residues on the substrate-binding face of RNase 1 is shown in Figure 2.2b. The manner in which RI recognizes RNase 1 and RNase A is similar. This similarity is evident from the superposition of the  $\beta 4$ – $\beta 5$  loop of RNase 1 and RNase A in the two complexes, as shown in Figure 2.3. Moreover, the total number of RI-contact residues (23) is conserved in RNase 1 and RNase A (Kobe and Deisenhofer 1995). In RNase 1, however, 13 residues form 19 hydrogen bonds with hRI, whereas 9 residues in RNase A form 11 hydrogen bonds with pRI (Table 2.2). Overall, the 19 hydrogen bonds observed between hRI and RNase 1 are shorter than the analogous ones between pRI and RNase A (Table 2.2). Likewise, 375 Å<sup>2</sup> more surface area is buried in the hRI-RNase 1 complex (2800 Å<sup>2</sup> *versus* 2425 Å<sup>2</sup>), indicative of a more intimate complex.

Previous studies on the interaction of RNase A and BS-RNase with RI focused on three structural regions that are remote from the active site: residues 38/39, residue 67, and residues in the  $\beta 4$ – $\beta 5$  loop (Lee and Raines 2005; Rutkoski et al. 2005). The hydrogen

bonding network and electron density of these regions in the hRI·RNase 1 complex are depicted in Figures 3 and 4. Based on this information, two variants of RNase 1 were designed in which residues were replaced in all three of these regions. One variant (G38R/R39G/N67R/N88R RNase 1) mimics the most cytotoxic of known RNase A variants (D38R/R39D/N67R/G88R RNase A) by swapping the amino acids in positions 38/39 and installing arginine residues at positions 67 and 88. The other RNase 1 variant (R39D/N67D/N88A/G89D/R91D RNase 1) is focused on the same regions, but instead uses Coulombic repulsion to suppress the binding of RI.

*Ribonucleolytic Activity.* The ability of a ribonuclease to cleave RNA in the presence of RI correlates closely with its cytotoxicity *in vitro* (Bretscher et al. 2000). For a ribonuclease variant to achieve its full cytotoxic potential, an amino-acid substitution that decreases RI binding must not be detrimental to catalytic activity (Dickson et al. 2003). Consequently, variants of RNase 1 were assayed for their catalytic activity toward a tetranucleotide substrate in buffer that lacks oligo(vinylsulfonic acid), a potent inhibitor of ribonucleolytic activity (Kelemen et al. 1999; Smith et al. 2003). Values of  $k_{\text{cat}}/K_{\text{M}}$  for RNase A, RNase 1, and their variants are given in Table 2.3. The  $k_{\text{cat}}/K_{\text{M}}$  value for wild-type RNase 1 is 10-fold higher than that reported previously (Leland et al. 2001). A similar increase in the catalytic activity was observed for RNase A when contaminating oligo(vinylsulfonic acid) was removed from the reaction buffer (Smith et al. 2003). The  $k_{\text{cat}}/K_{\text{M}}$  values for the RNase 1 variants are within 6-fold of that for the wild-type enzyme.

*Conformational Stability.* The conformational stability of a ribonuclease is linked to its susceptibility to proteolysis and, consequently, its cytotoxicity (Klink and Raines 2000).

The  $T_m$  values for all RNase 1 variants are shown in Table 2.3. The  $T_m$  value of wild-type RNase 1 is close to that reported previously (Leland et al. 2001). In agreement with previous studies, incorporation of charged patches on the surface of RNase 1 does not reduce the  $T_m$  value by more than 6 °C (Selzer et al. 2000). Neither arginine nor aspartate substitutions at residues 38/39, residue 67, or residues in the  $\beta 4$ – $\beta 5$  loop disturb the conformational stability significantly, as G38R/R39G/N67R/N88R RNase 1 and R39D/N67D/N88A/G89D/R91D RNase 1 have  $T_m$  values comparable to that of wild-type RNase 1 (61 and 58 °C, respectively). Thus, all of the variants have high conformational stability at physiological temperature.

*Evasion of Ribonuclease Inhibitor.* RI binds multiple members of the RNase A superfamily with equilibrium dissociation constants in the femtomolar range (Lee et al. 1989b), forming one of the tightest known noncovalent interactions among biomolecules. Replacing residues 38, 39, 67, and 88 in RNase A (D38R/R39D/N67R/G88R RNase A) increased the equilibrium dissociation constant of the hRI-RNase A complex by seven orders of magnitude (Table 2.3) (Rutkoski et al. 2005). In marked contrast, the analogous variant in RNase 1 (G38R/R39G/N67R/N88R RNase 1) had an affinity for RI near that reported previously for wild-type RNase 1 (Table 2.3) (Boix et al. 1996; Suzuki et al. 1999; Gaur et al. 2001).

This surprising observation led us to reinvestigate the affinity of wild-type RNase 1 for hRI. Previously, the stability of the hRI-RNase 1 complex had been determined by measuring the inhibition of catalytic activity. The  $K_i$  values ( $2 \times 10^{-11}$ ,  $5.2 \times 10^{-12}$ , or  $2 \times 10^{-13}$  M (Boix et al. 1996; Suzuki et al. 1999; Gaur et al. 2001)) obtained by this method

are lower than the concentration of wild-type RNase 1 used in the experiment itself. Accordingly, these values can only be an upper limit to the true  $K_d$  value (Stone and Hofsteenge 1986; Leland et al. 2001).

We determined the dissociation rate of the hRI·RNase 1 complex by monitoring the release of fluorescently-labeled RNase 1 over time (Figure 2.5). We found that the hRI·RNase 1 complex (Table 2.4) has a half-life ( $t_{1/2} = \ln 2/k_d$ ) of 81 days, which puts its value of  $k_d$  closer to that of the hRI-angiogenin complex ( $t_{1/2} = 62$  days) than that of the hRI·RNase A complex ( $t_{1/2} = 13$  h) (Lee et al. 1989b). To calculate the value of  $K_d$  of the hRI·RNase 1 complex, the value of  $k_a$  was assumed to be similar to that for the association of hRI with angiogenin or RNase A. These  $k_a$  values are within twofold of each other, and are close to the diffusion limit (Stone and Hofsteenge 1986; Lee et al. 1989b). The  $k_a$  value of RNase A was assumed herein for wild-type RNase 1 due to the similarity of the sequence and structure of RNase A with those of RNase 1. Using  $k_a = 3.4 \times 10^8 \text{ M}^{-1}\text{s}^{-1}$  (Lee et al. 1989b), the value of  $K_d (= k_d/k_a)$  for the hRI·RNase 1 complex was then calculated to be  $2.9 \times 10^{-16} \text{ M}$ , which is at least 690-fold lower than any reported previously for the hRI·RNase 1 complex (Boix et al. 1996; Suzuki et al. 1999; Gaur et al. 2001), 150-fold lower than that for the hRI·RNase A complex and comparable to that of the hRI-angiogenin complex ( $7.1 \times 10^{-16} \text{ M}$ ) (Lee et al. 1989b).

Designing a variant to overcome the extraordinary stability of the hRI·RNase 1 complex required a new strategy. Instead of inserting sterically bulky residues at the complementarity regions, multiple aspartate residues and one alanine residue were substituted in the same regions. The value of  $K_d = 1.7 \text{ }\mu\text{M}$  for the resulting variant,

R39D/N67D/N88A/G89D/R91D RNase 1, is close to the highest measured for any RNase A variant ( $2.9 \mu\text{M}$ ) (Cho et al. 2005; Rutkoski et al. 2005), despite the high stability of the wild-type complex. These substitutions reduced the affinity of hRI for RNase 1 by  $5 \times 10^9$ -fold, which is the greatest evasion yet reported for a mammalian ribonuclease. When the aspartate substitutions in R39D/N67D/N88A/G89D/R91D RNase 1 are replaced with an isologous amino acid, leucine (R39L/N67L/N88A/G89L/R91L RNase 1), the variant loses 50-fold in RI evasion.

The influence of electrostatics on the binding of hRI to RNase 1 variants was analyzed by determining the value of  $k_d$  for the complexes formed by hRI and these two RNase 1 variants (Table 2.4). The value of  $k_d$  increases by  $9 \times 10^5$ -fold upon substitution of R39L/N67L/N88A/G89L/R91L. Yet, the value of  $k_d$  increases by only twofold upon aspartate substitution (R39D/N67D/N88A/G89D/R91D RNase 1). The values of  $k_a$  for these two variants were calculated by using values of  $K_d$  from Table 2.3, values of  $k_d$  from Table 2.4, and equation (1). The association rate constant is affected more substantially by both leucine substitution (110-fold decrease) and aspartate substitutions (25-fold decrease). The substantial change in the value of  $k_a$  with both leucine and aspartate substitution demonstrates a contribution gained by both the loss of attractive forces (leucine substitution) and gain of repulsive forces (aspartate substitution). Overall, the  $5 \times 10^9$ -fold decrease in binding affinity of hRI for R39D/N67D/N88A/G89D/R91D RNase 1 contains significant contributions from both an increase in the value of  $k_d$  ( $2.2 \times 10^6$ -fold) and a decrease in that of  $k_a$  ( $2.7 \times 10^3$ -fold).

The impact of individual substitutions in R39D/N67D/N88A/G89D/R91D RNase 1 to its overall binding constant for hRI was elucidated by the reversion of each substitution in R39D/N67D/N88A/G89D/R91D RNase 1 to the residue in the wild-type enzyme. In this analysis, single substitutions with little impact on RI affinity had small values of  $\Delta\Delta G$  (Table 2.3). The energetic contributions of the substitutions increased in the order: N88A < G89D < N67D < R39D < R91D. In this analysis, installing an aspartate residue at position 91 contributed 2.7 kcal/mol to evasion, whereas an alanine residue at position 88 contributed only 0.3 kcal/mol.

*Molecular charge.* The cytotoxicity of a ribonuclease is modulated by its molecular charge (Futami et al. 2001; Lee and Raines 2005; Rutkoski et al. 2005; Notomista et al. 2006). This interplay is apparent in the data shown in Figure 2.6 and listed in Table 2.3. D38R/R39D/N67R/G88R RNase A ( $Z = +6$ ) and R39D/N67D/N88A/G89D/R91D RNase 1 ( $Z = 0$ ) have similar conformational stability, ribonucleolytic activity, and affinity for RI, but their  $IC_{50}$  values for K-562 cells differ by 87-fold (Table 2.3). R39D/N67D/N88A/G89D/R91D RNase 1 has an  $IC_{50}$  of only 13.3  $\mu M$ , making it more toxic than wild-type RNase 1, but twofold less toxic than G88R RNase A (Leland et al. 1998).

The  $IC_{50}$  values for all of the other variants of RNase 1 listed in Table 2.3 fall outside the measurable range of the assay ( $IC_{50} > 25 \mu M$ ). R39L/N67L/N88A/G89L/R91L RNase 1 and N67D/N88A/G89D/R91D RNase 1 killed approximately 60% of the K-562 cells at 25  $\mu M$  (Figure 2.6b), indicative of  $IC_{50}$  values only slightly above 25  $\mu M$ . The lack of cytotoxicity for RNase 1 variants other than R39D/N67D/N88A/G89D/R91D RNase 1

is likely due to an increased affinity for RI when compared to R39D/N67D/N88A/G89D/R91D RNase 1 (Table 2.3).

## 2.4 Discussion

Ribonuclease inhibitor is a 50-kDa resident of the cytosol that comprises 0.1% of all cellular proteins (Haigis et al. 2003; Dickson et al. 2005). RI serves as a sentry for rogue ribonucleases and through its horseshoe-shaped binding surface, inhibits the ribonucleolytic activity of members of the RNase A superfamily (Kobe and Deisenhofer 1995; Papageorgiou et al. 1997; Iyer et al. 2005). RI manifests this control despite the low sequence identity between RNase A family members (Beintema 1987), which are evolving rapidly (Rosenberg et al. 1995). The structural basis for the interaction of RI with four RNase A family members (RNase 1, RNase A, angiogenin, and EDN) has been determined by Deisenhofer, Acharya, and their coworkers (Kobe and Deisenhofer 1995; Papageorgiou et al. 1997; Iyer et al. 2005). A thorough comparison of the recognition by RI of structurally diverse ribonucleases (angiogenin and EDN) has been reported previously (Iyer et al. 2005). Here, we focus on recognition of RNase 1 and RNase A, two ribonucleases with high sequence identity.

*Recognition of RNase 1 by RI.* The fast atomic density evaluator (FADE) algorithm revealed regions of high shape-complementarity in the pRI-RNase A complex (Mitchell et al. 2001; Rutkoski et al. 2005). By inserting disruptive substitutions in those regions, D38R/R39D/N67R/G88R RNase A ( $K_d = 510$  nM) (Rutkoski et al. 2005) and C31A/C32A/G38R/K39D/G88R BS-RNase ( $K_d = 110$  nM) (Lee and Raines 2005) were

developed, and each was found to have significantly decreased affinity for hRI. Using the same reasoning, we designed G38R/R39G/N67R/N88R RNase 1 (Table 2.3). This variant of RNase 1, however, retained subnanomolar affinity for hRI and was not cytotoxic to K-562 cells (Figure 2.6). Consequently, we sought to reveal the distinguishing aspects of the recognition of RNase 1 and RNase A by hRI.

Hydrogen bonds play an important role in the stability of protein-protein complexes, as well as the conformational stability of individual proteins (Jeffrey and Saenger 1991; Pace et al. 1996; Pace 2001; Rose et al. 2006). Hydrogen bonds between functional groups of opposite charge (*i.e.*, salt bridges) are especially strong (Fersht et al. 1985). Overall, the hRI·RNase 1 complex has both more intermolecular hydrogen bonds than does the pRI·RNase A complex and more between residues of opposite charge (Table 2.2). Moreover, those hydrogen bonds that are conserved are shorter in the hRI·RNase 1 complex. The hRI·RNase 1 complex also buries an additional 375 Å<sup>2</sup> of surface area, which could also enhance its stability (Vallone et al. 1998; Pace 2001; Parsegian 2006). In line with the more intimate complex formed by hRI and RNase 1, RNase 1 dissociates from hRI 150-fold more slowly than does RNase A from hRI (Figure 2.5; Table 2.3) (Lee et al. 1989b). The slower dissociation rate ( $t_{1/2}$  = 81 days) for the hRI·RNase 1 complex is in the range of that for the hRI-angiogenin complex ( $t_{1/2}$  = 62 days) (Lee et al. 1989b). Accordingly, hRI seems to have coevolved with human ribonucleases in a manner that would enable hRI to abrogate more effectively any lethal ribonucleolytic activity. The greater stability of the hRI·RNase 1 complex also explains why the design of RI-evasive



RNase 1 variants has been more difficult than the design of RI-evasive RNase A variants (Gaur et al. 2001; Leland et al. 2001; Bosch et al. 2004).

To characterize differential binding within the hRI·RNase 1 and pRI·RNase A complexes, we investigated the energetic contribution of the residues in RNase 1 that are analogous to the residues in high shape-complementarity regions of RNase A (Rutkoski et al. 2005). These residues are Arg39, Asn67, and residues in the  $\beta 4$ – $\beta 5$  loop.

*Residue 39.* Arg39 of RNase A had the highest shape complementarity score of any RNase A residue in the pRI·RNase A complex (Rutkoski et al. 2005) and was proposed to be a secondary anchor residue (Rajamani et al. 2004). When Arg39 was replaced with an aspartate residue in G88R RNase A to create R39D/G88R RNase A, the R39D substitution instilled 725-fold lower RI affinity. In RNase 1, Arg39 interacts even more extensively with hRI, forming 2 hydrogen bonds that are absent in the pRI·RNase A complex (Figure 2.4a). Specifically, Arg39 of RNase 1 makes a bidentate hydrogen bond with the side chain of Glu401 and a main-chain hydrogen bond with the main chain of Tyr434. Consequently, the energetic consequence of the R39D substitution ( $\Delta\Delta G = 2.1$  kcal/mol; Table 2.3) is the second highest among the residues studied herein.

*Residue 67.* Interactions with Asn67 had been exploited previously to develop RI variants that bind to angiogenin but not to RNase 1 or RNase A. Incorporating a tryptophan at positions 408 and 410 hindered the interaction of hRI with Asn67 of RNase 1 and RNase A, yielding a variant of hRI that bound only to angiogenin (Kumar et al. 2004). Asn67 had been proposed to be a primary anchor residue in the pRI–RNase A interface, due to its burial of surface area and its lack of molecular motion (Rajamani et al. 2004).

Asn67 in RNase 1 forms a main-chain hydrogen bond to Tyr437 (Table 2.2) and is in van der Waals contact with Leu409 and Gly410 of hRI. We find, however, that replacing Asn67 to hinder interaction with residues 408–410 in hRI does not produce a large effect on binding, as an aspartate residue at position 67 only destabilizes the complex by  $\Delta\Delta G = 1.9$  kcal/mol (Table 2.3). Hence, Arg39 and Arg91 provide more energetic stabilization than does Asn67 to the hRI·RNase 1 complex.

*$\beta 4$ – $\beta 5$  loop.* Replacing Gly88 with an arginine residue in the  $\beta 4$ – $\beta 5$  loop of RNase A had been found previously to decrease the affinity of pRI for RNase A by  $10^4$ -fold (Leland et al. 1998) and the affinity of BS-RNase for hRI by 250-fold (Leland et al. 1998; Lee and Raines 2005). In the crystalline hRI·RNase 1 complex, the  $\beta 4$ – $\beta 5$  loop adopts a similar conformation to that of RNase A in the pRI·RNase A complex (Figure 2.3). One major difference is with residue 88, as Asn88 of RNase 1 forms a hydrogen bond with Glu264 instead of residing in the pocket formed by Trp261 and Trp263. (The numbering of RI residues herein refers to their position in hRI, which has four more N-terminal residues than does pRI.) Asn88 in RNase 1 is located on the outer surface of the hRI–RNase 1 interface. This location seems to be able to accommodate the bulk of an arginine residue (Gaur et al. 2001) (or even a carbohydrate chain (Ribó et al. 1994)) while maintaining high affinity for RI.

Gly89 of RNase 1 has been proposed to constitute the structural analogue of Gly88 in RNase A (Leland et al. 1998; Gaur et al. 2001; Bosch et al. 2004). Yet, replacing Gly89 with arginine in RNase 1 does not yield a cytotoxic variant (Gaur et al. 2001; Bosch et al. 2004). Gly89 in RNase 1 overlays more closely with Ser89 in RNase A (Figure 2.3), but

Gly89 is unable to form a hydrogen bond with Glu206, as does Ser89 in RNase A (Kobe and Deisenhofer 1995). Gly89 in RNase 1 is within van der Waals distance of Trp261 and Trp263 in hRI·RNase 1, but due to the increased stability of the hRI·RNase 1 complex, a single G89R substitution does not lower the affinity enough to make this variant cytotoxic (Gaur et al. 2001).

Among the five residues investigated, Arg91 had the greatest influence on the stability of the hRI·RNase 1 complex ( $\Delta\Delta G = 2.7$  kcal/mol, Table 2.3). Arg91 makes contact with hRI in the concave anionic surface of hRI (Figure 2.7), forming two hydrogen bonds with Glu287. Lys91 has been proposed to play a secondary role in anchoring RNase A to pRI (Rajamani et al. 2004), but Arg91 of RNase 1 could serve as a primary targeting residue in binding to hRI. Replacing Arg91 with an aspartate residue severs the hydrogen bonds formed with Glu287 of hRI, and replaces a favorable Coulombic interaction with an unfavorable one.

*Energetics of RI-evasion.* Charged amino acids comprise 19% of all exposed amino acids on a protein surface (Miller et al. 1987). (Sheinerman and Honig 2002) Fewer charged residues are exposed, however, in the average protein–protein interface. Charge–charge interactions in protein–protein interfaces are disfavored by the large energetic penalty incurred by desolvation of the exposed charge upon binding (Norel et al. 2001; Sheinerman and Honig 2002). The energetic penalty of desolvation can be circumvented by leaving key charged residues partially exposed to solvent upon complex formation (Sheinerman and Honig 2002). In Figure 2.4, the electron density for multiple solvent molecules is visible surrounding favorable Coulombic interactions between hRI and

RNase 1. This residual exposure to solvent diminishes the energetic desolvation penalty and allows electrostatics to remain a driving force to complex formation.

The cationicity of the RNase 1 surface (Figure 2.7) facilitates the binding of its anionic substrates (Park and Raines 2003). RI exploits this cationicity to inhibit RNase 1 rapidly and strongly using long-range Coulombic interactions (Shaul and Schreiber 2005). In a theoretical study of 14 enzyme-inhibitor complexes, all were found to suffer a net destabilization by electrostatic interactions, due to the energetic penalty of breaking hydrogen bonds to water in the unbound state (Norel et al. 2001). RI-ribonuclease complexes are, however, atypical (Shaul and Schreiber 2005). The hRI-angiogenin complex has  $\Delta U = -12.3$  kcal/mol and a calculated rate increase due to electrostatics of  $10^6$   $\text{M}^{-1}\text{s}^{-1}$  (Shaul and Schreiber 2005). Figure 2.7 highlights the distribution of positive and negative charges on hRI and RNase 1. In these highly charged proteins, the favorable electrostatic interaction of key solvent-exposed charged residues like Arg39 and Arg91 of RNase 1 appear to drive complex formation (Figures 4 and 7).

Arg39 and Arg91 contribute more free energy to complex formation than do Asn67, Asn88, or Gly89 (Table 2.3). Because Arg39 and Arg91 are the only charged residues changed in R39L/N67L/N88A/G89L/R91L RNase 1 and electrostatics determine the association rate (Selzer and Schreiber 1999; Selzer et al. 2000), data with R39L/N67L/N88A/G89L/R91L RNase 1 can be used to estimate the influence of Arg39 and Arg91 on the association rate. Replacing Arg39 and Arg91 with leucine residues to give R39L/N67L/N88A/G89L/R91L RNase 1 decreases the association rate by 110-fold (Table 2.4). Hence, Arg39 and Arg91 serve a special role in the hRI-RNase 1 complex, one

that we define as “electrostatic targeting residues”. A residue that directs the formation of a protein–protein complex could also provide the major energetic force to maintain a stable complex. Arg39 and Arg91 fit these criteria, as they strongly affect the association rate of the complex (Table 2.4). Then, Arg39 and Arg91 keep RNase 1 bound to hRI through multiple hydrogen bonds with anionic residues (Figure 2.4), allowing other contacts in the complex to form.

*Rates of Association and Dissociation.* Electrostatics can guide the formation of protein–protein complexes through space and can increase the rate of association beyond that of diffusion alone (Selzer and Schreiber 1999; Selzer et al. 2000; Tang et al. 2006). We measured the association and dissociation rates for two of the RNase 1 variants listed in Table 2.3, thereby dissecting equation (1) into its component parts (Shaul and Schreiber 2005). Changes in the values of both  $k_d$  ( $2.2 \times 10^6$ -fold increase) and  $k_a$  ( $2.8 \times 10^3$ -fold decrease) make a substantial contribution to the ability of R39D/N67D/N88A/G89D/R91D RNase 1 to evade hRI (Table 2.4). The effect of the electrostatic forces that originate from charged residues 39, 67, 89, and 91 in this aspartate variant can be discerned with a comparison to the isologous leucine variant, R39L/N67L/N88A/G89L/R91L RNase 1. The decrease to the value of  $k_a$  upon leucine substitution (110-fold from the loss of attractive forces) and then aspartate substitution (25-fold from the gain of repulsive forces) highlights the contribution of electrostatic forces to the stability of the hRI·RNase 1 complex and reinforces previous calculations on the importance of electrostatics in the affinity of ribonucleases for RI (Shaul and Schreiber 2005).

*RNase 1 as a Chemotherapeutic Agent.* Ribonucleases show great promise as cancer chemotherapeutic agents (Leland and Raines 2001). ONC, a homologue of RNase 1 from the Northern leopard frog, is currently in phase III clinical trials for the treatment of malignant mesothelioma (Mikulski et al. 2002). A chemotherapeutic agent based on a human ribonuclease have multiple advantages over ONC, including enhanced catalytic activity (Rutkoski et al. 2005), decreased renal toxicity (Vasandani et al. 1996; Vasandani et al. 1999), and decreased immunogenicity (Matousek et al. 2003). To endow ribonucleases that are not naturally cytotoxic with cytotoxic activity requires the consideration of multiple biochemical attributes, including ribonucleolytic activity, cationic charge, conformational stability, and (especially) RI evasion (Dickson et al. 2003; Rutkoski et al. 2005).

Variants of RNase 1, unlike those of RNase A, have been difficult to engineer with decreased affinity for hRI (Gaur et al. 2001; Bosch et al. 2004). The data reported herein reveal the origin of this difficulty. The hRI·RNase 1 complex has a more extensive and tighter network of hydrogen bonds than does the pRI·RNase A complex (Table 2.2). This structural data is manifested in the stability of the hRI·RNase 1 complex, which has a subfemtomolar  $K_d$  value (Table 2.3), which is 150-fold less than that of the hRI·RNase A complex (Lee et al. 1989b). Accordingly, cytotoxic variants of RNase 1 must overcome greater RI inhibition to become cytotoxic. We have overcome this barrier by designing a variant of RNase 1 with an affinity for RI in the micromolar range.

R39D/N67D/N88A/G89D/R91D RNase 1 has a  $5 \times 10^9$ -fold decrease in affinity for RI, making it the most RI-evasive engineered ribonuclease reported to date. This RNase 1

variant, which has nearly wild-type ribonucleolytic activity and conformational stability, is cytotoxic (Figure 2.6; Table 2.3). Its cytotoxic activity is, however, likely compromised by its overall neutrality ( $Z = 0$ ), as net charge is known to correlate with cytotoxic activity among ribonucleases with similar ribonucleolytic activity, conformational stability, and affinity for RI (Rutkoski et al. 2005; Notomista et al. 2006). The cytotoxicity of a ribonuclease can be increased, however, by adding nine arginine residues to the C-terminus (Fuchs and Raines 2005). Accordingly, liberating RNase 1 from inhibition by hRI overcomes the major barrier to endowing RNase 1 with cytotoxic activity.

## 2.5 Conclusions

RI and its cognate ribonucleases represent a unique system for characterizing a protein-protein complex. Toward this end, we have examined the interaction of RNase 1, which is the human homologue of RNase A, and hRI. We find that the affinity of RNase 1 for hRI is subfemtomolar, indicative of the imperative of regulating ribonucleolytic activity in humans. By determining the three-dimensional structure of the hRI-RNase 1 complex at atomic resolution, we were able to reveal those residues that are responsible for its extraordinary stability. We were also able to design an RNase 1 variant that retains its ribonucleolytic activity and conformational stability but has only micromolar affinity for hRI. Arg39 and Arg91 of RNase 1 are especially important in this context. These two “electrostatic targeting residues” (1) substantially increase the association rate of the complex, and (2) form tight hydrogen bonds that maintain the complex. Together, these data provide detailed insight into one of the most stable protein-protein complexes, and

represent a key step in the development of human ribonucleases as chemotherapeutic agents.



**Table 2.1** Crystallographic, data processing, and refinement statistics; values in parentheses refer to the highest resolution shell

<i>Data Collection Statistics</i>	
Space group	P2 <sub>1</sub> 2 <sub>1</sub> 2 <sub>1</sub>
Unit cell parameters	$a=71.338$ , $b=107.546$ , $c=155.036$
alpha beta gamma	90.00 90.00 90.00
X-ray energy (keV)	12.399
X-ray wavelength (Å)	0.99997
Overall resolution range (Å)	47.17–1.95 (2.00–1.95)
Number of reflections	measured 573,939, unique 84,446
Completeness (%)	97.0 (72.6)
$R_{\text{merge}}^a$	0.078 (0.424)
Redundancy	6.8 (3.6)
Mean $I/\sigma(I)$	16.96 (2.94)
<i>Phasing</i>	
MR correlation coefficient (MOLREP) <sup>d</sup>	0.223
MR model <sup>d</sup>	1DFJ
<i>Refinement and Model Statistics from REFMAC 5.2.0005</i>	
Number of reflections (total)	80,141
$R_{\text{cryst}}^b$ ( $R_{\text{free}}^c$ )	0.175 (0.236)
RMSD bonds (Å)	0.016
RMSD angles (°)	1.515
ESU based on $R_{\text{free}}^c$ (Å) <sup>d</sup>	0.166
Average $B$ factor (Å <sup>2</sup> )	28.04
Number of water molecules	854
<i>Ramachandran plot</i>	
Residues in most favorable region	86.8%
Residues in additional allowed region	12.8%
Residues in generously allowed region	0.4%
Residues in disallowed region	0.0%
<sup>a</sup> $R_{\text{merge}} = 3 \sum_i  I_i(h) - \langle I(h) \rangle  / 3 \sum_i I_i(h)$ , where $I_i(h)$ is the intensity of an individual measurement of the reflection and $\langle I(h) \rangle$ is the mean intensity of the reflection. <sup>b</sup> $R_{\text{cryst}} = 3 \sum_h  F_{\text{obs}} - F_{\text{calc}}  / 3 \sum_h F_{\text{obs}}$ , where $F_{\text{obs}}$ and $F_{\text{calc}}$ are the observed and calculated structure-factor amplitudes, respectively. <sup>c</sup> $R_{\text{free}}$ was calculated as $R_{\text{cryst}}$ using 5.0% of the randomly selected unique reflections that were omitted from structure refinement. <sup>d</sup> Abbreviations used: MR, molecular replacement; ESU, estimated standard uncertainty.	

**Table 2.2** Intermolecular hydrogen bonds ( $r_{X\cdots X} < 3.35$  Å) in the structures of the crystalline hRI·RNase 1 and pRI·RNase A complexes<sup>a</sup>

PDB Entry 1Z7X (Chains Y and Z)			PDB Entry 1DFJ (Chains E and I)		
Residue			Residue		
RNase 1	hRI	$r$ (Å)	RNase A	pRI	$r$ (Å)
Arg4	Trp438	2.74	—	—	—
Arg4	Trp438	2.91	—	—	—
Lys7	Ser460	2.80	Lys7	Ser456	3.20 <sup>b</sup>
Gln11	Ser460	2.94	—	—	—
—	—	—	Asn24	Asp117	2.72
Arg31	Gln10	2.79	—	—	—
Arg31	Asp35	2.82	—	—	—
Arg32	Asp36	2.67	—	—	—
Arg32	Asp36	2.74	—	—	—
Arg39	Tyr434	2.74	—	—	—
Arg39	Glu401	2.76	Arg39	Glu397	2.32
Arg39	Glu401	3.03	—	—	—
Lys41	Asp435	2.57	—	—	—
Asn67	Tyr437	2.87	Asn67	Val405	2.81
—	—	—	Asn67	Val405	2.83
—	—	—	Gln69	Asp407	3.19
Asn71	Tyr437	2.75	Asn71	Tyr437	2.36
Asn88	Glu264	2.71	Gly88	Trp257	3.24
Gly89	Trp261	2.97	Ser89	Glu202	2.97
Arg91	Glu287	2.61	—	—	—
Arg91	Glu287	2.93	—	—	—
—	—	—	Glu111	Glu436	2.89
Glu111	Tyr437	2.58	Glu111	Tyr433	3.00

<sup>a</sup> Hydrogen bonds were identified using the program PDBsum (Laskowski et al. 2005).

<sup>b</sup> No definitive electron density.

**Table 2.3** Biochemical parameters of RNase 1, RNase A, and their variants

Ribonuclease	$T_m^a$ (°C)	$k_{cat}/K_M^b$ ( $10^6 \text{ M}^{-1} \text{ s}^{-1}$ )	$K_d^c$ (nM)	$\Delta G^d$ (kcal/mol)	$\Delta\Delta G^e$ (kcal/mol)	$IC_{50}^f$ (μM)	Z
Wild-type RNase A	64 <sup>g</sup>	52 ± 4 <sup>g</sup>	44 × 10 <sup>-6h</sup>			>25	+4
D38R/R39D/N67R/ G88R RNase A	56 <sup>g</sup>	38 ± 6 <sup>g</sup>	510 ± 30 <sup>g</sup>			0.15 ± 0.01	+6
Wild-type RNase 1	57	21 ± 2	29 × 10 <sup>-8i</sup>			>25	+6
G38R/R39G/N67R/ N88R RNase 1	61	4.2 ± 0.4	0.032 ± 0.016	6.9		>25	+8
R39D/N67D/N88A/ G89D/R91D	58	6.3 ± 0.5	(1.7 ± 0.5) × 10 <sup>3</sup>	13.3		13.3 ± 1.7	0
R39L/N67L/N88A/ G89L/R91L	65	30 ± 3	30 ± 1	10.9	2.4	>25	+4
N67D/N88A/G89D/ R91D RNase 1	51	16 ± 6	45 ± 15	11.2	2.1	>25	+2
R39D/N88A/G89D/ R91D RNase 1	57	10 ± 3	68 ± 8	11.4	1.9	>25	+1
R39D/N67D/G89D/ R91D RNase 1	54	3.3 ± 0.5	(1.0 ± 0.1) × 10 <sup>3</sup>	13.0	0.3	>25	0
R39D/N67D/N88A/ R91D RNase 1	51	10 ± 1	278 ± 50	12.2	1.1	>25	+1
R39D/N67D/N88A/ G89D RNase 1	57	5 ± 1	16 ± 3	10.6	2.7	>25	+2

<sup>a</sup> Values of  $T_m$  (±2 °C) for RNase 1 and its variants were determined in PBS by UV spectroscopy.

<sup>b</sup> Values of  $k_{cat}/K_M$  (±SE) were determined for catalysis of 6-FAM-dArU(dA)<sub>2</sub>-6-TAMRA cleavage at 25 °C in 0.10 M MES-NaOH buffer (OVS-free), pH 6.0, containing 0.10 M NaCl (Kelemen et al. 2000).

<sup>c</sup> Values of  $K_d$  (±SE) were determined for the complex with hRI at 25 °C (Abel et al. 2002).

<sup>d</sup> Values of  $\Delta G$  were calculated with the equation:  $\Delta G = -RT \ln(K_d^{\text{wild-type}}/K_d^{\text{variant}})$ .

<sup>e</sup> Values of  $\Delta\Delta G = \Delta\Delta G^{\text{R39D/N67D/N88A/G89D/R91D RNase 1}} - \Delta\Delta G^{\text{RNase 1 variant}}$ .

<sup>f</sup> Values for  $IC_{50}$  (±SE) are for the incorporation of [*methyl*-<sup>3</sup>H]thymidine into the DNA of K-562 cells treated with the ribonuclease, and were calculated with equation (4).

<sup>g</sup> From ref (Rutkoski et al. 2005).

<sup>h</sup> From ref (Lee et al. 1989b).

<sup>i</sup> Calculated with the value of  $k_d$  for the hRI·RNase 1 complex (Table 4), the value of  $k_a = 3.4 \times 10^8 \text{ M}^{-1} \text{ s}^{-1}$  for hRI + RNase A (Lee et al. 1989a), and the equation:  $K_d = k_d/k_a$ .

**Table 2.4** Rate constants for the binding of hRI to RNase 1 and its variants

RNase 1	$k_d$ (s <sup>-1</sup> )	$k_a$ (M <sup>-1</sup> s <sup>-1</sup> )
wild-type	$(9.9 \pm 0.7) \times 10^{-8}$ <sup>a</sup>	$3.4 \times 10^8$ <sup>b</sup>
R39D/N67D/N88A/G89D/R91D	$0.22 \pm 0.03$ <sup>c</sup> ( $2.2 \times 10^6$ )	$1.2 \times 10^5$ <sup>d</sup> ( $2.8 \times 10^3$ )
R39L/N67L/N88A/G89L/R91L	$0.092 \pm 0.003$ <sup>c</sup> ( $9.3 \times 10^5$ )	$3.1 \times 10^6$ <sup>d</sup> ( $1.1 \times 10^2$ )

<sup>a</sup> The value of  $k_d$  ( $\pm$ SE) was determined by following the release of diethylfluorescein-labeled RNase 1 from hRI over time and fitting the curve to equation (3).

<sup>b</sup> The value of  $k_a$  is from ref (Lee et al. 1989a). Both angiogenin and RNase A have association rates within twofold of each other (Lee et al. 1989a), and so the association rate of RNase A was chosen for comparison due to the greater similarity of its sequence and structure with those of RNase 1.

<sup>c</sup> Values of  $k_d$  ( $\pm$ SE) were determined by following the release of a fluorescein-labeled RNase 1 variant from hRI over time and fitting the curves to equation (3). Values in parentheses represent the fold increase from wild-type RNase 1.

<sup>d</sup> Values of  $k_a$  were calculated with the equation:  $K_d = k_d/k_a$ . Numbers in parentheses represent the fold decrease from wild-type RNase 1.

**Figure 2.1** Structure of the crystalline complex of hRI (green) and RNase 1 (blue). Ribbon diagram of the contents of the asymmetric unit in which the N-terminal  $\beta$ -strands of hRI from two molecular complexes form an anti-parallel  $\beta$ -sheet. The image was created with the program PyMOL (DeLano Scientific, South San Francisco, CA).

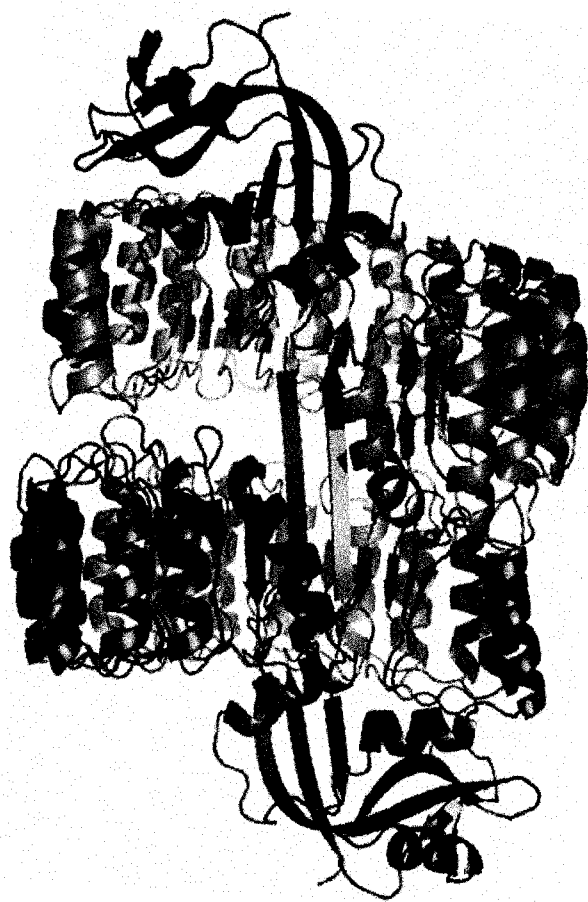


**Figure 2.2** Contact residues from the crystal structures of hRI·RNase 1 and pRI·RNase A. (a) Amino acid sequence alignment of RNase A and RNase 1. hRI contacts for both chains of RNase 1 in the unit cell are given. The secondary structure of RNase A is identified with h ( $\alpha$ -helix), s ( $\beta$ -strand), or t (turn). Residues in van der Waals or hydrophobic contact with RI are in blue. Residues with a hydrogen bond to RI are in red. Conserved cysteine residues are in yellow. Catalytic residues are enclosed in black boxes. (b) Three-dimensional structure of RNase 1, chain Z. Residues are colored using the same scheme as in panel a, except that active-site residues are not highlighted. The image was created with the program PyMOL.

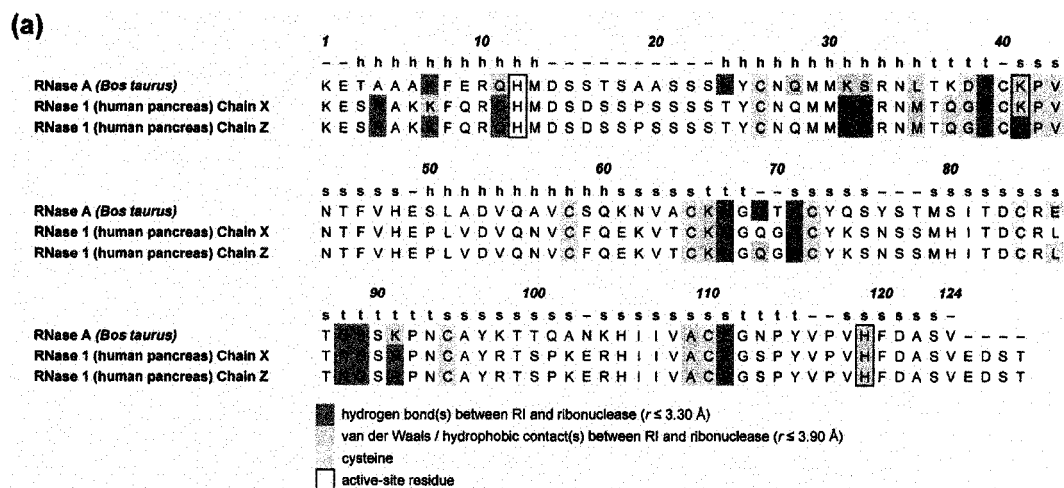




**Figure 2.3** Comparison of the  $\beta 4$ – $\beta 5$  loop of RNase 1 (purple) and RNase A (blue) when bound to RI (green).  $\alpha$ -Carbon atoms of RNase 1 and RNase A were superimposed with the program Sequoia, and images were created with the program PyMOL. (a) Structure of the  $\beta 4$ – $\beta 5$  loops. Sidechains of residues 88–91 are shown as sticks. Amino acids are labeled with the color corresponding to the color of the ribonuclease. (b) Orientation of the  $\beta 4$ – $\beta 5$  loops bound to RI. A model of RNase A (PDB entry 1DFJ, chain E) bound to hRI (chain Y) was created based on its alignment to RNase 1 (chain Z). Hydrogen bonds are shown as dotted lines. Hydrogen bonds between hRI and RNase A are hypothesized based on the alignment of hRI (chain Y) and pRI (chain I).

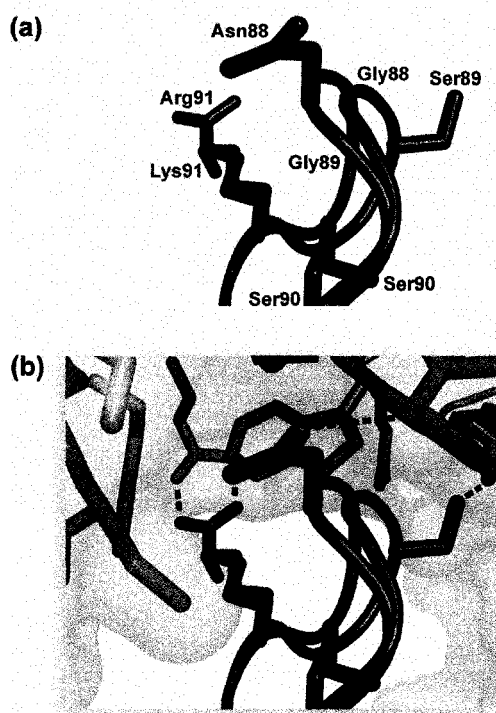


**Figure 2.4** Electron density at  $1\sigma$  ( $2F_{\text{obs}} - F_{\text{calc}}$ ) of key contact residues between hRI (green) and RNase 1 (purple). Specific residues shown in detail are (a) Arg39, (b) Asn67, and (c) Arg91. Highlighted regions are shown in wall-eyed stereo; interprotein hydrogen bonds are displayed by black dotted lines. Images were created with the program PyMOL.

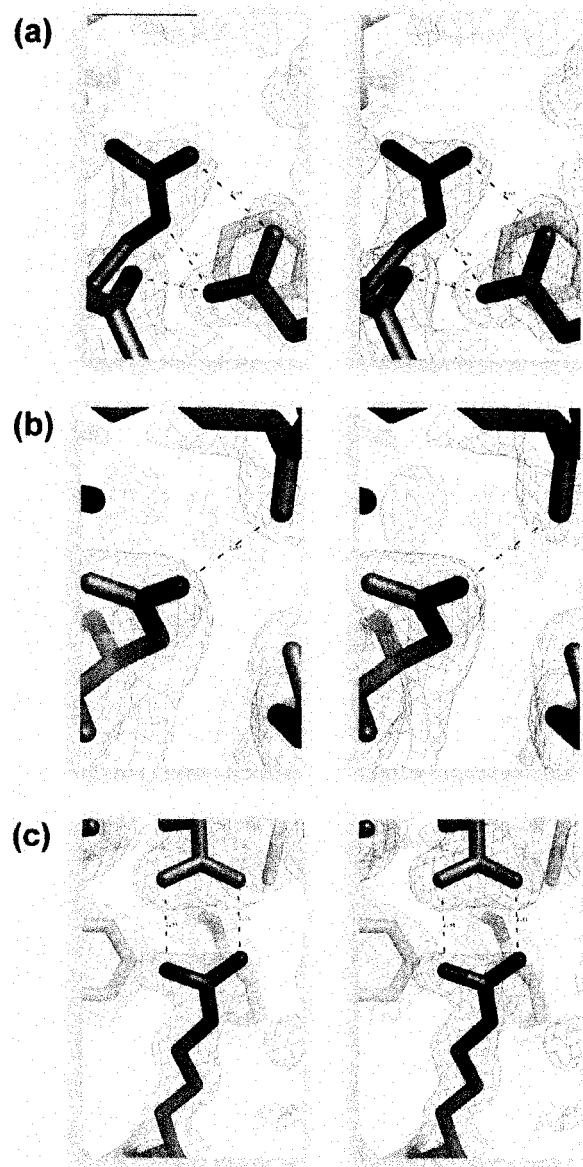


**Figure 2.5** Dissociation rate of the complex between wild-type RNase 1 and hRI. The release of diethylfluorescein-labeled RNase 1 (100 nM) from hRI (100 nM) was followed over time after addition of a 50-fold molar excess of angiogenin (5  $\mu$ M) (●) or after addition of an identical volume of PBS (○). The initial fluorescence of unbound RNase 1 was used as the end-point for complete RNase 1 release. Data points are the mean ( $\pm$ SE) of six separate measurements and are normalized for the average fluorescence of rhodamine 110 (10 nM).

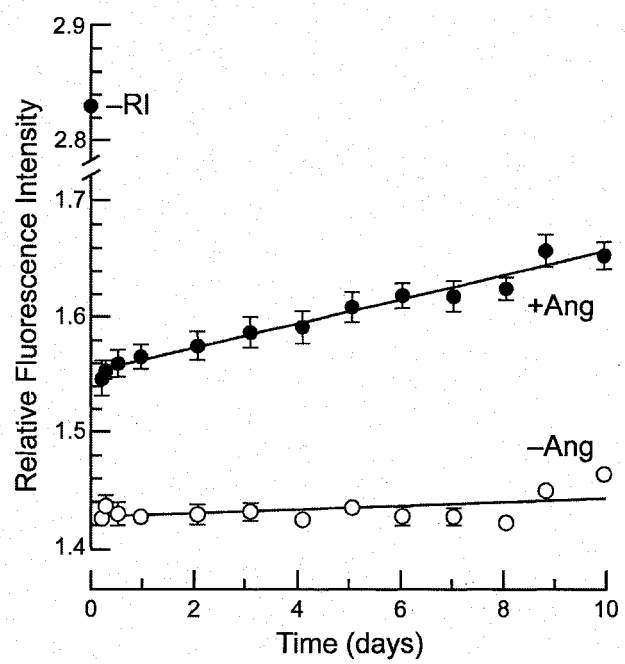


**Figure 2.6** Affinity for hRI and cytotoxic activity of ribonucleases. (a) Affinity of hRI for RNase 1 variants was determined by using a competition assay with fluorescein-labeled A19C/G88R RNase A (50 nM). Data points are the mean ( $\pm$ SE) of at least three separate measurements. RNase 1 variants in order of decreasing affinity for hRI: R39D/N67D/N88A/G89D (red  $\diamond$ ), R39L/N67L/N88A/G89L/R91L (blue  $\diamond$ ), N67D/N88A/G89D/R91D (red  $\blacksquare$ ), R39D/N88A/G89D/R91D (red  $\blacktriangle$ ), R39D/N67D/N88A/R91D (red  $\blacktriangledown$ ), R39D/N67D/G89D/R91D (red  $\bullet$ ), and R39D/N67D/N88A/G89D/R91D ( $\diamond$ ). (b) Effect of ribonucleases on the proliferation of K-562 cells was determined by monitoring the incorporation of [*methyl*- $^3$ H]thymidine into cellular DNA in the presence of ribonucleases. Data points are the mean ( $\pm$ SE) of at least three separate experiments carried out in triplicate. Ribonucleases in order of decreasing cytotoxic activity: D38R/R39D/N67R/G88R RNase A ( $\diamond$ ), G88R RNase A ( $\Gamma$ ), R39D/N67D/N88A/G89D/R91D RNase 1 ( $\diamond$ ), R39L/N67L/N88A/G89L/R91L RNase 1 (blue  $\diamond$ ), and N67D/N88A/G89D/R91D RNase 1 (red  $\blacksquare$ ). R39D/N67D/N88A/G89D RNase 1 (red  $\diamond$ ), G38R/R39G/N67R/N88R RNase 1 (green  $\diamond$ ), wild-type RNase 1 ( $\circ$ ), and other variants of RNase 1 (not shown) have negligible cytotoxic activity.

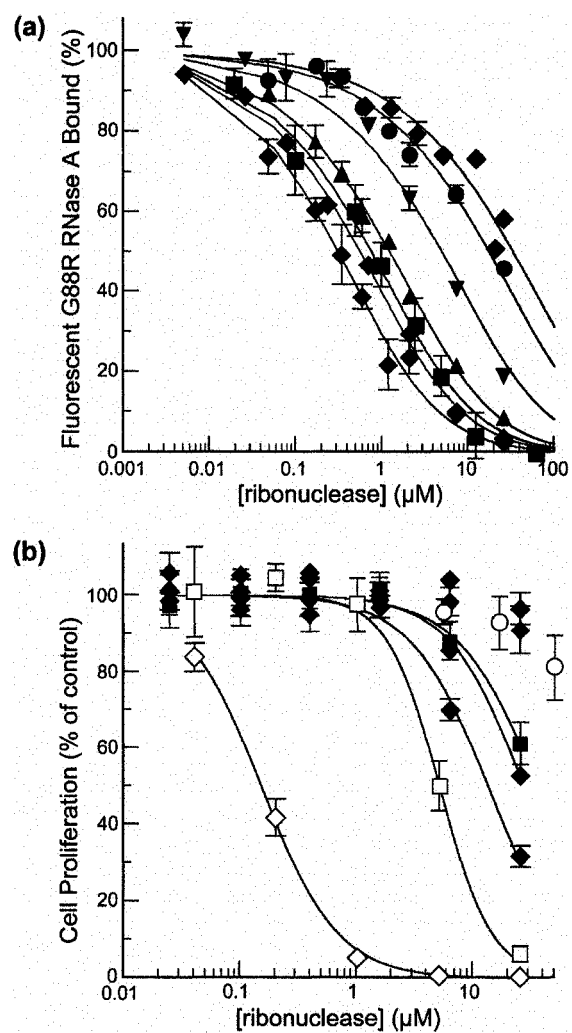
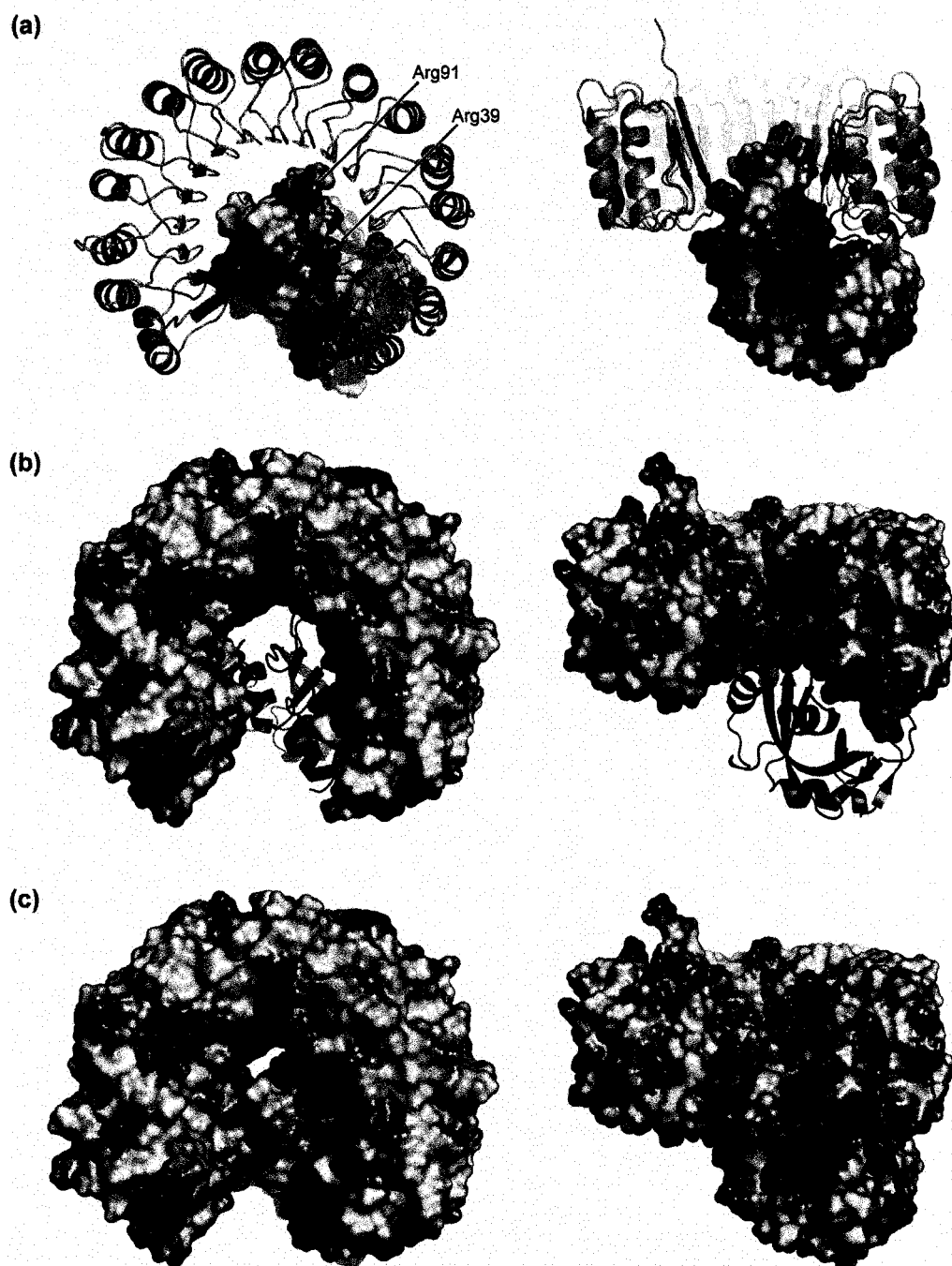




**Figure 2.7** Electrostatic representation of the interaction between hRI (green) and RNase 1 (purple). Protein contact potential of RNase 1 (a), hRI (b), and the hRI-RNase 1 complex (c) are shown. Residues 39 and 91 are labeled in panel a. The intensity of the blue (positive) and red (negative) coloration is indicative of the local electrostatic environment. Vacuum electrostatics were calculated and images were created with the program PyMOL.



## Chapter Three

### **Cytotoxic Ribonucleases: The Dichotomy of Coulombic Forces**

Portions of this chapter are being published as:

Johnson, R.J., Chao, T-Y., Lavis, L.D., Raines, R.T. (2007) Cytotoxic Ribonucleases: The Dichotomy of Coulombic Forces. *Biochemistry*. In Press. I performed all of the research described in this chapter, except the flow cytometry (TY Chao) and the synthesis of the latent fluorophore (LD Lavis).

### 3.1 Abstract

Cells tightly regulate their contents. Still, nonspecific Coulombic interactions between cationic molecules and anionic membrane components can lead to adventitious endocytosis. Here, we characterize this process in a natural system. To do so, we create variants of human pancreatic ribonuclease (RNase 1) that differ in net molecular charge. By conjugating a small-molecule latent fluorophore to these variants and using flow cytometry, we are able to determine the kinetic mechanism for RNase 1 internalization into live human cells. We find that internalization increases with solution concentration and is not saturable. Internalization also increases with time to a steady-state level, which varies linearly with molecular charge. In contrast, the rate constant for internalization ( $t_{1/2} = 2$  h) is independent of charge. We conclude that internalization involves an extracellular equilibrium complex between the cationic proteins and abundant anionic cell-surface molecules, followed by rate-limiting internalization. The enhanced internalization of more cationic variants of RNase 1 is, however, countered by their increased affinity for the cytosolic ribonuclease inhibitor protein, which is anionic. Thus, Coulombic forces mediate extracellular and intracellular equilibria in a dichotomous manner that both endangers cells and defends them from the potentially lethal enzymatic activity of ribonucleases.

### 3.2 Introduction

Cells control their intracellular environment through careful gating of the influx of extracellular material (Conner and Schmid 2003; Polo and Di Fiore 2006). To distinguish between molecules to be internalized from those to be excluded, cells use specific

interactions with cell-surface proteins, lipids, and carbohydrates. Nonspecific interactions mediated by Coulombic forces can also lead to internalization, often in an unregulated manner (Murray and Honig 2002; Conner and Schmid 2003; Cho and Stahelin 2005; Mulgrew-Nesbitt et al. 2006; Polo and Di Fiore 2006). Such nonspecific interactions can be modulated by increasing, decreasing, or masking the cationic charge on the biomolecule (Murray and Honig 2002; Mulgrew-Nesbitt et al. 2006).

Two classes of molecules that exploit high cationicity to effect nonspecific adsorption to the cell surface and internalization are cell-penetrating peptides (CPPs) and ribonucleases (Fotin-Mleczek et al. 2005; Kaplan et al. 2005; Fuchs and Raines 2006; Notomista et al. 2006). CPPs have received considerable attention due to their ability to transport otherwise membrane-impermeable cargo into cells (Zorko and Langel 2005; Chauhan et al. 2006; Fuchs and Raines 2006). The detailed mechanism of CPP internalization is unclear, but is known to involve multiple steps. Those steps include binding to anionic cell-surface molecules, internalization in an ATP- and temperature-dependent manner, and ultimately translocation from endosomes into the cytoplasm (Drin et al. 2003; Haigis and Raines 2003; Fuchs and Raines 2004; Richard et al. 2005; Fuchs and Raines 2006; Notomista et al. 2006). Similar to cationic peptides, the endocytosis of pancreatic-type ribonucleases is facilitated by their cationic nature (Notomista et al. 2006). Ribonucleases bind to the cell surface through Coulombic interactions between positively charged residues and negatively charged cell-surface molecules (Notomista et al. 2006), and are endocytosed by a dynamin-independent pathway without the necessity for a specific receptor (D'Alessio and Riordan 1997; Leland and Raines 2001; Matousek 2001;

Haigis and Raines 2003; Makarov and Ilinskaya 2003; Benito et al. 2005; Arnold and Ulbrich-Hofmann 2006).

Pancreatic-type ribonucleases have diverse biological activities, including selective toxicity to cancerous cells (D'Alessio and Riordan 1997; Leland and Raines 2001; Matousek 2001; Makarov and Ilinskaya 2003; Benito et al. 2005; Arnold and Ulbrich-Hofmann 2006). The archetype of a cytotoxic ribonuclease is Onconase<sup>®</sup> (ONC), a ribonuclease isolated from the oocytes of *Rana pipiens* that is currently in confirmatory phase IIIb clinical trials for the treatment of malignant mesothelioma (Pavlakakis and Vogelzang 2006). The specific toxicity of ONC and engineered ribonucleases toward tumor cells relies on multiple biochemical attributes, such as evasion of the cytosolic ribonuclease inhibitor protein (RI (Dickson et al. 2005)), high ribonucleolytic activity, and resistance to proteolysis (Bretscher et al. 2000; Klink and Raines 2000; Dickson et al. 2003).

Cationic charge is also important for ribonuclease cytotoxicity. For example, the cytotoxicity of bovine pancreatic ribonuclease (RNase A, EC 3.1.27.5 (Raines 1998)) and microbial ribonucleases can be increased through mutagenic or chemical cationization (Futami et al. 2001; Futami et al. 2002; Ilinskaya et al. 2002; Ilinskaya et al. 2004; Fuchs et al. 2007). Traditional studies on the relationship between the cationicity and cytotoxicity of ribonucleases have used cell death as the read-out (Futami et al. 2001; Futami et al. 2002; Ilinskaya et al. 2002; Ogawa et al. 2002; Ilinskaya et al. 2004; Notomista et al. 2006; Fuchs et al. 2007). This phenotype is manifested, however, only after a complex, multi-step process (D'Alessio and Riordan 1997; Leland and Raines 2001; Matousek 2001;

Makarov and Ilinskaya 2003; Benito et al. 2005; Arnold and Ulbrich-Hofmann 2006).

Hence, a direct measurement of ribonuclease internalization is necessary to dissect the effect of cationicity on internalization.

Here, we isolate internalization from cell death by using a novel fluorogenic label with fluorescence that remains quiescent until an encounter with an intracellular esterase (Chandran et al. 2005; Lavis et al. 2007). By using this latent fluorophore along with flow cytometry, we directly quantitate the internalization of variants of human pancreatic ribonuclease (RNase 1; Figure 3.1A). We then characterize the effect of charge on two equilibria that mediate ribonuclease cytotoxicity. Our findings reveal new information about the role of Coulombic forces in protein–cell and protein–protein interactions.

### 3.3 Experimental Procedures

*Materials.* *Escherichia coli* strain BL21(DE3) was from Novagen (Madison, WI). 6-FAM–dArU(dA)<sub>2</sub>–6-TAMRA, a fluorogenic ribonuclease substrate, was from Integrated DNA Technologies (Coralville, IA). Enzymes were from Promega (Madison, WI). K-562 cells, which are an erythroleukemia cell line derived for a chronic myeloid leukemia patient, were from the American Type Culture Collection (Manassas, VA). Cell culture medium and supplements were from Invitrogen (Carlsbad, CA). [*methyl*-<sup>3</sup>H]Thymidine (6.7 Ci/mmol) was from Perkin–Elmer (Boston, MA). Protein purification columns were from GE Biosciences (Piscataway, NJ). MES buffer (Sigma–Aldrich, St. Louis, MO) was purified by anion-exchange chromatography to remove trace amounts of oligomeric vinylsulfonic acid (Smith et al. 2003). Phosphate-buffered saline (PBS) contained (in 1.00

L) NaCl (8.0 g), KCl (2.0 g), Na<sub>2</sub>HPO<sub>4</sub>·7H<sub>2</sub>O (1.15 g), KH<sub>2</sub>PO<sub>4</sub> (2.0 g), and NaN<sub>3</sub> (0.10 g) and had a pH of 7.4. All other chemicals were of commercial grade or better, and were used without further purification.

*Instrumentation.* Fluorescence spectroscopy was performed with a QuantaMaster1 photon-counting fluorimeter equipped with sample stirring (Photon Technology International, South Brunswick, NJ). Thermal denaturation data were collected using a Cary 3 double-beam spectrophotometer equipped with a Cary temperature-controller (Varian, Palo Alto, CA). [*methyl*-<sup>3</sup>H]Thymidine incorporation into genomic DNA was quantitated by liquid scintillation counting using a Microbeta TriLux liquid scintillation and luminescence counter (Perkin–Elmer, Wellesley, MA). The mass of RNase 1 and its variants was confirmed by matrix-assisted laser desorption/ionization time-of-flight (MALDI–TOF) mass spectrometry with a Voyager-DE-PRO Biospectrometry Workstation (Applied Biosystems, Foster City, CA) at the campus Biophysics Instrumentation Facility. Flow cytometry data were collected by using a FACSCalibur flow cytometer equipped with a 488-nm argon-ion laser (Becton Dickinson, Franklin Lakes, NJ). Microscopy images were obtained with a Nikon Eclipse TE2000-U confocal microscope equipped with a Zeiss AxioCam digital camera.

*Protein Purification and Labeling.* DNA encoding variants of RNase 1 were made by using plasmid pHP-RNase (Leland et al. 2001) and the Quikchange site-directed mutagenesis or Quikchange Multi site-directed mutagenesis kit (Stratagene, La Jolla, CA). RNase 1 variants were produced in *E. coli* and purified by using methods described previously for wild-type RNase 1 (Leland et al. 2001). D38R/R39D/N67R/G88R RNase A,



which is a highly cytotoxic variant (Rutkoski et al. 2005), was a gift from T. J. Rutkoski. Human RI was produced in *E. coli* and purified as described previously (Johnson et al. 2007c).

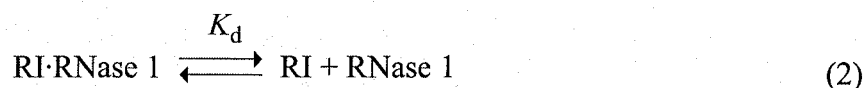
Variants with a free cysteine at position 19 were protected by reaction with 5,5'-dithio-bis(2-nitrobenzoic acid) (DTNB) (Riddles et al. 1983; Lavis et al. 2006). Immediately prior to latent-fluorophore attachment, TNB-protected ribonucleases were deprotected with a three-fold molar excess of dithiothreitol (DTT) and desalted by chromatography on a PD-10 desalting column (GE Biosciences, Piscataway, NJ). The maleimide-containing latent fluorophore was synthesized as described previously (Lavis et al. 2006). Deprotected ribonucleases were reacted for 4–6 h at 25 °C with a ten-fold molar excess of thiol-reactive latent fluorophore (Lavis et al. 2006). Conjugates were purified by chromatography using a HiTrap SP FF column. The molecular masses of RNase 1, its variants, and conjugates were confirmed by MALDI–TOF mass spectrometry. Protein concentration was determined by using a bicinchoninic acid assay kit from Pierce (Rockford, IL) with bovine serum albumin as a standard.

*Conformational Stability Measurements.* The conformational stability of RNase 1 and its variants was determined by following the change in UV absorbance at 287 nm with increasing temperature (Klink and Raines 2000). The temperature of PBS containing an RNase 1 variant (0.1–0.2 mg/mL) was heated from 20 to 80 °C at 0.15 °C/min. The  $A_{287}$  was followed at 1-°C intervals, and the absorbance change was fitted to a two-state model of denaturation, wherein the temperature at the midpoint of the transition curve corresponds to the value of  $T_m$ .

*Ribonucleolytic Activity Assays.* The ribonucleolytic activity of RNase 1 and its variants was determined by quantitating its ability to cleave 6-FAM-dArU(dA)<sub>2</sub>-6-TAMRA (Kelemen et al. 1999). Assays were carried out at 23 (±2) °C in 2.0 mL of 0.10 M MES–NaOH buffer (pH 6.0) containing NaCl (0.10 M). Fluorescence data were fitted to eq 1, in which  $\Delta I/\Delta t$  is the initial reaction velocity,  $I_0$  is the fluorescence intensity before addition of a ribonuclease,  $I_f$  is the fluorescence intensity after complete substrate hydrolysis, and  $[E]$  is the total ribonuclease concentration.

$$\frac{k_{\text{cat}}}{K_M} = \frac{(\Delta I / \Delta t)}{(I_f - I_0)[E]} \quad (1)$$

*RI-Binding Assays.* The affinity of RNase 1 variants for human RI was determined by using a fluorescent competition assay reported previously (Abel et al. 2002). Briefly, PBS (2.0 mL) containing DTT (5 mM), fluorescein-labeled G88R RNase A (50 nM), and various concentrations of an unlabeled RNase 1 variant was incubated at 23 (±2) °C for 20 min. The initial fluorescence intensity of the unbound fluorescein-labeled G88R RNase A was monitored for 3 min (excitation: 491 nm, emission: 511 nm). RI (50 nM) was then added, and the final fluorescence intensity was measured. The value of  $K_d$  for RI·RNase 1 complexes as defined in eq 2 was obtained by nonlinear least squares analysis of the binding isotherm using GraphPad Prism 4.02 (GraphPad Software, San Diego, CA). The  $K_d$  value for the complex between RI and fluorescein-labeled G88R RNase A was taken to be 1.4 nM (Rutkoski et al. 2005).



*Cytotoxicity Assays.* The effect of RNase 1 and its variants on the proliferation of K-562 cells was assayed as described previously (Leland et al. 2001; Haigis et al. 2002b; Rutkoski et al. 2005). After a 44-h incubation with ribonuclease, K-562 cells were treated with [*methyl*-<sup>3</sup>H]thymidine for 4 h, and the incorporation of radioactive thymidine into cellular DNA was quantitated by liquid scintillation counting. Results are shown as the percentage of [*methyl*-<sup>3</sup>H]thymidine incorporated relative to control cells. Data are the average of three measurements for each concentration, and the entire experiment was repeated in triplicate. Values for IC<sub>50</sub> were calculated by fitting the curves by nonlinear regression with eq 3 (Rutkoski et al. 2005; Johnson et al. 2007c), in which *y* is the total DNA synthesis following the [*methyl*-<sup>3</sup>H]thymidine pulse and *h* is the slope of the curve.

$$y = \frac{100\%}{1 + 10^{(\log(\text{IC}_{50}) - \log[\text{ribonuclease}])h}} \quad (3)$$

*Flow Cytometry Assays.* The internalization of ribonuclease variants with latent fluorophore attached (Figure 3.1B) was followed by monitoring the unmasking of fluorescence by intracellular esterases. K-562 cells from near confluent flasks were collected by centrifugation and resuspended at a density of  $1 \times 10^6$  cells/mL in fresh RPMI 1640. Labeled ribonuclease (10  $\mu\text{M}$ ) or unlabeled RNase 1 (10  $\mu\text{M}$ ) was added to 250  $\mu\text{L}$  of RPMI containing  $1 \times 10^6$  cells/mL of K-562 cells. K-562 cells were allowed to

incubate at 37 °C for varying times with the ribonucleases. To quench internalization, K-562 cells were collected by centrifugation at 750g for 3 min at 4 °C, and cell pellets were resuspended gently in ice-cold PBS (250 µL). Samples remained on ice until analyzed by flow cytometry.

Latent fluorophore fluorescence was detected through a 530/30-nm band-pass filter. Cell viability was determined by staining with propidium iodide, which was detected through a 660-nm long-pass filter. The mean channel fluorescence intensity of 20,000 viable cells was determined for each sample using CellQuest software and used for subsequent analysis. To determine the steady-state rate constant for ribonuclease internalization, fluorescence intensity data were fitted to eq 4, in which  $F_{\max}$  is the fluorescence intensity upon reaching the steady-state and  $k_1$  is the rate constant for ribonuclease internalization into K-562 cells.

$$F = F_{\max}(1 - e^{-k_1 t}) \quad (4)$$

*Microscopy.* Confocal microscopy was used to observe ribonuclease localization. K-562 cells were prepared as described for flow cytometry. Latent fluorophore-labeled RNase 1 variant (10 µM) or fluorescein-labeled RNase 1 variant (10 µM) were added to 250 µL of RPMI 1640 containing K-562 cells ( $1 \times 10^6$  cells/mL) and incubated at 37 °C for 30 min. Cell nuclei were stained by the addition of Hoechst 33342 (2 µg/mL) for the final 5 min of incubation. Excitation at 408 nm was provided by a blue-diode laser, and emission light was passed through a filter centered at 450 nm with a 35-nm band-pass.

Excitation at 488 nm was provided by an argon-ion laser, and emission light was passed through a filter centered at 515 nm with a 40-nm band-pass. Excitation at 543 nm was provided by a HeNe laser, and emission light was passed through a filter centered at 605 nm with a 75-nm band-pass.

### 3.4 Results

*Design of RNase 1 Variants.* Recently, we reported on variants of RNase 1 that evade the inhibitory action of RI (Johnson et al. 2007c). In these variants, positions 39, 67, 88, 89, and 91 of RNase 1 were determined to be important contact residues between human RI and RNase 1 (Figure 3.1A). By engendering Coulombic repulsion at these positions, a variant of RNase 1 (DDADD) was endowed with  $5 \times 10^9$ -fold lower affinity for RI. This variant was, however, only moderately toxic to human chronic myeloid leukemia cells *in vitro* ( $IC_{50} = 13.3 \mu M$ ) (Johnson et al. 2007c).

The lowered cytotoxicity of this RNase 1 variant when compared to other ribonucleases with similar biochemical characteristics was proposed to result from its net neutral charge, which could diminish its cellular internalization (Johnson et al. 2007c). To investigate the effect of both positively and negatively charged amino acid substitutions at these same positions in RNase 1 on ribonuclease internalization and RI evasion, a series of RNase 1 variants were constructed (Table 3.1). To maintain a basal level of RI evasion and cytotoxicity, these RNase 1 variants maintained an aspartate or leucine substitution at positions 39 and 91, as these residues contributed most to the evasion of RI (Johnson et al. 2007c). Then, the net charge of the RNase 1 variant was varied by incorporating positively

or negatively charged residues at positions 67, 88, or 89, which are known to contribute less to the stability of the RI-RNase 1 complex. These substitutions neither create nor destroy a canonical nuclear localization signal, which could contribute to cytotoxicity (Bosch et al. 2004). The resulting RNase 1 variants had a net charge ( $Z$ ) ranging from 0 to +6.

*Biochemical Properties of RNase 1 Variants.* The cytotoxicity of a ribonuclease is governed by the biochemical parameters listed in Table 3.1 (Bretscher et al. 2000; Klink and Raines 2000; Dickson et al. 2003): conformational stability, ribonucleolytic activity, RI affinity, and molecular charge of the RNase 1 variants. The conformational stability of a ribonuclease, which provides a measure of its vulnerability to proteolysis, correlates with its cytotoxic activity (Klink and Raines 2000). Conformational stability could not, however, have had a significant effect on the cytotoxicity of the RNase 1 variants, as each  $T_m$  value is within 8 °C of that of wild-type RNase 1 and significantly above physiological temperature (37 °C). Like conformational stability, ribonucleolytic activity correlates with cytotoxicity (Kim et al. 1995a; Bretscher et al. 2000). Here, however, each of the RNase 1 variants cleaved an RNA substrate with a  $k_{cat}/K_M$  value that was within 3-fold of that of the wild-type enzyme (Kelemen et al. 1999).

The biochemical attribute that varied most dramatically between the different RNase 1 variants was the affinity for RI (Table 3.1), which is known to be an important factor in cytotoxicity (Leland et al. 1998; Bretscher et al. 2000; Haigis et al. 2002b; Rutkoski et al. 2005). Consequently, the 1500-fold range of affinities for RI, between the

most RI-evasive variant (DDADD RNase 1;  $K_d = 1.7 \mu\text{M}$ ) and the least RI-evasive variant (LRRRD RNase 1;  $K_d = 1.1 \text{ nM}$ ), foreshadows a large range of cytotoxic activity.

*Ribonuclease Cytotoxicity.* Surprisingly, the RNase 1 variants varied little in their cytotoxic activity (Figure 3.2; Table 3.1). None of the RNase 1 variants was as cytotoxic as D38R/R39D/N67R/G88R RNase A. This variant of the bovine enzyme is both highly evasive of RI ( $K_d = 510 \text{ nM}$ ) and highly cationic, having a net molecular charge (*i.e.*, Arg + Lys – Asp – Glu) of  $Z = +6$  (Rutkoski et al. 2005).

*Ribonuclease Internalization.* To determine whether the molecular charge of an RNase 1 variant affects its cellular internalization, we employed a synthetic latent fluorophore (Figure 3.1B) (Chandran et al. 2005; Lavis et al. 2006). This latent fluorophore is not fluorescent until activated by an intracellular esterase, allowing for the direct and continuous visualization of protein internalization (Figure 3.1C,D). RNase 1, like RNase A, has eight cysteine residues that form four disulfide bonds in the native enzyme. To enable the attachment of the latent fluorophore, we replaced Pro19 of each RNase 1 variant with a cysteine residue. Position 19 was chosen because it is remote from the regions of interest (Figure 3.1A), and attachment of fluorescent groups at this position is not known to have a detectable effect on the ribonucleolytic activity, RI-affinity, or cell-surface binding of ribonuclease variants (Abel et al. 2002; Haigis and Raines 2003). The latent fluorophore was attached to Cys19 of each ribonuclease by a standard maleimide coupling reaction (Lavis et al. 2006).

The internalization of latent fluorophore-conjugated ribonuclease variants was observed by fluorescence microscopy and quantitated by flow cytometry. Initial

experiments revealed that the amount of ribonuclease internalized into live human cells increased linearly during the first 2 h (Figure 3.3A) and accumulated in endocytic vesicles (Figure 3.3B). Bright-field images indicated that the cells were alive and appeared to have normal physiology during the time course of the experiments (Figure 3.1D).

Detailed experiments were then performed to quantify the internalization of a ribonuclease as a function of time (Figure 3.4A), its net charge (Figure 3.4B), and its concentration (Figure 3.4C). Using eq 4 and the data in Figure 3.4A, the values of  $t_{1/2}$  ( $= \ln 2/k_1$ ) for the internalization of the RNase 1 variants were calculated to be  $(110 \pm 17)$  min for RNase 1,  $(131 \pm 16)$  min for DRRDD RNase 1, and  $(129 \pm 26)$  min for DDADD RNase 1. These  $t_{1/2}$  values are indistinguishable, suggesting that each variant is endocytosed by the same mechanism.

The amount of ribonuclease internalized into K-562 cells in 30 min was related linearly to the net charge of the ribonuclease (Figure 3.4B). The relative amount of ribonuclease internalized at 30 min also increased by greater than 4-fold between the RNase 1 variants with the lowest and highest net charge (DDADD ( $Z = 0$ ) and LRRRD ( $Z = +6$ ), respectively). Two variants of RNase 1 (DRRRD and LRRRD, with the G89R substitution underlined) were internalized to a somewhat greater extent than expected based on their net charge. These two variants are the only ones with a G89R substitution.

The amount of ribonuclease internalized into K-562 cells in 30 min increased with the solution concentration of the ribonuclease, at least up to  $10 \mu\text{M}$  (Figure 3.4C). These data suggest that the binding of RNase 1 to the cell surface is not saturable (Haigis and Raines 2003), consistent with internalization being mediated by a non-specific interaction



with an abundant cell-surface molecule rather than by a specific interaction with a receptor. Again, internalization correlated with net charge, as more wild-type RNase 1 ( $Z = +6$ ) than its DRRDD ( $Z = +3$ ) or DDADD ( $Z = 0$ ) variant was internalized at each concentration.

### 3.5 Discussion

*Dual Influence of Coulombic Forces.* Coulombic forces can lead to the unregulated internalization of cationic peptides and proteins into cells (Murray and Honig 2002; Conner and Schmid 2003; Cho and Stahelin 2005; Mulgrew-Nesbitt et al. 2006; Polo and Di Fiore 2006). To assess the biological consequences of increasing the charge of a ribonuclease, we created RNase 1 variants with a range of net charges (Table 3.1). We then quantitated their cellular internalization by using a latent fluorophore (Figure 3.1B) and flow cytometry. This combination obviated any signal from ribonucleases bound to the cell membrane (Figure 3.1C) without the need for protease treatment or washing steps (Richard et al. 2005; Lavis et al. 2006), permitting more timely and precise measurements than are accessible with any other method.

The net charge of a ribonuclease has a positive linear relationship with its internalization (Figure 3.4B). The two variants with the highest internalization based on their net charge have an arginine residue at position 89 (DRRRD and LRRRD). Installing arginine in the analogous site of RNase A yielded G88R RNase A, which was the first monomeric mammalian ribonuclease endowed with cytotoxicity (Leland et al. 1998). This cytotoxicity was attributed to a  $10^4$ -fold decrease in affinity for RI (Leland et al. 1998). Our analyses of the G89R variants of RNase 1 suggest, however, that this substitution in

RNase A could instill the added benefit of increasing cellular internalization. Our data also indicate that a positive net charge is *not* essential for ribonuclease internalization, as a neutral RNase 1 variant (DDADD) is internalized significantly and is cytotoxic (Figures 2 and 4; Table 3.1). Instead, the disposition of charge could govern the internalization of ribonucleases (Notomista et al. 2006) and other proteins (Fuchs and Raines 2007).

The opposite trend is observed between charge and the affinity for RI, which is highly anionic ( $Z = -22$ ). In Figure 3.4D, the net charge of RNase 1 variants substituted at positions 39, 67, 88, 89, and 91 is plotted *versus* the  $K_d$  value for their complex with RI. An inverse relationship between the net charge of an RNase 1 variant and its affinity for RI is observed, reinforcing the unusual nature of the RI–RNase 1 interaction and the importance of Coulombic forces to RI–RNase 1 complex formation (Johnson et al. 2007c).

Hence, two competing equilibria involving ribonuclease charge seem to imperil and protect cells from the cytotoxic activity of rogue ribonucleases (Haigis and Raines 2003). In these equilibria, increasing the positive charge of a ribonuclease increases its internalization but also increases its RI affinity (Figure 3.4), yielding RNase 1 variants with similar cytotoxic activity (Figure 3.2; Table 3.1). These competing equilibria make net charge a difficult variable to optimize in the design of cytotoxic ribonucleases.

*Mechanism of Ribonuclease Internalization.* The internalization of a ribonuclease seems to limit its cytotoxicity, as microinjected ribonucleases are cytotoxic at picomolar concentrations (Saxena et al. 1991). Thus, fully understanding the factors involved in ribonuclease internalization could lead to more effective ribonuclease chemotherapeutics (Haigis and Raines 2003). The cationicity of RI-evasive ribonucleases correlates with their

cytotoxicity (Futami et al. 2001; Futami et al. 2002; Ilinskaya et al. 2002; Ilinskaya et al. 2004) and destabilization of anionic membranes (Notomista et al. 2006). The endocytic mechanism is dynamin-independent (Haigis and Raines 2003), but the remaining steps in the pathway are unknown.

Further insight into the mechanism of ribonuclease internalization can be gathered by comparing its kinetic mechanism to that of CPPs. CPP internalization reaches a steady-state level, like that of ribonucleases (Figure 3.4A) (Hallbrink et al. 2001; Drin et al. 2003). The half-time for the internalization of a CPP ( $t_{1/2} \leq 60$  min (Drin et al. 2003; Zorko and Langel 2005)) is, however, less than that for the internalization of an RNase 1 variant ( $t_{1/2} = 2$  h, Figure 3.4A). This difference in rate constant likely arises from the difference in molecular mass, as CPPs carrying large cargo internalize more slowly (Zorko and Langel 2005). As with ribonucleases (Figure 3.4C), CPP internalization is dose-dependent (Drin et al. 2003). These similarities are consistent with ribonucleases and CPPs having similar internalization mechanisms.

The steady-state kinetics of CPP internalization have been interpreted in terms of an equilibrium formed between CPP free in solution and CPP bound to anionic cell-surface molecules, concomitant with the degradation of the CPP (Hallbrink et al. 2001; Drin et al. 2003; Zorko and Langel 2005). Based on the similarities between CPPs and ribonucleases, the same explanation seems to be applicable for ribonucleases: an extracellular pre-equilibrium is formed between ribonuclease free in solution and bound to the cell surface. Further evidence for the existence of such a prior equilibrium is provided by the charge dependence of internalization. All three ribonucleases tested had a similar half-time for

internalization (2 h), indicative of the same mechanism of internalization. Yet, their steady-state level of internalization varied by up to 4-fold based on their net charge (Figure 3.4A). Thus, ribonucleases that are more cationic have higher affinities for anionic cell-surface molecules, shifting the extracellular distribution toward the cell-surface bound state. This shift in distribution leads to more ribonucleases being internalized in the rate-limiting step ( $k_1$ ), but without affecting the internalization rate of any individual molecule.

Based on these data, we propose a model for the effect of ribonuclease charge on internalization and cytotoxicity (Figure 3.5). First, ribonucleases form an extracellular equilibrium with an anionic cell-surface molecule that is mediated by the cationicity of the ribonuclease. A candidate for this cell-surface molecule is heparan sulfate, which is an abundant glycosaminoglycan necessary for the efficient internalization of ribonucleases (Soncin et al. 1997) and CPPs (Fuchs and Raines 2004), as well as a cationic variant of the green fluorescent protein (Fuchs and Raines 2007). Second, an intracellular equilibrium based on ribonuclease charge is formed upon ribonuclease translocation to the cytosol (Figure 3.5). This second equilibrium between ribonucleases bound by RI and those that evade RI is apparent by the opposing trends depicted in Figure 3.4B,D. In these figures, ribonucleases that are internalized at a higher rate (Figure 3.4B) are not necessarily more cytotoxic (Figure 3.4) because they are also bound more tightly by RI (Figure 3.4D).

Finally, the Coulombic interactions characterized herein could have clinical significance. Cells derived from cancerous tissue tend to be more anionic than cells derived from similar normal tissue (Slivinsky et al. 1997; Orntoft and Vestergaard 1999). In contrast, RI levels are constant in cells with a cancerous and noncancerous origin (Haigis

et al. 2003). Accordingly, variation in the position of the extracellular equilibrium (Figure 3.5) could contribute to the therapeutic index of ONC and other ribonucleases.

### **3.6 Conclusions**

Understanding how cationic proteins enter human cells and exerting control over this process portends the development of better chemotherapeutics. Toward this end, we developed a method to quantitate the effect of the net charge of a ribonuclease on its cellular internalization. We found ribonuclease internalization to be related linearly to net charge and to reach a steady-state level of internalization based on that net charge. These two characteristics suggest that ribonuclease internalization is controlled by an extracellular equilibrium formed between ribonuclease molecules free in solution and those bound to anionic moieties on the cell surface. This extracellular equilibrium is then counteracted by an intracellular equilibrium in which more cationic ribonucleases bind more tightly to RI. Thus, these two equilibria cause cells to entice and then entrap ribonucleases.

Table 3.1: Properties of Wild-Type RNase 1 and its Variants

RNase 1 <sup>a</sup>	$T_m$ (°C) <sup>b</sup>	$k_{cat}/K_M$ <sup>c</sup> ( $10^6 \text{ M}^{-1}\text{s}^{-1}$ )	$K_d$ (nM) <sup>d</sup>	$IC_{50}$ ( $\mu\text{M}$ ) <sup>e</sup>	$Z$
wild type <sup>f</sup>	57	$21 \pm 2$	$29 \times 10^{-8}$ <sup>f</sup>	>25	+6
DDADD <sup>f</sup>	58	$6.3 \pm 0.5$	$(1.7 \pm 0.5) \times 10^3$	$13.3 \pm 1.7$	0
LLALL <sup>f</sup>	65	$30 \pm 3$	$30 \pm 1$	>25	+4
DRRDD	53	$14 \pm 3$	$28 \pm 4$	$5.69 \pm 0.37$	+3
DRRRD	49	$6.7 \pm 0.6$	$1.3 \pm 0.2$	$10.8 \pm 0.93$	+5
LRRDD	54	$19 \pm 2$	$1.8 \pm 0.1$	$16.2 \pm 1.3$	+4
LRRRD	53	$9.1 \pm 2$	$1.1 \pm 0.2$	>25	+6

<sup>a</sup> RNase 1 variants are named according to their amino acid composition at residues 39, 67, 88, 89, and 91. Hence, DDADD RNase 1 refers to the R39D/N67D/N88A/G89D/R91D variant.

<sup>b</sup> Values of  $T_m$  ( $\pm 2$  °C) were determined in PBS by UV spectroscopy.

<sup>c</sup> Values of  $k_{cat}/K_M$  ( $\pm$ SE) were determined for catalysis of 6-FAM-dArU(dA)<sub>2</sub>-6-TAMRA cleavage at 25 °C in 0.10 M MES-NaOH buffer (OVS-free), pH 6.0, containing 0.10 M NaCl and were calculated with eq 1.

<sup>d</sup> Values of  $K_d$  ( $\pm$ SE) were determined for the complex with human RI (eq 2) at 25 °C.

<sup>e</sup> Values of  $IC_{50}$  ( $\pm$ SE) are for incorporation of [*methyl*-<sup>3</sup>H]thymidine into the DNA of K-562 cells treated with the ribonuclease, and were calculated with eq 3.

<sup>f</sup> From ref. (Johnson et al. 2007c).

**Figure 3.1** Design of ribonuclease variants and latent fluorophore. (A) Ribbon diagram of RNase 1 (PDB entry 1Z7X, chain Z). Residues substituted herein are depicted in red. The image was created with the program PyMOL (DeLano Scientific, South San Francisco, CA). (B) Structure of latent fluorophore before and after activation by cellular esterases. (C,D) Confocal microscopy images of unwashed K-562 cells incubated at 37 °C for 30 min with fluorescein-labeled RNase 1 (10  $\mu$ M; C) or latent fluorophore-labeled RNase 1 (10  $\mu$ M; D). Nuclei were stained by adding Hoechst 33342 (2  $\mu$ g/mL) during the final 5 min of incubation. Insets: bright-field images. Scale bar: 10  $\mu$ m.

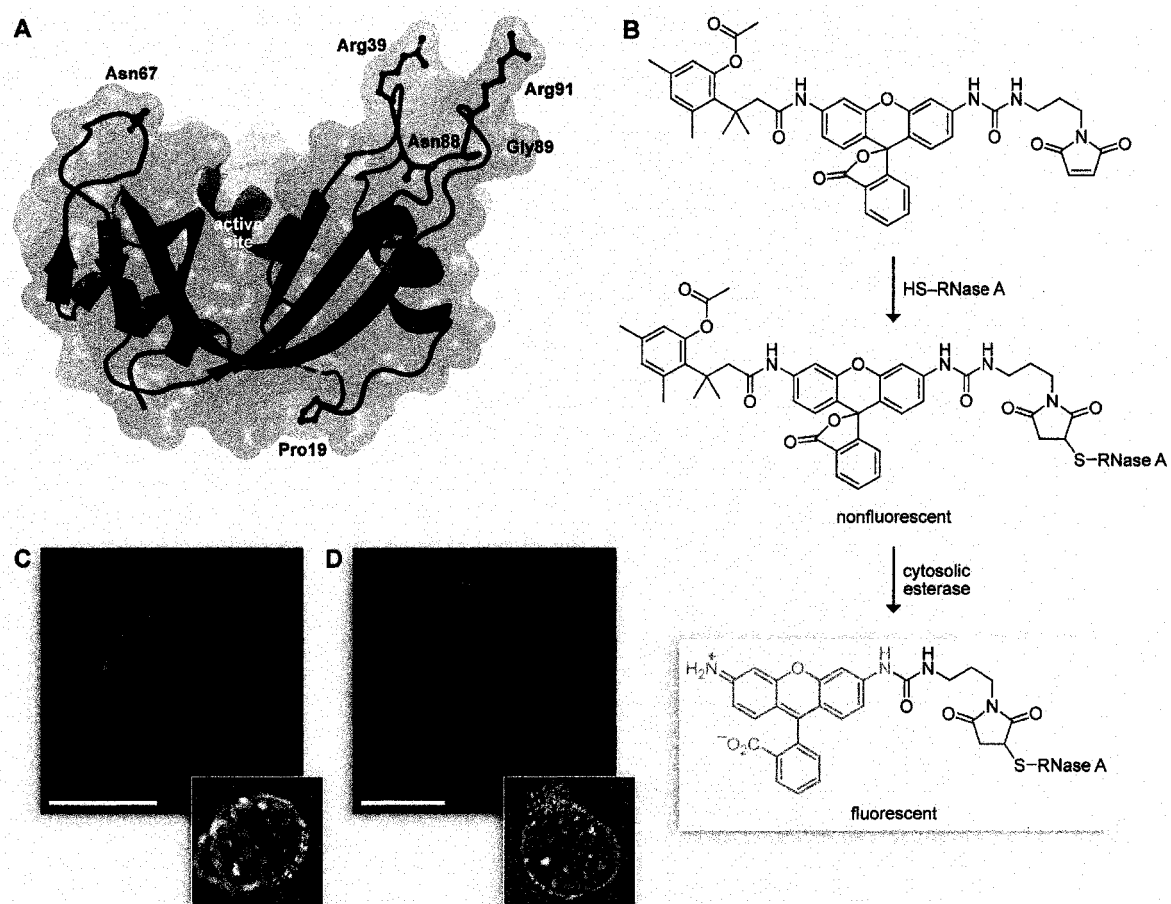




**Figure 3.2** Cytotoxicity of ribonuclease variants. Effect of ribonucleases on the proliferation of K-562 cells was determined by monitoring the incorporation of [*methyl*-<sup>3</sup>H]thymidine into cellular DNA in the presence of ribonucleases. Data points are mean values ( $\pm$ SE) from  $\geq 3$  experiments, each carried out in triplicate, and were fitted to eq 3. Variants in order of increasing cytotoxicity: D38R/R39D/N67R/G88R RNase A ( $\diamond$ ); DRRDD RNase 1 ( $\blacklozenge$ ); DRRRD RNase 1 ( $\blacktriangledown$ ); DDADD RNase 1 ( $\bullet$ ); LRRDD RNase 1 ( $\blacktriangle$ ); LRRRD RNase 1 ( $\blacksquare$ ); and wild-type RNase 1 ( $\circ$ ).

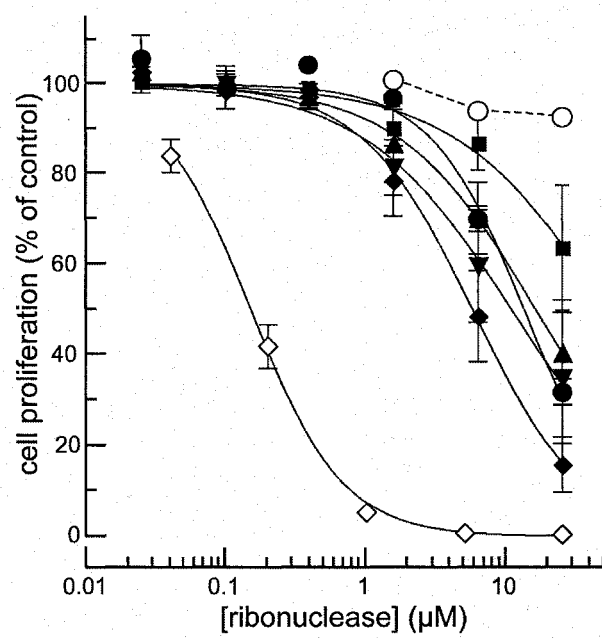


**Figure 3.3** Kinetics of ribonuclease internalization. (A) Initial velocity of cellular internalization versus time ( $\leq 2$  h). Internalization was determined by incubating latent fluorophore-labeled RNase 1 ( $\circ$ ) with K-562 cells at 37 °C. Incubations were quenched at known times by immersing the K-562 cells in ice-cold PBS and storing them on ice before quantitation by flow cytometry. Data points are mean values ( $\pm$ SE) from  $\geq 3$  cell populations. (B) Confocal microscopy images of unwashed K-562 cells incubated at 37 °C for varying time periods (0–6 h) with latent fluorophore-labeled RNase 1 (10  $\mu$ M). Nuclei were stained by adding Hoechst 33342 (2  $\mu$ g/mL) during the final 5 min of incubation. Scale bar: 10  $\mu$ m.

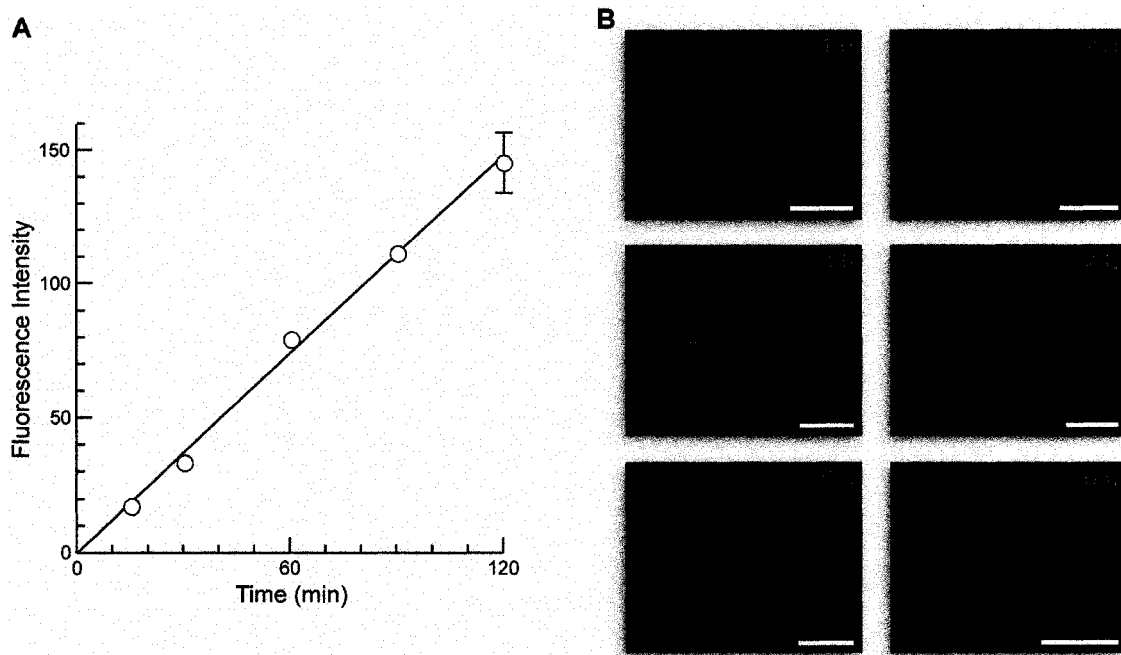


**Figure 3.4** Properties of RNase 1, its variants, and RNase A: wild-type RNase 1 ( $\circ$ ), DDADD RNase 1 ( $\bullet$ ), DRRDD RNase 1 ( $\blacklozenge$ ), LRRDD RNase 1 ( $\blacktriangle$ ), LLALL RNase 1 ( $\square$ ), DRRRD RNase 1 ( $\blacktriangledown$ ), LRRRD RNase 1 ( $\blacksquare$ ), and wild-type RNase A ( $\diamond$ ). (A) Plot of internalization of a ribonuclease into K-562 cells *versus* time. Internalization was measured by using flow cytometry and following the fluorescence manifested by activation of a latent fluorophore attached to the ribonuclease (10  $\mu$ M) after incubation for the specified times points. Data points are mean values ( $\pm$ SE) for 20,000 cells from  $\geq$  3 cell populations, and were fitted to eq 4. (B) Plot of internalization of a ribonuclease into K-562 cells *versus* its net charge. Internalization was monitored as in panel A, except that all incubations were for 30 min at 37  $^{\circ}$ C. (C) Plot of internalization of a ribonuclease into K-562 cells *versus* its concentration. Internalization was followed as in panel A, except for the variable concentration of ribonuclease (0.1, 1.0, or 10  $\mu$ M). (D) Semilog plot of affinity of a ribonuclease for RI *versus* its net charge. Data points are mean values ( $\pm$ SE). Variants of RNase 1 from ref are indicated by an asterick and their amino acids at positions 39, 67, 88, 89, and 91, with “–” indicating the wild-type residue.

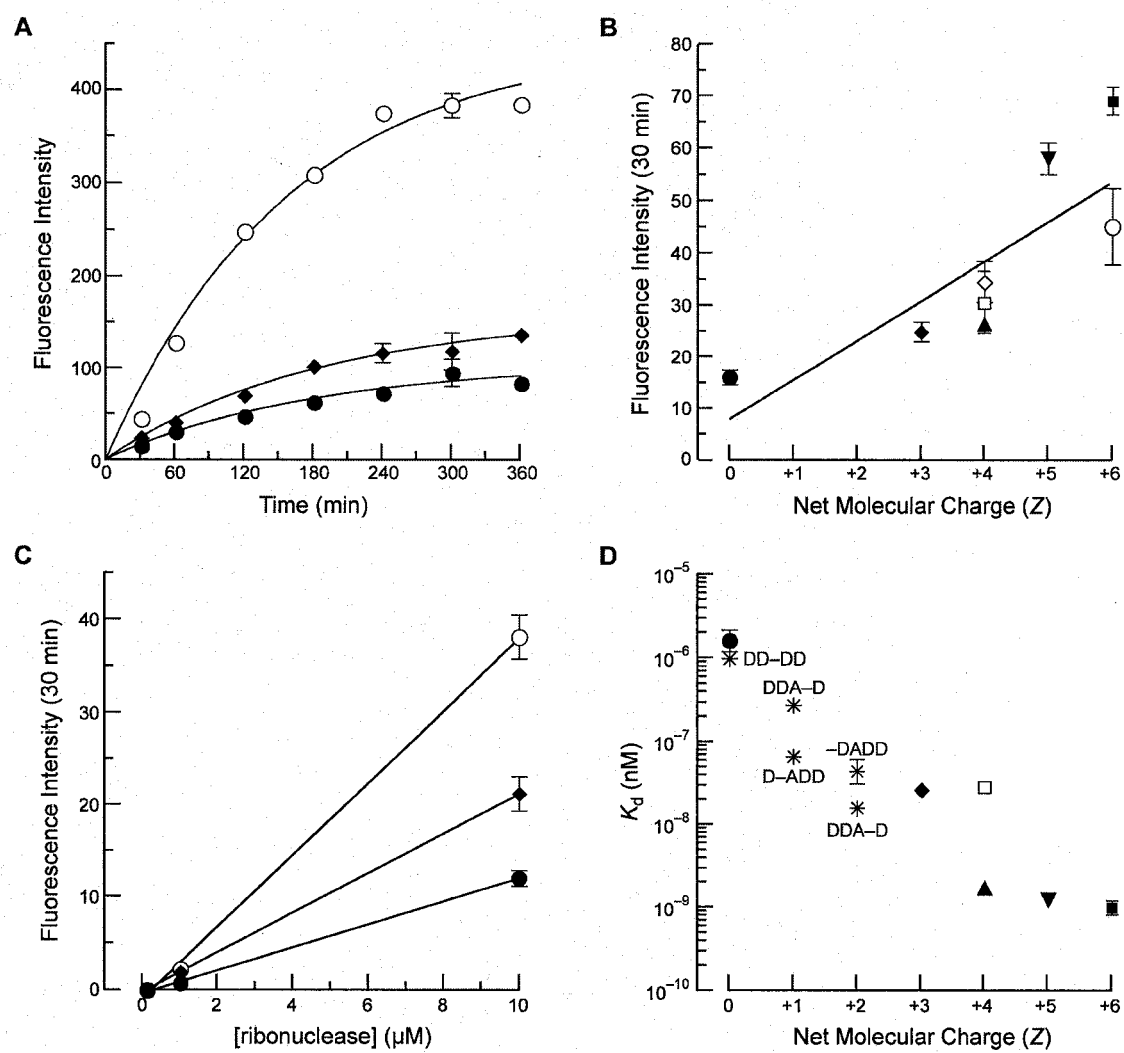
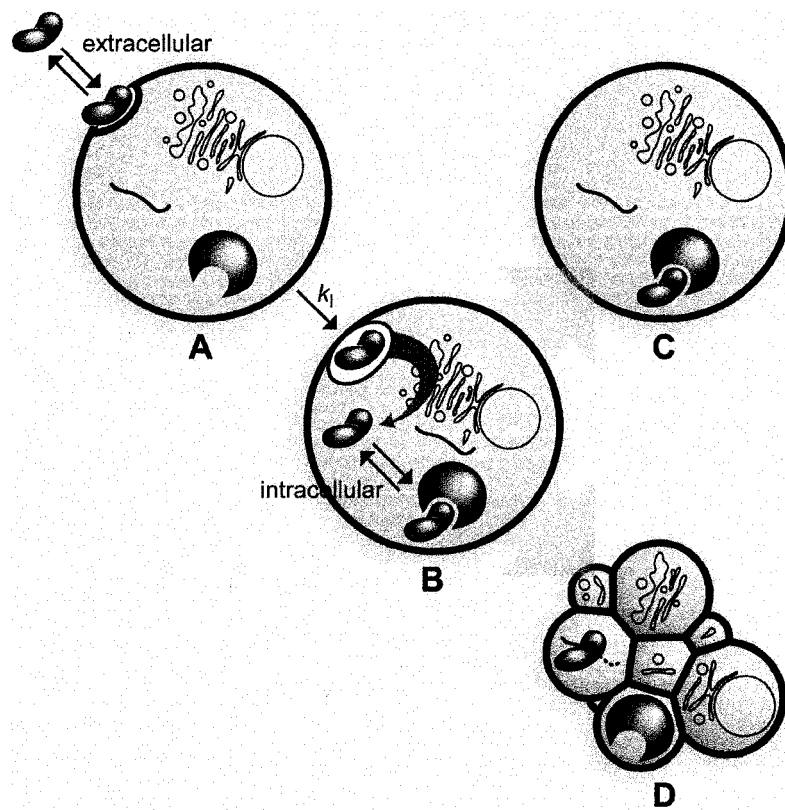


**Figure 3.5** Coulombic effects on ribonuclease-mediated cytotoxicity. Cationic and anionic molecules are depicted in blue and red, respectively. (A) Ribonucleases form an extracellular equilibrium complex with abundant anionic cell-surface molecules, such as heparan sulfate. Bound ribonucleases are internalized into endosomes with rate constant  $k_i$ . (B) Internalized ribonucleases translocate to the cytosol by an unknown mechanism. (C) In the cytosol, ribonucleases form an intracellular equilibrium complex with RI. (D) Ribonucleases that evade RI degrade cellular RNA, leading to apoptosis.





## **Chapter Four**

### **Intraspecies Regulation of Ribonucleolytic Activity**

Portions of this chapter are in preparation for publication as:

Johnson, R.J., Lavis, L.D., Raines, R.T. (2007) Intraspecies Regulation of Ribonucleolytic Activity. Submitted. I performed all of the research described in this chapter, except the synthesis of diethylfluorescein and development of methods for the oxidative resistance experiment (LD Lavis).

#### 4.1 Abstract

**ABSTRACT:** The evolutionary rate of proteins involved in obligate protein–protein interactions is slower and the degree of co-evolution higher than that for non-obligate protein–protein interactions. The co-evolution of the proteins involved in certain non-obligate interactions is, however, essential to cell survival. To gain insight into the co-evolution of one such non-obligate protein pair, the ribonuclease inhibitor (RI) proteins and pancreatic ribonucleases from cow (*Bos taurus*) and human (*Homo sapiens*) were produced in *Escherichia coli* and purified, and their physicochemical properties were analyzed. The two intraspecies complexes are found to be extremely tight (bovine  $K_d = 0.69$  fM; human  $K_d = 0.34$  fM). Human RI binds to its cognate ribonuclease (RNase 1) with 100-fold higher affinity than to the bovine ribonuclease (RNase A). In contrast, bovine RI binds to RNase 1 and RNase A with nearly equal affinity. This broader specificity is consistent with there being more pancreatic-type ribonucleases in cows (20) than humans (13). Human RI also has 4-fold less resistance to oxidation by hydrogen peroxide than does bovine RI. This decreased oxidative stability of human RI, which is caused largely by Cys74, implies a larger role for human RI in regulating cellular redox homeostasis. The oxidative and conformational stabilities of both RIs increase upon complex formation with ribonucleases, indicating that RI has evolved to maintain its tight regulation of ribonucleases, even when confronted with extreme environmental stress. Thus, the role of RI in protecting cells from ribonucleolytic activity seems to supplant its role in regulating oxidative damage, as even under extreme oxidative stress, it remains bound to ribonucleases.

## 4.2 Introduction

The discovery of extensive protein–protein interaction networks has facilitated investigations on protein evolution (Gavin et al. 2002; Ho et al. 2002; Krogan et al. 2006). For example, the rate of evolution within a protein–protein interaction network, has been found to depend on the number of binding partners, the concentration of each protein, and the evolutionary age of the proteins (Fraser et al. 2002; Lemos et al. 2004; Hahn and Kern 2005; Mintseris and Weng 2005; He and Zhang 2006; Liao et al. 2006; Saeed and Deane 2006). These relationships extend to subclasses of interactions, as obligate protein–protein interactions, which are defined as interactions necessary for the stability of an individual protein (Nooren and Thornton 2003), evolve at a slower rate and show a greater degree of co-evolution than do non-obligate interactions, which are interactions between proteins that can remain stable independently (Mintseris and Weng 2005). Nonetheless, the co-evolution of certain non-obligate protein–protein interactions, such as particular receptor–ligand and enzyme–inhibitor interactions, can be essential for cell survival (Nooren and Thornton 2003). To understand the co-evolution of such a non-obligate pair, we have investigated the complex formed between the cytosolic ribonuclease inhibitor protein (RI)<sup>1</sup> and ribonucleases, where failure to inhibit ribonucleolytic activity can lead to cell death (Leland et al. 1998; Raines 1998; Leland and Raines 2001; Smith and Raines 2006).

The ribonuclease A superfamily is a vertebrate-specific family of enzymes that has undergone rapid evolution by positive selection (Beintema 1987; Beintema et al. 1988b; Beintema et al. 1997; Zhang et al. 1998; Singhania et al. 1999). The superfamily has expanded rapidly (Cho et al. 2005; Cho and Zhang 2006), with only three members in fish

(*Danio rerio*) (Pizzo et al. 2006) and chicken (*Gallus gallus*) (Cho et al. 2005; Nitto et al. 2006), but 20 and 13 members in cow (*Bos taurus*) (Cho and Zhang 2006) and human (*Homo sapiens*) (Cho et al. 2005), respectively. Ribonucleases are controlled by the tight inhibition of RI (Haigis et al. 2003; Dickson et al. 2005), which binds to some members of the ribonuclease A superfamily with affinities in the femtomolar range (Lee et al. 1989b; Johnson et al. 2007c). RI is able to exert this affinity using its large concave surface area (Kobe and Deisenhofer 1995; 1996; Johnson et al. 2007c), even though the sequence identity among superfamily members is <30% (Dickson et al. 2005; Johnson et al. 2007c). RI evolved rapidly by exon duplication around the time of ribonuclease expansion (Haigis et al. 2002a), suggesting co-evolution of the protein families, but this direct relationship has not been demonstrated (Dickson et al. 2005).

Despite RNase A being perhaps the most studied of all enzymes (Raines 1998), little is known about its cognate inhibitor, bovine RI (bRI). In contrast, human RI (hRI) is known to bind to ribonucleases from such evolutionary distant organisms as fish, chickens, and cows (Kobe and Deisenhofer 1995; 1996; Nitto et al. 2006; Pizzo et al. 2006). Yet, we demonstrated recently that the affinity of hRI for bovine pancreatic ribonuclease (RNase A; EC 3.1.27.5 (Raines 1998)) is significantly lower than that for human pancreatic ribonuclease (RNase 1), suggesting a co-evolution of affinity between RI and its species-specific ribonucleases (Johnson et al. 2007c).

Here, we report on the heterologous production, purification, and characterization of bRI. We find that bRI forms a highly stable complex with both RNase A and RNase 1. bRI is also found to be stabilized to both thermal and oxidative stress upon ribonuclease

binding. This and other findings provide insight into the molecular evolution of a non-obligate protein–protein interaction and its biological imperatives.

### 4.3 Experimental Procedures

*General.* *Escherichia coli* BL21 (DE3) cells and the plasmid pET22b(+) were from Novagen (Madison, WI). DNA oligonucleotides for PCR, sequencing, and mutagenesis were from Integrated DNA Technologies (Coralville, IA). Protein purification columns were from GE Healthcare (Piscataway, NJ). MES buffer (Sigma Chemical, St. Louis, MO) was purified by anion–exchange chromatography to remove trace amounts of oligomeric vinylsulfonic acid (Smith et al. 2003). Restriction and PCR enzymes were from Promega (Madison, WI). All other chemicals were of commercial grade or better, and were used without further purification.

Terrific broth (TB) contained (in 1.00 L) tryptone (12 g), yeast extract (24 g), glycerol (4 mL),  $\text{KH}_2\text{PO}_4$  (2.31 g), and  $\text{K}_2\text{HPO}_4$  (12.54 g). Phosphate-buffered saline (PBS), pH 7.4, contained (in 1.00 L) NaCl (8.0 g), KCl (2.0 g),  $\text{Na}_2\text{HPO}_4 \cdot 7\text{H}_2\text{O}$  (1.15 g),  $\text{KH}_2\text{PO}_4$  (2.0 g), and  $\text{NaN}_3$  (0.10 g).

Circular dichroism (CD) data were collected with a model 62A DS CD spectrometer (Aviv, Lakewood, NJ) equipped with a temperature controller. The molecular mass of each ribonuclease and RI was determined by matrix-assisted laser desorption/ionization–time-of-flight (MALDI–TOF) mass spectrometry using a Voyager-DE-PRO Biospectrometry Workstation (Applied Biosystems, Foster City, CA). CD and MALDI–TOF mass spectrometry experiments were performed at the campus Biophysics Instrumentation

Facility. The fluorescence intensity in microtiter plates was recorded in a Perkin–Elmer EnVision 2100 plate reader equipped with a FITC filter set (excitation at 485 nm with 14 nm bandwidth; emission at 535 nm with 25 nm bandwidth; dichroic mirror cutoff at 505 nm) in the campus W.M. Keck Center for Chemical Genomics.

*RI Cloning and Purification.* The sequence of bRI was identified by its hypothetical annotation in the GenBank database (<http://www.ncbi.nlm.nih.gov/Genbank/index.html>). bRI (gi:78369509) was labeled as “*Bos taurus* similar to ribonuclease inhibitor”. Its amino-acid sequence had 74% identity to that of hRI (Supplementary Figure 1) (Johnson et al. 2007c). DNA primers were designed to amplify the cDNA encoding bRI and to incorporate *Nde*I and *Hind*III restriction sites at the 5’ and 3’ ends, respectively. cDNA encoding bRI was amplified by PCR from a bovine brain cDNA library (BioChain Institute Inc., Hayward, CA). The PCR product was inserted into plasmid pCR4-TOPO (Invitrogen, Carlsbad, CA), and sequence analysis was performed to ensure proper amplification. The cDNA encoding bRI was then inserted into plasmid pET22b(+) for protein production. A plasmid that encodes hRI (Rutkoski et al. 2005; Johnson et al. 2007c) was used to create cysteine-residue variants of hRI using the Quikchange site-directed mutagenesis kit (Stratagene, La Jolla, CA). Both wild-type RI proteins and variants of hRI were produced and purified using the procedure described previously (Klink et al. 2001; Johnson et al. 2007c).

*Ribonuclease Purification and Labeling.* RNase 1, RNase A, and their free cysteine residue variants were purified from inclusion bodies using the oxidative folding procedure described previously (Rutkoski et al. 2005; Johnson et al. 2007c). Plasmids containing

DNA encoding wild-type RNase 1 and RNase A were used to create variants with a free cysteine residue at position 19 (Lavis et al. 2006; Johnson et al. 2007c) using the Quikchange site-directed mutagenesis kit (Stratagene, La Jolla, CA). Position 19 was chosen as the attachment site, because attachment of fluorescent groups at this position does not have a detectable effect on the ribonucleolytic activity or RI-affinity of the resulting variants (Abel et al. 2002; Haigis et al. 2003). Variants of RNase 1 and RNase A with a free cysteine were initially protected by reaction with 5,5'-dithio-bis(2-nitrobenzoic acid) (DTNB) (Riddles et al. 1983; Lavis et al. 2006; Johnson et al. 2007c). Immediately before fluorophore attachment, protected variants were deprotected by using a 3-fold molar excess of dithiothreitol (DTT) and desalted by chromatography using a PD-10 desalting column (Amersham Biosciences, Piscataway, NJ). Deprotected ribonuclease variants were reacted for 4–6 h at 25 °C with a 10-fold molar excess of 2',7'-diethylfluorescein-5-iodoacetamide, which was synthesized as described previously (Lavis et al. 2007). Diethylfluorescein-labeled ribonucleases were purified by chromatography using a HiTrap SP FF column. The molecular masses of RNase 1, RNase A, their variants, and conjugates were confirmed by MALDI-TOF mass spectrometry.

*Dissociation Rate.* The dissociation rates of the RI-ribonuclease complexes were determined by using a procedure described previously (Johnson et al. 2007c). Briefly, diethylfluorescein-labeled ribonuclease (100 nM) in D-PBS containing tris(2-carboxyethyl)phosphine (TCEP, 0.10 mM) and bovine serum albumin (BSA, 0.10 mg·mL<sup>-1</sup>; Sigma Chemical) was added to a 96-well microtiter plate, and the initial fluorescence was measured. RI was then added at equimolar concentrations (100 nM) and incubated

with a labeled ribonuclease at 25 °C for 5 min. A 50-fold molar excess of human angiogenin (5  $\mu$ M) (purified as described previously (Leland et al. 2002)) was added to scavenge dissociated RI, and the change in fluorescence was measured at various time points. To ensure that the stability of the proteins was maintained over the extended duration of the experiment, additional data points were monitored under the same conditions, only without the addition of angiogenin. Data are the mean ( $\pm$ SE) of six replicates standardized for the mean fluorescence of six replicates of a rhodamine 110 standard (10 nM) and normalized for the fluorescence before RI addition ( $F_0$ ) and for the maximum fluorescence change of the fully dissociated hRI·RNase A complex. Fluorescence data were fitted to eq 1 with the program GraphPad Prism 4.02 (GraphPad Software, San Diego, CA) to determine the dissociation rate ( $k_d$ ), wherein  $F_0$  is the fluorescence before the addition of angiogenin, and  $F_\infty$  is the fluorescence before RI addition. Initial fluorescence data (<4 h) were not included in the analysis of RI·RNase 1 complexes, as they showed a rapid burst in fluorescence similar to that observed in previous dissociation rate determinations (Lee et al. 1989b; Johnson et al. 2007c). Initial fluorescence data were, however, included in the analysis of the RI·RNase A complexes, as the fluorescence change for their dissociation was greater than the initial burst.

$$F = F_0 + (F_\infty - F_0)(1 - e^{-k_d t}) \quad (\text{eq 1})$$

*Conformation and Conformational Stability.* CD spectroscopy was used to assess the secondary structural conformation of RI-ribonuclease complexes (Johnson et al. 2006).



Complexes between RI (25  $\mu$ M) and ribonuclease (28  $\mu$ M) were formed by incubation in PBS containing DTT (2 mM) at 25 °C for 30 min. A slight molar excess of ribonuclease was added to ensure that all RI molecules were complexed with ribonuclease. The CD signal contributed by the excess ribonuclease was then masked by the higher CD signal from RI. Additionally, free ribonuclease (28  $\mu$ M) and free RI (25  $\mu$ M) were prepared for CD measurement using conditions identical to those used to prepare RI-ribonuclease complexes. CD spectra were acquired from 260 to 205 nm in 1-nm increments at 25 °C, and the background CD spectrum of PBS containing DTT (2 mM) was subtracted from each spectrum. CD spectra are shown as the mean residue weight ellipticity at each wavelength (Johnson et al. 2007b).

CD spectroscopy was also used to evaluate the conformational stability of the RI-ribonuclease complexes (Johnson et al. 2006). The preparation of free RI, free ribonuclease, and RI-ribonuclease complexes was the same as for CD spectra determination. Protein solutions were heated from 25 °C to 75 °C in 2-°C increments. The change in molar ellipticity at 222 nm was measured after a 2-min equilibration at each temperature. CD data at 222 nm were fitted to a two-state model with the program GraphPad Prism 4.02 to determine the values of  $T_m$  (Becktel and Schellman 1987; Pace 1990).

*Oxidative Stability.* The stability of RI and RI-ribonuclease complexes to oxidation by hydrogen peroxide ( $H_2O_2$ ) was assessed by using a method similar to that described previously (Kim et al. 1999), except that the decrease in the fluorescence of diethylfluorescein-labeled ribonuclease upon RI-binding was used to quantitate binding

instead of indirectly following RI-binding through measurement of ribonucleolytic activity (Abel et al. 2002; Lavis et al. 2007). Immediately prior to assaying oxidative stability, purified RI was dialyzed for 16 h at 4 °C against 20 mM Hepes–HCl buffer, pH 7.6, containing KCl (50 mM) and DTT (200 µM), such that the final concentration of DTT in the H<sub>2</sub>O<sub>2</sub> reactions was ≤50 µM. Fresh H<sub>2</sub>O<sub>2</sub> (30% v/v, Fisher Scientific, Fair Lawn, NJ or Sigma Chemical) was diluted to 2% v/v in 20 mM Hepes–HCl buffer, pH 7.6, containing KCl (50 µM) (Buffer A). H<sub>2</sub>O<sub>2</sub> solution (2% v/v) was then serially diluted (10 solutions of 56:100) with Buffer A (final range = 1–0.003% v/v H<sub>2</sub>O<sub>2</sub>). RI-ribonuclease complexes were formed between RI (10 µM) and ribonuclease (10 µM) in Buffer A and incubated for 15 min at 23 °C prior to H<sub>2</sub>O<sub>2</sub> treatment. Free RI and ribonuclease were treated identically with the same volume of Buffer A. H<sub>2</sub>O<sub>2</sub> dilutions (5 µL) and RI, ribonuclease, or RI-ribonuclease complex (5 µL of a 10 µM solution) were added jointly to a 96-well PCR plate (Bio-Rad Laboratories, Hercules, CA). Plates were heated at 37 °C for 30 min in a PTC-100 thermal cycler equipped with a heated lid (Bio-Rad Laboratories). After 30 min, Buffer A (10 µL) was added to RI-ribonuclease complex and ribonuclease wells, RNase 1 (10 µL of a 5 µM solution) was added to hRI wells, and RNase A (10 µL of a 5 µM solution) was added to bRI wells. Plates were incubated for an additional 5 min in the thermocycler at 37 °C, and an aliquot (8 µL) from each well was then added to D-PBS (392 µL, Invitrogen, Grand Island, NY) containing BSA (0.10 mg·mL<sup>-1</sup>) and DTT (5 mM). To quantitate the fluorescence change upon RI-binding, an aliquot (100 µL) from the D-PBS dilution was transferred to a 96-well black non-binding surface polystyrene plate (Corning, Corning, NY). Data were converted to the fraction of RI oxidized by

normalizing for the fluorescence of the unbound complex and were fitted to eq 2 to determine  $IC_{50}$  values. The fluorescence intensity of diethylfluorescein-labeled ribonucleases remained constant over the range of  $H_2O_2$  concentrations used in the assay, indicating that any change observed was not due to an effect of  $H_2O_2$  on the fluorophore or free ribonuclease.

$$y = \frac{100\%}{1 + 10^{(\log(IC_{50}) - \log[H_2O_2])^h}} \quad (\text{eq 2})$$

*Sequence and Phylogenetic Analysis.* Sequence alignments of RI and ribonuclease (Figure 1 and Supplementary Figures 1–3) were performed with the program Clustal W (Chenna et al. 2003). Cladograms of RI and ribonuclease were made with the program MegAlign in the Lasergene software package (DNASTAR, Madison, WI). Bootstrap values were calculated by using 2,000 replicates, and values >40 are reported. Accession codes for RI sequences used for alignment are *Bos taurus* (gi: 78369509), *Rattus norvegicus* (gi: 77416905), *Mus musculus* (gi: 78099143), *Gallus gallus* (gi: 57529989), *Sus scrofa* (gi: 1942101), *Pan troglodytes* (gi: 38503347), *Homo sapiens* (gi: 71042211). Accession codes for ribonuclease sequences used for alignment are *Bos taurus* brain (gi: 27806923), *Bos taurus* seminal (gi: 32441267), *Bos taurus* pancreatic (gi: 48429071), *Rattus norvegicus* (gi: 71361661), *Mus musculus* (gi: 133221), *Gallus gallus* (gi: 45383972), *Sus scrofa* (gi: 133225), *Pan troglodytes* (gi: 38503271), *Homo sapiens* (gi: 71042210).

#### 4.4 Results

With their large concave surface areas, the structural family of leucine-rich repeats (LRRs), for which RI is the prototype, is well-suited to recognize diverse ligands (Figure 1A) (McEwan et al. 2006). Accordingly, RI has served as a structural model for protein–protein recognition (Dickson et al. 2005). Multiple biological roles have been assigned to RI, including protecting cells from rogue ribonucleases and scavenging free radicals (Haigis et al. 2003; Dickson et al. 2005; Wang and Li 2006; Monti et al. 2007). The latter activity is attributed to the 29–32 free cysteine residues found in RI, whose oxidation leads to irreversible inactivation of the protein (Kim et al. 1999; Park and Raines 2001).

The amino-acid sequences of RIs from multiple organisms (Supplementary Figure 2) have been reported, and some of these proteins have been characterized (Burton et al. 1980; Burton and Fucci 1982; Hofsteenge et al. 1988; Lee et al. 1988; Kawanomoto et al. 1992). In 1980, bRI was isolated and found to inhibit ribonucleolytic activity (Burton et al. 1980). Its amino-acid sequence and biochemical characteristics were, however, unknown (Burton et al. 1980; Wang and Li 2006). The amino acid sequence of bRI (Figure 1B) was annotated in the GenBank registry as “*Bos taurus* similar to ribonuclease inhibitor” (gi:78369509). The sequence of bRI was 74% identical to hRI (Supplementary Figure 1) and had the consensus A-Type and B-Type repeating architecture of ribonuclease inhibitors (Figure 1B) (Dickson et al. 2005). bRI contains 29 of the 32 cysteine residues in hRI and was able to be produced and purified by a procedure identical to that used for hRI (Klink et al. 2001; Johnson et al. 2007c), yielding 5 mg of bRI per liter of *E. coli*

culture. bRI, hRI, and their complexes with RNase A and RNase 1 were then analyzed biochemically to understand the factors that influence complex stability and determine the biological necessity for intraspecies regulation of ribonucleolytic activity.

*Dissociation Rate for RI-Ribonuclease Complexes.* The RI-ribonuclease complex is one of the tightest known biological interactions (Lee et al. 1989b; Teufel et al. 2003; Johnson et al. 2007c). The association rate constant for complex formation between RI and ribonucleases is close to the diffusion limit ( $10^9 \text{ M}^{-1} \text{ s}^{-1}$ ) (Stone and Hofsteenge 1986; Lee et al. 1989b; Johnson et al. 2007c), due to the strong electrostatic nature of the interaction (Shaul and Schreiber 2005; Johnson et al. 2007c). Yet, the dissociation rate constants of the hRI-RNase 1 and hRI-RNase A complexes differ significantly, owing to differences in the hydrogen bonds and van der Waals contacts made between hRI and the two ribonucleases (Johnson et al. 2007c).

The dissociation rate constants for the complexes of bRI and hRI with RNase A and RNase 1 were determined by using a competition experiment described previously (Lee et al. 1989b; Johnson et al. 2007c). The observed increase in fluorescence as the RI-ribonuclease complex dissociates is shown in Figure 2, and the  $k_d$  values determined by fitting the resulting data to eq 1 are listed in Table 1. Only the hRI-RNase A complex dissociated completely over the length of the experiment (Figure 2A) with a  $t_{1/2}$  ( $= \ln 2/k_d$ ) of 14 h, which is nearly identical to the value determined previously (13 h) (Lee et al. 1989b). All of the other RI-ribonuclease complexes were <50% dissociated after 15 days (Figure 2). Their  $k_d$  values were within twofold of each other (Table 1) and their  $t_{1/2}$  values (34 days for bRI-RNase A, 78 days for bRI-RNase 1, and 68 days for hRI-RNase 1) were

within twofold of that for the hRI-angiogenin complex ( $t_{1/2} = 60$  days) (Lee et al. 1989b). The clustering of the  $k_d$  values of the most stable RI-ribonuclease complexes suggests that an upper limit for the half-lives of the dissociation rate of an RI-ribonuclease complex has been reached at approximately three months (Table 1) (Lee et al. 1989b).

By assuming that all of the complexes have association rate constants close to the diffusion limit (Johnson et al. 2007c), the equilibrium dissociation constants ( $K_d$ ) of the complexes can be estimated. The  $K_d$  values for the bRI-RNase A, bRI-RNase 1, and hRI-RNase 1 complexes are between 0.30–0.69 fM, whereas the hRI-RNase A complex has at least 50-fold lower stability (30 fM) (Table 1). Overall, both bRI and hRI are tight inhibitors of ribonucleases, but bRI binds more tightly to both human and bovine ribonucleases.

*Conformation and Conformational Stability.* Proteins are stabilized upon binding to small-molecule ligands (Sturtevant 1987; Brandts and Lin 1990; Hytonen et al. 2004; Mayhood and Windsor 2005) or with other proteins (Donovan and Beardslee 1975; Makarov et al. 1994). The magnitude of the stabilization is often related directly to the affinity of the protein for the ligand (Brandts and Lin 1990; Waldron and Murphy 2003; Mayhood and Windsor 2005). To determine whether the conformational stability of bRI and hRI increases upon complex formation and whether this increase correlates with complex stability, the conformational stability of each RI-ribonuclease complex was determined by CD spectroscopy (Figure 3) (Kelly et al. 2005; Mayhood and Windsor 2005; Johnson et al. 2006).

The far-UV CD spectra of free RI, free ribonuclease, and RI-ribonuclease complexes are depicted in Figures 3A and 3B. bRI and hRI have similar CD spectra, with a maxima at 222 nm being indicative of similar secondary structure and three-dimensional architecture (Kelly et al. 2005). When complexed with a ribonuclease, the maxima of the CD spectra for hRI and bRI shifts to 225 nm. Complexes between RI and ribonuclease were formed with a slight molar excess of ribonuclease (28  $\mu\text{M}$ ) to RI (25  $\mu\text{M}$ ) to ensure complete complex formation by RI and to allow accurate determination of the conformational stability of RI. The ellipticity of RI with its regular repeating  $\alpha$ -helix,  $\beta$ -strand architecture (Figure 1A) overwhelms the ellipticity of the ribonucleases (ellipticity bRI at  $[\theta]_{222\text{ nm}} = -14,100\text{ deg}\cdot\text{cm}^2\cdot\text{dmol}^{-1}$  and RNase A at  $[\theta]_{222\text{ nm}} = -7,600\text{ deg}\cdot\text{cm}^2\cdot\text{dmol}^{-1}$ ), making it possible to measure only the change in the conformational stability of RI upon complex formation (Figure 3A and B).

The stability of the RI-ribonuclease complexes as a function of temperature is shown in Figures 3C and 3D. The mid-points of each transition curve ( $T_m$ ) were obtained by fitting the data to a two-state model and are listed in Table 1 (Becktel and Schellman 1987). Unbound hRI ( $T_m = 54\text{ }^\circ\text{C}$ ) is slightly more stable than is unbound bRI ( $T_m = 51\text{ }^\circ\text{C}$ ), but bRI gains more stability upon forming a complex with either ribonuclease. The  $T_m$  values of both RIs increase by  $>10\text{ }^\circ\text{C}$  upon complex formation with ribonuclease. The hRI-RNase A complex was the least stable of the four complexes, in accord with its having the largest dissociation rate constant (Figure 2).

*Oxidative Stability.* With its 29–32 free cysteine residues and abundance in the cytosol, RI serves a regulatory role in redox homeostasis (Monti et al. 2007) and acts as a

scavenger of free radicals (Wang and Li 2006). RI scavenges reactive oxygen species such as superoxide anion, hydroxyl radical, and singlet oxygen with  $IC_{50}$  values below 10  $\mu\text{g/mL}$ , making it a powerful cellular antioxidant (Wang and Li 2006). To investigate the oxidative stability of bRI and hRI and to determine how complex formation affects their oxidative stability, the vulnerability of both RIs to oxidation by  $\text{H}_2\text{O}_2$  was tested (Trost 1991; Kim et al. 1999; Lavis et al. 2007).

The binding curves obtained after incubating bRI, hRI, or RI-ribonuclease complexes with  $\text{H}_2\text{O}_2$  are shown in Figure 4, and the  $IC_{50}$  values (% v/v  $\text{H}_2\text{O}_2$ ) are listed in Table 1. The oxidative stability value for hRI ( $IC_{50} = 0.017\%$  v/v  $\text{H}_2\text{O}_2$ ) was close to that measured previously by evaluating the inhibition of ribonucleolytic activity by hRI (0.007% v/v) (Kim et al. 1999). The oxidative stability of bRI (29 cysteine residues) (Figure 1B) was, however, 4-fold higher than that of hRI (32 cysteine residues). bRI has both of the adjacent cysteine pairs that were shown to be important to the oxidative resistance of hRI (Kim et al. 1999). Yet, native bRI has oxidative stability similar to that of previously characterized oxidation-resistant variants of hRI (Table 2) (Kim et al. 1999).

The decreased oxidative stability of hRI compared to bRI could be due to the replacement of three residues in bRI with cysteine in hRI (Figure 1). Two of these cysteine residues, Cys74 and Cys408 (hRI numbering), were attractive candidates for decreasing the oxidative stability. The sulfur atoms of Cys74 and Cys29 are within 6 Å and could form a destabilizing disulfide bond upon oxidation, as seen for adjacent free cysteine residues in hRI (Kim et al. 1999); Cys408 has the highest solvent accessible surface area of any cysteine residue in hRI, as calculated for chain Y from PDB accession code 1Z7X with



the program POPS (Cavallo et al. 2003). Both Cys74 and Cys408 in hRI were replaced with the corresponding residues in bRI, C74L and C408G, and the oxidative stabilities of the resulting variants are shown in Figure 4C. C408G hRI appears to be more sensitive to oxidation, as its stability curve shows a steeper transition to the oxidized form. In the three-dimensional structure of the hRI·RNase 1 complex (Johnson et al. 2007c), Cys408 forms molecular contacts with Asn67 of RNase 1. As oxidative stability is measured in relation to RI-binding, substitution of Cys408 with a glycine residue could weaken the affinity for RNase 1, making hRI more susceptible to rapid oxidation. Yet, C408G hRI ( $IC_{50} = (0.023 \pm 0.002) \% \text{ v/v } H_2O_2$ ) still has near identical oxidative stability to wild-type hRI, whereas C74L hRI ( $IC_{50} = (0.043 \pm 0.005) \% \text{ v/v } H_2O_2$ ) has 2.5-fold higher oxidative stability than wild-type hRI, putting its stability within twofold of that of bRI (Table 1). Substitution of position 74 with an additional cysteine residue in hRI serves to explain the additional sensitivity of hRI to oxidation and could represent an adaptative substitution that permits greater control over the concentration of RI based on the cellular redox environment.

Upon complex formation with RNase A, bRI gains an additional 4-fold in oxidative stability and remains stably bound to RNase A at up to 0.30% v/v  $H_2O_2$  (0.13 M  $H_2O_2$ ), again underscoring the extraordinary stability of the RI-ribonuclease complex. Surprisingly, complex formation with RNase 1 elicits a twofold decrease in the oxidative stability of bRI. This decrease could be due to changes in the bRI structure upon RNase 1 binding, as seen upon RNase A binding to porcine RI (Kobe and Deisenhofer 1995), allowing better access to reactive sulfhydryl groups. Additionally, RNase 1, being more cationic than RNase A (Johnson et al. 2007a), could preferentially shift the  $pK_a$  of nearby cysteine residues (Lavis

et al. 2007), thereby favoring the transition from the thiol (RSH) to the more reactive thiolate ( $RS^-$ ) form (Shaked et al. 1980; Szajewski and Whitesides 1980) and facilitating disulfide bond formation (Kim et al. 1999). hRI, in contrast, has slightly increased oxidative stability upon complex formation with both RNase A and RNase 1, respectively (Table 1). Overall, the oxidative stability of RI-ribonuclease complexes seems to mirror the conformational stability.

#### 4.5 Discussion

Unregulated ribonucleolytic activity is potentially damaging to essential cellular processes (Leland et al. 1998; Raines 1998; Leland et al. 2001; Smith and Raines 2006). To protect themselves, cells have evolved RI (Haigis et al. 2002a; Haigis et al. 2003; Dickson et al. 2005). RI might have co-evolved with its ribonuclease ligands (Haigis et al. 2002a; Dickson et al. 2005), as mammalian RIs do not bind to ribonuclease homologues from frogs (Tomita et al. 1979; Wu et al. 1993) and hRI has 100-fold higher affinity for human RNase 1 than for bovine RNase A (Johnson et al. 2007c). This relationship is not definitive, however, as two of three new ribonucleases identified from fish (*Danio rerio*) are bound by hRI (Pizzo et al. 2006).

The structural basis of the possible co-evolution of ribonucleases and RI (Figure 1A) has been elucidated for four RNase A superfamily members: RNase A, angiogenin (RNase 5), eosinophil-derived neurotoxin (RNase 2), and RNase 1 (Kobe and Deisenhofer 1995; 1996; Papageorgiou et al. 1997; Iyer et al. 2005; Johnson et al. 2007c). The structural contacts within the hRI-RNase 1 complex (PDB accession code 1Z7X) were

extracted and the conservation of these RI residues are compared in Table 2 (Johnson et al. 2007c). If RI and ribonuclease have co-evolved, contact residues are likely to be conserved between RI proteins. For example, bRI and chicken RI have amino acid sequence identities to hRI of 74 and 49%, respectively (Supplementary Figure 1), but for contact residues, the sequence identities to hRI are 93 and 61%, respectively (Table 2). The greater conservation of contact residues is consistent with the existence of selective pressure that maintains the high affinity of RI for ribonucleases. Also, a phylogenetic tree of these RI proteins from diverse organisms (Figure 5A) has an architecture and rate of evolution similar to that of the phylogenetic tree of ribonucleases from the same organisms (Figure 5B) (Hofsteenge et al. 1988; Lee et al. 1988; Kawanomoto et al. 1992). To gain insight into the co-evolution of affinity of this femtomolar protein–protein complex and to address whether an evolutionary imperative exists for species-specific regulation of ribonucleolytic activity, RI from cow and human were produced in *E. coli* and purified along with their cognate ribonucleases.

Binding of proteins to small ligands can increase the thermal stability of the protein through the influence of the ligand on the unfolding equilibrium of the protein (Sturtevant 1987; Brandts and Lin 1990; Waldron and Murphy 2003; Mayhood and Windsor 2005). The increase in thermal stability ( $\Delta T_m$ ) can be related directly to the binding affinity ( $K_d$ ) of the ligand for the protein (Matulis et al. 2005), but only when the association rates and binding enthalpies of the ligands are equivalent (Waldron and Murphy 2003). These same principles of thermal stabilization can also be applied to protein–protein complexes, where complex formation increases the thermal stability of the individual proteins (Donovan and

Beardslee 1975; Makarov et al. 1994). Both RI and ribonuclease are thermally stabilized upon RI-ribonuclease complex formation (Table 1). All of the complexes between bRI or hRI and ribonuclease have  $\Delta T_m > 10^\circ\text{C}$  from free RI, with the bRI-RNase A complex having the largest change at  $>17\text{--}18^\circ\text{C}$ . This  $\Delta T_m$  upon ligand binding for RI-ribonuclease complex is similar to the  $\Delta T_m$  measured for avidin upon complex formation with biotin ( $\Delta T_m = 33.5^\circ\text{C}$ ), another protein-ligand complex with femtomolar binding affinity (Hytonen et al. 2004). Additionally, the thermal stabilization of RI-ribonuclease complexes is similar to the barnase-barstar complex, the bacterial analogue of RI-ribonuclease (Makarov et al. 1994). The barnase-barstar complex, whose formation is essential to bacterial cell survival, has a  $\Delta T_m$  of  $20^\circ\text{C}$ , essential ribonuclease inhibitor-ribonuclease interactions have  $\Delta T_m$  in the  $10\text{--}20^\circ\text{C}$  range.

For RI-ribonuclease complexes,  $\Delta T_m$  should serve as a good indicator of binding affinity (Waldron and Murphy 2003; Matulis et al. 2005), as the association rates and the binding enthalpies for RNase 1 and RNase A should be nearly identical (Johnson et al. 2007c). The dissociation rate constants and  $\Delta T_m$  for RI-ribonuclease complexes do align (Table 1), as the hRI-RNase A complex has the fastest dissociation rate and the lowest  $\Delta T_m$  ( $10^\circ\text{C}$ ), whereas both bRI-ribonuclease complexes have identical  $k_d$  values and  $\Delta T_m$  values. This direct relationship between binding affinity and thermal stability suggests that the thermal stability of RI-ribonuclease complexes could be used in future studies to estimate their binding affinities.

Besides inhibiting ribonucleases, RI also serves a role in regulating cellular redox homeostasis, where it uses its 29–32 free cysteine residues to scavenge free radicals

(Blázquez et al. 1996; Wang and Li 2006; Monti et al. 2007). The oxidation of its cysteine residues to disulfide bonds leads to its rapid degradation in the cell (Blázquez et al. 1996). RI in primates seems to have evolved greater sensitivity to oxidation through the addition of a specific cysteine residue, Cys74 (Figure 4C), whose conversion to leucine increases the oxidative stability of hRI by 2.5-fold. This increased sensitivity of hRI to oxidation could facilitate greater regulation of the cellular concentration of hRI through modulation of the cellular redox environment and thus permit more sensitive control over ribonuclease biology.

Upon formation of a complex with an intraspecies ribonuclease, the oxidative stability of RI increases (Table 1 and Figure 4), lowering its availability to compensate for oxidative stress. Thus, the role of RI in regulating ribonucleolytic activity appears to supersede its role in regulating oxidative damage, as even under extreme oxidative stress (*e.g.*, 0.13 M H<sub>2</sub>O<sub>2</sub> for the bRI-RNase A complex), it remains bound to ribonucleases. Apparently, the two biological roles for RI (Dickson et al. 2005), regulating ribonucleases and redox homeostasis, are functionally distinct. Other cellular biomolecules can regulate the cellular redox environment (Valko et al. 2006), but no other cellular inhibitors of ribonucleases are known (Dickson et al. 2005). Consequently, RI needs to maintain its high affinity for ribonucleases in order to protect cellular RNA, even under severely oxidizing conditions (Leland et al. 1998; Raines 1998; Smith and Raines 2006).

The kinetic inhibition of ribonucleases by RI is essentially permanent, as both bRI and hRI bind RNase A and RNase 1 with  $K_d$  values that are below 30 fM and with  $t_{1/2}$  values for the complexes (except the hRI-RNase A complex) that extend beyond 5 weeks

(Table 1). Interestingly, bRI does not show the same species-specific affinity preference of hRI (Johnson et al. 2007c). Rather, bRI maintains broader specificity for ribonucleases (Table 1 and Figure 2) and greater oxidative stability than hRI (Figure 4). Cows have more ribonucleases (20; (Cho and Zhang 2006)) than do humans (13; (Cho et al. 2005)), including three with high similarity to RNase 1 from three different tissues (Figure 5B). Accordingly, bRI might need to maintain broader specificity so as to recognize more ribonucleases. Additionally, the biological role of RNase A is to digest dietary RNA in a cow stomach (Barnard 1969), but new biological roles for RNase 1 in vertebrates seem to be evolving, as bursts of gene duplication and gene deactivation are observed in *Carnivora* (Yu and Zhang 2006). hRI might be evolving new biological roles along with RNase 1 and adding new levels of cellular regulation through its sensitivity to oxidative stress. Addressing these evolutionary questions will require the purification and identification of RI proteins from additional organisms, and performing analyses similar to those performed for ribonucleases (Beintema et al. 1988a; Beintema et al. 1988b; Beintema et al. 1997; Cho et al. 2005; Cho and Zhang 2006).

#### 4.6 Conclusions

The complexes between RI and ribonucleases serve as an ideal model system to investigate the co-evolution of an essentially permanent protein–protein complex. To control ribonucleolytic activity and protect cells from damaging ribonucleolytic activity, the RI-ribonuclease complex remains intact when confronted by severe thermal or oxidative stress. Yet, hRI shows increased sensitivity to oxidation, largely due to Cys74,

suggesting greater regulation of the cellular concentration of hRI through modulation of the cellular redox environment. hRI also displays greater variation in binding affinity for ribonucleases, as it binds RNase 1 with significantly higher affinity than RNase A, whereas bRI maintains broader specificity, binding both ribonucleases with high affinity.

**Table 4.1:** Biochemical parameters for bRI, hRI, and RI-ribonuclease complexes.

	$k_d$ ( $10^{-7} \text{ s}^{-1}$ ) <sup>a</sup>	$K_d$ ( $10^{-16} \text{ M}$ ) <sup>b</sup>	$T_m$ ( $^{\circ}\text{C}$ ) <sup>c</sup>	$\text{IC}_{50}$ (% v/v $\text{H}_2\text{O}_2$ ) <sup>d</sup>
bRI	—	—	$51.3 \pm 0.1$	$0.071 \pm 0.010$
bRI-RNase A	$2.36 \pm 0.05$	6.9	$68.6 \pm 0.3$	$0.30 \pm 0.004$
bRI-RNase 1	$1.03 \pm 0.07$	3.0	$68.0 \pm 0.2$	$0.029 \pm 0.008$
hRI	—	—	$54.1 \pm 0.1$	$0.017 \pm 0.004$
hRI-RNase A	$119 \pm 2$	350	$64.2 \pm 0.1$	$0.042 \pm 0.016$
hRI-RNase 1	$1.17 \pm 0.05$	3.4	$66.6 \pm 0.2$	$0.028 \pm 0.004$

<sup>a</sup> Values of  $k_d$  ( $\pm$ SE) were determined by following the release of diethylfluorescein-labeled ribonuclease from the RI-ribonuclease complex over time and fitting the resulting data to eq 1.

<sup>b</sup> Values of  $K_d$  ( $\pm$ SE) were calculated using the relationship  $K_d = k_d/k_a$  and the  $k_a$  value for hRI + RNase A (Lee *et al.* 1989b).

<sup>c</sup> Values of  $T_m$  ( $\pm$ SE) were determined by CD spectroscopy in PBS containing DTT (2 mM).

<sup>d</sup> Values of  $\text{IC}_{50}$  ( $\pm$ SE) are for the oxidative stability to  $\text{H}_2\text{O}_2$  and were calculated with eq 2.

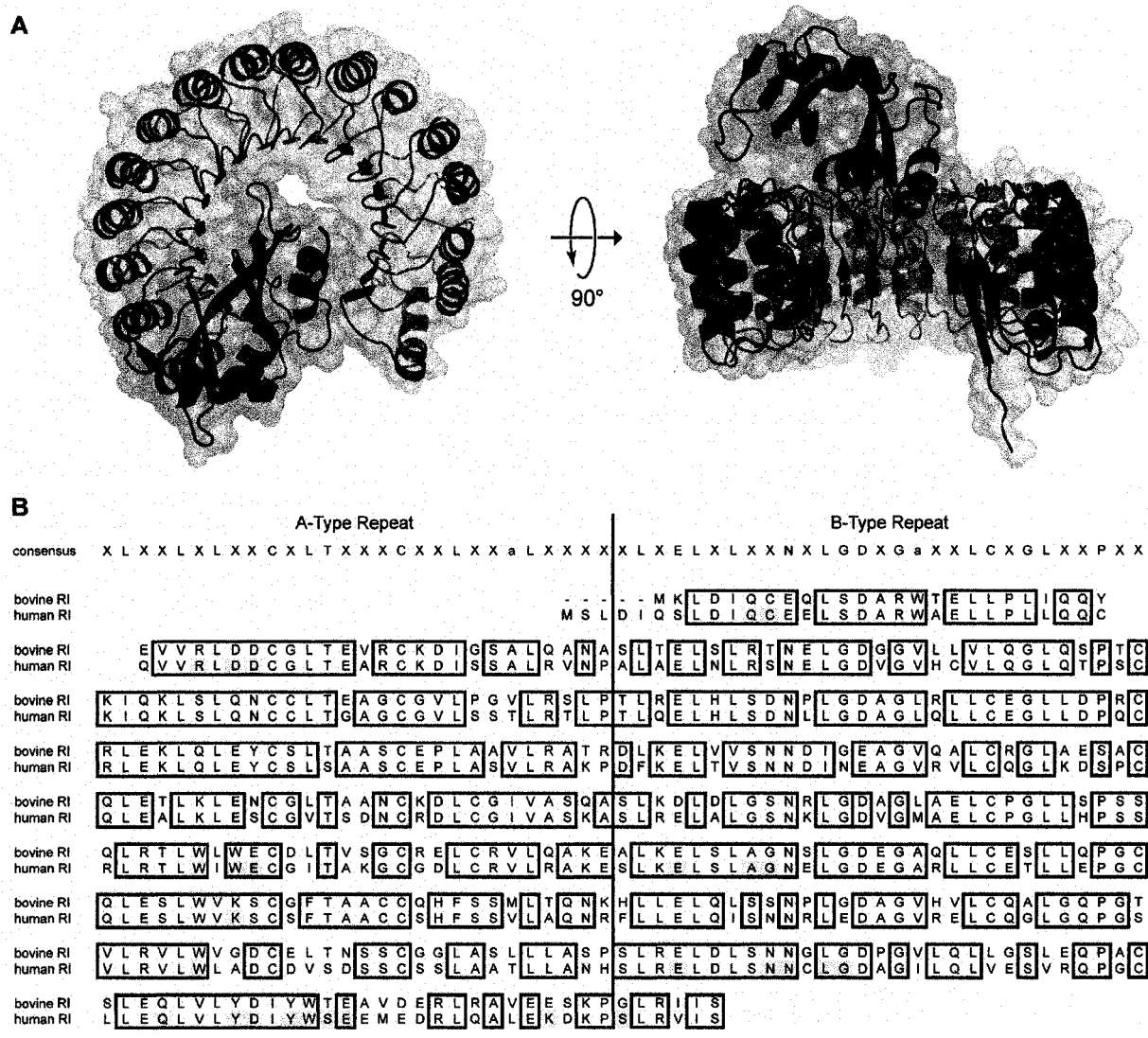


Table 4.2: Conservation of ribonuclease-contact residues in RIs<sup>a</sup>

human	chimp	cow	pig	mouse	rat	chicken
Q10	Q	Q	H	Q	Q	Q
C11	C	C	C	C	C	C
R33	R	R	R	R	R	R
R35	D	D	D	D	D	D
D36	D	D	D	D	D	D
W261	W	W	W	W	W	W
W263	W	W	W	W	W	W
E264	E	E	E	E	D	D
E287	E	E	E	E	E	E
A291	A	A	A	A	A	I
G292	G	G	G	S	G	D
K320	K	K	K	K	K	R
W375	W	W	C	W	W	W
E401	E	E	E	E	E	E
N406	N	N	N	N	N	Y
N407	N	N	N	N	N	N
C408	C	G	C	C	C	T
L409	L	L	V	M	M	L
G410	G	G	G	G	G	E
Q430	Q	Q	Q	Q	Q	Q
Y434	Y	Y	Y	Y	Y	Y
D435	D	D	D	D	D	D
Y437	Y	Y	Y	Y	Y	F
W438	W	W	W	W	W	W
S439	S	T	T	T	T	G
E440	E	E	E	N	D	P
R457	R	R	R	R	R	K
S460	S	S	S	S	S	S

<sup>a</sup> Contact residues for hRI-RNase 1 were taken from PDB accession code 1Z7X (chains Y and Z) (Johnson et al. 2007c). RI residues from other organisms are taken from the alignment in Figure 4.7.

**Figure 4.1** Structure and sequence of RI. (A) Ribbon diagram of the hRI (green)-RNase 1 (purple) complex (chains Y and Z from PDB accession code 1Z7X) (Johnson et al. 2007c). Images were made using PyMOL (DeLano Scientific, South San Francisco, CA). (B) Sequence alignment of the protein sequences of bRI and hRI. Conserved amino acids are shown with black boxes and contact residues ( $<3.9$  Å) within the hRI-RNase 1 complex are shaded yellow (chains Y and Z from PDB accession code 1Z7X) (Johnson et al. 2007c). Alignments were performed using the program Clustal W (Chenna et al. 2003). Consensus sequences for A-Type and B-Type repeats of RI-like LRRs were adapted from ref (Dickson et al.



**Figure 4.2** Dissociation of RI-ribonuclease complexes. The release of diethylfluorescein-labeled ribonuclease (100 nM) from RI (100 nM) was followed over time after the addition of a 50-fold molar excess of angiogenin (5  $\mu$ M) (open symbols) or after the addition of PBS (closed symbols). Data points are the mean ( $\pm$ SE) of six separate measurements and are normalized for the average fluorescence of rhodamine 110 (10 nM) and for the fluorescence of unbound RNase A from hRI·RNase A. The initial fluorescence of unbound ribonuclease was used as the end-point for complete ribonuclease release (Johnson et al. 2007c). (A) Dissociation of bRI·RNase A ( $\triangle$ ) and hRI·RNase A ( $\circ$ ); (B) Dissociation of bRI·RNase 1 ( $\square$ ) and hRI·RNase 1 ( $\diamond$ ).

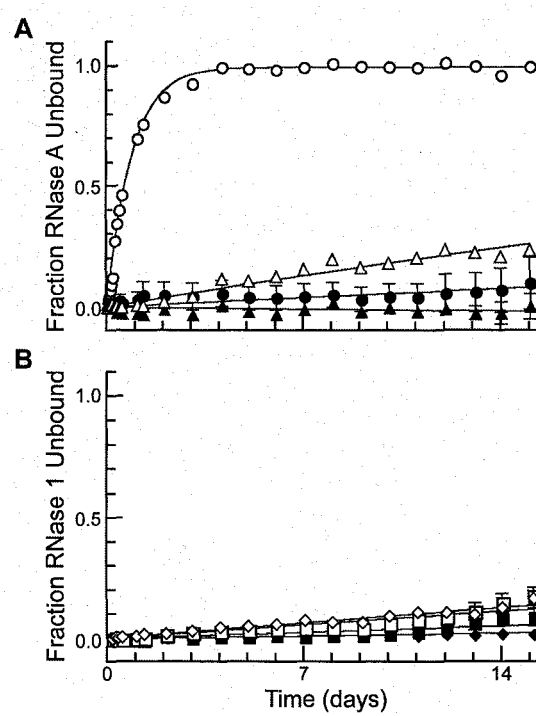


**Figure 4.3** Conformation and conformational stability of RI-ribonuclease complexes. (A and B) Far-UV CD spectra of RI, ribonuclease, and RI-ribonuclease complex (25  $\mu$ M RI and 28  $\mu$ M ribonuclease in PBS containing DTT (2 mM)). (C and D) Thermal denaturation of RI, ribonuclease, and RI-ribonuclease complex (25  $\mu$ M RI and 28  $\mu$ M ribonuclease in PBS containing DTT (2 mM)). Molar ellipticity at 222 nm was monitored after a 2 min equilibration at each temperature. Data were fitted to a two-state model to determine values for  $T_m$  (Table 1) (Becktel and Schellman 1987). Panels A and C depict data for RNase A ( $\triangle$ ), bRI ( $\square$ ), bRI·RNase A ( $\blacktriangle$ ), and bRI·RNase 1 ( $\blacksquare$ ); panels B and D depict data for RNase 1 ( $\diamond$ ), hRI ( $\circ$ ), hRI·RNase 1 ( $\blacklozenge$ ), and hRI·RNase A ( $\bullet$ ).

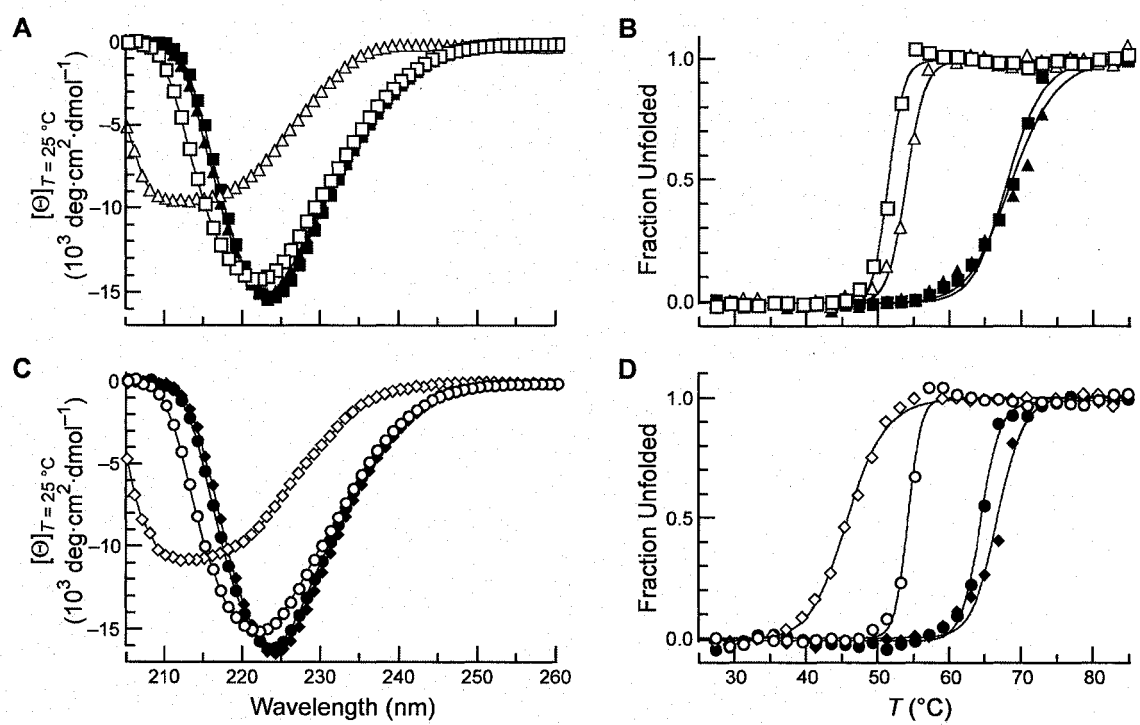


**Figure 4.4** Stability to hydrogen peroxide oxidation ( $\text{H}_2\text{O}_2$ ) of RI and RI-ribonuclease complexes. The decrease in fluorescence intensity of diethylfluorescein-labeled ribonuclease upon binding to RI was used to measure the oxidative stability of free RI and RI-ribonuclease complexes (Kim et al. 1999; Abel et al. 2002; Lavis et al. 2007). The complex formed by RI (10  $\mu\text{M}$ ) and ribonuclease (10  $\mu\text{M}$ ) was incubated in serial dilutions of  $\text{H}_2\text{O}_2$  buffered in 20 mM Hepes-HCl buffer, pH 7.6, containing KCl (50 mM) and DTT ( $\leq 50 \mu\text{M}$ ) for 30 min at 37 °C. Data points are the mean ( $\pm$  SE) of three independent experiments and were normalized for the maximum fluorescence of the unbound ribonuclease. Data were fitted to eq 2 to determine values of  $\text{IC}_{50}$  (Table 1). Panel A depicts data for bRI ( $\square$ ), bRI-RNase A ( $\blacktriangle$ ), and bRI-RNase 1 ( $\blacksquare$ ); panel B depicts data for hRI ( $\circ$ ), hRI-RNase 1 ( $\blacklozenge$ ), and hRI-RNase A ( $\bullet$ ); panel C depicts data for hRI ( $\circ$ ), C74L hRI ( $\blacktriangledown$ ), and C408G hRI ( $\triangledown$ ).



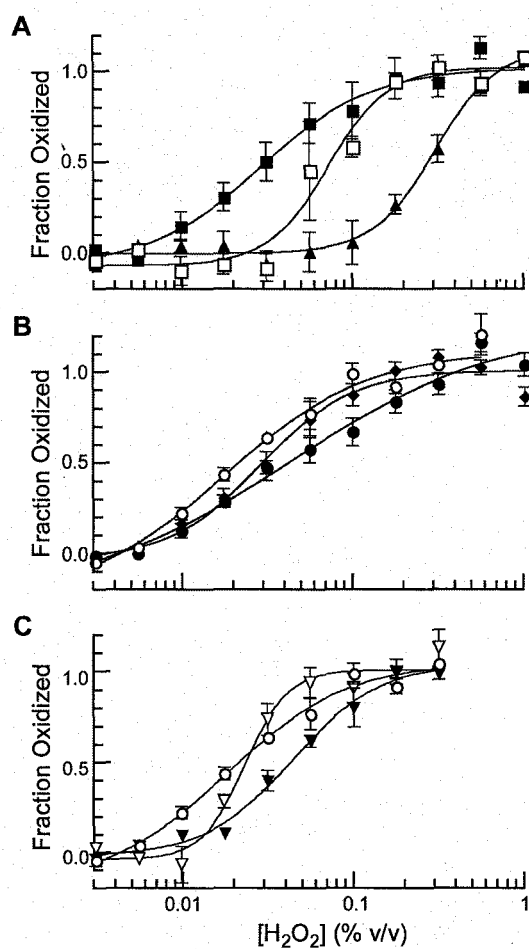


**Figure 4.5** Phylogenetic tree of RIs (a) and ribonucleases (b) from various organisms. Cladograms of RI and ribonuclease were made with the program MegAlign from the Lasergene software package (DNASTAR, Madison, WI). Bootstrap values were calculated using 2,000 replicates, and values >40 are reported. The bar indicates the distance for 0.10 substitutions per site. GenBank accession codes for RI and ribonuclease sequences are listed in the experimental procedures, and sequence alignments are shown in Supplementary Figures 2 and 3.

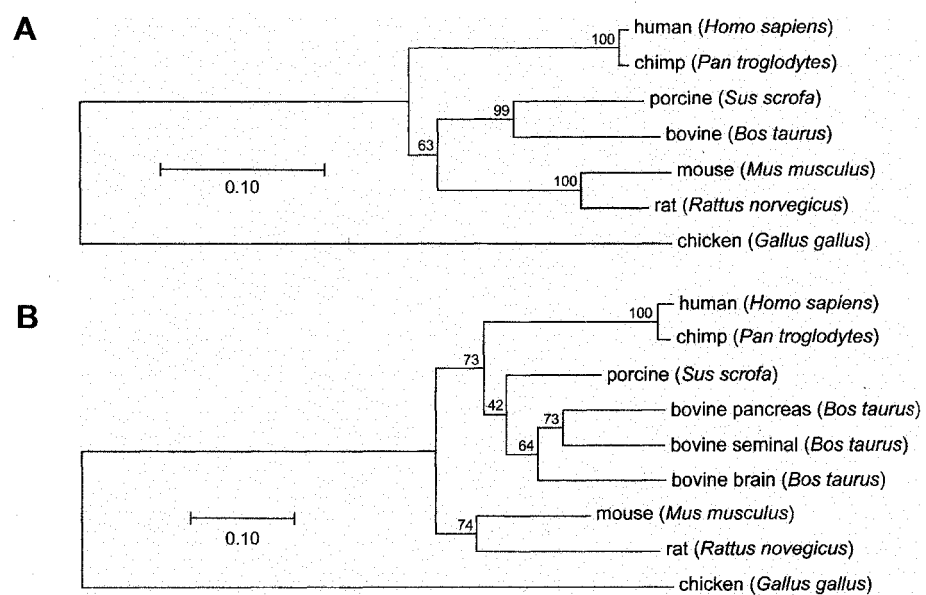


**Figure 4.6** Percent identity between RIs (A) and ribonucleases (B) from Figure 4.5. Percent identities were determined using the default values in Clustal W (Chenna et al. 2003).

**A**

Percent Identity	human RI	chimp RI	mouse RI	rat RI	bovine RI	porcine RI	chicken RI
human RI		98	73	75	74	77	49
chimp RI	98		73	75	74	77	49
mouse RI	73	73		90	76	76	48
rat RI	75	75	90		76	76	50
bovine RI	74	74	76	76		84	49
porcine RI	77	77	76	76	84		47
chicken RI	49	49	48	50	49	47	

**B**

Percent Identity	human RNase	chimp RNase	mouse RNase	rat RNase	bovine RNase	porcine RNase	chicken RNase
human RNase		97	70	65	69	75	30
chimp RNase	97		68	65	69	75	31
mouse RNase	70	68		76	70	74	35
rat RNase	65	65	78		66	66	27
bovine RNase	69	69	70	66		79	28
porcine RNase	75	75	74	66	79		31
chicken RNase	30	31	35	27	28	31	

**Figure 4.7** Multiple sequence alignment of RI used to construct the phylogenetic tree in Figure 4.5A. Conserved residues are shown as black boxes. Sequence alignments of RI were performed using the default values in Clustal W (Chenna et al. 2003). Accession codes for RI are listed in the experimental procedures.

human R1 ( <i>Homo sapiens</i> )	M S L D I Q S L D I Q C E E L S D A R W A E L L P L L Q Q C Q V V R L D D C G L T E A R C K D I S S A L R V N P A L A E	60
chimp R1 ( <i>Pan troglodytes</i> )	M S L D I Q S L D I Q C E E L S D A R W A E L L P L L Q Q C Q V V R L D D C G L T E A R C K D I S S A L R V N P A L A E	60
mouse R1 ( <i>Mus musculus</i> )	- - - - M S L D I Q C E E L S D A R W T E L L P L I Q Q Y E V V R L D D C G L T E V R C K D I S S A V Q A N P A L T E	55
rat R1 ( <i>Rattus norvegicus</i> )	- - - - M S L D I Q C E E L S D A R W T E L L P L I Q Q Y E V V R L D D C G L T E V R C K D I S S A I Q A N P A L T E	55
bovine R1 ( <i>Bos taurus</i> )	- - - - M K L D I Q C E E L S D A R W T E L L P L I Q Q Y E V V R L D D C G L T E V R C K D I G S A L Q A N A S L T E	55
porcine R1 ( <i>Sus scrofa</i> )	- - - - M N L D I H C E E L S D A R W T E L L P L I Q Q Y E V V R L D D C G L T E E H C K D I G S A L R A N P S L T E	55
chicken R1 ( <i>Gallus gallus</i> )	- - - - M D L D I Q C E E M N P S R W A E L L S T M K S C S T I R L D D C N L S S S N C K D I S S I H T N P S L K E	55
human R1 ( <i>Homo sapiens</i> )	L N L R S N E L G D V G V H C V L Q G L Q T P S C K I Q K L S L Q N C G L T A G G G V L S S T L R T L P T L Q E L H L	120
chimp R1 ( <i>Pan troglodytes</i> )	L N L R S N E L G D V G V H C V L Q G L Q S P S C K I Q K L S L Q N C G L T A G G G V L S S T L R T L P T L Q E L H L	120
mouse R1 ( <i>Mus musculus</i> )	L S L R T N E L G D V G V G L V L Q G L Q N P T C K I Q K L S L Q N C G L T A G G G V L S S T L R T L P T L Q E L H L	115
rat R1 ( <i>Rattus norvegicus</i> )	L S L R T N E L G D A G V G L V L Q G L Q N P T C K I Q K L S L Q N C G L T A G G G V L S S T L R T L P T L Q E L H L	115
bovine R1 ( <i>Bos taurus</i> )	L S L R T N E L G D G V G L V L Q G L Q S P T C K I Q K L S L Q N C G L T A G G G V L S S T L R T L P T L Q E L H L	115
porcine R1 ( <i>Sus scrofa</i> )	L C L R T N E L G D A G V H L V L Q G L Q S P T C K I Q K L S L Q N C G L T A G G G V L S S T L R T L P T L Q E L H L	115
chicken R1 ( <i>Gallus gallus</i> )	L K L N N N E L G D A G I E Y L C K G L T P S C S L Q K L W L Q N C N L T A S C E T L R S V L S A Q P S L T E L H V	115
human R1 ( <i>Homo sapiens</i> )	S D N L L G D A G L Q L L C E G L L D P Q C R L E K L Q L E Y C S L S A A S C E P L A S V L R A K P D F K E L T V S N N	180
chimp R1 ( <i>Pan troglodytes</i> )	S D N L L G D A G L Q L L C E G L L D P Q C R L E K L Q L E Y C S L S A A S C E P L A S V L R A K P D F K E L T V S N N	180
mouse R1 ( <i>Mus musculus</i> )	N D N P L G D A G L K L L C E G L L D P Q C R L E K L Q L E Y C N L T A T S C E P L A S V L R V K A D F K E L V L S N N	175
rat R1 ( <i>Rattus norvegicus</i> )	N D N P L G D E G L K L L C E G L L D P Q C R L E K L Q L E Y C N L T A T S C E P L A S V L R V K P D F K E L V L S N N	175
bovine R1 ( <i>Bos taurus</i> )	S D N P L G D A G L R L L C E G L L D P Q C R L E K L Q L E Y C S L T A A S C E P L A A V L R A T R D L K E L V S N N	175
porcine R1 ( <i>Sus scrofa</i> )	S D N P L G D A G L R L L C E G L L D P Q C H L E K L Q L E Y C R L T A A S C E P L A S V L R A T R A L K E L T V S N N	175
chicken R1 ( <i>Gallus gallus</i> )	G D N K L G T A G V K V L C Q G L M N P N C K L Q K L Q L E Y C E L T A D I V E A L N A A L Q A K P T L K E L S L S N N	175
human R1 ( <i>Homo sapiens</i> )	D I N E A G V R V L C Q G L K D S P C Q L E A L K L E S C G V T S D N C R D L C G I V A S K A S L R E L A L G S N K L G	240
chimp R1 ( <i>Pan troglodytes</i> )	D I N E A G V R V L C Q G L K D S P C Q L E A L K L E S C G V T S D N C R D L C G I V A S K A S L R E L A L G S N K L G	240
mouse R1 ( <i>Mus musculus</i> )	D L H E P G V R I L C Q G L K D S A C Q L E S L K L E N C G I T A A N C K D L C D V A S K A S L Q E L D L S S N K L G	235
rat R1 ( <i>Rattus norvegicus</i> )	D I H E A G I H T L C Q G L K D S A C Q L E S L K L E N C G I T A A N C K D L C D V A S K A S L Q E L D L S S N K L G	235
bovine R1 ( <i>Bos taurus</i> )	D I G E A G V Q A L C R G L A E S A C Q L E T L K L E N C G L T P A N C K D L C G I V A S Q A S L R E L D L S S N K L G	235
porcine R1 ( <i>Sus scrofa</i> )	D I G E A G A R V L G Q G L A D S A C Q L E T L L H L E N C G L T P A N C K D L C G I V A S Q A S L R E L D L S S N K L G	235
chicken R1 ( <i>Gallus gallus</i> )	T L G D T A V K Q L C R G L V E A S C D L E L L L H L E N C G I T S D S C R D J S A V L S S K P S L L D L A V G D N K I G	235
human R1 ( <i>Homo sapiens</i> )	D V G M A E L C P G L L H P S S R L R T L W I W E C G I T A K G C G D L C R V L R A K E S L K E L S L A G N E L G D E G	300
chimp R1 ( <i>Pan troglodytes</i> )	D V G M A E L C P G L L H P S S R L R T L W I W E C G I T A K G C G D L C R V L R A K E S L K E L S L A G N E L G D E G	300
mouse R1 ( <i>Mus musculus</i> )	N A G I A A L C P G L L L P S C K L R T L W L W E C D I T A E G C K D L C R V L R A K Q S L K E L S L A S N E L K D E G	295
rat R1 ( <i>Rattus norvegicus</i> )	N T G I A A L C S G L L L P S C R L R T L W L W E C D I T A E G C K D L C R V L R A K Q S L K E L S L A G N E L K D E G	295
bovine R1 ( <i>Bos taurus</i> )	D A G L A E L C P G L L S P S S Q L R T L W L W E C D I T A S G C R E L C R V L Q A K E A L K E L S L A G N S L G D E G	295
porcine R1 ( <i>Sus scrofa</i> )	D A G I A E L C P G L L S P A S L K T L W L W E C D I T A S G C R D L C R V L Q A K E T L K E L S L A G N S L G D E G	295
chicken R1 ( <i>Gallus gallus</i> )	D T G L A L L C Q G L L H P N C K I Q K L W L W D C D L T S A S C K D L S R V F S T K E T L L E V S L I D N N L R D S G	295
human R1 ( <i>Homo sapiens</i> )	A R L L C E T L L E P G C Q L E S L W V K S C S F T A A C C S H F S S V L A Q N R F L L E L Q I S N N R L E D A G V R E	360
chimp R1 ( <i>Pan troglodytes</i> )	A R L L C E T L L E P G C Q L E S L W V K S C S F T A A C C S H F S S V L A Q N K F L L E L Q I S N N R L E D A G V Q E	360
mouse R1 ( <i>Mus musculus</i> )	A R L L C E S L L E P G C Q L E S L W I K T C S L T A A S C P Y F C S V L T K S R S L F E L Q M S N N P L G D E G V Q E	355
rat R1 ( <i>Rattus norvegicus</i> )	A Q L L C E S L L E P G C Q L E S L W K T C S L T A A S C P H F C S V L T K N R S L F E L Q M S N N P L G D A G V H V	355
bovine R1 ( <i>Bos taurus</i> )	A Q L L C E S L L Q P G C Q L E S L W V K S C S F T A A C C Q H F S S M L T Q N K H L L E L Q L S S N P L G D A G V H V	355
porcine R1 ( <i>Sus scrofa</i> )	A R L L C E S L L Q P G C Q L E S L W V K S C S L T A A C C Q H V S L M L T Q N K H L L E L Q L S S N K L G D S G I Q E	355
chicken R1 ( <i>Gallus gallus</i> )	M E M L C Q A L K D P K A H L Q E L W V R E C G L T A A C C K A V S S V L S V N K H L Q V L H I G E N K L G N A G V E I	355
human R1 ( <i>Homo sapiens</i> )	L C Q G L G Q P G S V L R V L W L A D C D V S D S S C S S L A A T L L A N H S L R E L D L S N N C L G D A G I L Q L V E	420
chimp R1 ( <i>Pan troglodytes</i> )	L C Q G L G Q P G S V L R V L W L A D C D V S D S S C S S L A A T L L A N H S L R E L D L S N N C L G D A G I L Q L V E	420
mouse R1 ( <i>Mus musculus</i> )	L C K A L S Q P D T V L R V L W L G D C D V T N S G C S S L A V L L A N R S L R E L D L S N N C M G D N G V L Q L L E	415
rat R1 ( <i>Rattus norvegicus</i> )	L C K A L S Q P D T V L R V L W L G D C D V T N S G C S S L A V L L A N R S L R E L D L S N N C M G D N G V L Q L L E	415
bovine R1 ( <i>Bos taurus</i> )	L C Q A L S Q P G T V L R V L W V G D C E L T N S S C G G L A S L L A S P S L R E L D L S N N G L G D P G V L Q L L G	415
porcine R1 ( <i>Sus scrofa</i> )	L C Q A L S Q P G T T L R V L C L G D C E V T N S G C S S L A S L L A N R S L R E L D L S N N C V G D P G V L Q L L G	415
chicken R1 ( <i>Gallus gallus</i> )	L C E G L L H P N C N I H S L W L G N C D I T A A C C A T L A N V M V T K Q N L T E L D L S Y N T L E D E G V M K L C E	415
human R1 ( <i>Homo sapiens</i> )	S V R Q P G C L L E Q L V L Y D I Y W S E E M E D R L Q A L E K D K P S L R V I S	461
chimp R1 ( <i>Pan troglodytes</i> )	S V R Q P G C L L E Q L V L Y D I Y W S E E M E D R L Q A L E K D K P S L R V I S	461
mouse R1 ( <i>Mus musculus</i> )	S L K Q P S C I L Q Q L V L Y D I Y W T N E V E E Q L R A L E E E R P S L R I I S	456
rat R1 ( <i>Rattus norvegicus</i> )	S L K Q P S C I L Q Q L V L Y D I Y W T N E V E E Q L R A L E E E R P S L R I I S	456
bovine R1 ( <i>Bos taurus</i> )	S L E Q P G C A L E Q L V L Y D I Y W T E A V D E R L Q A L E E S K P G L R I I S	456
porcine R1 ( <i>Sus scrofa</i> )	S L E Q P G C A L E Q L V L Y D I Y W T E A V D E R L Q A L E E S K P G L R I I S	456
chicken R1 ( <i>Gallus gallus</i> )	A V R N P N C K M Q Q L I L Y D I F W G P E V D D E L Q A L E E A R P D V K I I S	456

**Figure 4.8** Multiple sequence alignment of ribonucleases used to construct the phylogenetic tree in Figure 4.5B. The sequences of bovine seminal ribonuclease and bovine brain ribonuclease are not shown for clarity. Conserved residues are shown as black boxes. Sequence alignments of ribonucleases were performed using the default values in Clustal W (Chenna et al. 2003). Accession codes for ribonucleases are listed in the experimental procedures.



human ( <i>Homo sapiens</i> )	KESRAKKFQRQHMDLSDSSPSSSSTYCNQMRRRRNM-TQGLCKPVNTFVHEPLVDVQNV	58
chimpanzee ( <i>Pan troglodytes</i> )	KESRAKKFQRQHMDLSDSSPSSSSTYCNQMRRRRNM-TQGRCKPVNTFVHEPLVDVQNV	58
mouse ( <i>Mus musculus</i> )	RESSADKFQRQHMDLSDSSPSSSSTYCNQMRRRRNM-TNGSCKPVNTFVHEPLVDVQAV	58
rat ( <i>Rattus norvegicus</i> )	RESSADKFQRQHMDLSDSSPSSSSTYCNQMRRRRNM-TNGSCKPVNTFVHEPLVDVQAV	58
bovine ( <i>Bos taurus</i> )	KETAAAKFQRQHMDLSDSSPSSSSTYCNQMRRRRNM-TKDRCKPVNTFVHEPLVDVQAV	58
porcine ( <i>Sus scrofa</i> )	KESPAKKFQRQHMDLSDSSPSSSSTYCNQMRRRRNM-TQGRCKPVNTFVHEPLVDVQAV	58
chicken ( <i>Gallus gallus</i> )	-VPTYQDFLRTHVDFPKTSFPNIAAYCNVMVRRGINVHGRCKSLNTFVHTDPRNLNTLC	59
human ( <i>Homo sapiens</i> )	FQEKVTCCKNGQGNCYKSNSSSMHIIDCRLTNGSRYPNCAVYRTSPKERHIIVACEGSPYVPV	118
chimpanzee ( <i>Pan troglodytes</i> )	FQEKVTCCKNGQGNCYKSNSSSMHIIDCRLTNGSRYPNCAVYRTSPKERHIIVACEGSPYVPV	118
mouse ( <i>Mus musculus</i> )	SQENVTCCKNRKSNKYSSALHIIDCHLKGNSKYPNCDYKTTQYQKHIIVACEGNPYVPV	118
rat ( <i>Rattus norvegicus</i> )	SQENVTCCKNRKSNKYSSALHIIDCHLKGNSKYPNCDYKTTQYQKHIIVACEGNPYVPV	118
bovine ( <i>Bos taurus</i> )	SQKNVACCKNGQTNKYQSYSTMSIIDCRQETGSSSKYPNCAVYKTTQANKHIIVACEGNPYVPV	118
porcine ( <i>Sus scrofa</i> )	SQKNVACCKNGQTNKYQSYSTMSIIDCRQETGSSSKYPNCAVYKTTQANKHIIVACEGNPYVPV	118
chicken ( <i>Gallus gallus</i> )	INQ-----PNRALRTTQQQLPVTDCKLIRS--HPTCSYTGNGFNHRVRVGCWGG--LPV	109
human ( <i>Homo sapiens</i> )	FDASVEDST	128
chimpanzee ( <i>Pan troglodytes</i> )	FDASVEDST	128
mouse ( <i>Mus musculus</i> )	FDA TV - - -	124
rat ( <i>Rattus norvegicus</i> )	FDA SV - - -	124
bovine ( <i>Bos taurus</i> )	FDA SV - - -	124
porcine ( <i>Sus scrofa</i> )	FDA SV - - -	124
chicken ( <i>Gallus gallus</i> )	HL DGTFP - -	116

## **Chapter Five**

### **A Ribonuclease Zymogen Activated by the NS3 Protease of Hepatitis C Virus**

Portions of this chapter were published as:

Johnson, R.J., Lin, S.R., Raines, R.T. (2006) A Ribonuclease Zymogen Activated by the NS3 Protease of the Hepatitis C Virus. *FEBS J.* **273**, 5457-5465. I performed or supervised all of the research described in this chapter.

## 5.1 Abstract

Translating proteases as inactive precursors, or zymogens, protects cells from the potentially lethal action of unregulated proteolytic activity. Here, we impose this strategy on bovine pancreatic ribonuclease (RNase A) by creating a zymogen in which quiescent ribonucleolytic activity is activated by the NS3 protease of the hepatitis C virus.

Connecting the N- and C-termini of RNase A with a 14-residue linker was found to diminish its ribonucleolytic activity by both occluding an RNA substrate and dislocating active-site residues, which are devices used by natural zymogens. After cleavage of the linker by the NS3 protease, the ribonucleolytic activity of the RNase A zymogen increased by 105-fold. Both before and after activation, the RNase A zymogen displayed high conformational stability and evasion of the endogenous ribonuclease inhibitor protein of the mammalian cytosol. Thus, the creation of ribonuclease zymogens provides a means to control ribonucleolytic activity and has the potential to provide a new class of antiviral chemotherapeutic agents.

## 5.2 Introduction

Proteolysis is an essential biological activity that requires tight regulation (Neurath 1984; Salvesen and Abrams 2004). One strategy employed by cells to control proteolysis is to encode proteolytic enzymes as inactive precursors—zymogens (Khan and James 1998). Zymogens are translated with N-terminal polypeptides, or prosegments, that inhibit proteolytic activity, typically by occluding substrate binding (Borgono and Diamandis 2004), distorting the active site (Khan and James 1998), or altering the substrate binding

cleft (Freer et al. 1970; Kossiakoff et al. 1977). When proteolytic activity is required, the inhibitory N-terminal prosegment is removed by autocatalytic cleavage, by cleavage by another protease, or by a conformational change invoked by the local environment (Khan and James 1998).

After processing of a zymogen to a mature protease, a cell can restrict proteolytic activity by employing cellular inhibitors (Khan and James 1998; Salvesen and Abrams 2004). Only this type of regulation is used to control the enzymatic activity of ribonucleases (Haigis et al. 2003; Dickson et al. 2005), which like proteases can degrade an essential biopolymer. The regulation of pancreatic-type ribonucleases is accomplished by ribonuclease inhibitor (RI (Lee et al. 1989b)), a cytosolic protein that binds to bovine pancreatic ribonuclease (RNase A (Cuchillo et al. 1997; Raines 1998), EC 3.1.27.5) and its mammalian homologs with extremely high affinity ( $K_i \approx 10^{-15}$  M). By evading the inhibition of RI, variants of RNase A become toxic to human cells (Leland and Raines 2001; Matousek 2001; Loverix and Steyaert 2003; Makarov and Ilinskaya 2003; Arnold and Ulbrich-Hofmann 2006).

Inspired by protease zymogens, we recently created a zymogen of RNase A in which a 14-residue linker connects the N- and C-termini (Plankum et al. 2003). The linker acts like the prosegment of a natural zymogen—inhibiting the native ribonucleolytic activity of RNase A but allowing the manifestation of near wild-type activity upon cleavage. The linker contained a sequence recognized by the plasmepsin II protease from the malarial parasite *Plasmodium falciparum*. Incubation with that protease restored the ribonucleolytic

activity of RNase A. We reasoned that this strategy could be general, in that the sequence of the linker could correspond to the recognition sequence of other proteases.

Hepatitis C virus (HCV (Major et al. 2001; Lindenbach and Rice 2005)), a positive-stranded RNA virus of the family *Flaviviridae* (Burke and Monath 2001; Lindenbach and Rice 2001), is estimated to infect 170 million people (*i.e.*, 2% of humanity) (World Health Organization 1999). This malady can lead to serious liver diseases such as cirrhosis and hepatocellular carcinoma, making infection by HCV the leading indicator of liver transplantation in the United States (Fishman et al. 1996). Like other RNA viruses, HCV translates its 9.6-kb genome as one single polyprotein, which is then co- and post-translationally cleaved by cellular endopeptidases and viral proteases to form at least four structural and six nonstructural proteins (Fishman et al. 1996). Nonstructural protein 3 (NS3) of the HCV polyprotein is a chymotrypsin-like serine protease (Tomei et al. 1993). The NS3 protein is essential for viral replication, cleaving the viral polyprotein at four positions (Urbani et al. 1997; Zhang et al. 1997).

Here, we report on an RNase A zymogen with a linker that corresponds to a sequence cleaved by the HCV NS3 protease. We investigate physicochemical properties of this RNase A zymogen both before and after its proteolytic activation, including its enzymatic activity, conformational stability, and affinity for RI. Characterization of this zymogen provides new insight into zymogen action. Moreover, the ensuing merger of the attributes of a cytotoxic ribonuclease with an enzymatic activity reliant on the HCV NS3 protease portends a new approach to antiviral therapies.

### 5.3 Experimental Procedures

*Materials.* *Escherichia coli* BL21(DE3) and pET28a(+) were from Novagen (Madison, WI). Enzymes were obtained from Promega (Madison, WI). Protein purification columns were from Amersham Biosciences (Piscataway, NJ). MES buffer (Sigma–Aldrich, St. Louis, MO) was purified by anion-exchange chromatography to remove trace amounts of oligomeric vinylsulfonic acid (OVS) (Smith et al. 2003). Poly(C) (Sigma–Aldrich, St. Louis, MO) was precipitated with ethanol prior to use to remove short RNA fragments. All other chemicals were of commercial grade or better, and were used without further purification.

Phosphate-buffered saline (PBS) contained (in 1.00 liter) NaCl (8.0 g), KCl (2.0 g), Na<sub>2</sub>HPO<sub>4</sub>·7H<sub>2</sub>O (1.15 g), KH<sub>2</sub>PO<sub>4</sub> (2.0 g), and NaN<sub>3</sub> (0.10 g) and had a pH of 7.4.

*Instrumentation.* Circular dichroism (CD) experiments were performed with a model 62A DS CD spectrometer (Aviv, Lakewood, NJ) equipped with a temperature controller. The mass of RNase A zymogens was confirmed by matrix-assisted laser desorption/ionization time-of-flight (MALDI-TOF) mass spectrometry using a Voyager-DE-PRO Biospectrometry Workstation (Applied Biosystems, Foster City, CA). CD and MALDI-TOF mass spectrometry experiments were performed at the Biophysics Instrumentation Facility.

UV–visible spectroscopy was performed with a Cary 3 double-beam spectrophotometer equipped with a Cary temperature controller (Varian, Palo Alto, CA). Fluorescence spectroscopy was performed with a QuantaMaster 1 photon-counting fluorometer equipped with sample stirring (Photon Technology International, South

Brunswick, NJ).

*Zymogen Preparation.* Plasmids that direct the production of HCV RNase A zymogens were derived from plasmid pET22b(+)/19N (Plainkum et al. 2003). The linker-encoding region of that plasmid was replaced with DNA encoding GEDVVCCSMSYGAG (to yield the “2C” zymogen) or GEDVVACSMSYGAG (to yield the “1C” zymogen) by using the QuikChange mutagenesis kit (Stratagene, La Jolla, CA). These sequences correspond to preferred NS5A/5B recognition sequences of the NS3 protease (Urbani et al. 1997; Zhang et al. 1997). The production, folding, and purification of RNase A zymogens were performed as described for other RNase A variants (Leland et al. 1998), except that oxidative folding was done for a minimum of 72 h at 4 °C and pH 7.8 with 0.50 M arginine in the folding buffer (1C *m/z* 15,142, expected: 15,116; 2C *m/z* 15,162, expected: 15,148).

*Protease Preparation.* Clone B cells (Blight et al. 2000) were a generous gift of C. M. Rice. Total cellular RNA was isolated from these cells by using the TRIZOL reagent (Invitrogen, Carlsbad, CA) (Lohmann et al. 1999; Blight et al. 2000). A One-Step RT-PCR kit (Qiagen, Valencia, CA) was used to amplify DNA encoding residues 1–181 of the NS3 gene, flanked by *Nde*I and *Xho*I restriction sites (Taremi et al. 1998). The resulting DNA fragment was inserted into plasmid pET-28a(+), which encodes an N-terminal His<sub>6</sub> tag. As in previous systems to produce the NS3 protease (Taremi et al. 1998), DNA encoding 12 residues of the NS4A protein of HCV and a flexible Gly–Ser–Gly–Ser tether was inserted upstream of the NS3 gene. The protein encoded by the resulting plasmid is referred to as the “NS4A/NS3 protease”.

NS4A/NS3 protease was purified by methods published previously (Taremi et al. 1998) and found to be >95% pure by SDS-PAGE and had the expected molecular mass ( $m/z$  21424, expected: 21407). Purified NS4A/NS3 protease was dialyzed exhaustively against 50 mM Tris-HCl buffer, pH 7.5, containing NaCl (0.30 M), glycerol (10% v/v), Tween 20 (0.025% v/v), and DTT (0.005 M), and aliquots were flash-frozen at  $-80^{\circ}\text{C}$ . The enzymatic activity of purified NS4A/NS3 was assayed by monitoring the change in retention time of a fluorescent peptide substrate (Bachem, King of Prussia, PA) during reverse-phase  $\text{C}_{18}$  HPLC. An inactivate variant of NS4A/NS3 protease with Ser139 replaced with an alanine residue did not cleave the fluorescent substrate, as had been reported previously (Tomei et al. 1993).

*Detection of Thiol Groups.* DTNB reacts with thiol groups (but not disulfide bonds) to produce a yellow chromophore that can be used to quantitate the number of thiol groups (Riddles et al. 1983). Solutions of the 1C and 2C zymogens were diluted to concentrations of 0.00625, 0.01325, 0.0265, and 0.053 mM with 100 mM Tris-HCl buffer, pH 8.3, containing EDTA (0.01 M). A 10-fold molar excess of DTNB (as 50 mM Tris-HCl buffer, pH 7.5, containing NaCl (0.10 M), EDTA (0.05 M), and DTNB (0.005 M)) was added to each dilution, and the DTNB was allowed to react for 30 min at  $25^{\circ}\text{C}$ . The number of free cysteines was determined by UV absorption using  $\epsilon_{412\text{ nm}} = 14.15\text{ M}^{-1}\text{cm}^{-1}$  for 2-nitro-5-thiobenzoic acid (Riddles et al. 1983).

*Activation of Zymogens.* RNase A zymogens were activated by mixing them with 0.5 molar equivalents of NS4A/NS3 protease in reaction buffer (which was 50 mM Tris-HCl buffer, pH 7.5, containing NaCl (0.3 M), glycerol (10% v/v), Tween 20 (0.025% v/v),



and DTT (0.005 M) (Taremi et al. 1998)) and incubating the resulting mixture at 37 °C for 15 min. Activation was stopped by dilution (1:>10) into 0.10 M MES–NaOH buffer, pH 6.0, containing NaCl (0.10 M) and placement of the reaction mixture on ice. Reaction mixtures were subjected to SDS–PAGE in the presence of DTT to assess zymogen activation.

*Ribonucleolytic Activity.* The ability of a ribonuclease to catalyze the cleavage of poly(C) ( $\epsilon_{268\text{ nm}} = 6,200\text{ M}^{-1}\text{cm}^{-1}$  per nucleotide) was monitored by measuring the increase in UV absorption upon cleavage ( $\Delta\epsilon_{250\text{ nm}} = 2,380\text{ M}^{-1}\text{cm}^{-1}$  (Leland et al. 1998)). Assays were performed at 25 °C in 0.10 M MES–NaOH buffer, pH 6.0, containing NaCl (0.10 M), poly(C) (10  $\mu\text{M}$  to 1.5 mM), and enzyme (1.5 nM for wild-type RNase A; 1 and 3  $\mu\text{M}$  for the 1C and 2C unactivated zymogens, respectively; 6 and 100 nM for the 1C and 2C activated zymogens, respectively). Initial velocity data were used to calculate values of  $k_{\text{cat}}$ ,  $K_{\text{M}}$ , and  $k_{\text{cat}}/K_{\text{M}}$  with the program DELTAGRAPH 5.5 (Red Rock Software, Salt Lake City, UT).

*Zymogen Conformation and Conformational Stability.* CD spectroscopy was used to assess the conformation of the unactivated and activated 1C zymogens. A solution of zymogen (0.5 mg/mL in PBS) was incubated for 5 min at 10 °C, and a CD spectrum was acquired from 260 to 210 nm in 1-nm increments.

CD spectroscopy was also used to evaluate the conformational stability of the unactivated and activated 1C zymogens (Lee and Raines 2003). A solution of zymogen (0.5 mg/mL in PBS) was heated from 10 to 80 °C in 2-°C increments, and the change in molar ellipticity at 215 nm was monitored after a 2-min equilibration at each temperature. RNase A zymogens were activated as before, and NS4A/NS3 protease was removed from

the reaction mixture by using His-Select spin columns (Sigma–Aldrich). CD spectra were fitted to a two-state model for denaturation to determine the value of  $T_m$ .

*Ribonuclease Inhibitor Evasion.* Porcine RI (pRI) was purified as described previously (Klink et al. 2001). The affinity of the unactivated and activated 1C zymogen for pRI was determined using a fluorescent competition assay described previously, with minor modifications (Abel et al. 2002). Briefly, fluorescein-labeled G88R RNase A (50 nM) and various concentrations of unlabeled RNase A zymogen were added to 2.0 ml of PBS containing DTT (5 mM), and the resulting solution was incubated at 23 ( $\pm 2$ ) °C for 20 min. After this incubation, the initial fluorescence intensity of the unbound fluorescein-labeled G88R RNase A was monitored for 3 min (excitation: 491 nm, emission: 511 nm). pRI was then added to 50 nM, and the final fluorescence intensity was measured. Values for  $K_d$  were obtained by nonlinear least-squares analysis of the binding isotherm with the program DELTAGRAPH 5.5 (Red Rock Software, Salt Lake City, UT). The value of  $K_d$  for the complex between pRI and fluorescein-labeled G88R RNase A was assumed to be 0.52 nM (Abel et al. 2002).

*Cytotoxic Activity.* The effect of an RNase A zymogen on the proliferation of K-562 cells was assayed as described previously (Plainkum et al. 2003; Rutkoski et al. 2005). After a 44-h incubation with a ribonuclease, K-562 cells were treated with [*methyl*- $^3\text{H}$ ]thymidine for 4 h, and the incorporation of radioactive thymidine into the cellular DNA was quantified by liquid scintillation counting. Results were the percentage of [*methyl*- $^3\text{H}$ ]thymidine incorporated into the DNA as compared to the incorporation into control K-562 cells to which only PBS was added. Data were the average of three

measurements for each concentration, and the entire experiment was repeated in duplicate. Values for  $IC_{50}$  were calculated by fitting the curves by nonlinear regression to a sigmoidal dose–response curve with the equation:

$$y = \frac{100\%}{1 + 10^{(\log(IC_{50}) - \log[\text{ribonuclease}]) \cdot h}} \quad (1)$$

In eq 1,  $y$  is the total DNA synthesis following the [*methyl*- $^3H$ ]thymidine pulse, and  $h$  is the slope of the curve.

*Molecular Modeling.* The atomic coordinates of RNase A were obtained from the Protein Data Bank (accession code: 7RSA) (Wlodawer et al. 1988). Models of both 1C and 2C RNase A zymogen were created with the program SYBYL (Tripos, St. Louis, MO) on an O2 computer (Silicon Graphics, Mountain View, CA) (Plainkum et al. 2003). SYBYL was used to connect the old N- and C-termini via the 14-residue linker, to replace residues 4, 88, 89, and 118 with cysteine, to cleave the polypeptide chain between residues 88 and 89, to create disulfide bonds between residues 4 and 118 and residues 88 and 89, and to minimize the conformational energy of the new residues (Plainkum et al. 2003).

## 5.4 Results

*Zymogen Design.* As a potential target for antiviral therapy, the HCV NS3 protease has a well-characterized structure and function (Lorenz et al. 2006). The HCV NS3 protease cleaves the HCV viral polyprotein at four specific locations, and the sequences of the cleavage sites are known (Urbani et al. 1997; Zhang et al. 1997). Of these, the cleavage

site between nonstructural proteins 5A and 5B (NS5A/5B) of the HCV polyprotein is cleaved most rapidly (Zhang et al. 1997). Consequently, the NS5A/5B sequence of GEDVV(C/A)CSMSYGAG was chosen as the linker for the HCV RNase A zymogen (Zhang et al. 1997). For full proteolytic activity, the NS3 protease recognition sequence requires ten residues of the NS5A/5B sequence with cysteine residues in the P1 and P2 positions, which immediately preceded the scissile bond. If the cysteine residue in the P1 position is replaced with alanine, the NS3 protease no longer cleaves the NS5A/5B peptide; a similar mutation at the P2 position results in only a 40% decrease in cleavage activity (Urbani et al. 1997; Zhang et al. 1997). The proximal cysteines in the NS5A/5B sequence could, however, form a disulfide bond (Zhang and Snyder 1989) that would alter the structure of the linker. Therefore, two HCV zymogen constructs were designed, one with a cysteine residue (2C zymogen) in the P2 position and one with an alanine residue there (1C zymogen). These two zymogens contain, in effect, a peptide that links residue 124 (C-terminus) with residue 1 (N-terminus).

In each zymogen, new N- and C-termini were created at residues 89 and 88, respectively (Plainkum et al. 2003). Disulfide bonds were used to link residues 88 and 89 and residues 4 and 118, as cysteines at these positions had been shown to increase the conformational stability of other RNase A variants by 10 and 5 °C, respectively (Klink and Raines 2000; Plainkum et al. 2003). A model of the 2C zymogen is shown in Fig. 1, highlighting the location of all seven possible disulfide bonds and the new termini at positions 89 and 88.

*Activation of Ribonucleolytic Activity.* An essential aspect of a functional zymogen is the resistance of the parent enzyme to cleavage by the activating protease. Accordingly, wild-type RNase A (25  $\mu$ M) was incubated for 60 min at 37 °C with equimolar NS4A/NS3 protease. After incubation, wild-type RNase A exhibited no significant loss in ribonucleolytic activity. Thus, RNase A is not a substrate for the NS4A/NS3 protease.

An RNase A zymogen should, however, be a substrate for its cognate protease but not other common proteases. The expected mass of the fragments produced by cleavage of the 1C zymogen and reduction of its disulfide bonds are 10.5 kDa (which is readily detectable by SDS–PAGE) and 4.6 kDa. Incubation of the 1C zymogen with a substoichiometric quantity of NS4A/NS3 protease led to its nearly complete processing after 15 min at 37 °C, as shown in Fig. 2. Incubation of the 1C zymogen for 15 min at 37 °C with trypsin, which is a common protease with high enzymatic activity, resulted in insignificant cleavage (molar ratio: 1:100 or 1:25 trypsin/1C zymogen; data not shown).

An RNase A zymogen should also have low ribonucleolytic activity before activation, and should regain nearly wild-type activity upon incubation with the NS4A/NS3 protease. The initial rates of poly(C) cleavage by unactivated 1C zymogen, activated 1C zymogen, and RNase A are depicted in Fig. 3, and the resulting steady-state kinetic parameters are listed in Table 1. The  $k_{\text{cat}}/K_{\text{M}}$  value for the cleavage of poly(C) by wild-type RNase A is higher than those reported previously (Leland et al. 1998) due to the removal from the assay buffer of OVS, which is a potent inhibitor of RNase A (Smith et al. 2003).

Wild-type RNase A has 430-fold and  $10^4$ -fold higher  $k_{\text{cat}}/K_{\text{M}}$  values for poly(C) cleavage than do the unactivated 1C and 2C zymogens, respectively (Table 1). The

decreased activity of unactivated zymogens is a result of both a smaller value of  $k_{\text{cat}}$  and a larger value of  $K_M$ . The  $k_{\text{cat}}/K_M$  value of the unactivated 1C zymogen is 33-fold higher than that of the unactivated 2C zymogen, and the difference is again the result of both a decrease in  $k_{\text{cat}}$  and an increase in  $K_M$ . The increase in  $k_{\text{cat}}$  values upon activation of the 1C and 2C zymogens suggests that the intact linker dislocates key catalytic residues.

The only difference between unactivated the 2C and 1C zymogens is the sulfur atom of the cysteine residue in the P2 position of the 2C zymogen. This difference enables the two adjacent cysteine residues in the linker of 2C zymogen to form a disulfide bond. A reaction with 5,5'-dithio-bis(2-nitrobenzoic acid) (DTNB) was used to determine the number of free thiols in the 1C and 2C zymogens. The results indicated that the 1C and 2C zymogens have  $0.6 \pm 0.1$  and  $0.16 \pm 0.04$  free thiols per molecule, respectively (Riddles et al. 1983). These values suggest that the cysteine residues in the linker of the 2C zymogen do indeed form a disulfide bond. Disulfide bonds between adjacent cysteine residues can distort the conformation of an enzyme and diminish its catalytic activity (Park and Raines 2001). That effect is likely responsible for the ribonucleolytic activity of the unactivated 2C zymogen being lower than that of the unactivated 1C zymogen (Table 1). These data also suggest that the cysteine residue in the linker of 1C zymogen is at least partially buried in the unactivated zymogen, as the 1C zymogen appears to have 0.6 instead of 1.0 free cysteines.

Upon incubation with the NS4A/NS3 protease, the  $K_M$  value of activated 1C zymogen returns to wild-type levels, and the  $k_{\text{cat}}$  value is  $1/3$ -fold that of the wild-type enzyme, giving a  $k_{\text{cat}}/K_M$  value that is  $1/4$  that of wild-type RNase A (Table 1). The change in both kinetic parameters upon activation suggests that the linker affects substrate binding

and turnover by an unactivated RNase A zymogen, but that these affects are reversible.

The disulfide bond in the linker of activated 2C zymogen also influences the catalytic activity, as both its  $k_{\text{cat}}$  and  $K_{\text{M}}$  values remain lower than those of activated 1C zymogen.

The ratio of the  $(k_{\text{cat}}/K_{\text{M}})_{\text{activated}}$  value to the  $(k_{\text{cat}}/K_{\text{M}})_{\text{unactivated}}$  value provides an estimate of the effectiveness of the linker in modulating the ribonucleolytic activity and, in essence, provides a measure of the therapeutic index of a ribonuclease zymogen. For the 1C zymogen, the  $(k_{\text{cat}}/K_{\text{M}})_{\text{activated}}/(k_{\text{cat}}/K_{\text{M}})_{\text{unactivated}}$  ratio is 105 for the 1C zymogen and 13 for the 2C zymogen. Overall, the disulfide bond formed between the cysteine residues in the linker of the 2C zymogen seems to be detrimental to the ability of the linker to act as a zymogen prosegment. Accordingly, only the 1C zymogen was subjected to additional biochemical analyses.

*Zymogen Conformation and Conformational Stability.* The near-UV CD spectrum (170–250 nm) of a protein is a representation of protein secondary structure (Kelly et al. 2005). The CD spectra of unactivated and activated 1C zymogen are shown in Fig. 4A. Although deconvolution of the contribution of distinct secondary structural elements to the CD spectra of unactivated and activated 1C zymogen is difficult, activation of the 1C zymogen appears to have an effect on its CD spectrum and is thus likely to affect its conformation.

The conformational stability of both unactivated and activated 1C zymogen was determined by CD spectroscopy. The thermal denaturation curves are shown in Fig. 4B, and the resulting values of  $T_{\text{m}}$  are listed in Table 2. Both unactivated and activated 1C zymogen have  $T_{\text{m}}$  values well-above physiological temperature (37 °C) but below that of

wild-type RNase A (64 °C). As with the RNase A zymogen described previously (Plankum et al. 2003), the conformational stability of the 1C zymogen increases upon activation, perhaps due to the release of strain.

*Affinity for Ribonuclease Inhibitor and Cytotoxicity.* RI recognizes members of the RNase A superfamily with femtomolar affinity (Dickson et al. 2005). As many RI contacts with RNase A are in the active site (Kobe and Deisenhofer 1995), the linker in an RNase A zymogen could block RI binding. The affinity of pRI for the 1C zymogen was determined by using a competitive binding assay with fluorescein-labeled G88R RNase A (Abel et al. 2002). The resulting  $K_d$  values for the complexes of pRI with both unactivated and activated 1C zymogen are listed in Table 2. Unactivated 1C zymogen at 16  $\mu\text{M}$  did not compete with fluorescein-labeled G88R RNase A for binding to pRI, and the  $K_d$  value for the pRI complex with unactivated 1C zymogen was therefore estimated to be  $>1 \mu\text{M}$  (Rutkoski et al. 2005). The lack of affinity of unactivated 1C zymogen for pRI puts it in the range of the most RI-evasive of known RNase A variants (Rutkoski et al. 2005). Yet, unlike most RI-evasive variants, unactivated 1C zymogen was not toxic ( $\text{IC}_{50} > 25 \mu\text{M}$ ) to a standard cancer cell-line used to estimate ribonuclease cytotoxicity (Table 2).

In contrast, the value of  $K_d$  ( $= 13 \text{ nM}$ ) for the complex of pRI with activated 1C zymogen is greater than that of the unactivated 1C zymogen. Yet, the affinity of pRI for wild-type RNase A is still  $10^5$ -fold higher than that for the activated 1C zymogen (Table 2), suggesting that the cleaved linker still disturbs RI binding. The affinity of pRI for activated 1C zymogen is close to that measured previously for K7A/G88R RNase A ( $K_d = 17 \text{ nM}$ ) (Rutkoski et al. 2005). The change in binding affinity of pRI for unactivated and activated



1C zymogen provides additional evidence that the linker is flexible and that it moves away from the RNase A active site upon activation.

## 5.5 Discussion

*Basis for Zymogen Inactivity.* The cleavage of a peptide bond in natural zymogens leads to their activation by enabling the binding of substrate (Sohl et al. 1997), altering the conformation of active-site residues (Khan and James 1998), or constituting the substrate binding cleft (Freer et al. 1970; Kossiakoff et al. 1977). For example, formation of the “oxyanion hole” and substrate binding cleft occurs upon activation of chymotrypsinogen (Freer et al. 1970; Khan and James 1998). Based on our molecular modeling, the linker of the RNase A zymogen appears to occlude the binding of substrate to the active site (Fig. 1). This model is supported by the low  $K_M$  values of the unactivated 1C and 2C zymogens (Table 1). Likewise, the intact linker of the unactivated zymogen inhibits RI binding to the active site more than does the cleaved linker (Table 2). Still, the cleaved linker, which is not excised from the zymogen, continues to instill the ability to evade RI upon the activated zymogen. This continued evasion contrasts with the behavior of some natural zymogens, which bind tightly to endogenous inhibitors upon activation (Khan and James 1998; Salvesen and Abrams 2004).

If the linker merely occludes the substrate from binding to the RNase A zymogens and has no influence on the conformation of active-site residues, then activation would have no effect on the turnover number ( $k_{cat}$ ) (Sohl et al. 1997). Yet, the  $k_{cat}$  values for the unactivated 1C zymogen ( $3.8 \text{ s}^{-1}$ ) and 2C zymogen ( $0.70 \text{ s}^{-1}$ ) are significantly lower than

those of the activated zymogens (Table 1). This decrease in  $k_{cat}$  value prior to activation suggests that key active-site residues are dislocated by the intact linker. Changes in the CD spectra upon activation are likewise indicative of a conformational change (Fig. 4).

Consequently, the low activity of the RNase A zymogen appears to arise from both substrate occlusion and an alteration of active-site residues. Thus, two strategies used by natural zymogens (Sohl et al. 1997; Khan and James 1998) are replicated in our artificial one. Most importantly, the intact linker diminishes the ribonucleolytic activity of the 1C zymogen, but allows for its reconstitution upon cleavage.

*Therapeutic Potential.* The NS3 protease of HCV is a major drug target (Tan et al. 2002). Design of small-molecule inhibitors of the NS3 protease is, however, problematic because of its shallow substrate-binding cleft (Pizzi et al. 1994; Kim et al. 1996; Yao et al. 1999). Herein, we take the opposite tact. Rather than trying to inhibit the enzymatic activity of the NS3 protease, we attempt to exploit that activity to activate an RNase A zymogen.

By comparing the ribonucleolytic activity and RI affinity of unactivated and activated 1C zymogen to those of other RNase A variants, we can estimate the therapeutic potential of an HCV RNase A zymogen. Unactivated 1C zymogen was not toxic to K-562 cells (Table 2) and has ribonucleolytic activity comparable to those of nontoxic ribonucleases, such as K41A/G88R RNase A (Thompson et al. 1995; Bretscher et al. 2000). Upon activation, the ribonucleolytic activity of 1C RNase A zymogen increases by 105-fold, approaching that of wild-type RNase A. Combining the ribonucleolytic activity of the activated 1C zymogen with its affinity for RI enables an estimate of its toxicity to cells

containing the NS3 protease (Bretscher et al. 2000; Rutkoski et al. 2005). For example, the activated 1C zymogen has greater ribonucleolytic activity than that of K7A/G88R RNase A and similar RI affinity (Rutkoski et al. 2005). K7A/G88R RNase A has  $IC_{50} = 1.1 \mu M$  for K-562 cell proliferation.

In conjunction with a positive activation ratio, the 1C zymogen also combines an increased  $T_m$  upon activation, making the activated ribonuclease more stable than the unactivated one. Thus, 1C RNase A zymogen has the necessary attributes for selective cytotoxicity to HCV, including a high ratio of  $(k_{cat}/K_M)_{activated}/(k_{cat}/K_M)_{unactivated}$  (105-fold), high conformational stability, and an ability to evade RI. Testing the toxicity of an RI-evasive 1C zymogen for HCV-infected cells (as opposed to K-562 cells; Table 2) is thus a worthwhile goal.

## 5.6 Conclusions

Unchecked ribonucleolytic activity is potentially lethal to cells, which have evolved RI to modulate this activity (Haigis et al. 2002a; Haigis et al. 2003). Transforming ribonucleases into zymogens represents another general strategy for controlling ribonucleolytic activity. We have developed an RNase A zymogen that is activated by the NS3 protease of HCV. The linker of our RNase A zymogen inhibits its activity by a mechanism similar to proteolytic zymogens—by sterically blocking substrate binding to the ribonuclease active site and dislocating key active-site residues. The linker of RNase A zymogens could serve an additional role in ribonuclease cytotoxicity by decreasing the affinity of RI for RNase A, even following activation. The HCV RNase A zymogen has the

necessary characteristics of a ribonuclease therapeutic, including wild-type activity after activation, a  $T_m$  value above physiological temperature, and low affinity for RI. By exploiting the proteolytic activity of NS3, RNase A zymogens could be selectively activated and circumvent the known mechanisms of microbial resistance, allowing for development of a ribonuclease-based therapeutic for HCV.

<b>Table 5.1.</b> Enzymatic activity of ribonuclease A zymogens <sup>a</sup>							
	$(k_{\text{cat}})_{\text{unactivated}}$	$(k_{\text{cat}})_{\text{activated}}$	$(K_{\text{M}})_{\text{unactivated}}$	$(K_{\text{M}})_{\text{activated}}$	$(k_{\text{cat}}/K_{\text{M}})_{\text{unactivated}}$	$(k_{\text{cat}}/K_{\text{M}})_{\text{activated}}$	$(k_{\text{cat}}/K_{\text{M}})_{\text{activated}}/$ $(k_{\text{cat}}/K_{\text{M}})_{\text{unactivated}}$
Ribonuclease	(s <sup>-1</sup> )	(s <sup>-1</sup> )	(10 <sup>-6</sup> M)	(10 <sup>-6</sup> M)	(10 <sup>3</sup> M <sup>-1</sup> s <sup>-1</sup> )	(10 <sup>3</sup> M <sup>-1</sup> s <sup>-1</sup> )	
Wild-type	—	280 ± 29	—	3.3 ± 0.2	—	83,000 ± 7000	—
1C zymogen	3.8 ± 0.1	86 ± 5	20 ± 2	4.3 ± 0.7	190 ± 20	20,000 ± 3000	105
2C zymogen	0.70 ± 0.02	10 ± 1	120 ± 1	140 ± 20	5.8 ± 0.4	74 ± 4	13
<sup>a</sup> Values of $k_{\text{cat}}$ , $K_{\text{M}}$ , and $k_{\text{cat}}/K_{\text{M}}$ (±SE) were determined for catalysis of poly(C) cleavage at 25 °C in 0.10 M MES–NaOH buffer (OVS-free), pH 6.0, containing NaCl (0.10 M). Initial velocity data were used to calculate values of $k_{\text{cat}}$ , $K_{\text{M}}$ , and $k_{\text{cat}}/K_{\text{M}}$ with the program DELTAGRAPH 5.5 (Red Rock Software, Salt Lake City, UT).							

**Table 5.2.** Physicochemical properties of a ribonuclease A zymogen

Ribonuclease	$(T_m)_{\text{unactivated}}^a$	$(T_m)_{\text{activated}}^a$	$(K_d)_{\text{unactivated}}^b$	$(K_d)_{\text{activated}}^b$	$(IC_{50})_{\text{unactivated}}^c$
	$^{\circ}C$	$^{\circ}C$	$nM$	$nM$	$\mu M$
Wild-type	$64^d$	—	$44 \times 10^{-6e}$	—	$>25$
1C zymogen	$51.6 \pm 0.4$	$56.3 \pm 0.7$	$>(10^3)$	$13 \pm 0.2$	$>25$

<sup>a</sup> Values of  $T_m$  for HCV zymogens were determined in PBS by CD spectroscopy.

<sup>b</sup> Values of  $K_d$  ( $\pm$ SE) were determined for the complex with pRI at 23 ( $\pm$ 2)  $^{\circ}C$ .

<sup>c</sup> Values of  $IC_{50}$  are for the incorporation of [*methyl*- $^3H$ ]thymidine into the DNA of K-562 cells treated with a ribonuclease, and were calculated with Equation 1.

<sup>d</sup> From (Rutkoski et al. 2005).

<sup>e</sup> From (Vicentini et al. 1990) for the pRI-RNase A complex.

**Figure 5.1** Structural model of unactivated 2C zymogen with 88/89 termini, 14-residue linker, and seven disulfide bonds. The conformational energy of the side chains of variant residues were minimized with the program SYBYL (Tripos). Atoms of the linker and cysteine residues are shown explicitly; non-native cystines and old and new termini are labeled. The sequence of the linker is given with flexible residues in black, the NS5A/5B cleavage sequence in red, and the scissile bond designated with a slash (“/”).

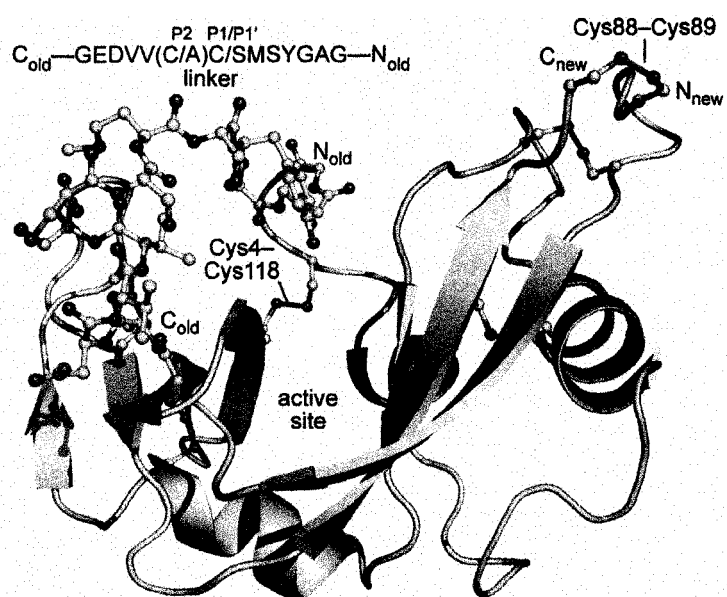




**Figure 5.2** Activation of 1C zymogen by the NS4A/NS3 protease. Activation at 37 °C was monitored at different times after the addition of 0.5 molar equivalents of NS4A/NS3 protease by SDS–PAGE in the presence of DTT. “std” is the protein molecular weight standard; “p” is NS4A/NS3 protease after a 15-min incubation at 37 °C; “z” is 1C zymogen after a 15-min incubation at 37 °C.

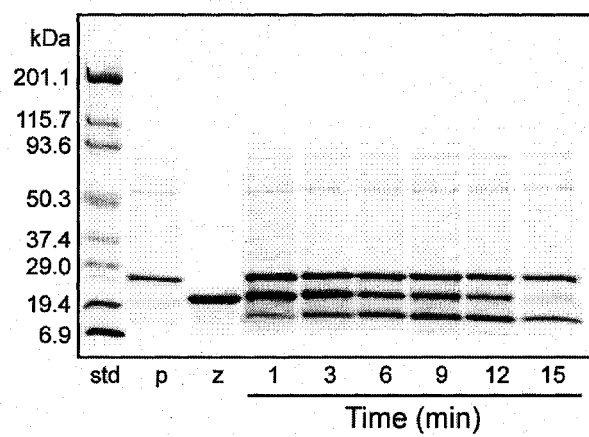


**Figure 5.3** Ribonucleolytic activity of unactivated 1C zymogen (●; 1.0  $\mu$ M), activated 1C zymogen (○; 6 nM), and wild-type RNase A (◆; 1.5 nM). Initial velocity data ( $v/[\text{ribonuclease}]$ ) were determined at increasing concentrations of poly(C). Data points are the average of three independent assays, and are shown  $\pm$ SE. Data were used to determine the values of  $k_{\text{cat}}$ ,  $K_{\text{M}}$ , and  $k_{\text{cat}}/K_{\text{M}}$  (Table 1).

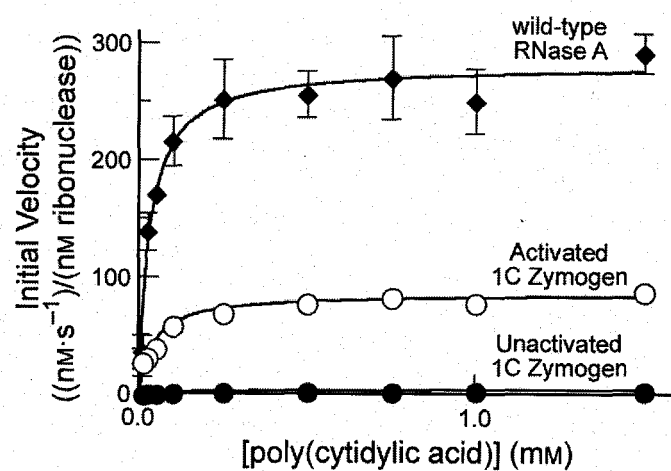
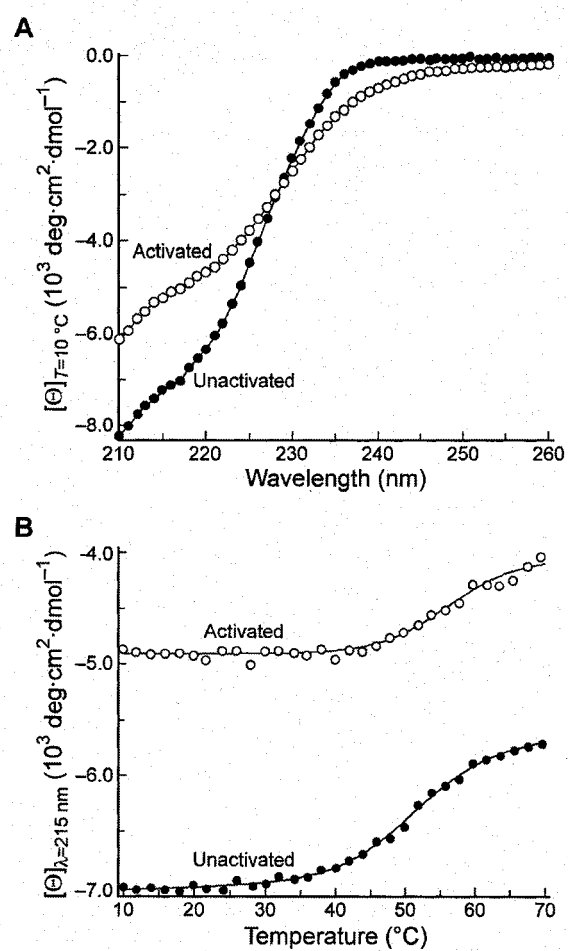


**Figure 5.4** Conformation and conformational stability of unactivated (●) and activated (○) 1C zymogens by circular dichroism. (A) Near-UV CD spectra of unactivated and activated 1C zymogens (0.5 mg/mL in PBS). (B) Thermal denaturation of unactivated and activated 1C zymogens (0.5 mg/mL in PBS). Molar ellipticity at 215 nm was monitored after a 2-min equilibration at each temperature. Data were fitted to a two-state model to determine values of  $T_m$  (Table 2).



## **Chapter Six**

### **Genetic Selection Reveals the Role of a Buried, Conserved Polar Residue**

Portions of this chapter were published as:

Johnson, R.J., Lin, S.R., Raines, R.T. (2007) Genetic Selection Reveals the Role of a Buried, Conserved Polar Residue. *Protein Sci.* **16**, In press. I performed or supervised all of the research described in this chapter.

## 6.1 Abstract

The burial of nonpolar surface area is known to enhance markedly the conformational stability of proteins. The contribution from the burial of polar surface area is less clear. Here, we report on the tolerance to substitution of Ser75 of bovine pancreatic ribonuclease (RNase A), a residue that has the unusual attributes of being buried, conserved, and polar. To identify variants that retain biological function, we used a genetic selection based on the intrinsic cytotoxicity of ribonucleolytic activity. Cell growth at 30, 37, and 44 °C correlated with residue size, indicating that the primary attribute of Ser75 is its small size. The side-chain hydroxyl group of Ser75 forms a hydrogen bond with a main-chain nitrogen. The conformational stability of the S75A variant, which lacks this hydrogen bond, was diminished by  $\Delta\Delta G = 2.5$  kcal/mol. Threonine, which can reinstate this hydrogen bond, provided a catalytically active RNase A variant at higher temperatures than did some smaller residues (including aspartate), indicating that a secondary attribute of Ser75 is the ability of its uncharged side chain to accept a hydrogen bond. These results provide insight on the imperatives for the conservation of a buried, polar residue.

## 6.2 Introduction

The conformational stability of a protein derives from the energetic difference between the unfolded and folded states. For the majority of proteins, this energetic difference ( $\Delta G^\circ_{\text{conf}}$ ) falls within the narrow range of  $-5$  to  $-15$  kcal/mol (Kumar et al. 2006; Rose et al. 2006). The small energetic distinction between the unfolded and folded states is maintained through the burial of nonpolar surface area, the formation of hydrogen bonds,



and other forces (Dill 1990; Myers and Pace 1996; Fleming and Rose 2005; Rose et al. 2006).

Conformational stability is only one attribute that leads to the existence of a residue at a particular position in an amino-acid sequence. Proteins often concede stability for function (Shoichet et al. 1995; Beadle and Shoichet 2002; DePristo et al. 2005; Pál et al. 2006). For example, altering residues in the active site of AmpC  $\beta$ -lactamase increases the stability of that enzyme, but greatly decreases its catalytic activity (Beadle and Shoichet 2002).

The selective pressures that determine the amino-acid composition at specific positions have been elucidated for nonpolar residues buried in the interior of a protein (Lim and Sauer 1989; 1991; Guo et al. 2004; Smith and Raines 2006). These residues are relatively invariant to substitution, as they are required to maintain the structural integrity of the protein, and they have lower substitution rates than expected by neutral drift (Choi et al. 2006). Still, it is unclear if these arguments also apply to buried polar residues.

Recently, the residues critical for the function of bovine pancreatic ribonuclease (RNase A) were revealed by using a novel genetic selection system (Smith and Raines 2006). Residues found to be essential included the canonical active-site residues (His12, Lys41, and His119), half-cystines, and residues buried in the hydrophobic core (Coll et al. 1999). Although serine is the most abundant residue in RNase A, only one of its fifteen serine residues was found to be critical (Smith and Raines 2006). That unique residue is Ser75, which is the most buried of the serine residues ( $ASA = 1.9 \text{ \AA}^2$ ; Figures 1A and 1B) and is highly conserved among homologous ribonucleases (Smith and Raines 2006). In the

hydrophobic core of RNase A, Ser75 forms two hydrogen bonds with Ile106, another essential residue that expedites protein folding (Coll et al. 1999). Predictably, replacing Ile106 with an alanine residue lowers the value of  $T_m$  by 14 °C (Coll et al. 1999). No variant at position 75 has been studied previously.

Here, we report on the biochemical attributes that lead to the conservation of a buried polar residue. To do so, we create RNase A variants with each of the twenty proteinogenic amino acids at position 75. We then subject these twenty variants to the extant genetic selection (Smith and Raines 2006), but at different temperatures so as to glean additional information. Finally, we characterize the five most interesting variants in detail. The results provide a comprehensive picture of the effect of a buried, polar residue on the conformational stability and catalytic activity of a protein, and serve to reveal the physicochemical attributes that lead to its evolutionary conservation.

### 6.3 Experimental Procedures

*General.* *Escherichia coli* BL21 (DE3) cells, *E. coli* Origami™ B (DE3) cells, and plasmid pET27b(+) were from Novagen (Madison, WI). The fluorogenic ribonuclease substrate, 6-FAM-dArU(dA)<sub>2</sub>-6-TAMRA, and DNA oligonucleotides for mutagenesis were from Integrated DNA Technologies (Coralville, IA). Protein purification columns and the pGEX vector were from GE Healthcare (Piscataway, NJ). MES buffer (Sigma–Aldrich, St. Louis, MO) was purified by anion-exchange chromatography to remove trace amounts of oligomeric vinylsulfonic acid (Smith et al. 2003). All other chemicals were of commercial grade or better, and were used without further purification.

Luria–Bertani (LB) agar contained (in 1.00 L) tryptone (10 g), yeast extract (5 g), NaCl (10 g), and agar (15 g). PBS, pH 7.4, contained (in 1.00 L) NaCl (8.0 g), KCl (2.0 g),  $\text{Na}_2\text{HPO}_4 \cdot 7\text{H}_2\text{O}$  (1.15 g),  $\text{KH}_2\text{PO}_4$  (2.0 g), and  $\text{NaN}_3$  (0.10 g).

Fluorescence spectroscopy was performed with a QuantaMaster1 photon-counting fluorimeter equipped with sample stirring (Photon Technology International, South Brunswick, NJ). CD data were collected with a model 62A DS CD spectrometer (Aviv, Lakewood, NJ) equipped with a temperature controller. Matrix-assisted laser desorption/ionization time-of-flight (MALDI–TOF) mass spectrometry was performed with a Voyager-DE-PRO Biospectrometry Workstation (Applied Biosystems, Foster City, CA). CD and MALDI–TOF mass spectrometry experiments were performed at the campus Biophysics Instrumentation Facility.

*Genetic Selection.* Variants of RNase A with all twenty amino acids at position 75 were created by using plasmid pGEX-RNase A, which was derived from pGEX-4T3 (Smith and Raines 2006), and the Quikchange site-directed mutagenesis kit (Stratagene, La Jolla, CA). Codons for position 75 substitution were chosen for optimized protein expression in *E. coli*, based on known codon usage (Aota et al. 1988). The presence of Met(–1) has been shown to have no discernable effect on the ribonucleolytic activity or conformational stability of RNase A (Kelemen et al. 1999). The identity of codons at position 75 and elsewhere was confirmed by DNA sequence analysis. Purified plasmid DNA from all twenty RNase A variants was transformed into Origami™ B (DE3) cells. Transformed Origami B (DE3) cells were spread onto LB agar containing ampicillin (100  $\mu\text{g}/\text{mL}$ ), kanamycin (20  $\mu\text{g}/\text{mL}$ ), and tetracycline (12.5  $\mu\text{g}/\text{mL}$ ), and allowed to grow at 23, 30, 37, or 44 °C for 48 h.

Results were confirmed by repeating the selection (*i.e.*, transformation, spreading, and growth).

*Protein Purification.* RNase A and variants of RNase A were purified from inclusion bodies by using the same high-yielding procedure described previously (delCardayré et al. 1995; Rutkoski et al. 2005). A pET27b(+) plasmid containing DNA that encodes wild-type RNase A was used to produce Ser75-variants of RNase A (Leland et al. 1998; Rutkoski et al. 2005), using the Quikchange site-directed mutagenesis kit (Stratagene, La Jolla, CA). The molecular mass of each purified RNase A variant was determined with MALDI-TOF mass spectrometry.

*Enzymatic Activity.* The ribonucleolytic activity of wild-type RNase A and its Ser75-variants was determined by using 6-FAM-dArU(dA)<sub>2</sub>-6-TAMRA as the substrate (Kelemen et al. 1999). Assays were carried out at 23 (±2) °C in 2.0 mL of 0.10 M MES-NaOH buffer, pH 6.0, containing NaCl (0.10 M). Fluorescence data were fitted to the equation:

$$k_{\text{cat}}/K_{\text{M}} = (\Delta I/\Delta t)/((I_{\text{f}} - I_0)[\text{E}]) \quad (1)$$

In equation 1,  $\Delta I/\Delta t$  represents the initial reaction velocity,  $I_0$  is the fluorescence intensity before the addition of a ribonuclease,  $I_{\text{f}}$  corresponds to the final fluorescence intensity after complete substrate hydrolysis, and  $[\text{E}]$  is the concentration of added ribonuclease.

*Secondary Structure and Conformational Stability.* CD spectroscopy was used to assess the secondary structure of the RNase A variants (delCardayré et al. 1995). A

solution of PBS containing an RNase A variant (0.5 mg/mL) was incubated for 5 min at 25 °C, and CD spectra were then acquired from 260 to 205 nm in 1-nm increments. CD spectra were collected at least twice for each RNase A variant, and data points are shown as the mean residue-weight ellipticity at each wavelength.

CD spectroscopy was also used to evaluate the conformational stability of the variants of RNase A (Johnson et al. 2006). PBS containing each of the RNase A variants (0.5 mg/mL) was heated from 25 to 75 °C in 2-°C increments. The change in molar ellipticity at 215 nm was measured after a 2-min equilibration at each temperature, and the entire experiment was repeated at least once. Raw CD data at 215 nm were used to determine the values of  $T_m$  and  $\Delta H_m$  using Igor Pro 5.04B (Wavemetrics Inc, Lake Oswego, Oregon) and the Gibbs–Helmholtz equation (Pace 1990; Eberhardt et al. 1996; Pace et al. 1998; Smith and Raines 2006):

$$\Delta G = \Delta H_m(1 - T/T_m) + \Delta C_p[T - T_m - T \ln(T/T_m)] \quad (2)$$

Values of  $\Delta C_p$  were held constant ( $\Delta C_p = 0$ ), as the  $\Delta C_p$  values calculated by fitting the raw CD data to equation 2 were small compared to  $\Delta H_m$ . Also, curve-fitting of the raw CD data with and without  $\Delta C_p$  had no affect on the  $T_m$  values and only slightly changed the  $\Delta H_m$  value for wild-type RNase A (< 5%). The values of  $\Delta \Delta G$  for the S75A and S75T variants were calculated at the  $T_m$  of wild-type RNase A by replacing  $T$  in equation 2 with the  $T_m$  values for S75A and S75T, respectively. Analogous values for S75C and S75R were not calculated because their large  $\Delta T_m$  values impose a high error in the calculation.

## 6.4 Results

*Genetic Selection at Serine 75.* RNase A produced in traditional *Escherichia coli* strains aggregates to form enzymatically inactive inclusion bodies, as its requisite four disulfide bonds cannot form in the reducing environment of the cytosol (delCardayré et al. 1995). Engineered *E. coli* strains, such as the Origami™ strain (Novagen, Madison, WI), provide a more oxidizing cytosol wherein RNase A can fold (Smith and Raines 2006). Folded RNase A catalyzes the degradation of bacterial RNA, resulting in cell death. Even leaky expression of wild-type RNase A from the uninduced  $P_{tac}$  promoter is adequate to cause cell death (Smith and Raines 2006).

We used the ability of properly folded, active RNase A to elicit cell death to explore the role of Ser75. Twenty plasmids encoding variants in which position 75 was substituted with all 20 natural amino acids were created by site-directed mutagenesis, and these plasmids were transformed individually into Origami cells. The transformed Origami cells were grown at four different temperatures (23, 30, 37, and 44 °C) and selected for growth. At 23 °C, no variant reduced the ribonucleolytic activity enough to allow for the growth of *E. coli* cells (data not shown). Results at the other three temperatures are shown in Figure 6.1C. At 44 °C, which is 17 °C lower than the  $T_m$  value of wild-type RNase A (Table 6.1), only serine (wild-type) or its substitution with glycine, alanine, or threonine significantly inhibited cell growth. At 30 °C, 12 variants were identified (glycine, alanine, serine, cysteine, proline, aspartate, threonine, asparagine, valine, histidine, methionine, and arginine) that inhibited cell growth. The amino-acid substitutions that diminished

ribonucleolytic activity sufficiently to allow for the growth of *E. coli* cells are depicted in Figure 6.1D, in which the amino acids are listed in the order of their van der Waals volume (Creighton 1993). The inhibition of growth correlates with the van der Waals volume of the amino-acid substitution. At 44 °C, the amino-acid substitutions that retain enzymatic activity are the smallest amino acids with the exception of threonine, which has a van der Waals volume that is larger than cysteine, proline, or aspartate. The ability of the threonine substitution at position 75 to maintain the catalytic activity and stability of RNase A at 44 °C, even with its larger van der Waals volume, suggests that it still forms a hydrogen bond with Ile106.

Data from 37 and 30 °C follow a similar pattern, where growth of the Origami cells is related to the van der Waals volume of the substituted amino acid (Figure 6.1D). At 30 °C, there are also outliers to this trend. For example, the van der Waals volume of arginine is 24 Å<sup>2</sup> greater than that of methionine, which is the amino acid with the next closest volume that inhibited growth (Figure 6.2B). To understand better the relationship between the van der Waals volume and hydrogen-bonding capability of amino-acid substitutions at position 75 and the resulting ribonucleolytic activity and conformational stability of the RNase A variants, five variants (serine, alanine, threonine, cysteine, and arginine) were isolated (Table 6.2) and subjected to detailed analysis. These variants were chosen based on their small size (alanine), ability to form a hydrogen bond with Ile106 (serine and threonine), and unexpected retention of ribonucleolytic activity in the genetic selection (cysteine and arginine).

*Physiochemical Properties of RNase A Variants.* To insure that all five RNase A variants were folded properly at 25 °C, far-UV circular dichroism (CD) spectroscopy was used to discern any changes in secondary structure (Kelly et al. 2005). Each variant was found to have a similar CD spectrum (Figure 6.2A), suggesting that substitution at position 75 does not have a large effect on the secondary structure of RNase A. This result is consistent with studies in other proteins that show that single substitutions tend to have small effects on global protein structure (Matthews 1987; Stites et al. 1991; Chen et al. 1993). RNase A variants with lower conformational stability (Table 6.1; arginine and cysteine) did, however, have lower mean residue-weight ellipticity, consistent with minor changes to local secondary structure.

To characterize these RNase A variants further, their conformational stabilities were determined by monitoring their CD spectrum at 215 nm as a function of temperature (Figure 6.2B) (Johnson et al. 2006). The temperature at the midpoint of the transition curve ( $T_m$ ) and associated change in enthalpy ( $\Delta H_m$ ) are listed in Table 6.1. A large range of conformational stabilities was generated upon substitution at position 75. Alanine and threonine residues decrease the value of  $T_m$  by 8 °C, whereas arginine decreases the  $T_m$  by 23 °C. A similar trend is observed for the values of  $\Delta H_m$ , except for the S75C variant, which has a  $\Delta H_m$  value that is 32 kcal/mol greater than that of wild-type RNase A. The S75C variant exhibits a steady increase in ellipticity following denaturation (Figure 6.2B), suggesting that a two-state model for its unfolding is invalid. This anomalous behavior could be caused by the free cysteine residue in S75C RNase A eliciting dimerization via disulfide bond formation, leading to aggregation. Otherwise, the  $T_m$  values for the purified



RNase A variants closely follow the growth inhibition results (Figure 6.2). The  $T_m$  values of the S75T and S75A variants are  $>44$  °C, that of the S75C variant is  $>37$  °C, and that of the S75R is  $>30$  °C (Table 6.1), demonstrating the ability of the genetic selection to report accurately on conformational stability.

This large variation in other physicochemical attributes of the variants is not reflected in their catalytic activity (Table 6.1). At 25 °C, all variants have ribonucleolytic activity within twofold of the wild-type enzyme, suggesting, as do the data in Figure 6.2A, that each variant assumes the structure of wild-type RNase A at 25 °C. This negligible effect of substitution at position 75 on ribonucleolytic activity is most likely true for any amino-acid substitution, as the growth of all transformed *E. coli* cells was inhibited at 23 °C (data not shown). Thus, position 75 in RNase A strongly influences the conformational stability of the enzyme, but does not affect its ribonucleolytic activity.

## 6.5 Discussion

*Role of a Buried Polar Residue in Conformational Stability.* The neutral theory of molecular evolution states that the vast majority of mutations do not affect the fitness of an organism (Kimura 1968; 1983). Still, amino-acid substitutions often do have detrimental effects on the structure and function of a particular protein (DePristo et al. 2005; Pál et al. 2006). Understanding the tolerance of specific conserved residues to substitution and the evolutionary pressures that select for conservation could reveal the underlying evolutionary mechanisms and facilitate identification of disease-inducing residues (Benner 2001; Guo et al. 2004; DePristo et al. 2005; Smith and Raines 2006). We have combined data from a

genetic selection with phylogenetic data to investigate these selective pressures as applied to a buried, polar residue.

As our model system, we chose RNase A, which is one of the best characterized proteins (D'Alessio and Riordan 1997; Raines 1998). In seminal work, Anfinsen used RNase A to show that “the native conformation is determined by the totality of interatomic interactions and hence by the amino acid sequence, in a given environment” (Anfinsen 1973). Subsequently, RNase A has been used to evaluate the factors involved in protein folding and stability, especially disulfide bond formation and prolyl peptide bond isomerization (Wedemeyer et al. 2000; Wedemeyer et al. 2002). The RNase A superfamily has also served as an archetype for studying many aspects of molecular evolution, including mammalian speciation (Beintema 1987; Beintema et al. 1988b; Beintema et al. 1997; Yu and Zhang 2006), adaptive parallel evolution (Schienman et al. 2006; Zhang 2006), the shuffling of disulfide bonds (Zhang 2007), and gene duplication (Sassi et al. 2007). Sequences of RNase A homologs have been reported from >200 organisms (Beintema 1987; Beintema et al. 1988b; Beintema et al. 1997; Nitto et al. 2006; Pizzo et al. 2006; Yu and Zhang 2006), making RNase A an exceptional protein with which to study the selective pressures that lead to amino-acid conservation.

We have focused on the basis for the conservation of a particular buried polar residue in RNase A, Ser75. Within the 266 known members of the RNase A superfamily (Smith and Raines 2006), Ser75 is conserved in 238 (89.5%). This level of conservation is indicative of biological importance. Recently, we showed that Ser75 is indeed critical to

ribonuclease function (Smith and Raines 2006). Still, whether Ser75 played a role in enzymatic catalysis or conformational stability (or both) had been unknown.

The 28 known ribonucleases that diverge from a serine residue at position 75 are listed in Table 6.3. Interestingly, each of these divergent ribonucleases has a residue that enables function at 30 °C in our genetic selection (Figures 1C and 1D). Moreover, most of the amino acids that replace serine at position 75 in these divergent ribonucleases fall into the subset of smaller amino acids that lead to cytotoxicity at 44 °C (glycine, threonine, and cysteine). This direct correlation between the ribonuclease sequence data (Table 6.3) and our genetic selection data (Figure 6.2) indicates that a small amino acid at position 75 is necessary for ribonucleases to function properly (Figure 6.1B).

Another salient characteristic of this buried polar residue is its ability to interact with proximal residues in the folded protein (Figures 1A and 1B). The hydrogen bond formed from the hydroxymethyl sidechain of Ser75 adds an additional  $\Delta\Delta G = 2.5$  kcal/mol of energetic stability to RNase A over other small amino acids, but this hydrogen bond does not seem to be the only selective pressure. Substitution with threonine maintains ribonucleolytic activity at 44 °C (Figures 1C and 1D), presumably because it can form a hydrogen bond from its hydroxyethyl side chain to Ile106. S75T RNase A is, however, not as stable as the S75A variant (Table 6.1). Adding a methylene group to the side chain of Ser75 (as in the S75T variant) disrupts the energetic stability of wild-type RNase A more than does removing the oxygen atom from its side chain (as in the S75A variant; Table 6.1). Thus, the amino acid at position 75 in ribonucleases, especially RNase A, appears to have been selected primarily because of its van der Waals volume. Among the amino acids with

a small van der Waals volume, serine has been selected because of the additional energetic stability imparted by its ability to form a hydrogen bond with Ile106. Similarly, a conserved glutamate residue in pyrrolidone carboxyl peptidases from hyperthermophiles is completely buried and stabilizes that protein by forming hydrogen bonds with main-chain atoms (Kaushik et al. 2006).

*Hydrogen Bonds and Conformational Stability.* The influence of hydrogen bonds on the conformational stability of proteins has generated much interest (Dill 1990; Myers and Pace 1996; Baldwin 2003). The recent observation by Rose and coworkers that virtually all of the nitrogens and oxygens in proteins participate in hydrogen bonds provides compelling evidence that these hydrogen bonds confer much stability (Fleming and Rose 2005; Rose et al. 2006). Pace and coworkers have demonstrated that intramolecular hydrogen bonds increase the packing density and van der Waals interactions of a protein (Schell et al. 2006). For example, the average volume occupied by a serine side chain decreases by  $1 \text{ \AA}^3$  when the side chain is engaged in a hydrogen bond.

Ser75 of RNase A appears to function in this dual manner. The main-chain nitrogen of Ile106 needs a hydrogen-bonding partner, and other residues are not in a position to fulfill that role. On average, replacing a serine residue with alanine results in  $\Delta\Delta G = -1.1 \pm 1.5$  kcal/mol for serine residues that are  $77 \pm 25\%$  buried from solvent (Myers and Pace 1996). Ser75 of RNase A falls on the extreme end of this continuum, having  $\Delta\Delta G = -2.5$  kcal/mol (Table 6.1) and being 98.1% buried. These data underscore the importance of the Ser75...Ile106 hydrogen bond to conformational stability. It is noteworthy that the stability conferred by Ser75 is comparable to that measured for the buried hydrogen bond between

the side chain of Tyr97 and main-chain oxygen of Lys41 of RNase A (Eberhardt et al. 1996), as well as buried hydrogen bonds in the microbial ribonucleases, RNase T1 and barnase (Shirley et al. 1992; Chen et al. 1993). A buried salt bridge in triosephosphate isomerase is likewise critical to the function of that enzyme (Silverman et al. 2001).

The importance of the Ser75...Ile106 hydrogen bond is apparent from its environment. The relative importance of a particular hydrogen bond to protein stability is related to its mobility (Pace et al. 2001). Ser75 is packed tightly in the interior of RNase A (Figure 6.1B), being surrounded by seven residues that lie within 3.9 Å. Thus, the Ser75...Ile106 hydrogen bond could contribute to stability not only by its satisfying the hydrogen-bonding requirement of Ile106, but also by eliciting an increase in van der Waals contacts within the hydrophobic core of RNase A.

## 6.6 Conclusions

By combining genetic selection with phylogenetic data, we sought to reveal the characteristics that select for a buried, polar residue and understand the tolerance to mutation of this conserved residue. A trend was observed in both genetic and evolutionary selection toward amino acids with small van der Waals volume, implying a requirement for a small amino acid at position 75 to maintain conformational stability. A serine substitution adds an additional 2.5 kcal/mol of energetic stability beyond an alanine residue due to its ability to form a hydrogen bond with Ile106, which could also increase the packing density of the protein interior. Ser75 functions largely to maintain the stability of RNase A, but has no direct impact on its catalytic activity at 25 °C. Our genetic selection

could be useful to probe the contribution of other ribonuclease residues to their biological function and the selective pressures responsible for their conservation.

**Table 6.1.** *Biochemical properties of wild-type RNase A and variants at Ser75*

RNase A	$T_m$ (°C) <sup>a</sup>	$\Delta T_m$ (°C) <sup>b</sup>	$\Delta H_m$ (kcal/mol) <sup>c</sup>	$\Delta\Delta G$ (kcal/mol) <sup>d</sup>	$k_{cat}/K_M$ ( $10^6 \text{ M}^{-1}\text{s}^{-1}$ ) <sup>e</sup>
Wild-type	$61.1 \pm 0.3$	—	$104.8 \pm 6.1$	—	$39 \pm 7$
S75A	$53.2 \pm 0.1$	7.9	$100.9 \pm 5.0$	-2.5	$22 \pm 5$
S75T	$52.2 \pm 0.1$	8.9	$103.2 \pm 4.2$	-2.8	$25 \pm 3$
S75C <sup>f</sup>	$43.2 \pm 0.1$	17.9	$137.1 \pm 6.0$	—	$41 \pm 9$
S75R <sup>f</sup>	$38.2 \pm 0.1$	22.9	$83.0 \pm 6.2$	—	$18 \pm 7$

<sup>a</sup> Values of  $T_m$  ( $\pm$ SE) for RNase A and variants were determined in PBS by CD spectroscopy (Johnson et al. 2006).

<sup>b</sup>  $\Delta T_m = (T_m)_{\text{wild-type}} - (T_m)_{\text{variant}}$

<sup>c</sup> Values of  $\Delta H_m$  ( $\pm$ SE) were determined by fitting the change in the molar ellipticity at 215 nm for each RNase A variant to equation 2 (Pace 1990; Eberhardt et al. 1996; Pace et al. 1998).

<sup>d</sup> Values of  $\Delta\Delta G$  ( $\pm$ SE) were calculated by replacing  $T$  in equation 2 with the  $T_m$  value of the variant (Pace 1990; Eberhardt et al. 1996; Pace et al. 1998).

<sup>e</sup> Values of  $k_{cat}/K_M$  ( $\pm$ SE) were determined for catalysis of 6-FAM-dArU(dA)<sub>2</sub>-6-TAMRA cleavage at 25 °C in 0.10 M MES-NaOH buffer, pH 6.0, containing 0.10 M NaCl (Kelemen et al. 1999; Smith et al. 2003).

<sup>f</sup> A value of  $\Delta\Delta G$  was not calculated for this variant because of its sensitivity to a small (and unknown) change in  $\Delta C_p$ .

**Table 6.2.** *Mass analysis of wild-type RNase A and variants at Ser75*

RNase A	<i>m/z</i> , Expected (Da)	<i>m/z</i> , Observed (Da) <sup>a</sup>
Wild-type	13690	13695
S75A	13674	13675
S75T	13704	13708
S75C	13706	13706
S75R	13759	13761
<sup>a</sup> Values were determined by MALDI-TOF mass spectrometry.		



**Table 6.3.** *Residues other than serine at position 75 (or the structurally analogous position) in the RNase A superfamily*

<i>RNase 4</i>		
RNAS4_BOVIN	<i>Bos taurus</i>	Gly
RNAS4_HUMAN	<i>Homo sapiens</i>	Gly
RNAS4_MOUSE	<i>Mus musculus</i>	Gly
RNAS4_PANTR	<i>Pan troglodytes</i>	Gly
RNAS4_RAT	<i>Rattus norvegicus</i>	Gly
Q9TV21_SAISC	<i>Saimiri sciureus</i>	Gly
RNAS4_PIG	<i>Sus scrofa</i>	Gly
<i>Frog Ribonucleases</i>		
Q9DFY6_RANCA	<i>Rana catesbeiana</i>	Asn
Q6EUW9_RANCA	<i>Rana catesbeiana</i>	Arg
Q6EUW8_RANCA	<i>Rana catesbeiana</i>	Arg
Q9DFY7_RANCA	<i>Rana catesbeiana</i>	Arg
Q9DFY5_RANCA	<i>Rana catesbeiana</i>	Arg
Q98SM2_RANCA	<i>Rana catesbeiana</i>	Pro
Q6EUW7_RANCA	<i>Rana catesbeiana</i>	Thr
RNASO_RANCA	<i>Rana catesbeiana</i>	Thr
Q9DFY8_RANCA	<i>Rana catesbeiana</i>	Thr
Q9DF78_RANCA	<i>Rana catesbeiana</i>	Thr
RNASL_RANCA	<i>Rana catesbeiana</i>	Thr
Q98SM1_RANCA	<i>Rana catesbeiana</i>	Thr
Q98SM0_RANCA	<i>Rana catesbeiana</i>	Thr
LECS_RANJA	<i>Rana japonica</i>	Thr
Q8UVX5_RANPI	<i>Rana pipiens</i>	Thr
Q9I8V8_RANPI	<i>Rana pipiens</i>	Thr
<i>Other Ribonucleases</i>		
ANG1_CHICK	<i>Gallus gallus</i>	Thr
05GAL6_CHICK	<i>Gallus gallus</i>	Thr
RSFR_CHICK	<i>Gallus gallus</i>	Thr
Q5NVS4_PONPY	<i>Pongo pymaeus</i>	Gly
O9JKG3_MUSR	<i>Mus caroli</i>	Cys

<sup>a</sup> From a compilation of 266 RNase A superfamily members listed as their EMBL accession numbers (Smith and Raines 2006).

**Figure 6.1** Genetic selection to reveal the influence of substitutions at position 75 to the activity and stability of RNase A. (A) Ribbon diagram of RNase A (green) in which the atoms of Ser75 and Ile106 are depicted explicitly and putative hydrogen bonds are shown with black dashed lines. (B) Space-filling model of Ser75 and Ile106 in the same orientation as panel A. Ser75 and Ile106 are in red, and all other RNase A residues are in gray. Images in panels A and B were created with PDB entry 7RSA (Wlodawer et al. 1988) and the program PyMOL (DeLano Scientific, South San Francisco, CA). (C) Growth of Origami™ *E. coli* cells that produce an RNase A variant containing the indicated amino acid residue at position 75. Plates were incubated at the indicated temperature for 48 h. Cells producing active and thus cytotoxic RNase A variants will be inviable; those producing inactive variants will be viable. (D) Graphical representation of the results from panel C. Amino acids are listed in order of increasing van der Waals volume (Richards 1974).

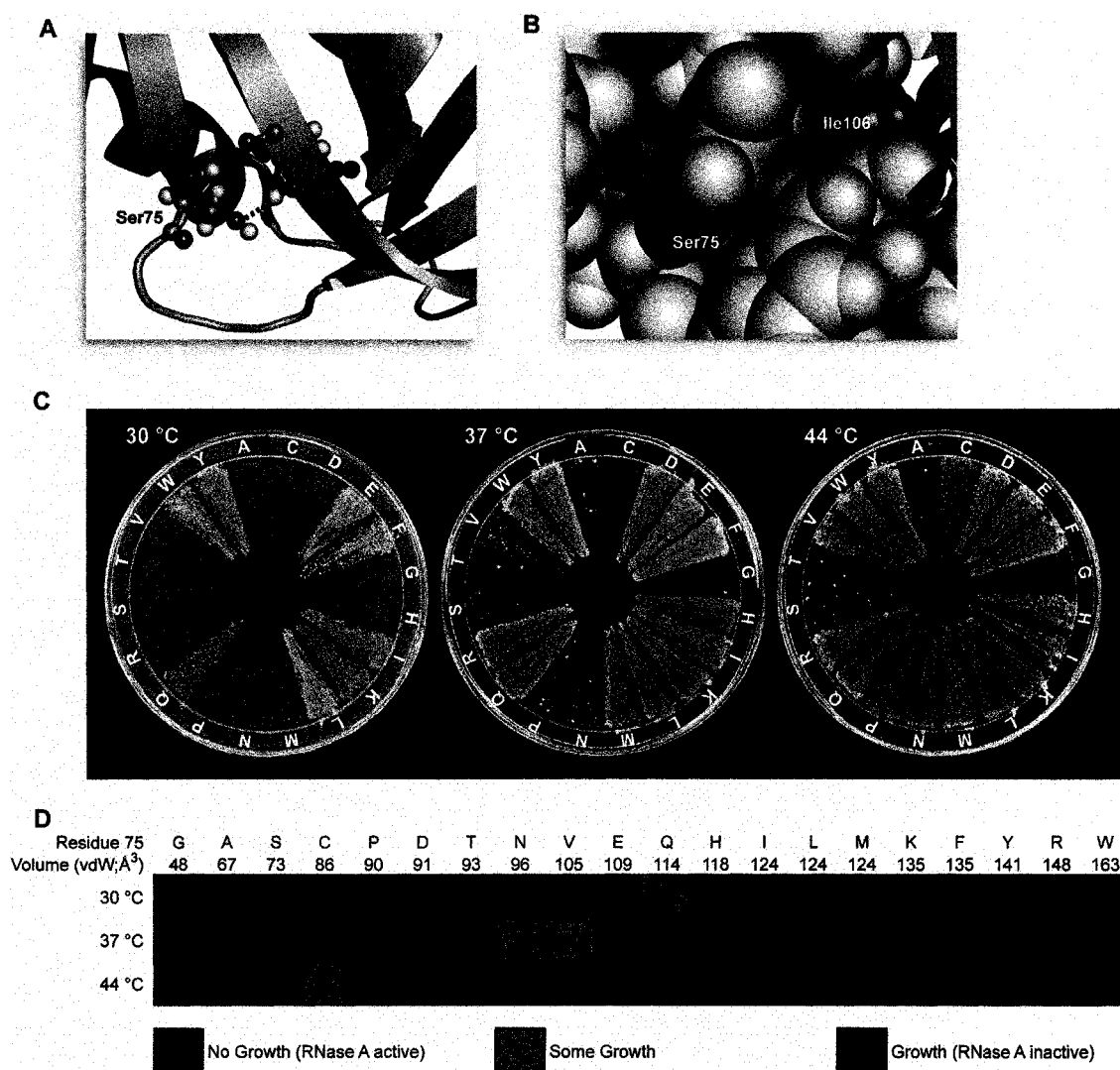
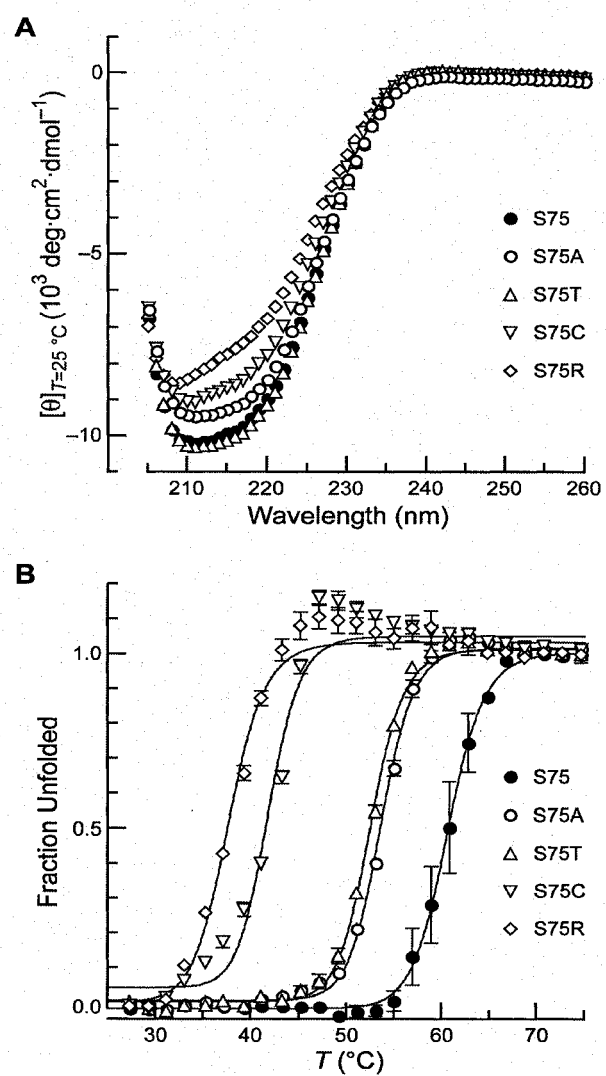


**Figure 6.2** Conformational stability of five variants of RNase A. (A) Far-UV CD spectra of the indicated position 75 variants of RNase A (0.5 mg/mL in PBS). (B) Thermal denaturation of the indicated position 75 variants of RNase A (0.5 mg/mL in PBS). Molar ellipticity at 215 nm was monitored after a 2-min equilibration at each temperature. Data points are mean values ( $\pm$ SE) from  $\geq 2$  experiments, and were fitted to a two-state model to determine values of  $T_m$  (Table 1).



## **Chapter Seven**

### **Conclusions and Future Directions**

## 7.1 Conclusions

Pancreatic ribonucleases have exciting potential as chemotherapeutics, due to their selective toxicity toward cancerous cells. With their high catalytic activity and low immunogenicity, mammalian ribonucleases are especially promising chemotherapeutic candidates. To understand the cytotoxic potential of mammalian ribonucleases, this dissertation sought to clarify the mechanism of their cytotoxicity.

Chapters Two and Three examined the effect of electrostatics on two aspects of ribonuclease cytotoxicity. Using the information from the hRI·RNase 1 complex crystal structure and electrostatic repulsion, Chapter Two describes the design and engineering of the most RI-evasive variant. This variant, R39D/ N67D/ N88A/ G89D/ R91D RNase 1, had greater than  $10^9$ -fold lower affinity for RI and was modestly toxic toward an erythroleukemia cell line.

Chapter Three showed that the low net molecular charge of this RI-evasive variant was inhibiting its internalization and consequently its cytotoxicity. Additionally, Coulombic forces were found to both endanger and defend cells from invading ribonucleases due to the competing extracellular and intracellular equilibria. These competing equilibria permit more positively charged ribonucleases to be internalized at a higher level, but upon cellular entry, these variants are bound more tightly by RI.

Chapter Four described the heterologous production and purification of bovine RI, the intraspecies binding partner of RNase A. Bovine RI was found to bind both RNase A and RNase 1 with high affinity, as compared to human RI, which bound its cognate ribonuclease, RNase 1, with 100-fold higher affinity. Bovine RI was also found to be 4-

fold more stable to oxidation than human RI, suggesting a greater role for human RI as an antioxidant.

Chapter Five examined the targeting of ribonuclease toxicity toward hepatitis C virus-infected cells by designing a zymogen, or inactive precursor of RNase A. This zymogen was activated by the NS3 protease of the hepatitis C virus, and this activation recapitulated many of the characteristics of proteolytic zymogens. Additionally, the RNase A zymogen was RI-evasive in both its unactivated and its activated form, and had high conformational stability.

The data contained in Chapter Six furthered work on residues essential to the catalytic activity of RNase A, by examining the contribution of a buried serine residue to the conformational stability and catalytic activity of RNase A. Serine 75 was found to contribute significantly to the conformational stability of RNase A through its small van der Waals volume and hydrogen bonds to isoleucine 106.

Overall, this dissertation furthered the understanding of ribonuclease cytotoxicity and expanded the potential of mammalian ribonucleases as cancer therapeutics.

## **7.2 Future Directions**

Ribonucleases offer the potential for many exciting studies on both protein structure–function relationship and their application to cancer therapy. Multiple aspects of this dissertation could be expanded to provide additional knowledge about ribonucleases and protein structure. The ribonuclease inhibitors from only a few species have been described currently, but with the determination of additional genome sequences, ribonuclease



inhibitors from other species could be identified and compared to those described in Chapter Four. This sequence comparison could be used to probe the co-evolution of ribonucleases with the ribonuclease inhibitor and to understand the biological role of the numerous free cysteine residues in the ribonuclease inhibitor.

The relationship between ribonuclease internalization and electrostatics could also be expanded using flow cytometry and latent fluorophores. Quantitation of cellular internalization over a wider range of net molecular charges encompassing a greater percentage of the residues in a ribonuclease would greatly expand the understanding of ribonuclease internalization. Additionally quantitation of ribonuclease internalization in both cancerous and noncancerous cells over a range of molecular charges would resolve whether the charge on a cancer cell determines the selectivity of the ribonuclease for cancerous cells.

Finally, studies on the residues critical to ribonucleolytic activity could be expanded to include additional members of the ribonuclease A superfamily. Other superfamily members such as RNase 2, 3, and 7 have been proposed to be cytotoxic in the absence of ribonucleolytic activity, so elucidating the residues necessary for their cytotoxicity could provide new information about their cytotoxic mechanism. Additionally, comparison of the critical residues from ribonucleases with divergent sequences could identify the residues essential to any ribonuclease and help in understanding the rapid evolution of ribonucleases in vertebrates.

## **Appendix I**

### **Tissue expression and ribonucleolytic activity of human ribonucleases 11–13**

### A1.1 Abstract

Ribonucleases perform many biological roles in the cell. Most of these roles are engendered by the ability of ribonucleases to degrade RNA efficiently. Yet, in the recently identified human ribonucleases 11–13, key catalytic residues are removed, suggesting that their biological roles are independent of RNA degradation. The mRNA for RNase 11–13 was also present in RNA isolated from 12 tissues, indicative of a common biological role, irrespective of cell type. To examine the potential ribonucleolytic activity of RNases 11–13, DNA encoding these ribonucleases was cloned and the resulting proteins expressed in *Escherichia coli*. All three ribonucleases were produced at high levels in *E. coli*, but aggregated into inclusion bodies. *In vitro* oxidative folding trials of the ribonucleases produced inconclusive results. Instead genetic selection for ribonucleolytic activity in the Origami *E. coli* strain indicates that RNase 12 has low catalytic activity caused by its N-terminus and its two conserved active-site residues. These initial studies indicated that RNases 11–13 are common components of all tissues and that RNase 12 has limited ribonucleolytic activity. Future studies on these ribonucleases could identify novel biological roles for ribonucleases.

### A1.2 Introduction

The pancreatic ribonuclease superfamily is a family of vertebrate specific enzymes with diverse biological roles (Beintema 1987; Beintema et al. 1988b; Beintema et al. 1997). Bovine pancreatic ribonuclease (RNase A), the prototype of a pancreatic ribonuclease superfamily member, was perhaps the most studied enzyme of the 20<sup>th</sup> century, due to its

small size and ease of purification (Raines 1998). Yet, its biological activity, digestion of dietary RNA in the ruminant gut, is fairly pedestrian (Barnard 1969). This biological activity is, however, atypical of the enzyme superfamily, as the family is undergoing rapid evolution concomitant with the addition of new biological roles (Singhania et al. 1999; Zhang et al. 2002).

Thirteen members of the pancreatic RNase A superfamily have been identified in humans (*Homo sapiens*), and varied biological roles have been assigned to these human ribonucleases (Cho et al. 2005). For instance, RNase 5 (angiogenin) induces blood vessel proliferation by transducing to the nucleus and binding to rRNA (Shapiro et al. 1986b; Tsuji et al. 2005). Additionally, RNase 2, 3, and 7 are involved in immune function and possess anti-microbial and anti-inflammatory activity (Rosenberg and Dyer 1995; Huang et al. 2007). The biological activities of various other members were, however, unknown (Cho et al. 2005).

The biological activities of most ribonucleases stem from their ability to degrade RNA, and substitution of the residues essential for RNA degradation eliminates their biological activity (Shapiro and Vallee 1989; Leland and Raines 2001; Lee and Raines 2003). Yet, in the recently identified ribonucleases 9–13, at least one of the three conserved catalytic residues (His12, Lys41, and His119 in RNase A) is substituted with a different amino acid, suggesting that RNA degradation is not essential to their biological activity (Figure A1.1). RNases 9–13 are also highly conserved across various mammalian species (Cho and Zhang 2006), indicative of conserved biological roles for these ribonucleases.

Two of these ribonucleases, RNases 9 and 10, are expressed at high concentrations in the male reproductive system and are inactive for RNA degradation (Zhu et al. 2007), but the other three ribonucleases, RNases 11–13, have not been studied to date. To determine the tissue specific expression of RNases 11–13, total RNA from 12 tissues was examined for the presence of the mRNA coding for these three ribonucleases. Additionally, the DNA encoding RNases 11–13 was amplified by PCR, inserted into DNA plasmids and expressed in *Escherichia coli*. RNase 12 was also tested for its toxicity toward a specific *E. coli* strain, as evidence for ribonucleolytic activity. These analyses provide preliminary information about the ribonucleolytic and biological activity of RNases 11–13.

### A1.3 Experimental Procedures

*General.* *Escherichia coli* BL21 (DE3) cells, *E. coli* Origami™ B (DE3) cells, and plasmid pET22b(+) were from Novagen (Madison, WI). DNA oligonucleotides for PCR and mutagenesis were from Integrated DNA Technologies (Coralville, IA). All other chemicals were of commercial grade or better, and were used without further purification.

Luria–Bertani (LB) agar contained (in 1.00 L) tryptone (10 g), yeast extract (5 g), NaCl (10 g), and agar (15 g). Terrific Broth (TB) contained (in 1.00 L) tryptone (12 g), yeast extract (24 g), glycerol (4 mL),  $\text{KH}_2\text{PO}_4$  (2.31 g), and  $\text{K}_2\text{HPO}_4$  (12.54 g). Phosphate-buffered saline (PBS; pH 7.4) contained (in 1.00 L) NaCl (8.0 g), KCl (2.0 g),  $\text{Na}_2\text{HPO}_4 \cdot 7\text{H}_2\text{O}$  (1.15 g),  $\text{KH}_2\text{PO}_4$  (2.0 g), and  $\text{NaN}_3$  (0.10 g).

*RNase 11–13 Cloning.* The sequences of RNase 11–13 and their GenBank accession codes were obtained from Cho et al. (2005). DNA primers were designed to amplify the

cDNAs encoding RNases 11–13 and to incorporate *Nde*I and *Bam*HI restriction sites at the 5' and 3' ends, respectively. The One-Step RT–PCR kit (Qiagen, Valencia, CA) was used to amplify DNA encoding RNases 11–13 from total RNA isolated from human testes (Stratagene, La Jolla, CA). The PCR products were inserted into plasmid pCR4-TOPO (Invitrogen, Carlsbad, CA), and sequence analysis was performed to ensure proper amplification. For protein expression, the PCR products were also inserted into plasmid pET-22b(+).

*Sequence Analysis.* Sequence alignments of ribonucleases (Figure A1.3) were performed with the program Clustal W (Chenna et al. 2003), using the amino-acid sequences for RNases 1, 5, and 12 obtained from (Cho et al. 2005).

*Protein Expression.* Plasmids that direct the expression of RNase 11–13 were transformed into *E. coli* BL21(DE3) cells and *E. coli* Origami B(DE3) cells, and a single colony was used to inoculate LB medium (25 mL) containing ampicillin (200 µg/mL) for BL21(DE3) cells or ampicillin (200 µg/mL), kanamycin (40 µg/mL), and tetracycline (12.5 µg/mL) for Origami B(DE3) cells. A starter culture was grown for 16 h at 37 °C and shaking at 225 rpm. Cultures were collected by centrifugation at 5,000g and resuspended in fresh LB medium. Resuspended cultures were used to inoculate cultures of TB medium (1.00 L) containing ampicillin (200 µg/mL) for BL21(DE3) cells or ampicillin (200 µg/mL), kanamycin (40 µg/mL), and tetracycline (12.5 µg/mL) for Origami B(DE3) cells. These cultures were grown at 37 °C with shaking at 225 rpm until  $OD_{600} \geq 3.0$ . Expression of the RNase 11, 12, or 13 cDNA was induced by adding IPTG (to 0.5 mM) and growing for 16 h at 18 °C and shaking at 225 rpm for BL21(DE3) cells or by adding IPTG (to 0.01

mM) and growing for 40 h at 12 °C and shaking at 225 rpm for Origami B(DE3) cells. Cells were collected by centrifugation (12,000g for 10 min) and resuspended in 30 mL of 50 mM Tris-HCl buffer, pH 7.5, containing NaCl (100 mM). Cells were lysed by two passes through a French pressure cell, and the inclusion bodies were collected by centrifugation at 18,000g for 45 min. Inclusion bodies were solubilized in 100 mM NaH<sub>2</sub>PO<sub>4</sub> buffer, pH 8.0, containing Tris-HCl (10 mM) and guanidine-HCl (6 M) (20 mL). The solubilized inclusion bodies were combined with Ni-NTA agarose (5–10 mL; Qiagen, Valencia, CA) and allowed to incubate for 1 h at 4 °C. Agarose resin containing the *E. coli* supernatant was loaded onto a gravity-flow column, and the resin was washed sequentially with 10 column volumes of 100 mM NaH<sub>2</sub>PO<sub>4</sub> buffer, pH 6.3, containing Tris-HCl (10 mM) and urea (8 M) and 10 column volumes of 100 mM NaH<sub>2</sub>PO<sub>4</sub> buffer, pH 5.9, containing Tris-HCl (10 mM) and urea (8 M). RNases 11–13 were eluted with two column volumes of 100 mM NaH<sub>2</sub>PO<sub>4</sub> buffer, pH 4.5, containing Tris-HCl (10 mM) and urea (8 M) and dialyzed against PBS or 50 mM Tris-HCl buffer containing NaCl (100 mM) for 16 h at 4 °C. Aliquots containing RNases 11–13 were incubated under oxidative folding conditions in either 100 mM Tris-HCl buffer, pH 8.0, containing NaCl (100 mM), reduced glutathione (1.0 mM), and oxidized glutathione (0.2 mM) or 100 mM Tris-HCl buffer, pH 8.0, containing L-arginine (0.5 M), reduced glutathione (3 mM), and oxidized glutathione (0.6 mM) at both 23 °C and 4 °C. Protein folding was assayed by chromatography on a G75 size-exclusion column (GE Healthcare, Piscataway, NJ) that had been equilibrated with 50 mM NaOAc-NaOH buffer, pH 5.0, containing NaCl (100 mM). Proper folding was determined by comparing the retention times of RNases 11–13 to the retention times

of folded ribonucleases, such as RNase A. Fractions were taken after induction with IPTG and after Ni-NTA purification to examine protein purity by SDS-PAGE.

*Genetic Selection.* Variants of RNase 12 were created by using the pET-22b plasmid encoding RNase 12 described above with the addition of a C-terminal extension of six histidine residues, and the Quikchange site-directed mutagenesis kit (Stratagene, La Jolla, CA). Codons for substitution were chosen for optimized protein expression in *E. coli*, based on known codon usage (Aota et al. 1988). The identity of substituted codons was confirmed by DNA-sequence analysis. Purified plasmid DNA from all RNase 12 variants was transformed into Origami™ B (DE3) cells. Transformed Origami B (DE3) cells were spread onto LB agar containing ampicillin (200 µg/mL), kanamycin (40 µg/mL), and tetracycline (12.5 µg/mL), and allowed to grow at 37 °C for 48 h. Most results were confirmed by repeating the selection (*i.e.*, transformation, spreading, and growth).

#### **A1.4 Results and Discussion**

*Sequence Analysis.* The amino-acid sequences of RNases 11–13 were recently identified, based on their similarity to the pancreatic RNase A superfamily (Cho et al. 2005). RNases 11–13 have many of the characteristics that define the RNase A superfamily, including the conserved cysteine residues (Figure A1.1) and N-terminal secretion sequence (Beintema 1987; Beintema et al. 1988b; Beintema et al. 1997). Yet, they were missing at least one of the conserved catalytic residues (Figure A1.1) (Cho et al. 2005). To determine their gene expression levels and biochemical characteristics, the DNA encoding each of these ribonucleases was amplified from RNA that was isolated from the



male testes. The DNA sequences for RNases 11–13 were amplified, sequenced, and inserted into a protein expression vector.

*Expression Pattern.* The tissue-specificity of the expression of RNases 11–13 was examined with RNA isolated from 12 tissues. The total RNA from these 12 tissues was probed by RT-PCR for the presence of RNA encoding RNases 11–13 (Figure A1.2). The RT-PCR was performed with the same DNA oligonucleotides employed in the initial PCR amplification. Thus, the DNA band observed in the RT-PCR reaction from the testes could serve as a standard with which to identify the DNA band representing RNases 11–13.

Figure A1.2 depicts the RT-PCR results for RNases 11–13, and Figure A1.3 quantitates the intensity of the major bands in Figure A1.2. RNase 11 has little variation in expression levels based on tissue type. Conversely, the expression of RNases 12 and 13 varies significantly by tissue type, with RNase 12 having decreased expression in RNA extracted from muscle, lymph node, pancreas, and penis tissue. Whereas, RNase 11 has increased expression in the RNA extracted from muscle and reproductive tissues, especially the testes. Although their expression levels vary by tissue type, these data suggest that RNases 11–13 are expressed ubiquitously and advocate for important biological roles for each ribonuclease.

*Protein Expression.* To determine the ribonucleolytic activity of RNases 11–13, the ribonucleases were expressed in and purified from *E. coli*. A variety of different expression and purification strategies were attempted using several *E. coli* strains. All three ribonucleases were expressed in *E. coli* as insoluble inclusion bodies (Figure A1.5), similar to other pancreatic ribonucleases (delCardayré et al. 1995; Leland et al. 2001). Both

RNase 11 and 12 were expressed in the *E. coli* BL21(DE3) strain upon induction at both 37 °C for 3 h and more significantly at 18 °C for 16 h. RNase 13, due to rare arginine codons present in its DNA, was expressed more significantly at lower temperatures (15 °C) and in *E. coli* cells lines that provided extra copies of rare arginine codons.

The oxidative folding of RNases 11–13 isolated from inclusion bodies was performed using procedures similar to those described for other pancreatic ribonucleases (Leland et al. 1998; Leland et al. 2001). The proper folding of RNases 11–13 under these oxidative folding conditions was assayed by chromatography using a size-exclusion column, and the retention times of RNases 11–13 were compared to those of folded ribonuclease standards. None of the ribonucleases were folded properly under these conditions. To purify the samples further prior to oxidative folding, a six-residue histidine sequence was added to the C-terminus, which permitted facile protein purification. RNases 11 and 12 were still induced at a significant level with the histidine sequence attached and could be purified to homogeneity in the denatured state by chromatography using Ni-NTA agarose (Figure A1.5). Purified, denatured RNases 11 and 12 were then subjected to similar oxidative folding conditions (Leland et al. 1998; Leland et al. 2001) and checked for proper folding by size-exclusion chromatography. Again, comparison to known folded ribonucleases suggested that RNases 11 and 12 failed to find their folded conformation under these conditions. Additional folding trials need to be conducted using a wider range of oxidative folding conditions to determine definitively if the folding of RNases 11–13 is possible *ex vivo*.

*Genetic Selection.* When expressed in the *E. coli* Origami™ strain (Novagen, Madison, WI), wild-type RNase A and RNase 5 are toxic (Smith and Raines 2006). This toxicity may be absent in RNases 11–13 due to their lack of an intact catalytic triad. To test for the toxicity of RNase 12, the wild-type enzyme was transformed into Origami cells and plated onto selective media in both the presence and absence of IPTG (Figure A1.6). Surprisingly, RNase 12 displayed toxicity upon induction with IPTG (100  $\mu$ M), suggesting that it has low catalytic activity (Smith and Raines 2006). To insure that the toxicity was due to the expression of RNase 12 and not the toxicity of the media or IPTG, a variant of RNase 12 was constructed with the N-terminal methionine residue converted to an alanine residue (M(-1)A). This variant of RNase 12 was not toxic, indicating that RNase 12 expression caused the observed toxicity (Figure A1.6).

Additional variants of RNase 12 were constructed that evaluated other residues in the enzyme for their affect on the observed toxicity, including prospective active-site residues (Figure A1.6A), N- and C-terminal residues (Figure A1.6B), and conserved cysteine residues (Figure A1.6C). RNase 12 contains two of the conserved catalytic residues, identified as His14 and Lys46, and an additional lysine residue (Lys47) proximal to Lys46 that could serve the role of Lys46 in stabilizing the transition state (Raines 2004; Cho et al. 2005). Single substitutions of either His14 or Lys46 with alanine residues did not, however, reduce the toxicity of RNase 12, but when His14 and Lys46 were substituted jointly with alanine residues, toxicity was abolished. These results indicate that His14 and Lys46 are vital to the observed toxicity of RNase 12 and possibly constitute the active site of the enzyme. As further evidence for the importance of His14 to the observed toxicity, deletion

of the first 12 residues of RNase 12 again obliterated its toxicity. Additional N-terminal or C-terminal deletions had no effect on the toxicity, suggesting that no third active-site residue exists, as the second catalytic histidine residue is often located near the C-terminus of the ribonuclease (Beintema 1987; Beintema et al. 1988b; Beintema et al. 1997).

Certain cysteine residues in RNase A are essential to its ribonucleolytic activity (Smith and Raines 2006), and these residues are conserved in RNase 12 (Figure A1.4). Yet, substitution of any of the putative cysteine pairs in RNase 12 did not affect its toxicity. These data suggest that the cysteine residues in RNase 12 might not be form disulfide bonds or do not serve the same important structural role as seen in RNase A. Overall, the genetic selection indicates that RNase 12 might have low ribonucleolytic activity that is facilitated by residues His14 and Lys46 and the N-terminus of the protein, but is not dependent on the conserved cysteine residues.

*Conclusions.* RNases 11–13 differ from most members of the pancreatic RNase A superfamily in the absence from their amino-acid sequence of at least one of the conserved active-site residues. The mRNA encoding these three ribonucleases was present at varying concentrations in 12 different tissues. Additionally, the DNA encoding these enzymes was cloned and the ribonucleases were expressed in *E. coli*. Purification and folding of the ribonucleases were performed, but purified, properly folded ribonuclease was not obtained. Genetic selection results for RNase 12 suggest that it has low ribonucleolytic activity facilitated by its N-terminus and residues His14 and Lys46. Further studies on RNases 11–13 could provide new information about the evolution of ribonucleases and their expanding biological roles.

**Figure A1.1** Comparison of conserved sequence elements within human members of pancreatic ribonuclease superfamily. Specific regions highlighted include the catalytic histidine residues, catalytic lysine residue, and structural cysteine residues. Sequence alignment and amino-acid composition are adapted from Cho et al. (2005).

	H <sub>12</sub>	CK <sub>1</sub> XXNTF	VPVH <sub>119</sub>	No. Conserved Cysteines
RNase 1 (human pancreatic ribonuclease)	H	CKPVNTF	VPVH	8
RNase 2 (human EDN)	H	CKNQNTF	VPVH	8
RNase 3 (human ECP)	H	CKNQNTF	VPVH	8
RNase 4 (human liver)	H	CKRNTF	VPVH	8
RNase 5 (angiogenin)	H	CKDINTF	VPVL	6
RNase 11	H	CKWSNMF	LTGH/MSWL	6
RNase 12	H	CKKEHVF	RPDS	8
RNase 13	P	CPKIHVV	KY/DPIG	8

**Figure A1.2** Expression of the RNA encoding RNases 11–13. The DNA sequence encoding RNases 11–13 was amplified from total RNA (Stratagene, La Jolla, CA) from various tissues by RT-PCR (Qiagen, Valencia, CA). Panels depict the results for (A) RNase 11; (B) RNase 12; and (C) RNase 13.

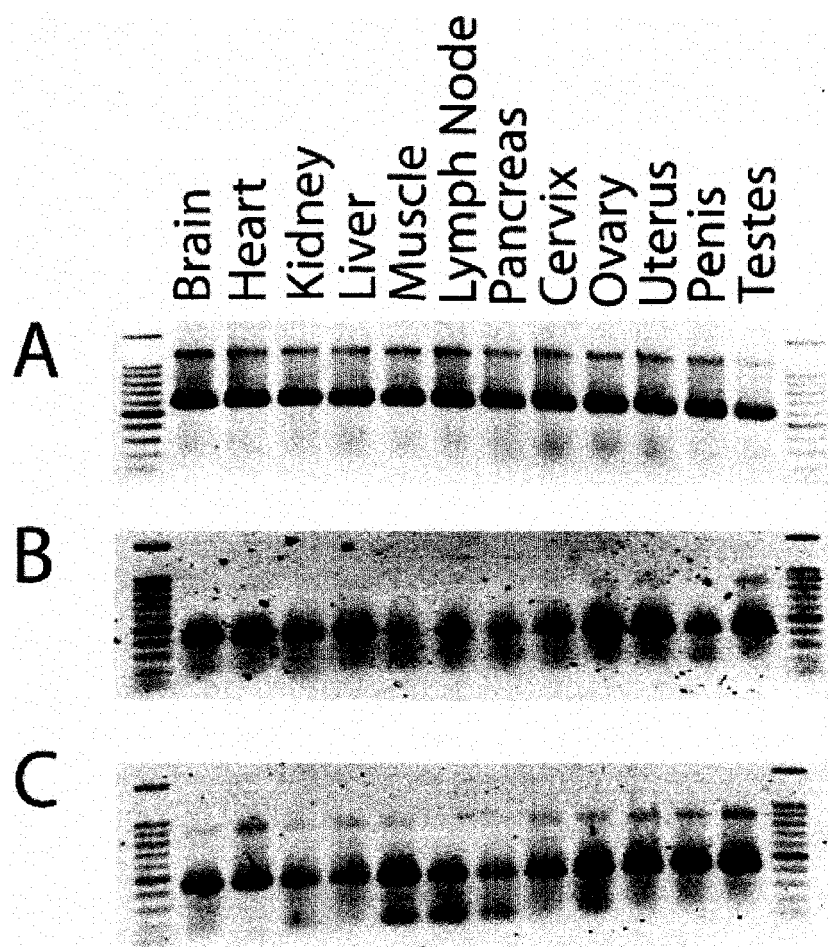




**Figure A1.3** Quantitation of mRNA expression data. Gel bands from Figure A1.2 were quantitated using TinyQuant v1.54 (University Health Network, Toronto, CA). Data were standardized by subtracting the background signal and by normalizing for the maximum band intensity for each ribonuclease.

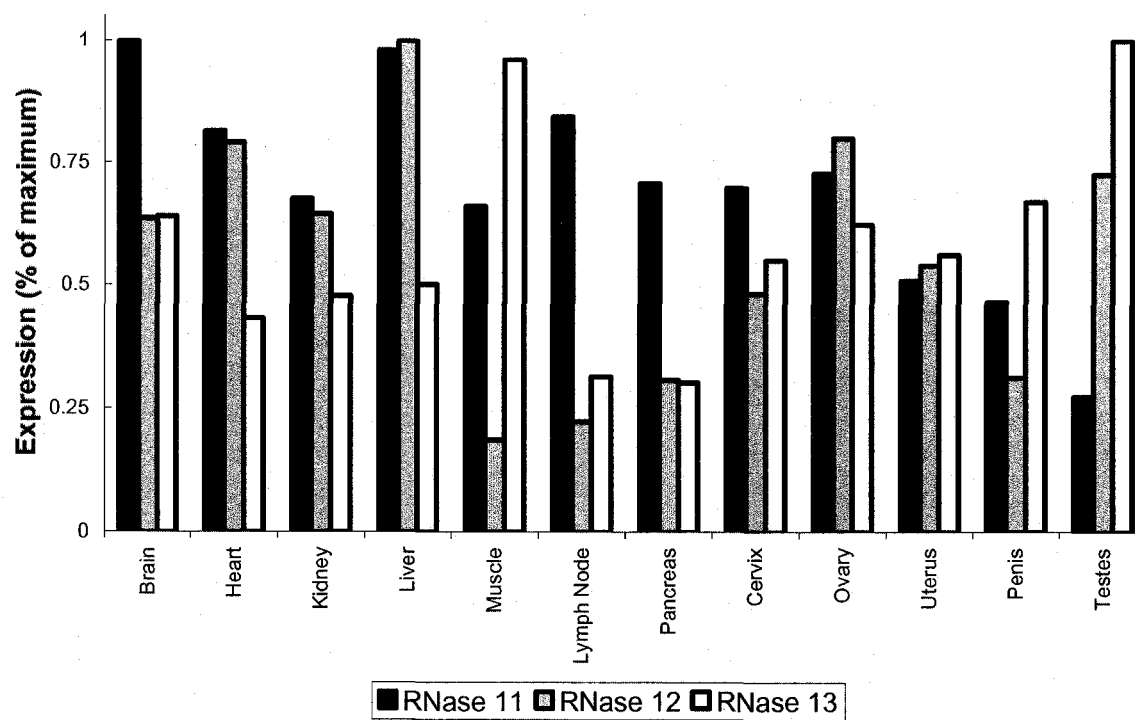


**Figure A1.4** Sequence alignment of RNase 1, RNase 5, and RNase 12 performed with the program Clustal W (Chenna et al. 2003). Yellow boxes highlight conserved cysteine residues, red boxes highlight conserved active site residues, and black boxes surround highly conserved residues as identified by Cho et al. (2005) and Smith & Raines (2006).

```

RNase 1      - - KESRAKKFQRQMDS-DSSPSSSSSTYCINQMRRRRNMTQG--RC[PVNT] 45
RNase 5 (ANG) - QDNSRYTHFLTQYDA-KPQ-GRDDRYCESIMRRRGLTS--PCDINT 44
RNase 12     VNDEAVMSTLEHLVDYPQNDVPVPARYCNHMLIQRVIREPDHTC[KEHV] 50

RNase 1      [F]VHEPLVDVQNVCFQEKVTCKN--GQGNCYKSNSSMHI TDCRLTNGSRYP 93
RNase 5 (ANG) [F]HGNKRSIKAIC--ENKNGNP--HRENLRISKSSFQVTTCKLHGGSPWP 90
RNase 12     [F]HERPRKINGICISPKKVACQNLSAIFCFQSE TKFKMTVCQLIEGTRY P 100

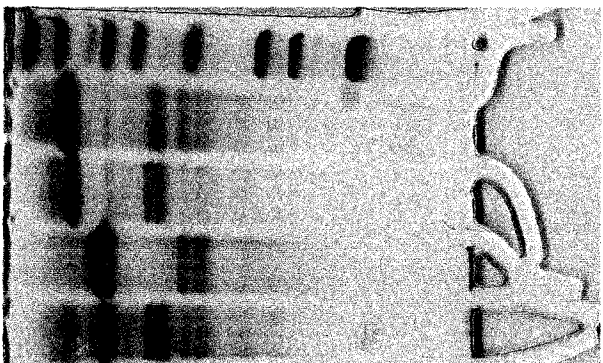
RNase 1      NCA[Y]RTSPKERHIIV[ACE]GSPYV[PV]FDASVEDST 128
RNase 5 (ANG) PCQYRATAGFRNVVV[ACE]NG--LPV[LDQSI]FRRP 123
RNase 12     AC[RY]HYSPTTEGFVLVTC[DD]LR--PDS[FLGYVK]-- 130

```

= Conserved Cysteine Residue  
 = Catalytic Residue  
 = Highly Conserved Residue

**Figure A1.5** Protein expression of RNases 11 and 12 in *E. coli* BL21(DE3) cells.

Samples for SDS-PAGE gel analysis were taken after induction at 18 °C for 16 h and after purification of the denatured proteins using Ni-NTA agarose (Qiagen, Valencia, CA).



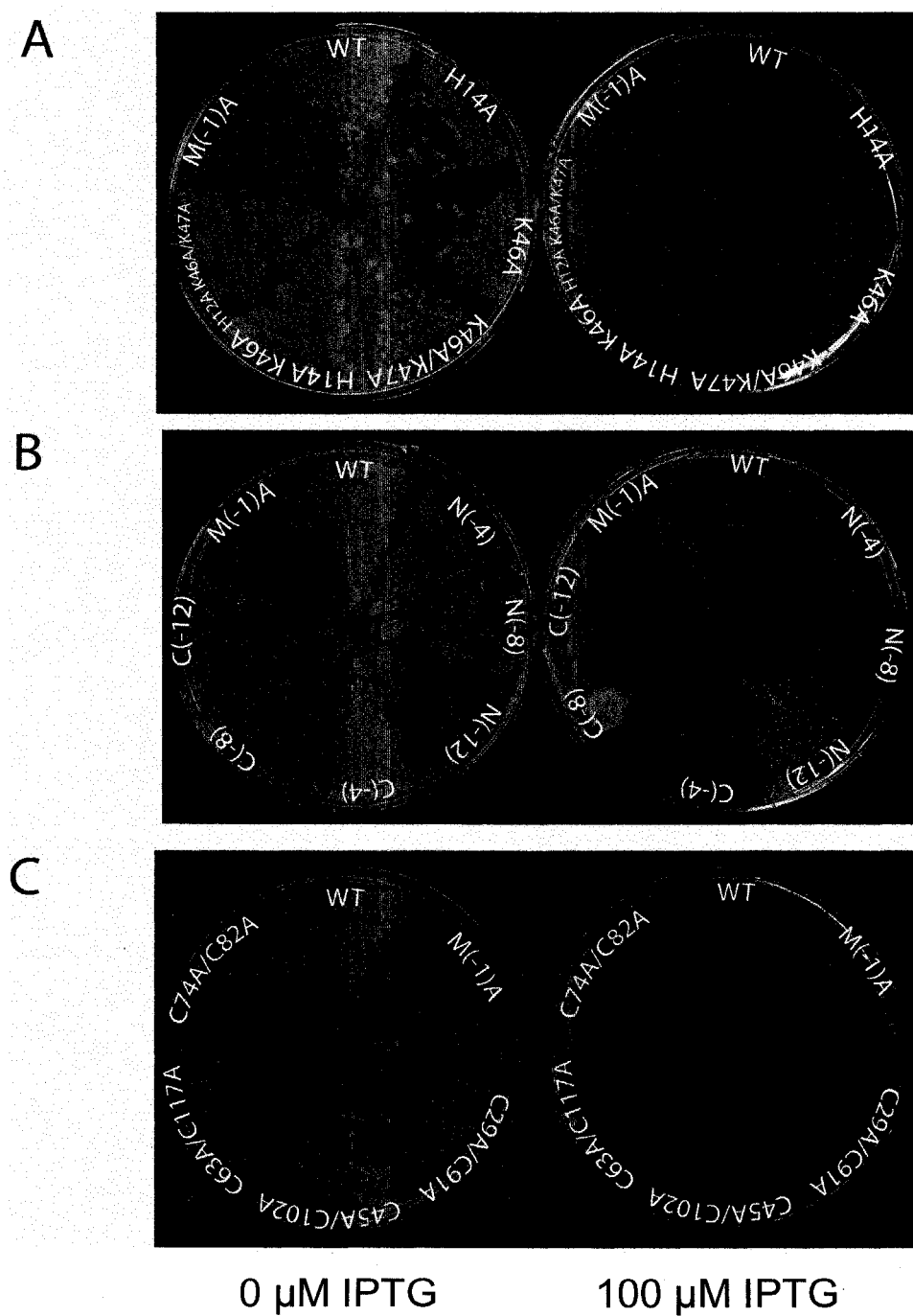
RNase 12 induction

RNase 12 Ni-NTA Purified

RNase 11 induction

RNase 11 Ni-NTA Purified

**Figure A1.6** Genetic selection for the critical residues to RNase 12 ribonucleolytic activity (Smith and Raines 2006). Plasmids containing variants of RNase 12 with specific residues substituted with alanine were transformed into *E. coli* Origami B (DE3) cells and plated onto LB-agar containing 200 µg/mL ampicillin, 40 µg/mL kanamycin, 12.5 µg/mL tetracycline, and 0 or 100 µM IPTG. Plates were incubated at 37 °C for 48 h. All plates contain wild-type RNase 12 and wild-type RNase 12 with the start codon methionine substituted with an alanine residue as controls. (A) Catalytic residues (Fig. A1.1) were substituted with alanine residues both separately and in concert. (B) N- and C-terminal residues in RNase 12 were deleted. The number of residues deleted from each variant is indicated in parentheses. (C) Conserved cysteine residues in RNase 12 were substituted with alanine residues.





## References

- Abel, R.L., Haigis, M.C., Park, C., and Raines, R.T. 2002. Fluorescence assay for the binding of ribonuclease A to the ribonuclease inhibitor protein. *Anal. Biochem.* **306**: 100-107.
- Anfinsen, C.B. 1973. Principles that govern the folding of protein chains. *Science* **181**: 223-230.
- Aota, S., Gojobori, T., Ishibashi, F., Maruyama, T., and Ikemura, T. 1988. Codon usage tabulated from the GenBank Genetic Sequence Data. *Nucleic Acids Res.* **16 Suppl**: r315-402.
- Ardelt, B., Ardelt, W., and Darzynkiewicz, Z. 2003. Cytotoxic ribonucleases and RNA interference (RNAi). *Cell Cycle* **2**: 22-24.
- Arnold, U., Schulenburg, C., Schmidt, D., and Ulbrich-Hofmann, R. 2006. Contribution of structural peculiarities of onconase to its high stability and folding kinetics. *Biochemistry* **45**: 3580-3587.
- Arnold, U., and Ulbrich-Hofmann, R. 2006. Natural and engineered ribonucleases as potential cancer therapeutics. *Biotechnol. Lett.* **28**: 1615-1622.
- Bailey, S. 1994. The CCP4 suite: Programs for protein crystallography. *Acta. Crystallogr. D Biol. Crystallogr.* **50**: 760-763.
- Baldwin, R.L. 2003. In search of the energetic role of peptide hydrogen bonds. *J. Biol. Chem.* **278**: 17581-17588.
- Barnard, E.A. 1969. Biological function of pancreatic ribonuclease. *Nature* **221**: 340-344.
- Beadle, B.M., and Shoichet, B.K. 2002. Structural bases of stability-function tradeoffs in enzymes. *J. Mol. Biol.* **321**: 285-296.
- Becktel, W.J., and Schellman, J.A. 1987. Protein stability curves. *Biopolymers* **26**: 1859-1877.
- Beintema, J.J. 1987. Structure, properties and molecular evolution of pancreatic-type ribonucleases. *Life Chem. Rep.* **4**: 333-389.
- Beintema, J.J., Breukelman, H.J., Carsana, A., and Furia, A. 1997. Evolution of vertebrate ribonucleases: Ribonuclease A superfamily. In *Ribonucleases: Structures and Functions*. (eds. G. D'Alessio, and J.F. Riordan), pp. 245-269. Academic Press, New York.

- Beintema, J.J., Hofsteenge, J., Iwama, M., Morita, T., Ohgi, K., Irie, M., Sugiyama, R.H., Schieven, G.L., Dekker, C.A., and Glitz, D.G. 1988a. Amino acid sequence of the nonsecretory ribonuclease of human urine. *Biochemistry* **27**: 4530-4538.
- Beintema, J.J., Schüller, C., Irie, M., and Carsana, A. 1988b. Molecular evolution of the ribonuclease superfamily. *Prog. Biophys. Molec. Biol.* **51**: 165-192.
- Beintema, J.J., Wietzes, P., Weickmann, J.L., and Glitz, D.G. 1984. The amino acid sequence of human pancreatic ribonuclease. *Anal. Biochem.* **136**: 48-64.
- Benito, A., Ribo, M., and Vilanova, M. 2005. On the track of antitumour ribonucleases. *Mol. Biosyst.* **1**: 294-302.
- Benner, S.A. 2001. Natural progression. *Nature* **409**: 459.
- Blanc, E., Roversi, P., Vornrhein, C., Flensburg, C., Lea, S.M., and Bricogne, G. 2004. Refinement of severely incomplete structures with maximum likelihood in BUSTER-TNT. *Acta Crystallogr. D Biol. Crystallogr.* **60**: 2210-2221.
- Blázquez, M., Fominaya, J.M., and Hofsteenge, J. 1996. Oxidation of sulfhydryl groups of ribonuclease inhibitor in epithelial cells is sufficient for its intracellular degradation. *J. Biol. Chem.* **271**: 18638-18642.
- Blight, K.J., Kolykhalov, A.A., and Rice, C.M. 2000. Efficient initiation of HCV RNA replication in cell culture. *Science* **290**: 1972-1974.
- Boix, E., Wu, Y., Vasandani, V.M., Saxena, S.K., Ardelt, W., Ladner, J., and Youle, R.J. 1996. Role of the N-terminus in RNase A homologues: Differences in catalytic activity, ribonuclease inhibitor interaction and cytotoxicity. *J. Mol. Biol.* **257**: 992-1007.
- Borgono, C.A., and Diamandis, E.P. 2004. The emerging roles of human tissue kallikreins in cancer. *Nat. Rev. Cancer* **4**: 876-890.
- Bosch, M., Benito, A., Ribo, M., Puig, T., Beaumelle, B., and Vilanova, M. 2004. A nuclear localization sequence endows human pancreatic ribonuclease with cytotoxic activity. *Biochemistry* **43**: 2167-2177.
- Brandts, J.F., and Lin, L.N. 1990. Study of strong to ultratight protein interactions using differential scanning calorimetry. *Biochemistry* **29**: 6927-6940.
- Bretscher, L.E., Abel, R.L., and Raines, R.T. 2000. A ribonuclease A variant with low catalytic activity but high cytotoxicity. *J. Biol. Chem.* **275**: 9893-9896.
- Burke, D.S., and Monath, T.P. 2001. Flaviviruses. In *Fields Virology*. (eds. D.M. Knipe, and P.M. Howley), pp. 1043-1125. Lippincott Williams & Wilkins, New York.

- Burton, L.E., Blackburn, P., and Moore, S. 1980. Ribonuclease inhibitor from bovine brain. *Int. J. Pept. Protein Res.* **16**: 359-364.
- Burton, L.E., and Fucci, N.P. 1982. Ribonuclease inhibitors from the livers of five mammalian species. *Int. J. Pept. Protein Res.* **19**: 372-379.
- Cavallo, L., Kleinjung, J., and Fraternali, F. 2003. POPS: A fast algorithm for solvent accessible surface areas at atomic and residue level. *Nucleic Acids Res.* **31**: 3364-3366.
- Chandran, S.S., Dickson, K.A., and Raines, R.T. 2005. Latent fluorophore based on the trimethyl lock. *J. Am. Chem. Soc.* **127**: 1652-1653.
- Chauhan, A., Tikoo, A., Kapur, A.K., and Singh, M. 2006. The taming of the cell penetrating domain of the HIV Tat: Myths and realities. *J. Control. Release* **117**: 148-162.
- Chen, Y.W., Fersht, A.R., and Henrick, K. 1993. Contribution of buried hydrogen bonds to protein stability. The crystal structures of two barnase mutants. *J. Mol. Biol.* **234**: 1158-1170.
- Chenna, R., Sugawara, H., Koike, T., Lopez, R., Gibson, T.J., Higgins, D.G., and Thompson, J.D. 2003. Multiple sequence alignment with the Clustal series of programs. *Nucleic Acids Res.* **31**: 3497-3500.
- Cho, S., Beintema, J.J., and Zhang, J. 2005. The ribonuclease A superfamily of mammals and birds: Identifying new members and tracing evolutionary histories. *Genomics* **85**: 208-220.
- Cho, S., and Zhang, J. 2006. Ancient expansion of the ribonuclease A superfamily revealed by genomic analysis of placental and marsupial mammals. *Gene* **373**: 116-125.
- Cho, W., and Stahelin, R.V. 2005. Membrane-protein interactions in cell signaling and membrane trafficking. *Annu. Rev. Biophys. Biomol. Struct.* **34**: 119-151.
- Choi, S.S., Vallender, E.J., and Lahn, B.T. 2006. Systematically assessing the influence of 3-dimensional structural context on the molecular evolution of mammalian proteomes. *Mol. Biol. Evol.* **23**: 2131-2133.
- Coling, D.E., Ding, D., Young, R., Lis, M., Stofko, E., Blumenthal, K.M., and Salvi, R.J. 2007. Proteomic analysis of cisplatin-induced cochlear damage: Methods and early changes in protein expression. *Hear Res.* **226**: 140-156.
- Coll, M.G., Protasevich, II, Torrent, J., Ribo, M., Lobachov, V.M., Makarov, A.A., and Vilanova, M. 1999. Valine 108, a chain-folding initiation site-belonging residue,

- crucial for the ribonuclease A stability. *Biochem. Biophys. Res. Commun.* **265**: 356-360.
- Conner, S.D., and Schmid, S.L. 2003. Regulated portals of entry into the cell. *Nature* **422**: 37-44.
- Creighton, T.E. 1993. *Proteins: structures and molecular properties*, 2nd ed. W.H. Freeman, New York, pp. xiii, 507 p.
- Cuchillo, C.M., Vilanova, M., and Nogués, M.V. 1997. Pancreatic ribonucleases. In *Ribonucleases: Structures and Functions*. (eds. G. D'Alessio, and J.F. Riordan), pp. 271-304. Academic Press, New York.
- D'Alessio, G., and Riordan, J.F. 1997. *Ribonucleases: Structures and Functions*. Academic Press, New York, pp. xix, 670 p.
- delCardayré, S.B., Ribó, M., Yokel, E.M., Quirk, D.J., Rutter, W.J., and Raines, R.T. 1995. Engineering ribonuclease A: Production, purification, and characterization of wild-type enzyme and mutants at Gln11. *Protein Eng.* **8**: 261-273.
- DePristo, M.A., Weinreich, D.M., and Hartl, D.L. 2005. Missense meanderings in sequence space: a biophysical view of protein evolution. *Nat. Rev. Genet.* **6**: 678-687.
- Dickson, K.A., Dahlberg, C.L., and Raines, R.T. 2003. Compensating effects on the cytotoxicity of ribonuclease A variants. *Arch. Biochem. Biophys.* **415**: 172-177.
- Dickson, K.A., Haigis, M.C., and Raines, R.T. 2005. Ribonuclease inhibitor: Structure and function. *Prog. Nucleic Acid Res. Mol. Biol.* **80**: 349-374.
- Dill, K.A. 1990. Dominant forces in protein folding. *Biochemistry* **29**: 7133-7155.
- Donovan, J.W., and Beardslee, R.A. 1975. Heat stabilization produced by protein-protein association. A differential scanning calorimetric study of the heat denaturation of the trypsin-soybean trypsin inhibitor and trypsin-ovomucoid complexes. *J. Biol. Chem.* **250**: 1966-1971.
- Drin, G., Cottin, S., Blanc, E., Rees, A.R., and Temsamani, J. 2003. Studies on the internalization mechanism of cationic cell-penetrating peptides. *J. Biol. Chem.* **278**: 31192-31201.
- Dykxhoorn, D.M., and Lieberman, J. 2005. The silent revolution: RNA interference as basic biology, research tool, and therapeutic. *Annu. Rev. Med.* **56**: 401-423.

- Eberhardt, E.S., Wittmayer, P.K., Templer, B.M., and Raines, R.T. 1996. Contribution of a tyrosine side chain to ribonuclease A catalysis and stability. *Protein Sci.* **5**: 1697-1703.
- Erickson, H.A., Jund, M.D., and Pennell, C.A. 2006. Cytotoxicity of human RNase-based immunotoxins requires cytosolic access and resistance to ribonuclease inhibition. *Protein Eng. Des. Sel.* **19**: 37-45.
- Esquela-Kerscher, A., and Slack, F.J. 2006. Oncomirs - microRNAs with a role in cancer. *Nat. Rev. Cancer* **6**: 259-269.
- Fersht, A.R., Shi, J.-P., Knill-Jones, J., Lowe, D.M., Wilkinson, A.J., Blow, D.M., Brick, P., Arter, P., Waye, M.M.Y., and Winter, G. 1985. Hydrogen bonding and biological specificity analysed by protein engineering. *Nature* **314**: 235-238.
- Fishman, J.A., Rubin, R.H., Koziel, M.J., and Periera, B.J. 1996. Hepatitis C virus and organ transplantation. *Transplantation* **62**: 147-154.
- Fleming, P.J., and Rose, G.D. 2005. Do all backbone polar groups in proteins form hydrogen bonds? *Protein Sci.* **14**: 1911-1917.
- Fominaya, J.M., and Hofsteenge, J. 1992. Inactivation of ribonuclease inhibitor by thiol-disulfide exchange. *J. Biol. Chem.* **267**: 24655-24660.
- Fotin-Mleczech, M., Fischer, R., and Brock, R. 2005. Endocytosis and cationic cell-penetrating peptides-a merger of concepts and methods. *Curr. Pharm. Des.* **11**: 3613-3628.
- Fraser, H.B., Hirsh, A.E., Steinmetz, L.M., Scharfe, C., and Feldman, M.W. 2002. Evolutionary rate in the protein interaction network. *Science* **296**: 750-752.
- Freer, S.T., Kraut, J., Robertus, J.D., Wright, H.T., and Xuong, N.H. 1970. Chymotrypsinogen: 2.5-angstrom crystal structure, comparison with alpha-chymotrypsin, and implications for zymogen activation. *Biochemistry* **9**: 1997-2009.
- Fuchs, S.M., and Raines, R.T. 2004. Pathway for polyarginine entry into mammalian cells. *Biochemistry* **43**: 2438-2444.
- Fuchs, S.M., and Raines, R.T. 2005. Polyarginine as a multifunctional fusion tag. *Protein Sci.* **14**: 1538-1544.
- Fuchs, S.M., and Raines, R.T. 2006. Internalization of cationic peptides: the road less (or more?) traveled. *Cell. Mol. Life Sci.* **63**: 1819-1822.

- Fuchs, S.M., and Raines, R.T. 2007. Arginine grafting to endow cell permeability. *ACS Chem. Biol.* **2**: 167-170.
- Fuchs, S.M., Rutkoski, T.J., Groeschl, R.T., and Raines, R.T. 2007. Increasing the cytotoxicity of ribonuclease A with arginine grafting. *Protein Eng. Des. Sel.* **20**: xxx-xxx.
- Futami, J., Maeda, T., Kitazoe, M., Nukui, E., Tada, H., Seno, M., Kosaka, M., and Yamada, H. 2001. Preparation of potent cytotoxic ribonucleases by cationization: Enhanced cellular uptake and decreased interaction with ribonuclease inhibitor by chemical modification of carboxyl groups. *Biochemistry* **26**: 7518-7524.
- Futami, J., Nukui, K., Maeda, T., Kosaka, M., Tada, H., Seno, M., and Yamada, H. 2002. Optimum modification for the highest cytotoxicity of cationized ribonuclease. *J. Biochem. (Tokyo)* **132**: 223-228.
- Gaur, D., Swaminathan, S., and Batra, J.K. 2001. Interaction of human pancreatic ribonuclease with human ribonuclease inhibitor. *J. Biol. Chem.* **276**: 24978-24984.
- Gavin, A.C., Bosche, M., Krause, R., Grandi, P., Marzioch, M., Bauer, A., Schultz, J., Rick, J.M., Michon, A.M., Cruciat, C.M., et al. 2002. Functional organization of the yeast proteome by systematic analysis of protein complexes. *Nature* **415**: 141-147.
- Getzoff, E.D., Cabelli, D.E., Fisher, C.L., Parge, H.E., Viezzoli, M.S., Banci, L., and Hallewell, R.A. 1992. Faster superoxide dismutase mutants designed by enhancing electrostatic guidance. *Nature* **358**: 347-351.
- Goldstrohm, A.C., Hook, B.A., Seay, D.J., and Wickens, M. 2006. PUF proteins bind Pop2p to regulate messenger RNAs. *Nat. Struct. Mol. Biol.* **13**: 533-539.
- Goldstrohm, A.C., Seay, D.J., Hook, B.A., and Wickens, M. 2007. PUF protein-mediated deadenylation is catalyzed by Ccr4p. *J. Biol. Chem.* **282**: 109-114.
- Greenway, M.J., Andersen, P.M., Russ, C., Ennis, S., Cashman, S., Donaghy, C., Patterson, V., Swingler, R., Kieran, D., Prehn, J., et al. 2006. ANG mutations segregate with familial and 'sporadic' amyotrophic lateral sclerosis. *Nat. Genet.* **38**: 411-413.
- Guo, H.H., Choe, J., and Loeb, L.A. 2004. Protein tolerance to random amino acid change. *Proc. Natl. Acad. Sci. U.S.A.* **101**: 9205-9210.
- Hahn, M.W., and Kern, A.D. 2005. Comparative genomics of centrality and essentiality in three eukaryotic protein-interaction networks. *Mol. Biol. Evol.* **22**: 803-806.
- Haigis, M.C., Haag, E.S., and Raines, R.T. 2002a. Evolution of ribonuclease inhibitor protein by exon duplication. *Mol. Biol. Evol.* **19**: 960-964.

- Haigis, M.C., Kurten, E.L., Abel, R.L., and Raines, R.T. 2002b. KFERQ sequence in ribonuclease A-mediated cytotoxicity. *J. Biol. Chem.* **277**: 11576-11581.
- Haigis, M.C., Kurten, E.L., and Raines, R.T. 2003. Ribonuclease inhibitor as an intracellular sentry. *Nucleic Acids Res.* **31**: 1024-1032.
- Haigis, M.C., and Raines, R.T. 2003. Secretory ribonucleases are internalized by a dynamin-independent endocytic pathway. *J. Cell Sci.* **116**: 313-324.
- Hallbrink, M., Floren, A., Elmquist, A., Pooga, M., Bartfai, T., and Langel, U. 2001. Cargo delivery kinetics of cell-penetrating peptides. *Biochim. Biophys. Acta* **1515**: 101-109.
- Hannon, G.J. 2002. RNA interference. *Nature* **418**: 244-251.
- He, X., and Zhang, J. 2006. Why do hubs tend to be essential in protein networks? *PLoS Genet.* **2**: e88.
- Ho, Y., Gruhler, A., Heilbut, A., Bader, G.D., Moore, L., Adams, S.L., Millar, A., Taylor, P., Bennett, K., Boutilier, K., et al. 2002. Systematic identification of protein complexes in *Saccharomyces cerevisiae* by mass spectrometry. *Nature* **415**: 180-183.
- Hofsteenge, J., Kieffer, B., Matthies, R., Hemmings, B.A., and Stone, S.R. 1988. Amino acid sequence of the ribonuclease inhibitor from porcine liver reveals the presence of leucine-rich repeats. *Biochemistry* **27**: 8537-8544.
- Huang, Y.C., Lin, Y.M., Chang, T.W., Wu, S.J., Lee, Y.S., Chang, M.D., Chen, C., Wu, S.H., and Liao, Y.D. 2007. The flexible and clustered lysine residues of human ribonuclease 7 are critical for membrane permeability and antimicrobial activity. *J. Biol. Chem.* **282**: 4626-4633.
- Hytonen, V.P., Nyholm, T.K., Pentikainen, O.T., Vaarno, J., Porkka, E.J., Nordlund, H.R., Johnson, M.S., Slotte, J.P., Laitinen, O.H., and Kulomaa, M.S. 2004. Chicken avidin-related protein 4/5 shows superior thermal stability when compared with avidin while retaining high affinity to biotin. *J. Biol. Chem.* **279**: 9337-9343.
- Ilinskaya, O.N., Dreyer, F., Mitkevich, V.A., Shaw, K.L., Pace, C.N., and Makarov, A.A. 2002. Changing the net charge from negative to positive makes ribonuclease Sa cytotoxic. *Protein Sci.* **11**: 2522-2525.
- Ilinskaya, O.N., Koschinski, A., Mitkevich, V.A., Repp, H., Dreyer, F., Pace, C.N., and Makarov, A.A. 2004. Cytotoxicity of RNases is increased by cationization and counteracted by K(Ca) channels. *Biochem. Biophys. Res. Commun.* **314**: 550-554.

- Iyer, S., Holloway, D.E., Kumar, K., Shapiro, R., and Acharya, K.R. 2005. Molecular recognition of human eosinophil-derived neurotoxin (RNase 2) by placental ribonuclease inhibitor. *J. Mol. Biol.* **347**: 637-655.
- Jeffrey, G.A., and Saenger, W. 1991. *Hydrogen bonding in biological structures*. Springer-Verlag, Berlin; New York, pp. xiv, 569 p.
- Johnson, R.J., Chao, T.-Y., Lavis, L.D., and Raines, R.T. 2007a. Cytotoxic ribonucleases: The dichotomy of Coulombic forces. *Biochemistry* **XX**: XXXX-XXXX.
- Johnson, R.J., Lin, S.R., and Raines, R.T. 2006. A ribonuclease zymogen activated by the NS3 protease of the hepatitis C virus. *FEBS J.* **273**: 5457-5465.
- Johnson, R.J., Lin, S.R., and Raines, R.T. 2007b. Genetic selection to reveal the role of a buried, conserved polar residue. *Protein Sci.* **16**: XXX-XXX.
- Johnson, R.J., McCoy, J.G., Bingman, C.A., Phillips, G.N., and Raines, R.T. 2007c. Inhibition of human pancreatic ribonuclease by the human ribonuclease inhibitor protein. *J. Mol. Biol.* **368**: 434-449.
- Kaplan, I.M., Wadia, J.S., and Dowdy, S.F. 2005. Cationic TAT peptide transduction domain enters cells by macropinocytosis. *J. Control. Release* **102**: 247-253.
- Kaushik, J.K., Iimura, S., Ogasahara, K., Yamagata, Y., Segawa, S., and Yutani, K. 2006. Completely buried, non-ion-paired glutamic acid contributes favorably to the conformational stability of pyrrolidone carboxyl peptidases from hyperthermophiles. *Biochemistry* **45**: 7100-7112.
- Kawanomoto, M., Motojima, K., Sasaki, M., Hattori, H., and Goto, S. 1992. cDNA cloning and sequence of rat ribonuclease inhibitor, and tissue distribution of mRNA. *Biochim. Biophys. Acta* **1129**: 335-338.
- Kelemen, B.R., Klink, T.A., Behlke, M.A., Eubanks, S.R., Leland, P.A., and Raines, R.T. 1999. Hypersensitive substrate for ribonucleases. *Nucleic Acids Res.* **27**: 3696-3701.
- Kelemen, B.R., Schultz, L.W., Sweeney, R.Y., and Raines, R.T. 2000. Excavating an active site: The nucleobase specificity of ribonuclease A. *Biochemistry* **39**: 14487-14494.
- Kelly, S.M., Jess, T.J., and Price, N.C. 2005. How to study proteins by circular dichroism. *Biochim. Biophys. Acta* **1751**: 119-139.
- Khan, A.R., and James, M.N. 1998. Molecular mechanisms for the conversion of zymogens to active proteolytic enzymes. *Protein Sci.* **7**: 815-836.



- Kim, B.-M., Schultz, L.W., and Raines, R.T. 1999. Variants of ribonuclease inhibitor that resist oxidation. *Protein Sci.* **8**: 430-434.
- Kim, J.-S., Soucek, J., Matousek, J., and Raines, R.T. 1995a. Catalytic activity of bovine seminal ribonuclease is essential for its immunosuppressive and other biological activities. *Biochem. J.* **308**: 547-550.
- Kim, J.-S., Soucek, J., Matousek, J., and Raines, R.T. 1995b. Structural basis for the biological activities of bovine seminal ribonuclease. *J. Biol. Chem.* **270**: 10525-10530.
- Kim, J.L., Morgenstern, K.A., Lin, C., Fox, T., Dwyer, M.D., Landro, J.A., Chambers, S.P., Markland, W., Lepre, C.A., O'Malley, E.T., et al. 1996. Crystal structure of the hepatitis C virus NS3 protease domain complexed with a synthetic NS4A cofactor peptide. *Cell* **87**: 343-355.
- Kimura, M. 1968. Evolutionary rate at the molecular level. *Nature* **217**: 624-626.
- Kimura, M. 1983. *The Neutral Theory of Molecular Evolution*. Cambridge University Press, New York.
- Klink, T.A., and Raines, R.T. 2000. Conformational stability is a determinant of ribonuclease A cytotoxicity. *J. Biol. Chem.* **275**: 17463-17467.
- Klink, T.A., Vicentini, A.M., Hofsteenge, J., and Raines, R.T. 2001. High-level soluble production and characterization of porcine ribonuclease inhibitor. *Protein Expr. Purif.* **22**: 174-179.
- Klink, T.A., Woycechowsky, K.J., Taylor, K.M., and Raines, R.T. 2000. Contribution of disulfide bonds to the conformational stability and catalytic activity of ribonuclease A. *Eur. J. Biochem.* **267**: 566-572.
- Kobe, B., and Deisenhofer, J. 1995. A structural basis of the interactions between leucine-rich repeats and protein ligands. *Nature* **374**: 183-186.
- Kobe, B., and Deisenhofer, J. 1996. Mechanism of ribonuclease inhibition by ribonuclease inhibitor protein based on the crystal structure of its complex with ribonuclease A. *J. Mol. Biol.* **264**: 1028-1043.
- Korostelev, A., Trakhanov, S., Laurberg, M., and Noller, H.F. 2006. Crystal structure of a 70S ribosome-tRNA complex reveals functional interactions and rearrangements. *Cell* **126**: 1065-1077.
- Kossiakoff, A.A., Chambers, J.L., Kay, L.M., and Stroud, R.M. 1977. Structure of bovine trypsinogen at 1.9 Å resolution. *Biochemistry* **16**: 654-664.

- Krogan, N.J., Cagney, G., Yu, H., Zhong, G., Guo, X., Ignatchenko, A., Li, J., Pu, S., Datta, N., Tikuisis, A.P., et al. 2006. Global landscape of protein complexes in the yeast *Saccharomyces cerevisiae*. *Nature* **440**: 637-643.
- Kumar, K., Brady, M., and Shapiro, R. 2004. Selective abolition of pancreatic RNase binding to its inhibitor protein. *Proc. Natl. Acad. Sci. U.S.A.* **101**: 53-58.
- Kumar, M.D., Bava, K.A., Gromiha, M.M., Prabakaran, P., Kitajima, K., Uedaira, H., and Sarai, A. 2006. ProTherm and ProNIT: Thermodynamic databases for proteins and protein-nucleic acid interactions. *Nucleic Acids Res.* **34**: D204-206.
- Lagos-Quintana, M., Rauhut, R., Lendeckel, W., and Tuschl, T. 2001. Identification of novel genes coding for small expressed RNAs. *Science* **294**: 853-858.
- Landre, J.B., Hewett, P.W., Olivot, J.M., Friedl, P., Ko, Y., Sachinidis, A., and Moenner, M. 2002. Human endothelial cells selectively express large amounts of pancreatic-type ribonuclease (RNase 1). *J. Cell. Biochem.* **86**: 540-552.
- Laskowski, R.A., Chistyakov, V.V., and Thornton, J.M. 2005. PDBsum more: New summaries and analyses of the known 3D structures of proteins and nucleic acids. *Nucleic Acids Res.* **33**: D266-D268.
- Lavis, L.D., Chao, T.-Y., and Raines, R.T. 2006. Fluorogenic label for biomolecular imaging. *ACS Chem. Biol.* **1**: 252-260.
- Lavis, L.D., Rutkoski, T.J., and Raines, R.T. 2007. Tuning the  $pK_a$  of fluorescein to optimize binding assays. *Anal. Chem.* **79**: XXX-XXX.
- Lee, F.S., Auld, D.S., and Vallee, B.L. 1989a. Tryptophan fluorescence as a probe of placental ribonuclease inhibitor binding to angiogenin. *Biochemistry* **28**: 219-224.
- Lee, F.S., Fox, E.A., Zhou, H.-M., Strydom, D.J., and Vallee, B.L. 1988. Primary structure of human placental ribonuclease inhibitor. *Biochemistry* **27**: 8545-8553.
- Lee, F.S., Shapiro, R., and Vallee, B.L. 1989b. Tight-binding inhibition of angiogenin and ribonuclease A by placental ribonuclease inhibitor. *Biochemistry* **28**: 225-230.
- Lee, J.E., and Raines, R.T. 2003. Contribution of active-site residues to the function of onconase, a ribonuclease with antitumoral activity. *Biochemistry* **42**: 11443-11450.
- Lee, J.E., and Raines, R.T. 2005. Cytotoxicity of Bovine Seminal Ribonuclease: Monomer versus Dimer. *Biochemistry* **44**: 15760-15767.
- Lee, L.P., and Tidor, B. 2001. Barstar is electrostatically optimized for tight binding to barnase. *Nat. Struct. Biol.* **8**: 73-76.

- Leich, F., Koditz, J., Ulbrich-Hofman, R., and Arnold, U. 2006. Tandemization endows bovine pancreatic ribonuclease with cytotoxic activity. *J. Mol. Biol.* **358**: 1305-1313.
- Leland, P.A., and Raines, R.T. 2001. Cancer chemotherapy—ribonucleases to the rescue. *Chem. Biol.* **8**: 405-413.
- Leland, P.A., Schultz, L.W., Kim, B.-M., and Raines, R.T. 1998. Ribonuclease A variants with potent cytotoxic activity. *Proc. Natl. Acad. Sci. U.S.A.* **98**: 10407-10412.
- Leland, P.A., Staniszewski, K.E., Kim, B.-M., and Raines, R.T. 2000. A synapomorphic disulfide bond is critical for the conformational stability and cytotoxicity of an amphibian ribonuclease. *FEBS Lett.* **477**: 203-207.
- Leland, P.A., Staniszewski, K.E., Kim, B.-M., and Raines, R.T. 2001. Endowing human pancreatic ribonuclease with toxicity for cancer cells. *J. Biol. Chem.* **276**: 43095-43102.
- Leland, P.A., Staniszewski, K.E., Park, C., Kelemen, B.R., and Raines, R.T. 2002. The ribonucleolytic activity of angiogenin. *Biochemistry* **41**: 1343-1350.
- Lemos, B., Meiklejohn, C.D., and Hartl, D.L. 2004. Regulatory evolution across the protein interaction network. *Nat. Genet.* **36**: 1059-1060.
- Liao, B.Y., Scott, N.M., and Zhang, J. 2006. Impacts of gene essentiality, expression pattern, and gene compactness on the evolutionary rate of mammalian proteins. *Mol. Biol. Evol.* **23**: 2072-2080.
- Lim, W.A., and Sauer, R.T. 1989. Alternative packing arrangements in the hydrophobic core of lambda repressor. *Nature* **339**: 31-36.
- Lim, W.A., and Sauer, R.T. 1991. The role of internal packing interactions in determining the structure and stability of a protein. *J. Mol. Biol.* **219**: 359-376.
- Lin, J.J., Newton, D.L., Mikulski, S.M., Kung, H.F., Youle, R.J., and Rybak, S.M. 1994. Characterization of the mechanism of cellular and cell free protein synthesis inhibition by an anti-tumor ribonuclease. *Biochem. Biophys. Res. Commun.* **204**: 156-162.
- Lindenbach, B.D., and Rice, C.M. 2001. *Flaviviridae: The viruses and their replication*. In *Fields Virology, 4th ed.* (eds. D.M. Knipe, and P.M. Howley), pp. 991-1041. Lippincott Williams & Wilkins, New York.
- Lindenbach, B.D., and Rice, C.M. 2005. Unravelling hepatitis C virus replication from genome to function. *Nature* **436**: 933-938.

- Lohmann, V., Korner, F., Koch, J., Herian, U., Theilmann, L., and Bartenschlager, R. 1999. Replication of subgenomic hepatitis C virus RNAs in a hepatoma cell line. *Science* **285**: 110-113.
- Lorenz, I.C., Marcotrigiano, J., Dentzer, T.G., and Rice, C.M. 2006. Structure of the catalytic domain of the hepatitis C virus NS2-3 protease. *Nature* **442**: 831-835.
- Loverix, S., and Steyaert, J. 2003. Ribonucleases and their anti-tumor activity. *Comp. Biochem. Physiol.* **129C**: 175-191.
- Major, M.E., Reherrmann, B., and Feinstone, S.M. 2001. Hepatitis C viruses. In *Fields Virology, 4th ed.* (eds. D.M. Knipe, and P.M. Howley), pp. 1127-1161. Lippincott Williams & Wilkins, New York.
- Makarov, A.A., and Ilinskaya, O.N. 2003. Cytotoxic ribonucleases: Molecular weapons and their targets. *FEBS Lett.* **540**: 15-20.
- Makarov, A.A., Protasevich, II, Lobachov, V.M., Kirpichnikov, M.P., Yakovlev, G.I., Gilli, R.M., Briand, C.M., and Hartley, R.W. 1994. Thermostability of the barnase-barstar complex. *FEBS Lett.* **354**: 251-254.
- Matousek, J. 2001. Ribonucleases and their antitumor activity. *Comp. Biochem. Physiol.* **129C**: 175-191.
- Matousek, J., Soucek, J., Slavik, T., Tomanek, M., Lee, J.E., and Raines, R.T. 2003. Comprehensive comparison of the cytotoxic activities of onconase and bovine seminal ribonuclease. *Comp. Biochem. Physiol. C Toxicol. Pharmacol.* **136**: 343-356.
- Matthews, B.W. 1987. Genetic and structural analysis of the protein stability problem. *Biochemistry* **26**: 6885-6888.
- Matulis, D., Kranz, J.K., Salemme, F.R., and Todd, M.J. 2005. Thermodynamic stability of carbonic anhydrase: Measurements of binding affinity and stoichiometry using ThermoFluor. *Biochemistry* **44**: 5258-5266.
- Mayhoad, T.W., and Windsor, W.T. 2005. Ligand binding affinity determined by temperature-dependent circular dichroism: Cyclin-dependent kinase 2 inhibitors. *Anal. Biochem.* **345**: 187-197.
- McDonald, I.K., and Thornton, J.M. 1994. Satisfying hydrogen bonding potential in proteins. *J. Mol. Biol.* **238**: 777-793.
- McEwan, P.A., Scott, P.G., Bishop, P.N., and Bella, J. 2006. Structural correlations in the family of small leucine-rich repeat proteins and proteoglycans. *J. Struct. Biol.* **155**: 294-305.

- McRee, D.E. 1999. XtalView/Xfit--A versatile program for manipulating atomic coordinates and electron density. *J. Struct. Biol.* **125**: 156-165.
- Michalak, P. 2006. RNA world - the dark matter of evolutionary genomics. *J. Evol. Biol.* **19**: 1768-1774.
- Mikulski, S.M., Costanzi, J.J., Vogelzang, N.J., McCachren, S., Taub, R.N., Chun, H., Mittelman, A., Panella, T., Puccio, C., Fine, R., et al. 2002. Phase II trial of a single weekly intravenous dose of ranpirnase in patients with unresectable malignant mesothelioma. *J. Clin. Oncol.* **20**: 274-281.
- Miller, S., Janin, J., Lesk, A.M., and Chothia, C. 1987. Interior and surface of monomeric proteins. *J. Mol. Biol.* **196**: 641-656.
- Mintseris, J., and Weng, Z. 2005. Structure, function, and evolution of transient and obligate protein-protein interactions. *Proc. Natl. Acad. Sci. U.S.A.* **102**: 10930-10935.
- Mitchell, J.C., Kerr, R., and Ten Eyck, L.F. 2001. Rapid atomic density methods for molecular shape characterization. *J. Mol. Graph. Model.* **19**: 325-330.
- Monti, D.M., and D'Alessio, G. 2004. Cytosolic RNase inhibitor only affects RNases with intrinsic cytotoxicity. *J. Biol. Chem.* **279**: 39195-39198.
- Monti, D.M., Montesano Gesualdi, N., Matousek, J., Esposito, F., and D'Alessio, G. 2007. The cytosolic ribonuclease inhibitor contributes to intracellular redox homeostasis. *FEBS Lett.* **581**: 930-934.
- Mulgrew-Nesbitt, A., Diraviyam, K., Wang, J., Singh, S., Murray, P., Li, Z., Rogers, L., Mirkovic, N., and Murray, D. 2006. The role of electrostatics in protein-membrane interactions. *Biochim. Biophys. Acta* **1761**: 812-826.
- Murray, D., and Honig, B. 2002. Electrostatic control of the membrane targeting of C2 domains. *Mol. Cell* **9**: 145-154.
- Murshudov, G.N., Vagin, A.A., and Dodson, E.J. 1997. Refinement of macromolecular structures by the maximum-likelihood method. *Acta Crystallogr. D Biol. Crystallogr.* **53**: 240-255.
- Myers, J.K., and Pace, C.N. 1996. Hydrogen bonding stabilizes globular proteins. *Biophys. J.* **71**: 2033-2039.
- Neurath, H. 1984. Evolution of proteolytic enzymes. *Science* **224**: 350-357.

- Nitto, T., Dyer, K.D., Czapiga, M., and Rosenberg, H.F. 2006. Evolution and function of leukocyte RNase A ribonucleases of the avian species, *Gallus gallus*. *J. Biol. Chem.* **281**: 25622-25634.
- Nooren, I.M., and Thornton, J.M. 2003. Diversity of protein-protein interactions. *EMBO J.* **22**: 3486-3492.
- Norel, R., Sheinerman, F., Petrey, D., and Honig, B. 2001. Electrostatic contributions to protein-protein interactions: fast energetic filters for docking and their physical basis. *Protein Sci.* **10**: 2147-2161.
- Notomista, E., Mancheno, J.M., Crescenzi, O., Di Donato, A., Gavilanes, J., and D'Alessio, G. 2006. The role of electrostatic interactions in the antitumor activity of dimeric RNases. *FEBS J.* **273**: 3687-3697.
- Ogawa, Y., Iwama, M., Ohgi, K., Tsuji, T., Irie, M., Itagaki, T., Kobayashi, H., and Inokuchi, N. 2002. Effect of replacing the aspartic acid/glutamic acid residues of bullfrog sialic acid binding lectin with asparagine/glutamine and arginine on the inhibition of cell proliferation in murine leukemia P388 cells. *Biol. Pharm. Bull.* **25**: 722-727.
- Orntoft, T.F., and Vestergaard, E.M. 1999. Clinical aspects of altered glycosylation of glycoproteins in cancer. *Electrophoresis* **20**: 362-371.
- Otwinowski, Z., and Minor, W. 1997. Processing of X-ray diffraction data collected in oscillation mode. *Methods Enzymol.* **276**: 307-326.
- Pace, C.N. 1990. Measuring and increasing protein stability. *Trends Biotechnol.* **8**: 93-98.
- Pace, C.N. 2001. Polar group burial contributes more to protein stability than nonpolar group burial. *Biochemistry* **40**: 310-313.
- Pace, C.N., Hebert, E.J., Shaw, K.L., Schell, D., Both, V., Krajcikova, D., Sevcik, J., Wilson, K.S., Dauter, Z., Hartley, R.W., et al. 1998. Conformational stability and thermodynamics of folding of ribonucleases Sa, Sa2 and Sa3. *J. Mol. Biol.* **279**: 271-286.
- Pace, C.N., Horn, G., Hebert, E.J., Bechert, J., Shaw, K., Urbanikova, L., Scholtz, J.M., and Sevcik, J. 2001. Tyrosine hydrogen bonds make a large contribution to protein stability. *J. Mol. Biol.* **312**: 393-404.
- Pace, C.N., Shirley, B.A., McNutt, M., and Gajiwala, K. 1996. Forces contributing to the conformational stability of proteins. *FASEB J.* **10**: 75-83.
- Pál, C., Papp, B., and Lercher, M.J. 2006. An integrated view of protein evolution. *Nat. Rev. Genet.* **7**: 337-348.

- Papageorgiou, A., Shapiro, R., and Acharya, K. 1997. Molecular recognition of human angiogenin by placental ribonuclease inhibitor—an X-ray crystallographic study at 2.0 Å resolution. *EMBO J.* **16**: 5162-5177.
- Park, C., and Raines, R.T. 2001. Adjacent cysteine residues as a redox switch. *Protein Eng.* **14**: 939-942.
- Park, C., and Raines, R.T. 2003. Catalysis by ribonuclease A is limited by the rate of substrate association. *Biochemistry* **42**: 3509-3518.
- Parsegian, V.A. 2006. *van der Waals Forces*. Cambridge University Press, New York.
- Pavlakakis, N., and Vogelzang, N.J. 2006. Ranpirnase—an antitumour ribonuclease: Its potential role in malignant mesothelioma. *Expert Opin. Biol. Ther.* **6**: 391-399.
- Pizzi, E., Tramontano, A., Tomei, L., La Monica, N., Failla, C., Sardana, M., Wood, T., and De Francesco, R. 1994. Molecular model of the specificity pocket of the hepatitis C virus protease: Implications for substrate recognition. *Proc. Natl. Acad. Sci. U.S.A.* **91**: 888-892.
- Pizzo, E., Buonanno, P., Di Maro, A., Ponticelli, S., De Falco, S., Quarto, N., Cubellis, M.V., and D'Alessio, G. 2006. Ribonucleases and angiogenins from fish. *J. Biol. Chem.* **281**: 27454-27460.
- Plainkum, P., Fuchs, S.M., Wiyakrutta, S., and Raines, R.T. 2003. Creation of a zymogen. *Nat. Struct. Biol.* **10**: 115-119.
- Polo, S., and Di Fiore, P.P. 2006. Endocytosis conducts the cell signaling orchestra. *Cell* **124**: 897-900.
- Pous, J., Canals, A., Terzyan, S.S., Guasch, A., Benito, A., Ribo, M., Vilanova, M., and Coll, M. 2000. Three-dimensional structure of a human pancreatic ribonuclease variant, a step forward in the design of cytotoxic ribonucleases. *J. Mol. Biol.* **303**: 49-60.
- Raines, R.T. 1998. Ribonuclease A. *Chem. Rev.* **98**: 1045-1065.
- Raines, R.T. 2004. Active site of ribonuclease A. In *Artificial Nucleases*. (ed. M.A. Zenkova), pp. 19-32. Springer-Verlag, Heidelberg, Germany.
- Rajamani, D., Thiel, S., Vajda, S., and Camacho, C.J. 2004. Anchor residues in protein-protein interactions. *Proc. Natl. Acad. Sci. U.S.A.* **101**: 11287-11292.
- Ran, S., Downes, A., and Thorpe, P.E. 2002. Increased exposure of anionic phospholipids on the surface of tumor blood vessels. *Cancer Res.* **62**: 6132-6140.

- Reiter, N.J., Nikstad, L.J., Allmann, A.M., Johnson, R.J., and Butcher, S.E. 2003. Structure of the U6 RNA intramolecular stem-loop harboring an S(P)-phosphorothioate modification. *RNA* **9**: 533-542.
- Ribó, M., Beintema, J.J., Osset, M., Fernández, E., Bravo, J., de Llorens, R., and Cuchillo, C.M. 1994. Heterogeneity in the glycosylation pattern of human pancreatic ribonuclease. *Biol. Chem. Hoppe-Seyler* **375**: 357-363.
- Richard, J.P., Melikov, K., Brooks, H., Prevot, P., Lebleu, B., and Chernomordik, L.V. 2005. Cellular uptake of unconjugated TAT peptide involves clathrin-dependent endocytosis and heparan sulfate receptors. *J. Biol. Chem.* **280**: 15300-15306.
- Richards, F.M. 1974. The interpretation of protein structures: total volume, group volume distributions and packing density. *J. Mol. Biol.* **82**: 1-14.
- Riddles, P.W., Blakeley, R.L., and Zerner, B. 1983. Reassessment of Ellman's reagent. *Methods Enzymol.* **91**: 49-60.
- Rodriguez, M., Benito, A., Tubert, P., Castro, J., Ribo, M., Beaumelle, B., and Vilanova, M. 2006. A cytotoxic ribonuclease variant with a discontinuous nuclear localization signal constituted by basic residues scattered over three areas of the molecule. *J. Mol. Biol.* **360**: 548-557.
- Rodriguez, M., Torrent, G., Bosch, M., Rayne, F., Dubremetz, J.F., Ribo, M., Benito, A., Vilanova, M., and Beaumelle, B. 2007. Intracellular pathway of Onconase that enables its delivery to the cytosol. *J. Cell. Sci.* **120**: 1405-1411.
- Rose, G.D., Fleming, P.J., Banavar, J.R., and Maritan, A. 2006. A backbone-based theory of protein folding. *Proc. Natl. Acad. Sci. U.S.A.* **103**: 16623-16633.
- Rosenberg, H.F., and Dyer, K.D. 1995. Eosinophil cationic protein and eosinophil-derived neurotoxin. *J. Biol. Chem.* **270**: 21539-21544.
- Rosenberg, H.F., Dyer, K.D., Tiffany, H.L., and Gonzalez, M. 1995. Rapid evolution of a unique family of primate ribonuclease genes. *Nature Genet.* **10**: 219-223.
- Rothenberg, M.E., and Hogan, S.P. 2006. The eosinophil. *Annu. Rev. Immunol.* **24**: 147-174.
- Ruoppolo, M., Vinci, F., Klink, T.A., Raines, R.T., and Marino, G. 2000. Contribution of individual disulfide bonds to the oxidative folding of ribonuclease A. *Biochemistry* **39**: 12033-12042.
- Rutkoski, T.J., Kurten, E.L., Mitchell, J.C., and Raines, R.T. 2005. Disruption of shape-complementarity markers to create cytotoxic variants of ribonuclease A. *J. Mol. Biol.* **354**: 41-54.



- Saeed, R., and Deane, C.M. 2006. Protein–protein interactions, evolutionary rate, abundance and age. *BMC Bioinformatics* **7**: 128.
- Salvesen, G.S., and Abrams, J.M. 2004. Caspase activation—stepping on the gas or releasing the brakes? Lessons from humans and flies. *Oncogene* **23**: 2774-2784.
- Sashital, D.G., Venditti, V., Angers, C.G., Cornilescu, G., and Butcher, S.E. 2007. Structure and thermodynamics of a conserved U2 snRNA domain from yeast and human. *RNA* **13**: 328-338.
- Sassi, S.O., Braun, E.L., and Benner, S.A. 2007. The evolution of seminal ribonuclease: pseudogene reactivation or multiple gene inactivation events? *Mol. Biol. Evol.* **24**: 1012-1024.
- Saxena, S.K., Rybak, S.M., Winkler, G., Meade, H.M., McGray, P., Youle, R.J., and Ackerman, E.J. 1991. Comparison of RNases and toxins upon injection into *Xenopus* oocytes. *J. Biol. Chem.* **266**: 21208-21214.
- Schell, D., Tsai, J., Scholtz, J.M., and Pace, C.N. 2006. Hydrogen bonding increases packing density in the protein interior. *Proteins* **63**: 278-282.
- Schienman, J.E., Holt, R.A., Auerbach, M.R., and Stewart, C.B. 2006. Duplication and divergence of 2 distinct pancreatic ribonuclease genes in leaf-eating African and Asian colobine monkeys. *Mol. Biol. Evol.* **23**: 1465-1479.
- Schreiber, G., and Fersht, A.R. 1996. Rapid, electrostatically assisted association of proteins. *Nat. Struct. Biol.* **3**: 427-431.
- Selzer, T., Albeck, S., and Schreiber, G. 2000. Rational design of faster associating and tighter binding protein complexes. *Nat. Struct. Biol.* **7**: 537-541.
- Selzer, T., and Schreiber, G. 1999. Predicting the rate enhancement of protein complex formation from the electrostatic energy of interaction. *J. Mol. Biol.* **287**: 409-419.
- Shaked, Z., Szajewski, R.P., and Whitesides, G.M. 1980. Rates of thiol-disulfide interchange reactions involving proteins and kinetic measurements of thiol  $pK_a$  values. *Biochemistry* **19**: 4156-4166.
- Shapiro, R., Fett, J.W., Strydom, D.J., and Vallee, B.L. 1986a. Isolation and characterization of a human colon carcinoma-secreted enzyme with pancreatic ribonuclease-like activity. *Biochemistry* **25**: 7255-7264.
- Shapiro, R., Riordan, J.F., and Vallee, B.L. 1986b. Characteristic ribonucleolytic activity of human angiogenin. *Biochemistry* **25**: 3527-3532.

- Shapiro, R., and Vallee, B.L. 1989. Site-directed mutagenesis of histidine-13 and histidine-114 of human angiogenin. Alanine derivatives inhibit angiogenin-induced angiogenesis. *Biochemistry* **28**: 7401-7408.
- Sharp, K., Fine, R., and Honig, B. 1987. Computer simulations of the diffusion of a substrate to an active site of an enzyme. *Science* **236**: 1460-1463.
- Shaul, Y., and Schreiber, G. 2005. Exploring the charge space of protein-protein association: a proteomic study. *Proteins* **60**: 341-352.
- Sheinerman, F.B., and Honig, B. 2002. On the role of electrostatic interactions in the design of protein-protein interfaces. *J. Mol. Biol.* **318**: 161-177.
- Shirley, B.A., Stanssens, P., Hahn, U., and Pace, C.N. 1992. Contribution of hydrogen bonding to the conformational stability of ribonuclease T1. *Biochemistry* **31**: 725-732.
- Shoichet, B.K., Baase, W.A., Kuroki, R., and Matthews, B.W. 1995. A relationship between protein stability and protein function. *Proc. Natl. Acad. Sci. U.S.A.* **92**: 452-456.
- Shoup, D., and Szabo, A. 1982. Role of diffusion in ligand binding to macromolecules and cell-bound receptors. *Biophys. J.* **40**: 33-39.
- Silverman, J.A., Balakrishnan, R., and Harbury, P.B. 2001. Reverse engineering the (beta/alpha)<sub>8</sub> barrel fold. *Proc. Natl. Acad. Sci. U.S.A.* **98**: 3092-3097.
- Singhania, N.A., Dyer, K.D., Zhang, J., Deming, M.S., Bonville, C.A., Domachowske, J.B., and Rosenberg, H.F. 1999. Rapid evolution of the ribonuclease A superfamily: Adaptive expansion of independent gene clusters in rats and mice. *J. Mol. Evol.* **49**: 721-728.
- Slivinsky, G.G., Hymer, W.C., Bauer, J., and Morrison, D.R. 1997. Cellular electrophoretic mobility data: A first approach to a database. *Electrophoresis* **18**: 1109-1119.
- Smith, B.D., and Raines, R.T. 2006. Genetic selection for critical residues in ribonucleases. *J. Mol. Biol.* **362**: 459-478.
- Smith, B.D., Soellner, M.B., and Raines, R.T. 2003. Potent inhibition of ribonuclease A by oligo(vinylsulfonic acid). *J. Biol. Chem.* **278**: 20934-20938.
- Sohl, J.L., Shiau, A.K., Rader, S.D., Wilk, B.J., and Agard, D.A. 1997. Inhibition of alpha-lytic protease by pro region C-terminal steric occlusion of the active site. *Biochemistry* **36**: 3894-3902.

- Soncin, F., Strydom, D.J., and Shapiro, R. 1997. Interaction of heparin with human angiogenin. *J. Biol. Chem.* **272**: 9818-9824.
- Stites, W.E., Gittis, A.G., Lattman, E.E., and Shortle, D. 1991. In a staphylococcal nuclease mutant the side-chain of a lysine replacing valine 66 is fully buried in the hydrophobic core. *J. Mol. Biol.* **221**: 7-14.
- Stone, S.R., and Hofsteenge, J. 1986. Kinetics of the inhibition of thrombin by hirudin. *Biochemistry* **25**: 4622-4628.
- Sturtevant, J.M. 1987. Biochemical applications of differential scanning calorimetry. *Annu Rev Phys Chem* **38**: 463-488.
- Suhasini, A.N., and Sirdeshmukh, R. 2006. Transfer RNA cleavages by onconase reveal unusual cleavage sites. *J. Biol. Chem.* **281**: 12201-12209.
- Suzuki, M., Saxena, S.K., Boix, E., Prill, R.J., Vasandani, V.M., Ladner, J.E., Sung, C., and Youle, R.J. 1999. Engineering receptor-mediated cytotoxicity into human ribonucleases by steric blockage of inhibitor interaction. *Nat. Biotechnol.* **17**: 265-270.
- Szajewski, R.P., and Whitesides, G.M. 1980. Rate constants and equilibrium-constants for thiol-disulfide interchange reactions involving oxidized glutathione. *J. Am. Chem. Soc.* **102**: 2011-2026.
- Tada, H., Onizuka, M., Muraki, K., Masuzawa, W., Futami, J., Kosaka, M., Seno, M., and Yamada, H. 2004. Insertional-fusion of basic fibroblast growth factor endowed ribonuclease 1 with enhanced cytotoxicity by steric blockade of inhibitor interaction. *FEBS Lett.* **568**: 39-43.
- Tafech, A., Bassett, T., Sparanese, D., and Lee, C.H. 2006. Destroying RNA as a therapeutic approach. *Curr. Med. Chem.* **13**: 863-881.
- Takeshita, F., and Ochiya, T. 2006. Therapeutic potential of RNA interference against cancer. *Cancer Sci.* **97**: 689-696.
- Tan, S.L., Pause, A., Shi, Y., and Sonenberg, N. 2002. Hepatitis C therapeutics: Current status and emerging strategies. *Nat. Rev. Drug Discov.* **1**: 867-881.
- Tang, C., Iwahara, J., and Clore, G.M. 2006. Visualization of transient encounter complexes in protein-protein association. *Nature* **444**: 383-386.
- Taremi, S.S., Beyer, B., Maher, M., Yao, N., Prosise, W., Weber, P.C., and Malcolm, B.A. 1998. Construction, expression, and characterization of a novel fully activated recombinant single-chain hepatitis C virus protease. *Protein Sci.* **7**: 2143-2149.

- Teufel, D.P., Kao, R.Y., Acharya, K.R., and Shapiro, R. 2003. Mutational analysis of the complex of human RNase inhibitor and human eosinophil-derived neurotoxin (RNase 2). *Biochemistry* **42**: 1451-1459.
- Thompson, J.E., Kutateladze, T.G., Schuster, M.C., Venegas, F.D., Messmore, J.M., and Raines, R.T. 1995. Limits to catalysis by ribonuclease A. *Bioorg. Chem.* **23**: 471-481.
- Tomei, L., Failla, C., Santolini, E., De Francesco, R., and La Monica, N. 1993. NS3 is a serine protease required for processing of hepatitis C virus polyprotein. *J. Virol.* **67**: 4017-4026.
- Tomita, Y., Goto, Y., Okazaki, T., and Shukuya, R. 1979. Liver ribonucleases from the bullfrog, *Rana catesbeiana*. Purification, properties and changes in activity during metamorphosis. *Biochim. Biophys. Acta* **562**: 504-514.
- Trost, B.M. 1991. *Comprehensive Organic Synthesis: Selectivity, Strategy, & Efficiency in Modern Organic Chemistry*. Pergamon Press. vol 6, pp 758-769, New York.
- Tsuji, T., Sun, Y., Kishimoto, K., Olson, K.A., Liu, S., Hirukawa, S., and Hu, G.F. 2005. Angiogenin is translocated to the nucleus of HeLa cells and is involved in ribosomal RNA transcription and cell proliferation. *Cancer Res.* **65**: 1352-1360.
- Urbani, A., Bianchi, E., Narjes, F., Tramontano, A., De Francesco, R., Steinkuhler, C., and Pessi, A. 1997. Substrate specificity of the hepatitis C virus serine protease NS3. *J. Biol. Chem.* **272**: 9204-9209.
- Vagin, A., and Teplyakov, A. 1997. MOLREP: An automated program for molecular replacement. *J Appl Crystallogr* **30**: 1022-1025.
- Valko, M., Rhodes, C.J., Moncol, J., Izakovic, M., and Mazur, M. 2006. Free radicals, metals and antioxidants in oxidative stress-induced cancer. *Chem. Biol. Interact.* **160**: 1-40.
- Vallone, B., Miele, A.E., Vecchini, P., Chiancone, E., and Brunori, M. 1998. Free energy of burying hydrophobic residues in the interface between protein subunits. *Proc. Natl. Acad. Sci. USA* **95**: 6103-6107.
- Vasandani, V.M., Burris, J.A., and Sung, C. 1999. Reversible nephrotoxicity of onconase and effect of lysine pH on renal onconase uptake. *Cancer Thermother. Pharmacol.* **44**: 164-169.
- Vasandani, V.M., Wu, Y.-N., Mikulski, S.M., Youle, R.J., and Sung, C. 1996. Molecular determinants in the plasma clearance and tissue distribution of ribonucleases of the ribonuclease A superfamily. *Cancer Res.* **56**: 4180-4186.

- Vicentini, A.M., Kieffer, B., Mathies, R., Meyhack, B., Hemmings, B.A., Stone, S.R., and Hofsteenge, J. 1990. Protein chemical and kinetic characterization of recombinant porcine ribonuclease inhibitor expressed in *Saccharomyces cerevisiae*. *Biochemistry* **29**: 8827-8834.
- Waldron, T.T., and Murphy, K.P. 2003. Stabilization of proteins by ligand binding: Application to drug screening and determination of unfolding energetics. *Biochemistry* **42**: 5058-5064.
- Wang, S., and Li, H. 2006. Radical scavenging activity of ribonuclease inhibitor from cow placenta. *Biochemistry (Moscow)* **71**: 520-524.
- Wedemeyer, W.J., Welker, E., Narayan, M., and Scheraga, H.A. 2000. Disulfide bonds and protein folding. *Biochemistry* **39**: 4207-4216.
- Wedemeyer, W.J., Welker, E., and Scheraga, H.A. 2002. Proline *cis-trans* isomerization and protein folding. *Biochemistry* **41**: 14637-14644.
- Wlodawer, A., Svensson, L.A., Sjölin, L., and Gilliland, G.L. 1988. Structure of phosphate-free ribonuclease A refined at 1.26 Å. *Biochemistry* **27**: 2705-2717.
- World Health Organization. 1999. Global surveillance and control of hepatitis C. Report of a WHO Consultation organized in collaboration with the Viral Hepatitis Prevention Board, Antwerp, Belgium. *J. Viral. Hepat.* **6**: 35-47.
- Wu, W., Sun, M., Zou, G.M., and Chen, J. 2007. MicroRNA and cancer: Current status and prospective. *Int. J. Cancer* **120**: 953-960.
- Wu, Y., Mikulski, S.M., Ardelt, W., Rybak, S.M., and Youle, R.J. 1993. A cytotoxic ribonuclease. *J. Biol. Chem.* **268**: 10686-10693.
- Yao, N., Reichert, P., Taremi, S.S., Prosise, W.W., and Weber, P.C. 1999. Molecular views of viral polyprotein processing revealed by the crystal structure of the hepatitis C virus bifunctional protease-helicase. *Structure Fold. Des.* **7**: 1353-1363.
- Yu, L., and Zhang, Y.P. 2006. The unusual adaptive expansion of pancreatic ribonuclease gene in carnivora. *Mol. Biol. Evol.* **23**: 2326-2335.
- Zhang, J. 2006. Parallel adaptive origins of digestive RNases in Asian and African leaf monkeys. *Nat. Genet.* **38**: 819-823.
- Zhang, J. 2007. Disulfide-bond reshuffling in the evolution of an ape placental ribonuclease. *Mol. Biol. Evol.* **24**: 505-512.

- Zhang, J., Rosenberg, H.F., and Nei, M. 1998. Positive Darwinian selection after gene duplication in primate ribonuclease genes. *Proc. Natl. Acad. Sci. U.S.A.* **95**: 3708-3713.
- Zhang, J., Zhang, Y.P., and Rosenberg, H.F. 2002. Adaptive evolution of a duplicated pancreatic ribonuclease gene in a leaf-eating monkey. *Nat. Genet.* **30**: 411-415.
- Zhang, R., Durkin, J., Windsor, W.T., McNemar, C., Ramanathan, L., and Le, H.V. 1997. Probing the substrate specificity of hepatitis C virus NS3 serine protease by using synthetic peptides. *J. Virol.* **71**: 6208-6213.
- Zhang, R., and Snyder, G.H. 1989. Dependence of formation of small disulfide loops in two-cysteine peptides on the number and types of intervening amino acids. *J. Biol. Chem.* **264**: 18472-18479.
- Zhu, C.F., Liu, Q., Zhang, L., Yuan, H.X., Zhen, W., Zhang, J.S., Chen, Z.J., Hall, S.H., French, F.S., and Zhang, Y.L. 2007. RNase9, an androgen-dependent member of the RNase A family, is specifically expressed in the rat epididymis. *Biol. Reprod.* **76**: 63-73.
- Zorko, M., and Langel, U. 2005. Cell-penetrating peptides: mechanism and kinetics of cargo delivery. *Adv. Drug Deliv. Rev.* **57**: 529-545.